Geology of the Qaqqanituaq Area and mafic and ultramafic geochemistry of the Hall Peninsula, Baffin Island, Nunavut

A Thesis Submitted to the College of

Graduate Studies and Research

In Partial Fulfillment of the Requirements

For the Degree of Master of Science

In the Department of Geological Sciences

University of Saskatchewan

Saskatoon

By Cameron Bruce MacKay

PERMISSION TO USE

In presenting this thesis in partial fulfillment of the requirements for a Postgraduate degree from the University of Saskatchewan, I agree that the Libraries of this University may make it freely available for inspection. I further agree that permission for copying of this thesis in any manner, in whole or in part, for scholarly purposes may be granted by the professor or professors who supervised my thesis work or, in their absence, by the Head of the Department or the Dean of the College in which my thesis work was done. It is understood that any copying or publication or use of this thesis or parts thereof for financial gain shall not be allowed without my written permission. It is also understood that due recognition shall be given to me and to the University of Saskatchewan in any scholarly use which may be made of any material in my thesis.

Requests for permission to copy or to make other uses of materials in this thesis/dissertation in whole or part should be addressed to:

Head of the Department of Geological Sciences
University of Saskatchewan
114 Science Place
Saskatoon, Saskatchewan
S7N 5E2, Canada

OR

Dean of the College of Graduate Studies and Research
University of Saskatchewan
107 Administration Place
Saskatoon, Saskatchewan
S7N 5A2, Canada

ABSTRACT

Recent regional bedrock mapping carried out on the Hall Peninsula, Baffin Island, Nunavut has revealed previously unknown rock units, structural relationships and metamorphic conditions achieved. Mafic and ultramafic rocks occur primarily intercalated with metasedimentary rocks in the east-central region of the Hall Peninsula. Focused mapping was carried out in the Quaqqanituaq Area (QA), now the type locality for metasedimentary-mafic/ultramafic occurrences on the Hall Peninsula. The QA records an east-west compression event, D1, which produced in the dominant regional S1 fabric and tight, nearly isoclinal F1 folds. The QA also records a north-south compression event, D3 (regional D2 event not observed in QA) resulting in an S3 crenulation cleavage and open F3 folds. U-Pb detrital zircon geochronology and U-Pb geochronology of a cross-cutting monzogranite dyke bracket sediment accumulation and mafic/ultramafic intrusion/extrusion between 2.13 and 1.87 Ga and place a maximum age on D1 at 1.87 Ga. Garnet – biotite – K-feldspar – ± sillimanite mineral assemblages observed in QA pelites indicate that upper amphibolite facies metamorphic conditions were reached. This observation is empirically confirmed by the implementation of winTWQ software which indicates that the peak pressure and temperature conditions reached in the QA were 4.8±2.1 kbars and 645±50°C. Whole-rock major and trace element geochemical data was obtained for 75 mafic and ultramafic samples from all regions of the Hall Peninsula including 20 from the QA. Mafic samples were classified on the basis of N-MORB normalized trace element geochemistry as being alkaline (La/Sm ~ 4.9; Gd/Yb ~ 2.7), calc-alkaline (La/Sm ~ 4.3; Gd/Yb ~ 2.4), tholeiitic (La/Sm ~ 2.1; Gd/Yb ~ 1.1), or transitional (La/Sm ~ 2.7; Gd/Yb ~ 1.6). A negative Nb anomaly, which is on average 5.4 times lower with respect to Th and Ce is observed in all mafic samples with the exception of alkaline mafic rocks. On the basis of their

geochemical profiles and comparative study of adjacent terrains, the mafic rocks are concluded result from partial melting a subduction modified mantle source during plume-initiated rifting of the North Atlantic Craton.

ACKOWLEDGEMENTS

The completion of this thesis would not have been possible without the care and support of many people and institutions. My supervisor Kevin Ansdell is thanked for selecting me to undertake this project and for his patient, tempered guidance and mentorship throughout the process. The Canada-Nunavut Geoscience Office initiated and funded the Hall Peninsula Integrated Geoscience Project, within the context of which my thesis project took place. Dave Mate, Celine Gilbert, Holly Steenkamp and Tommy Tremblay are thanked for their friendship and expertise. Diane Skipton, Rich From, Zoe Braden, Julie Leblanc-Dumas, Gabe Creason, Patricia Peyton, and Candice Sudlovenick are thanked for their friendship and good humour throughout our time together in the north. To all the people who call Baffin Island home, qujannamiik. The University of Saskatchewan is thanked for the use of its facilities as well as all Professors and staff who have provided guidance, knowledge and friendship throughout my time here. Marc St-Onge, Nicole Rayner and Mike Young are thanked for their collaboration on projects and knowledge shared. The Research Affiliate Program provided stipend support and NSERC Discovery grant to Kevin Ansdell provided additional financial support. Finally, I would like to thank my wife Emma, for always loving and supporting me unconditionally and for pushing me to be my best.

TABLE OF CONTENTS

LIST OF TABLES

LIST OF FIGURES

CHAPTER 1

HALL PENINSULA REGIONAL GEOLOGY AND PROJECT OVERVIEW

1.1 Introduction

This M.Sc. thesis is one of the projects undertaken as part of the Hall Peninsula Integrated Geoscience Program (HPIGP) conducted by the Canada-Nunavut Geoscience Office (CNGO). The Hall Peninsula is situated on Baffin Island in the eastern Canadian Arctic Archipelago (Figure 1.1). The primary goals of the HPIGP are to produce an updated geological map of the Hall Peninsula (Figure 1.2a and b); to discern where the Hall Peninsula crustal block fits with respect to known cratons, crustal structures and previously identified rock units; to identify prospective targets or favourable conditions for the exploration for and development of mineral resources on the Hall Peninsula; and to aid in the completion of thematic studies carried out by undergraduate and graduate students from across Canada which further the aforementioned goals of the HPIGP.

Figure 1.1 – Map of Baffin Island showing boundaries, selected place names, selected drainage names, and selected lines of latitude and longitude. Black polygon outlines the Hall Peninsula.

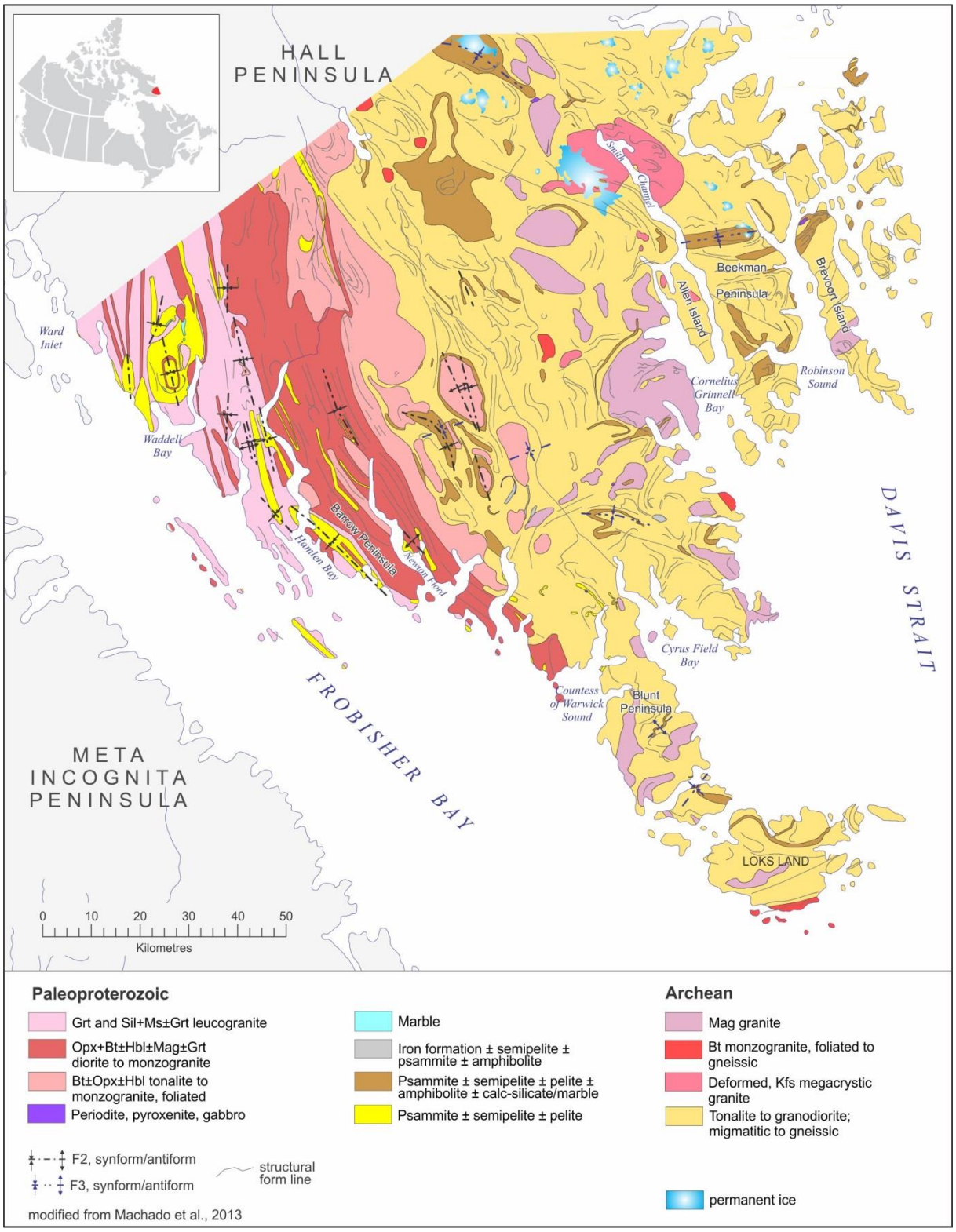

Figure 1.2a – Geology of southern Hall Peninsula, Baffin Island. Modified from Machado et al. (2013).

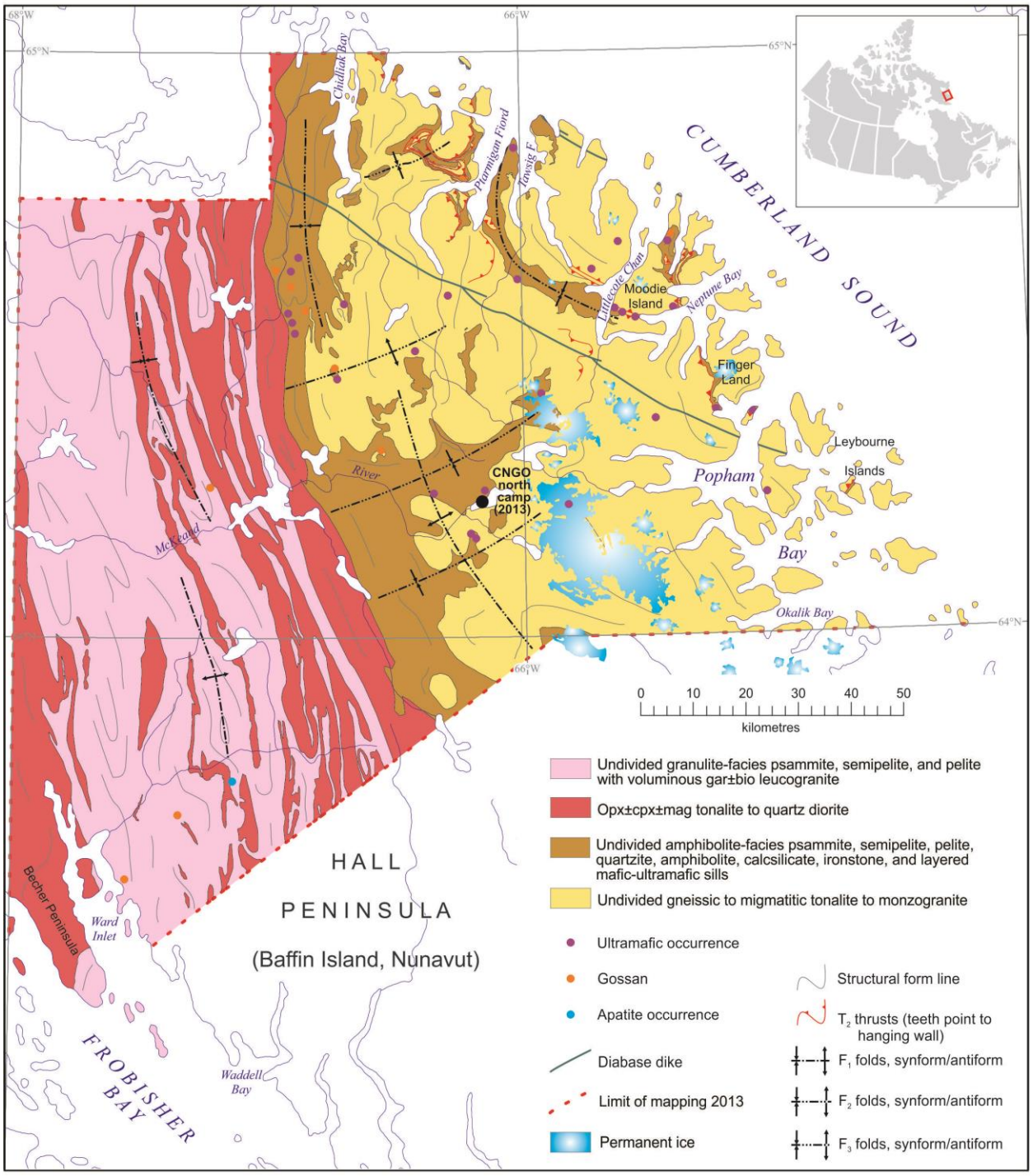

Figure 1.2b – Geology of northern Hall Peninsula, Baffin Island. Modified from Steenkamp and St-Onge (2014).

1.2 Regional Geology – Previous Work

The Hall Peninsula is situated within the northeastern portion of Paleoproterozoic Trans-Hudson Orogen, which represents the collision zone between the underriding Superior craton to the southwest and the upper Churchill plate collage to the northwest (Figure 1.3). The Churchill plate collage is made up of a number of distinct, Archean crustal blocks including the Slave craton, the North Atlantic (Nain) craton, the Rae craton, the Wyoming craton (not shown) and the Hearne craton (Figure 1.3). The locations of the boundaries between unique crustal blocks are problematic to define with certainty. However, broadly speaking, the Hall Peninsula is situated to south of the Rae craton, north of the Superior craton, west of the North Atlantic (Nain) craton and east of the Meta Incognita microcontinent (Figure 1.3).

Prior to the initiation of the HPIGP the geology of the Hall Peninsula was first studied in 1965 under the Geological Survey of Canada's Operation Amadjuak (Blackadar, 1967). This reconnaissance-scale mapping project outlined the major lithological units on the Hall Peninsula. This work was later refined by Scott (1996, 1999) who divided the geology of Hall Peninsula into three principal lithological domains: 1) a western metaplutonic domain dominated by orthopyroxene- and garnet-bearing monzogranites which was interpreted as an extension of the Paleopreoterozoic Cumberland Batholith; 2) a central metasedimentary domain composed of Paleoproterozoic siliciclastic rocks with lesser Paleoproterozoic metaplutonic rocks; and 3) an eastern metaplutonic domain dominated by Archean tonalitic gneisses, monzogranite and minor metasedimentary rocks (Scott, 1996; 1999). Scott's classification of these domains was based on: i) field observations made while conducting a transect through a well exposed corridor east of Iqaluit, NU (Figure 1.4); ii) the characterization of igneous and metamorphic events by

isotope dilution U-Pb dating of zircon, monazite and titanite; and iii) Pb-Pb laser ablation microprobe ICP-MS age dates obtained from detrital zircons (Scott, 1996; 1999). Results of geochronology conducted by Scott (1999) indicate that the western domain orthopyroxene and garnet-bearing monzogranites are ca. 1.869 – 1.850 Ga in age, the central metasedimentary domain rocks are almost exclusively Paleoproterozoic in age and that the eastern plutonic domain rocks crystallized between 2.92 and 2.80 Ga.

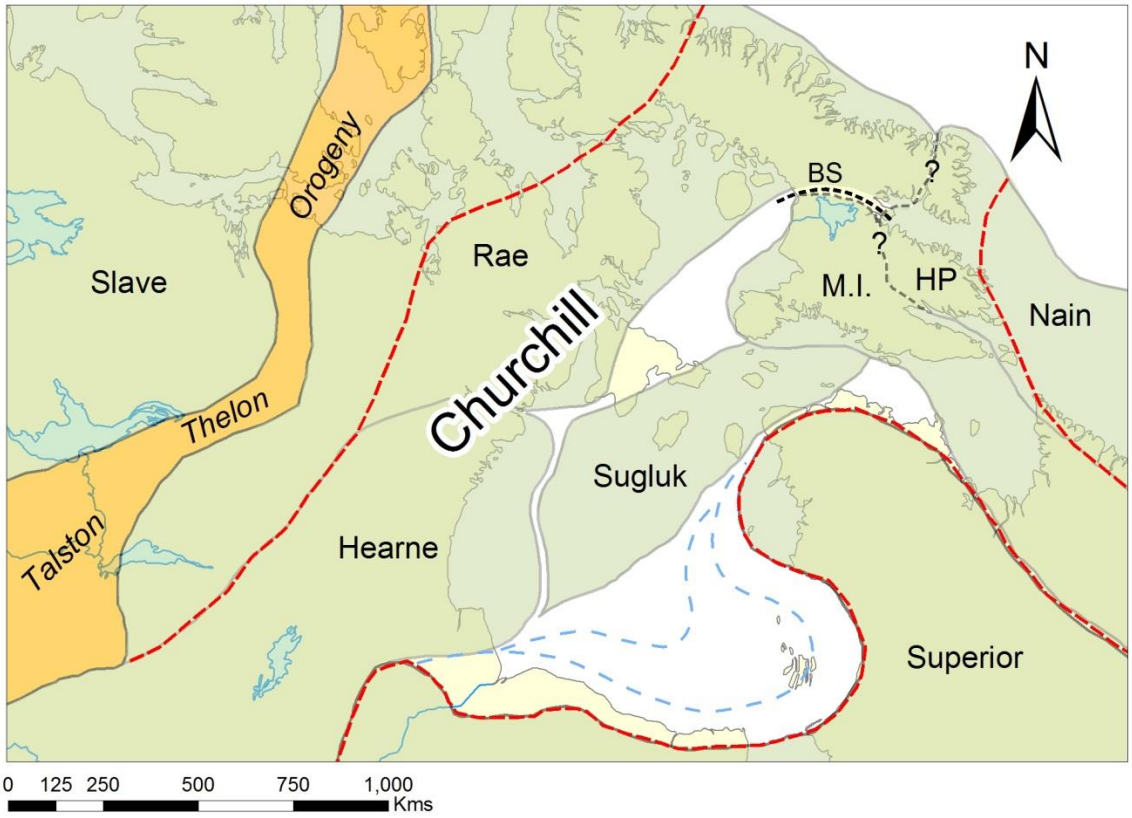

Figure 1.3 – Precambrian tectonic subdivisions of northeastern Canada modified after Corrigan (2012). Red dashed lines demarcate the area affected by Trans-Hudson orogenic processes. Blue dashed lines indicate possible extensions of the Superior craton at the Moho. Abbreviations: BS – Baffin Suture; HP – Hall Peninsula; M.I. – Meta Incognita microcontinent.

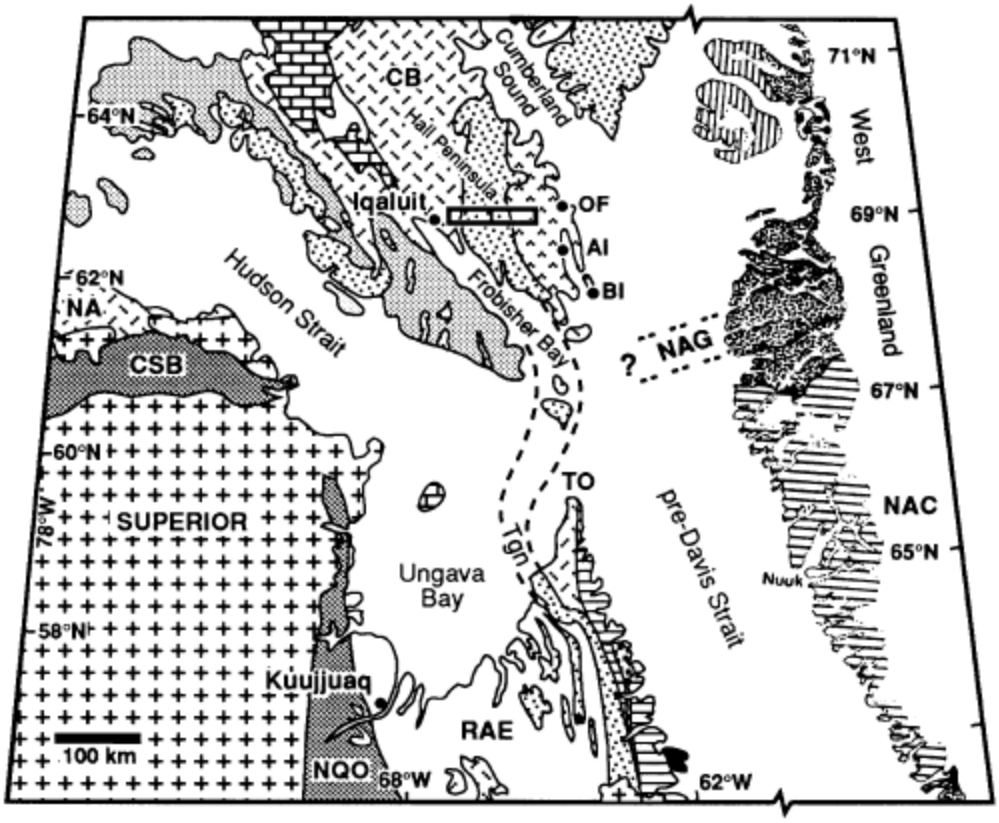

Figure 1.4 – Summary geological map from Scott (1999). Box east of Iqaluit indicates location of Scott (1996) transect. AI, Allan Island; BI, Brevoort Island; CB, Cumberland Batholith; CSB, Cape Smith belt; NA, Narsajuaq Arc; NAC, North Atlantic (Nain) craton; NAG, Nagssugtoqidian suture zone; NQO, New Quebec Orogen; OF, Okalik Fiord; Tgn, Tasiuyak paragneiss; TO, Torngat Orogen.

Regional tectono-stratigraphic correlations involving the Hall Peninsula block are numerous and contentious. Jackson and Taylor (1972) correlated the siliciclastic metasedimentary rocks of the Hall Peninsula with the Lake Harbour Group on the Meta Incognita microcontinent and similar metasedimentary rocks from northeastern Quebec. Hoffman (1989a) suggested that the Tasiuyak paragneiss of northern Quebec and Labrador might continue onto the Hall Peninsula (Figure 1.4). Hoffman's interpretation was based on a pronounced magnetic low anomaly that can be traced 1300 km from the Grenville orogen in southern Labrador to Cumberland Sound. Where exposed, the Abloviak shear zone of northern Quebec correlates with this magnetic low. The Abloviak shear zone is found in association with

the Tasiuyak paragneiss in northern Quebec and Labrador. Thus, both were interpreted to continue north through the Hall Peninsula (Figure 1.4) (Hoffman, 1989b). Corrigan (2012) follows this reasoning and then interprets the Hall Peninsula as being a part of the North Atlantic/Nain craton (Figure 1.3). St-Onge (2009) breaks from this interpretation by suggesting that the Hall Peninsula is part of the Meta Incognita microcontinent by correlating Paleoproterozoic metasedimentary packages; the Hoare Bay group, found on the Cumberland Peninsula and the Piling group exposed on the Rae craton of central Baffin Island. Based on this correlation, St-Onge (2009) placed a suture between the Rae craton to the north and the Meta Incognita microcontinent to the south, informally termed the Baffin suture (Figure 1.3). St-Onge also correlates – as did Jackson and Taylor (1972) – the Lake Harbour Group on the Meta-Incognita microcontinent with the metasedimentary rocks on Hall Peninsula.

1.3 Regional Geology – Interpretations based on new observations

1.3.1 Introduction

New observations following 1:250 000 scale bedrock mapping conducted by the CNGO in 2012 and 2013 (Figure 1.2a and b) have identified new rock units and led to reinterpretation of the litho-tectonic history of the Hall Peninsula. The Hall Peninsula can be broadly subdivided into two distinct lithological regions, a western region and an east-central region. The division between the two regions is roughly defined by a pronounced magnetic high anomaly (Figure 1.5).

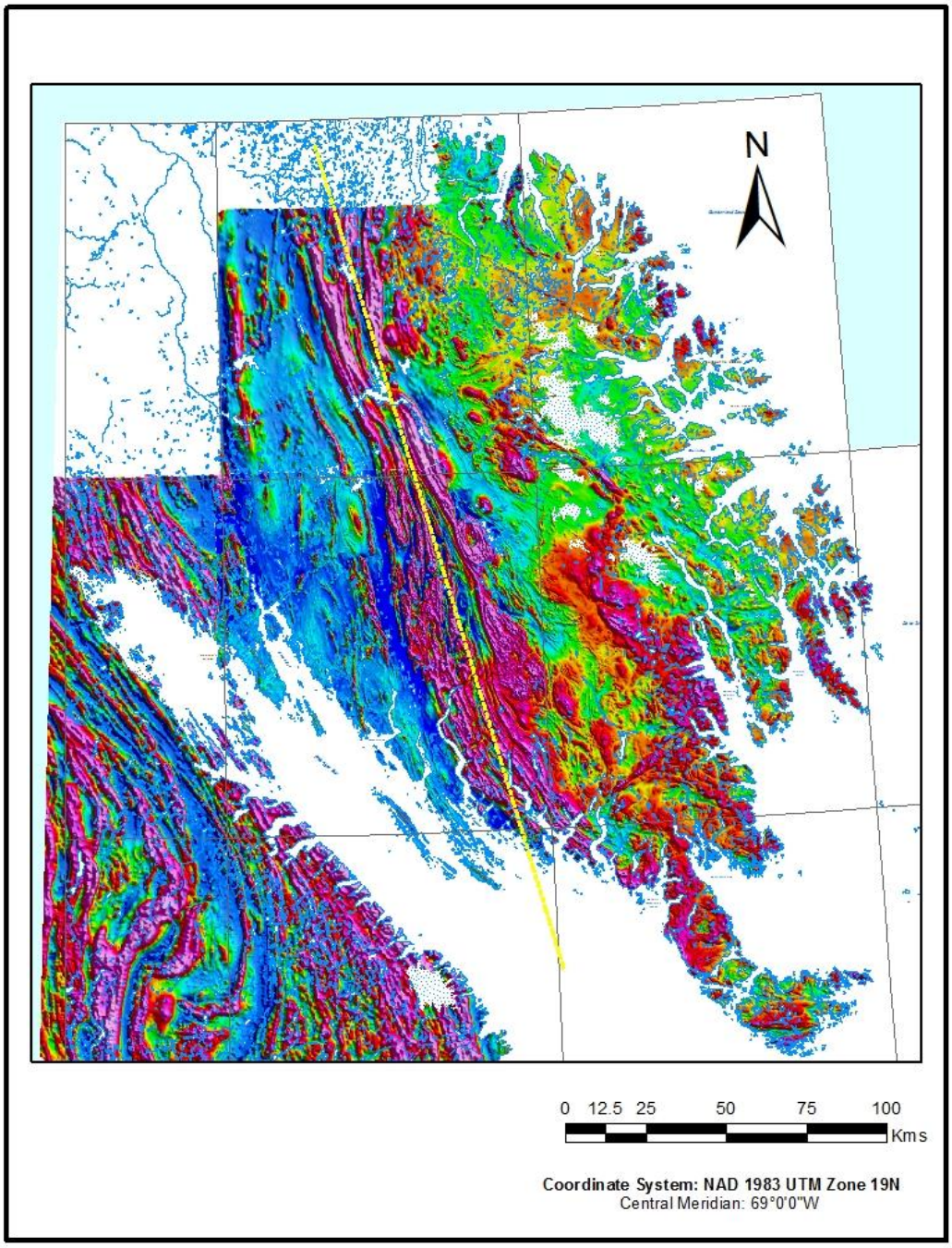

Figure 1.5 – Aeromagnetic map of Hall Peninsula Baffin Island, Nunavut modified from Dumont and Dostaker (2010). Yellow dashed line indicates approximate divide between western and east-central lithological regions of Hall Peninsula.

1.3.2 Overview of lithological units

The western region comprises metasedimentary rocks including pelites and psammites (Figure 1.6a) with lesser quartzite and marble/calc-silicate rocks (Figure 1.7a). The metasedimentary rocks are cut by a large volume 1892 ± 7 Ma (Rayner, 2014 a and b) orthopyroxene-bearing diorite-granodiorite-monzogranite suite (Figure 1.7c and 1.7d). The east-central region is dominated by complex Archean, crystalline gneissic rocks of predominantly biotite-tonalite composition (Figure 1.7e), dated at 2841 ± 3 Ma (Rayner, 2014a and b) with numerous other crystalline phases including monzogranite, syenogranite, granodiorite, trondjemite, gabbro, pyroxenite, amphibolite and a 2701 ± 2 Ma (Rayner, 2014a and b) rapakivi-granite (Figure 1.7f). The crystalline, gneissic basement rocks in the east-central region are overlain by metasedimentary rock packages comprising some combination of the following: quartzite, psammite, pelite, calc-silicate ± intrusive mafic and/or ultramafic sills and dykes (Figure 1.7g and 1.7h) and younger 1873 ± 6 (Rayner, 2014a and b) monzogranite intrusions. Figure 1.7 shows the location of the station where corresponding photographs from Figure 1.6 were taken.

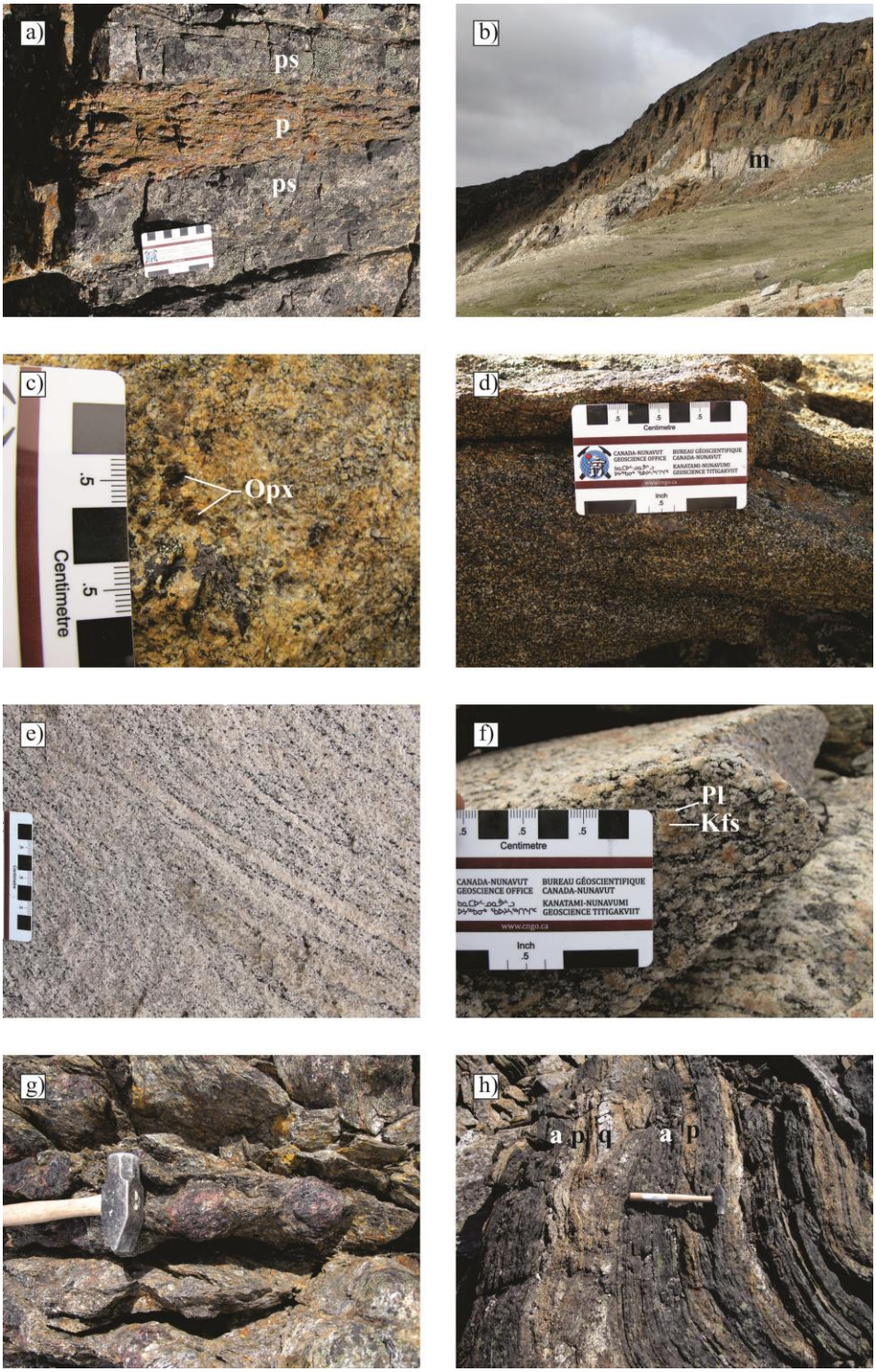

Figure 1.6 – a) Interbedded pelite (p) and psammite (ps). b) White marble (m) interbedded with other metasedimentary rocks. Marble thickness is approximately 2.5 metres at label. c) Orthopyroxene (Opx)-bearing monzogranite. d) Orthopyroxene-bearing diorite. e) Biotite-rich tonalite gneiss. f) Rapikivi granite: Kfs – K-feldspar, Pl – plagioclase. g) Pelitic rocks with decimetre-scale garnet porphyroblasts. Hammer head is 12 cm. h) Metasedimentary rocks intruded by amphibolite sills: a – amphibolite, p – pelite, q – quartzite. Hammer length is 40 cm.

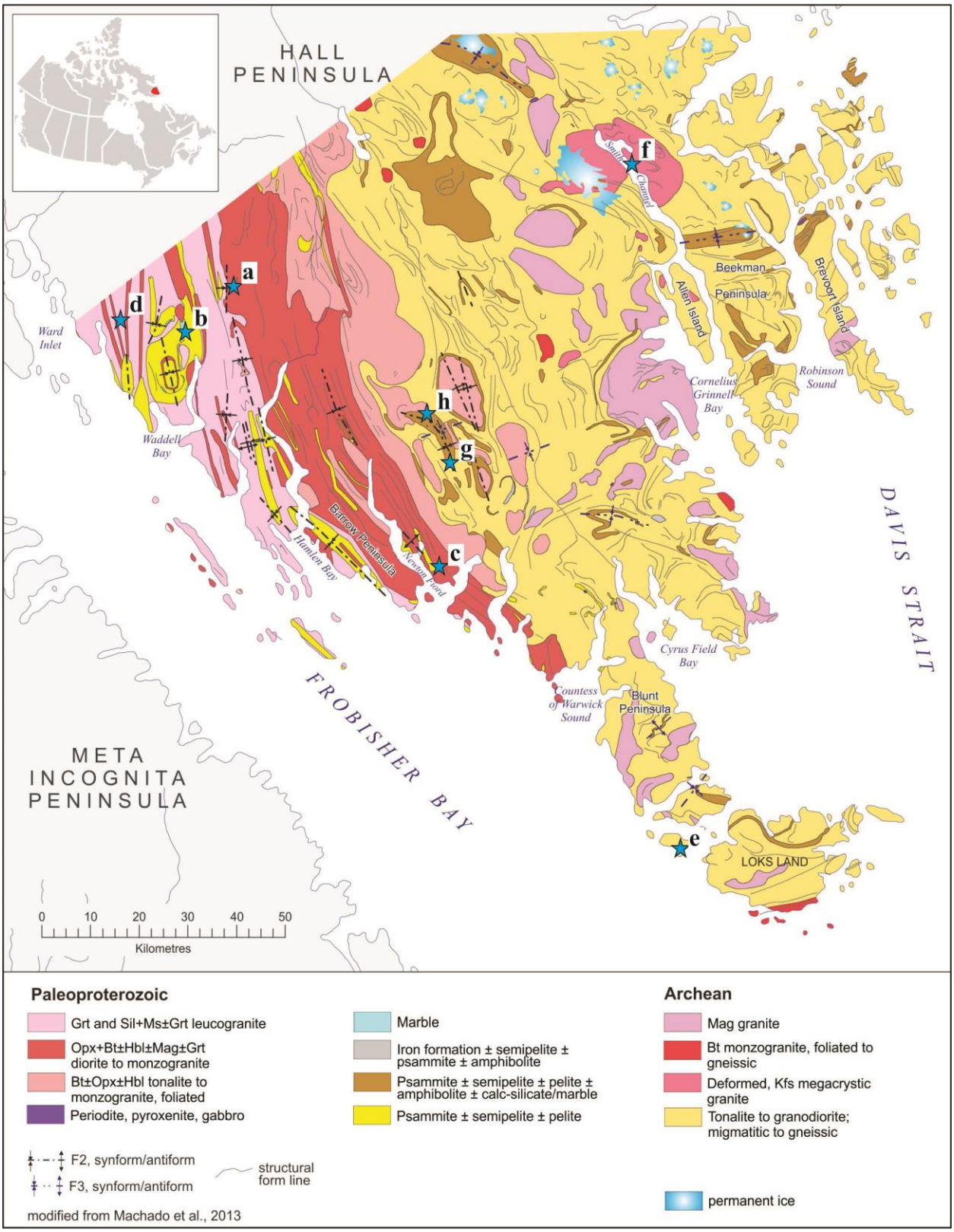

Figure 1.7 – Geology of southern Hall Peninsula, Baffin Island Nunavut. Modified from Machado, Bilodeau and St-Onge (2013). Blue stars indicate the location of rock unit photographs from Figure 1.6.

1.3.3 Structural observations and metamorphic overview

Following regional-scale and focused mapping conducted during the 2012 and 2013 field seasons, three dominant Paleoproterozoic deformation events were recognized. The initial deformation event (D1) resulted from east-west shortening. This event created isoclinal folds of bedding (F1) (Figure 1.8a) and the development of the dominant regional foliation (S1) (Figure 1.8b) which is axial planar to F1. D1 was overprinted by further east-west shortening (D2) that resulted in thick-skinned thrusts (T2) observed in rocks in the northeastern part of the Hall Peninsula west of Ptarmigan Fiord (Figure 1.8c) (Skipton and St-Onge, 2014). D1 and D2 are interpreted to be a part of the same event, with D1 occurring pre-to syn-thermal peak and D2 occurring post-thermal peak. During D1 and D2, metasedimentary rocks in the east-central region of Hall Peninsula were thrust over and tectonically imbricated within the Archean, crystalline orthogneiss basement. Later, the region was subjected to north-south shortening which resulted in south-vergent thick-skinned folding of previous fabrics (F3) and the development of an axial-planar crenulation cleavage (S3).

Broadly speaking, the metamorphic grade on the Hall Peninsula increases from lower amphibolite facies in the east, as suggested by garnet – biotite – K-feldspar ± sillimanite mineral assemblages in pelites (Figure 1.8g) with sillimanite becoming ubiquitous moving westward, to granulite facies in the west, evidenced by orthopyroxene-bearing granite, grano-diorite and diorite (Figure 1.8c and 1.8d) rocks and granitic melt pods/sweats (Figure 1.8d). Figures 1.9a and 1.9b show the location where corresponding photographs from Figure 1.8 were taken.

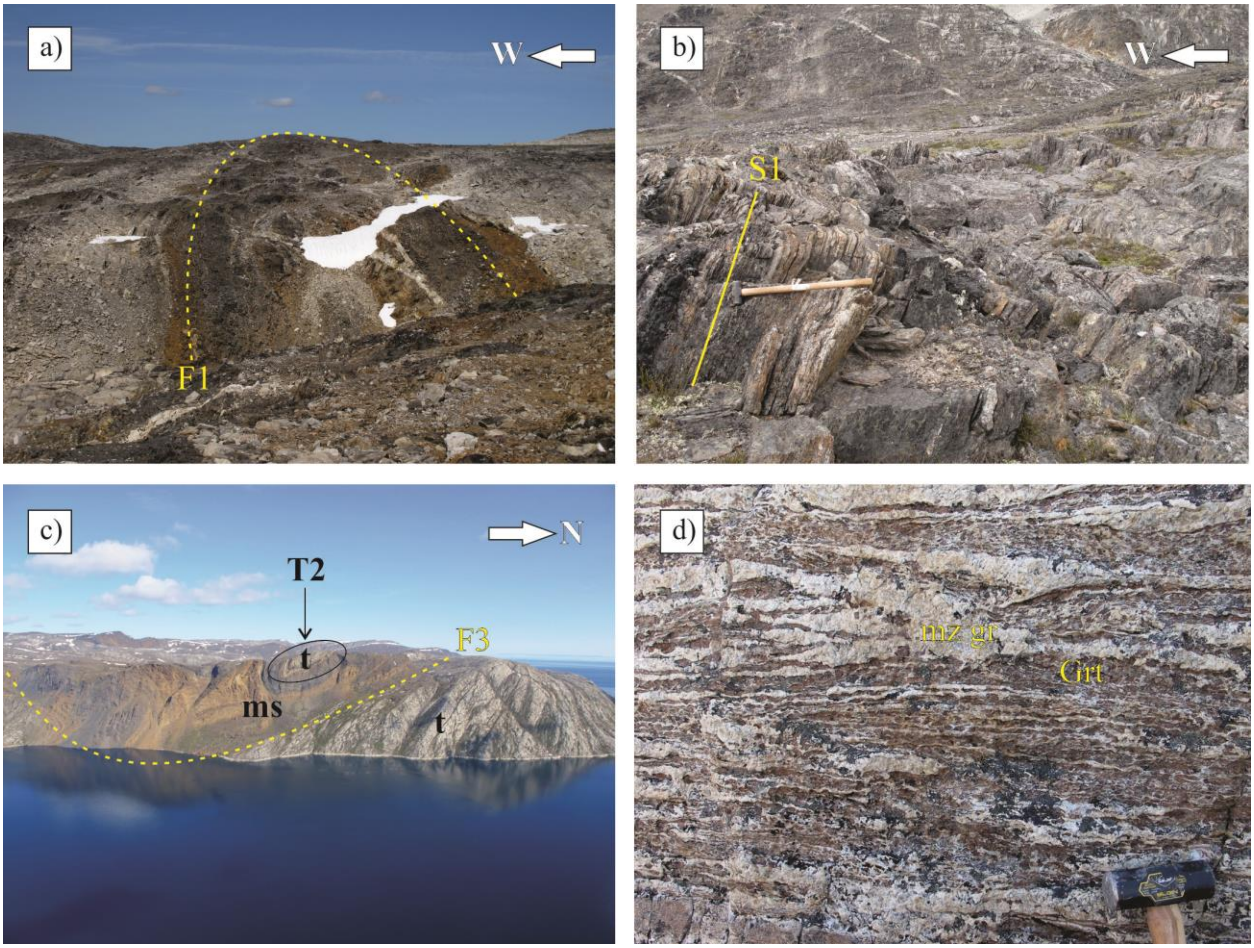

Figure 1.8 – a) Outcrop scale F1 fold. b) Steeply dipping S1 fabric. c) T2 thrust of Archean tonalite orthogneiss (t) onto Paleoproterozoic metasediments (ms) folded by F3 fold. d) Granulite grade metasediments with garnet restite (Grt) and monzogranite melt pods (mz gr). Hammer head is 15 cm.

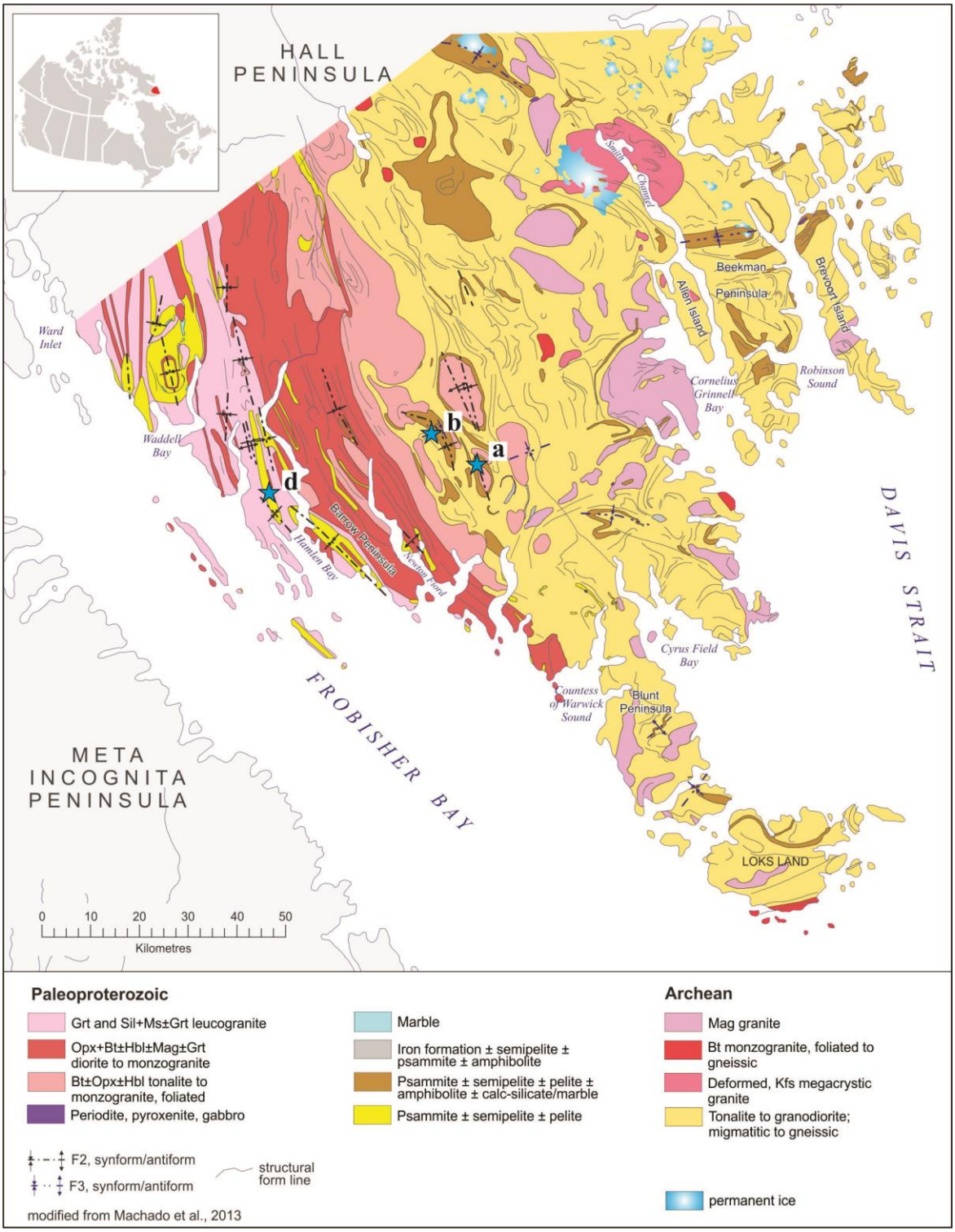

Figure 1.9a – Geology of southern Hall Peninsula, Baffin Island Nunavut. Modified from Machado, Bilodeau and St-Onge (2013). Blue stars indicate the location of rock unit photographs a, b and d from Figure 1.8.

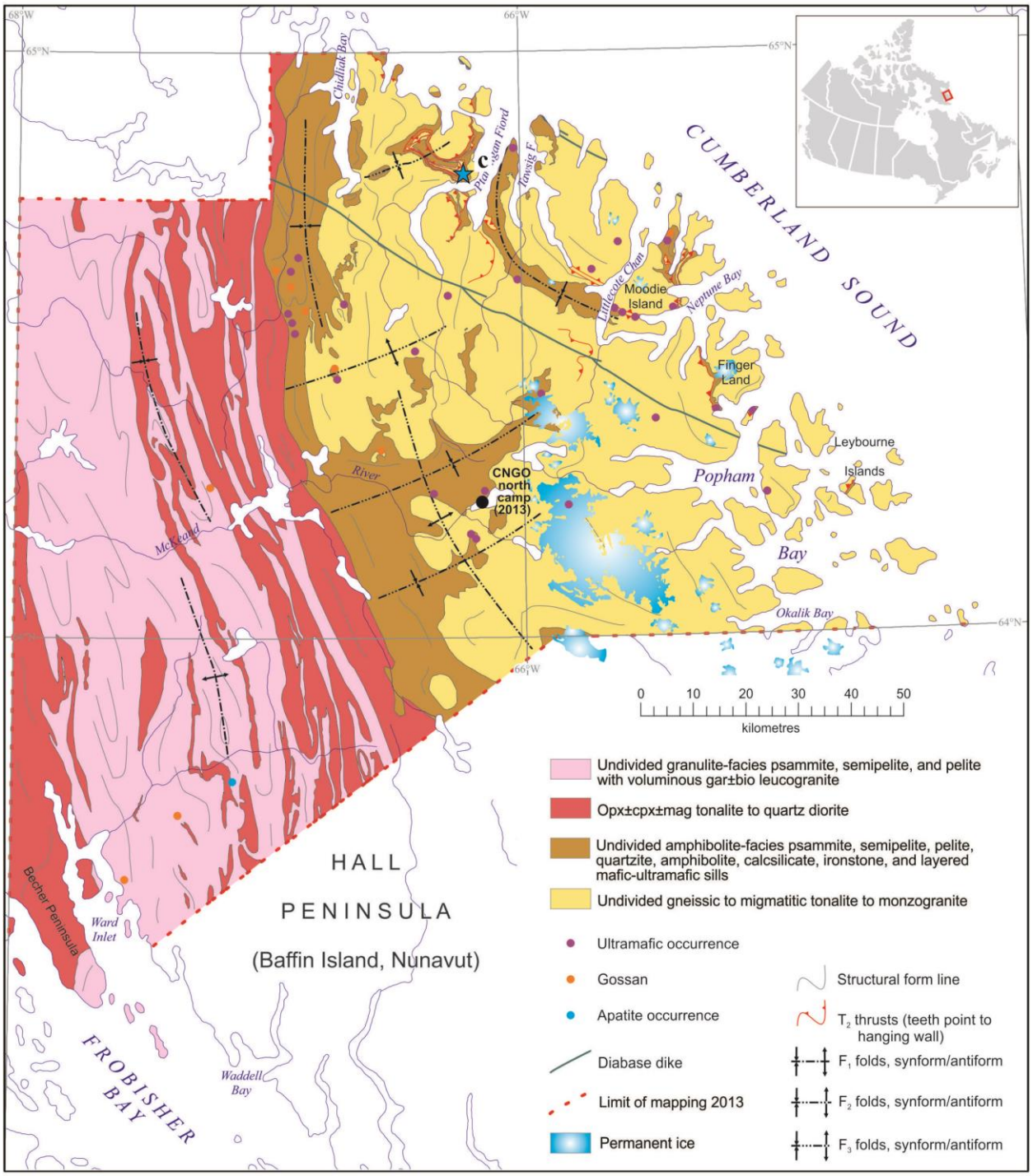

Figure 1.9b – Geology of northern Hall Peninsula, Baffin Island Nunavut. Modified from Steenkamp and St-Onge (2014). Blue stars indicate the location of rock unit photograph c from Figure 1.8.

1.3.4 Project overview

This aims of this thesis are twofold and in order to address both aims, this thesis will be split into two distinct, yet complimentary parts. First, a study the deformational, metamorphic and geochronological history of an important area in the southern Hall Peninsula will be conducted; and second, the characterization of the geochemistry and petrogenesis of the mafic and ultramafic rocks on the Hall Peninsula, Baffin Island, Nunavut will be carried out. This new information will then be compared with adjacent regions in order to suggest potential correlations between previously identified rock units, known cratons and crustal structures.

This topic was chosen because at the onset of the HPIGP, the geological history of the Hall Peninsula was poorly understood and no geochemical studies of mafic/ultramafic rocks had been conducted. In the summer of 2012, the HPIGP team completed the first of two mapping field seasons (2012 – southern Hall Peninsula (Figure 1.2a), 2013 – northern Hall Peninsula (Figure 1.2b), during the course of which, the understanding of the deformational and metamorphic history of the Hall Peninsula was improved through field observations. In addition, numerous exposures of mafic and ultramafic rocks were discovered. However, these occurrences represent very little of the total exposed outcrops and as such are not represented as a unique map unit on the Hall Peninsula regional geological map (Figure 1.2a and b). The vast majority of sizable mafic-rock-occurrences are found intercalated with metasedimentary rocks in the east-central region of the Hall Peninsula (Figure 1.2a and b). These two revelations – improved geologic understanding and knowledge of mafic/ultramafic rock distribution – informed the selection of a map area where the field relationships, deformation and metamorphism and geochronology were studied in order to improve the understanding of the geological context of the Hall Peninsula satisfying the first goal of this thesis. In addition, this

area records rock units and relationships which are representative of the metasedimentary packages into which the majority of mafic rocks are emplaced. This allows for the second part of this thesis, a geochemical study to characterize the mafic and ultramafic rocks throughout the whole of the Hall Peninsula to be conducted with the broader geological context in mind.

CHAPTER 2

QUAQQANITTUAQ AREA MAPPING PROJECT

2.1 Introduction

Using field observations from regional mapping during the 2012 field season, an area was selected in order to quantitatively study the deformation, metamorphism and geochronology of the central region of the Hall Peninsula, Baffin Island Nunavut. The area chosen is known as the Qaqqanittuaq area (QA) and is named in accordance with a traditional Inuit place name. The QA location (Figure 2.1) was chosen because of its proximity to the CNGO 2012 south camp (Figure 2.2); and because it has excellent exposure and it contains rock units and relationships that are representative of the supracrustal-mafic rock packages of the east-central region of Hall Peninsula.

Mafic/ultramafic-rock-occurrences on the Hall Peninsula are restricted in both volume and geographic distribution, occurring primarily intercalated within metasedimentary rocks in the east-central region. In addition to aiding in the understanding of the deformation, metamorphism and geochronology of the central region of the Hall Peninsula, studying the QA allows the geological relationships found therein to be extrapolated to other metasedimentary-mafic-rock-occurrences which allows for a better description of the geologic context into which the majority of mafic and ultramafic rocks were emplaced (Chapter 3).

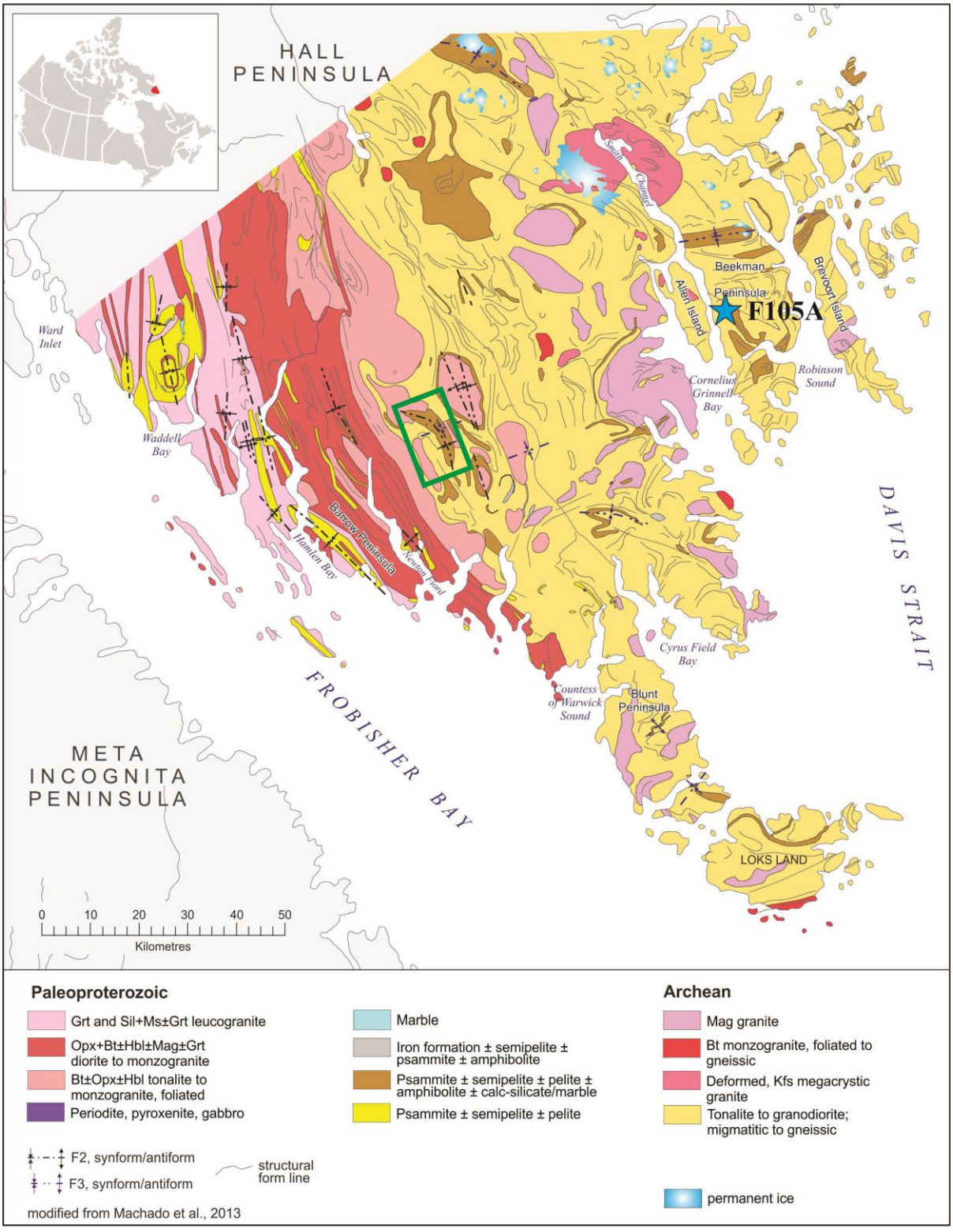

Figure 2.1 – Geology of southern Hall Peninsula, Baffin Island. Modified from Machado et al., (2013). Green box outlines the Qaqqanituaq area. Blue star indicates location of a 2841 ± 3 Ma (Rayner, 2014) tonalite sample correlated with QA structural basement.

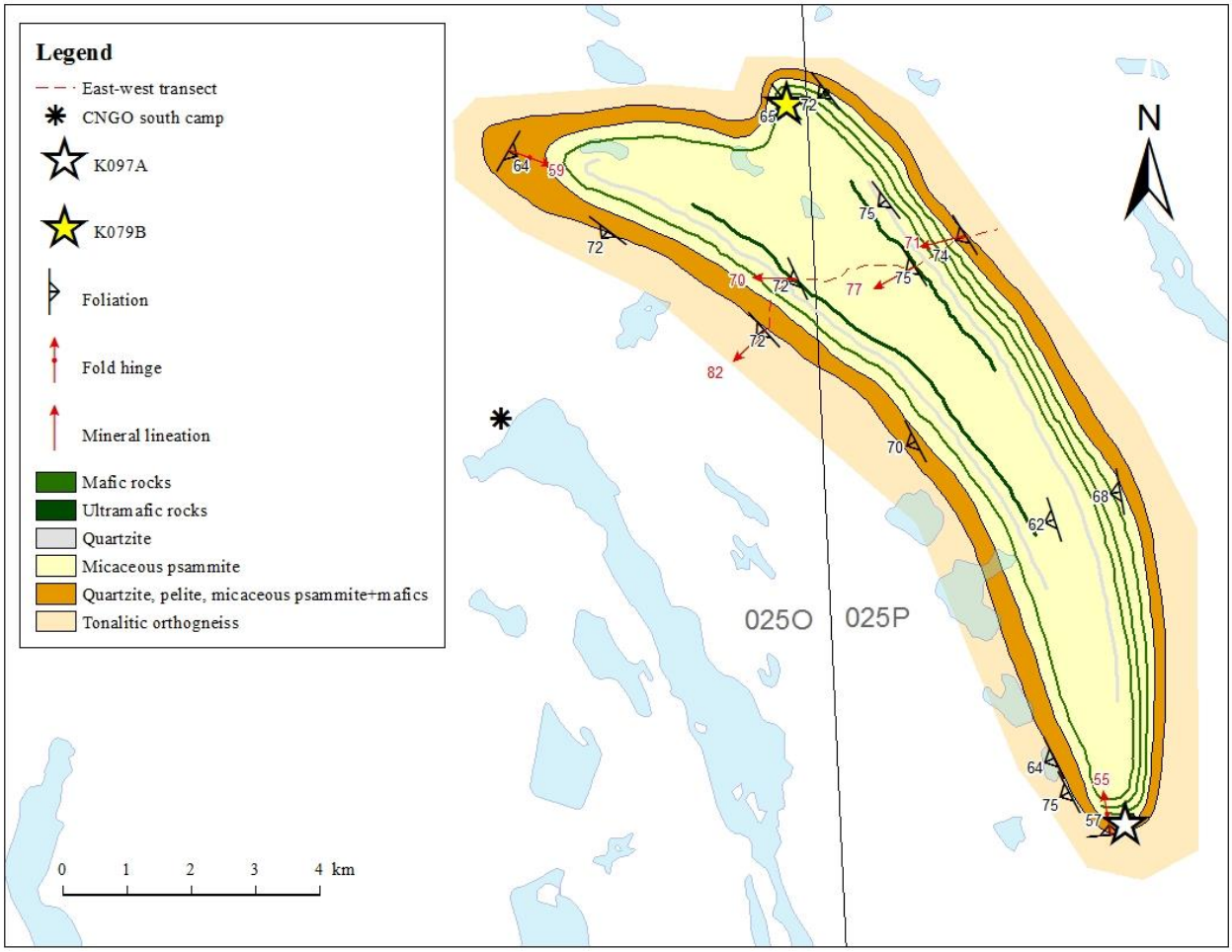

Figure 2.2 – Geology of Qaqqanituaq area.

Detailed mapping of the QA was completed by combining focused mapping in key areas, helicopter-assisted reconnaissance and a detailed east-west transect across the entire width of the central QA (Figure 2.2). Locations and measurements in the field were recorded on an HP iPAQ 210 device running GPS integrated GIS software.

In general, the QA forms a doubly-plunging, synformal structural basin approximately 15 km long by 3.5 km wide, that trends in a southeast-northwest direction (Figure 2.2). Field relationships described herein indicate that an Archean tonalite orthogneiss complex forms the

structural and possibly stratigraphic crystalline basement to a supracrustal sequence comprising siliciclastic strata interbedded with a series of mafic and ultramafic rocks and younger cross-cutting monzogranite dykes. Mineral assemblages indicate that rocks in the QA were subjected to upper-amphibolite-facies metamorphic conditions. In addition, there is evidence that the area was subjected to at least two distinct deformational events. Lithotectonic units will be discussed from oldest to youngest based on field relationships and the assumption that all supracrustal rocks are broadly contemporaneous.

2.2 Lithotectonic Units

2.2.1 Tonalite orthogneiss complex

The tonalite orthogneiss complex forms the structural base of the QA (Figure 2.2**).** The contact between the tonalite orthogneiss and the overlying metasediments is readily observable from the air (Figure 2.3a). The tonalite orthogneiss is composed predominantly of biotite tonalite (70%) Figure 2.3a, c, and d) and younger, cross-cutting white-weathering monzogranite (20%), and pink syenogranite (10%) (Figure 2.3b). Both the monzogranite and the syenogranite occur as thin sheets and stringers that are typically centimetres to decimetres in thickness (Figure 2.3b). However, metre-scale monzogranite intrusions have been observed. Amphibolite and pyroxenite enclaves, which are typically lenticular and range in scale from several centimetres to more than 10 m, are observed throughout the tonalite gneiss complex. The enclaves are interpreted to be deformed mafic inclusions and/or deformed, boudinaged, pre-metamorphic mafic dikes. Two generations of pegmatite dikes intrude the tonalite gneiss complex. The first is of syenogranite composition and is overprinted by the regional fabric. This type of dike is thought to represent a pegmatitic phase of the syenogranite intrusions pervasive throughout the tonalite gneiss complex.

The other pegmatite is broadly granitic in composition and cross-cuts all fabrics. While numerous other crystalline phases, including granodiorite, trondjemite, gabbro and a rapakivi-granite (Figure 1.6f) that has been dated at 2701 ± 2 Ma (Rayner, 2014a and b), occur within the tonalite orthogneiss complex in the southern Hall Peninsula, none of these rocks are observed in the QA map area. No tonalitic sample from the QA was dated, but the QA basement is correlated with a 2841 ± 3 Ma (Rayner, 2014) tonalite (sample F105A) from Beekman Peninsula (Figure 2.1)

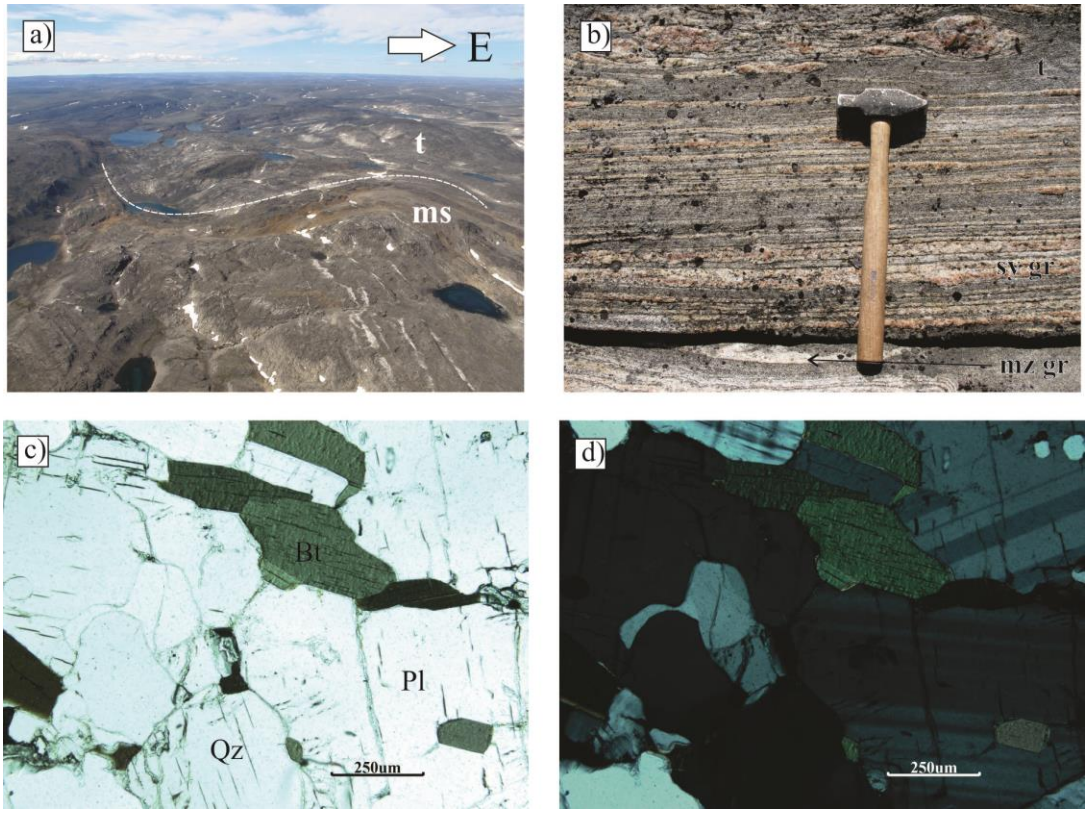

Figure 2.3 – Images of tonalite gneiss complex. a) Air photograph of parasitic fold at north end of QA (Figure 2.2) showing contact between tonalite orthogneiss (t) and metasediments (ms). b) Outcrop photograph: mz gr – monzogranite, sy gr – syenogranite, t – tonalite. Hammer length is 40 cm.c) Plane polarized light thin section image: Bt – biotite, Pl – plagioclase, Qz – quartz. d) Cross-polarized light image of a). See Figure 2.10 for outcrop photo location.

2.2.2 Micaceous psammite

Micaceous psammite comprises the bulk of the supracrustal rocks within the QA structural basin (Figure 2.2). The majority of the micaceous psammite is composed of quartzofeldspathic detritus (Figure 2.4a). However, in some areas throughout the unit there is a noticeable pelitic component which results in a quartz – plagioclase – biotite ± sillimanite ± garnet metamorphic mineral assemblage. Sillimanite occurs primarily as faserkiesel aggregates (Figure 2.4b) as well as fibrolite (Figure 2.4c and d). Garnet porphyroblasts are commonly rimmed by plagioclase (Figure 2.4e). This texture indicates that the grossular component of garnet has reacted to form plagioclase during decompression (Barker, 1990). The faserkiesel are strongly lineated in fold hinges (Figure 2.4f), while fibrolite and biotite are aligned defining the dominant regional, S1 fabric (Figure 2.3a and b).

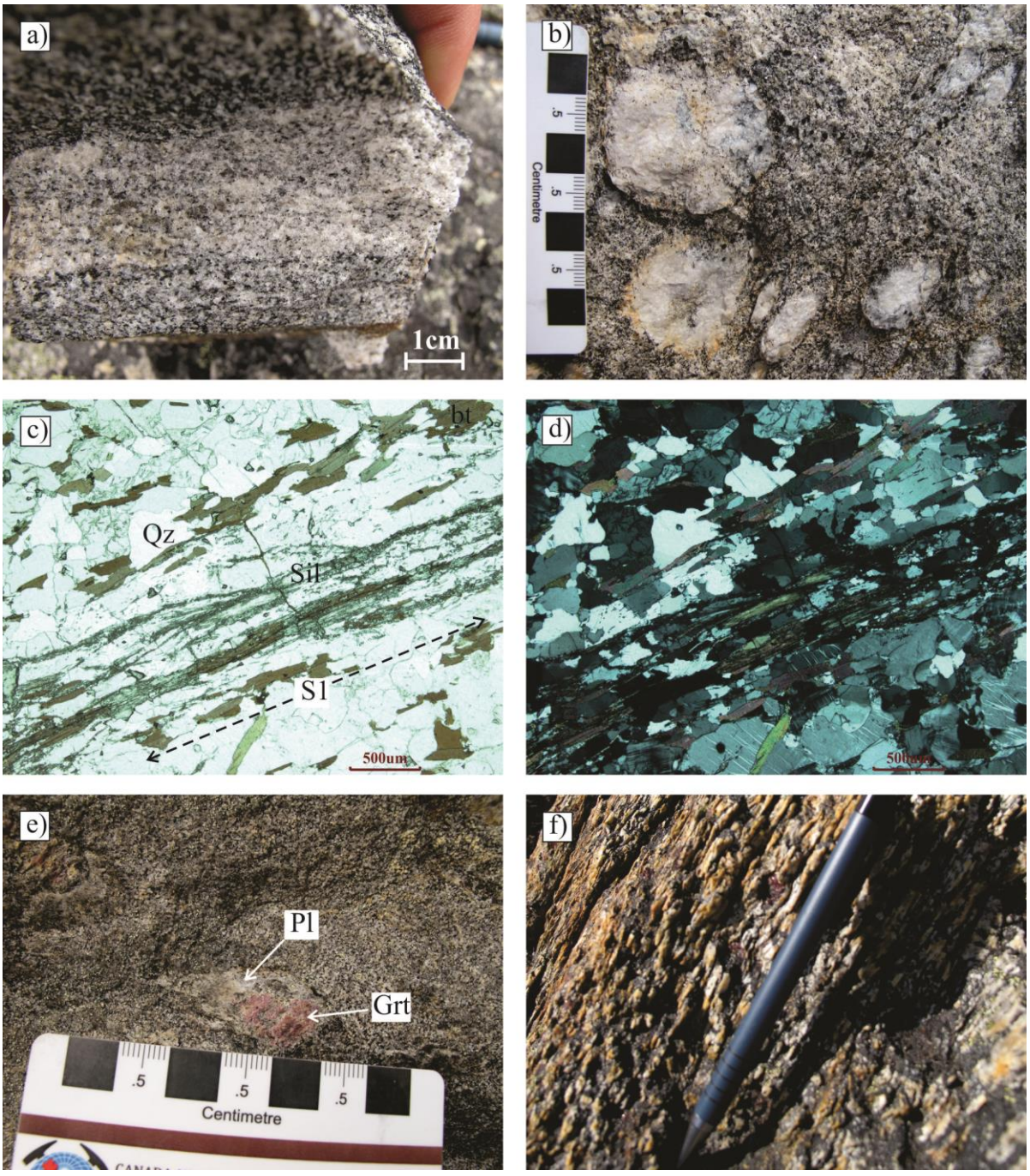

Figure 2.4 – Images of micaceous psammite. a) Hand sample comprising quartz, feldspar and biotite. b) Faserkiesel aggregates in outcrop c) Plane polarized light thin section image: Bt – biotite, Qz – quartz, Sil – sillimanite in fibrolite form, S1 – dominant regional fabric expressed in thin section. d) cross-polarized light thin section image of c). e) garnet porphyroblast (Grt) with plagioclase decompression corona (Pl). f) strongly lineated faserkiesel in fold hinge. Pen is 15 cm long. See Figure 2.10 for outcrop photo locations.

2.2.3 Quartzite

Fine- to medium-grained quartzite (Figure 2.5a) occurs as discrete, thin (<1m) laterally continuous layers. Quartzite occurs at or just above the contact between the tonalite gneiss complex and the supracrustal rocks at all observed localities. Quartzite also occurs in a distinct 1 – 2 m thick, boudinaged layer (Figure 2.5b) within the micaceous psammite that is traceable along strike. While dominated by quartz (>95%), the QA quartzites also contain both plagioclase and alkali-feldspar (2-4% combined) as well as trace amounts of garnet, graphite, apatite, zircon and biotite (Figure 2.5c).

The QA quartzite has undergone grain boundary migration recrystallization resulting in lobate, interfingering grain sutures (Figure 2.5d) consistent with observations made by Stipp et al. (2002). Locally, grains are observed both overgrowing and pinned by secondary mineral phases (Figure 2.5d). Grain size dimensions reach up to 4 millimeters (Figure 2.5c and d) with crystal growth interpreted to have occurred during peak thermal conditions. As such, intracrystalline deformation features such as undulose extinction (Figure 2.5d) and deformation lamellae (Figure 2.5d) are attributed to post-thermal-peak deformation.

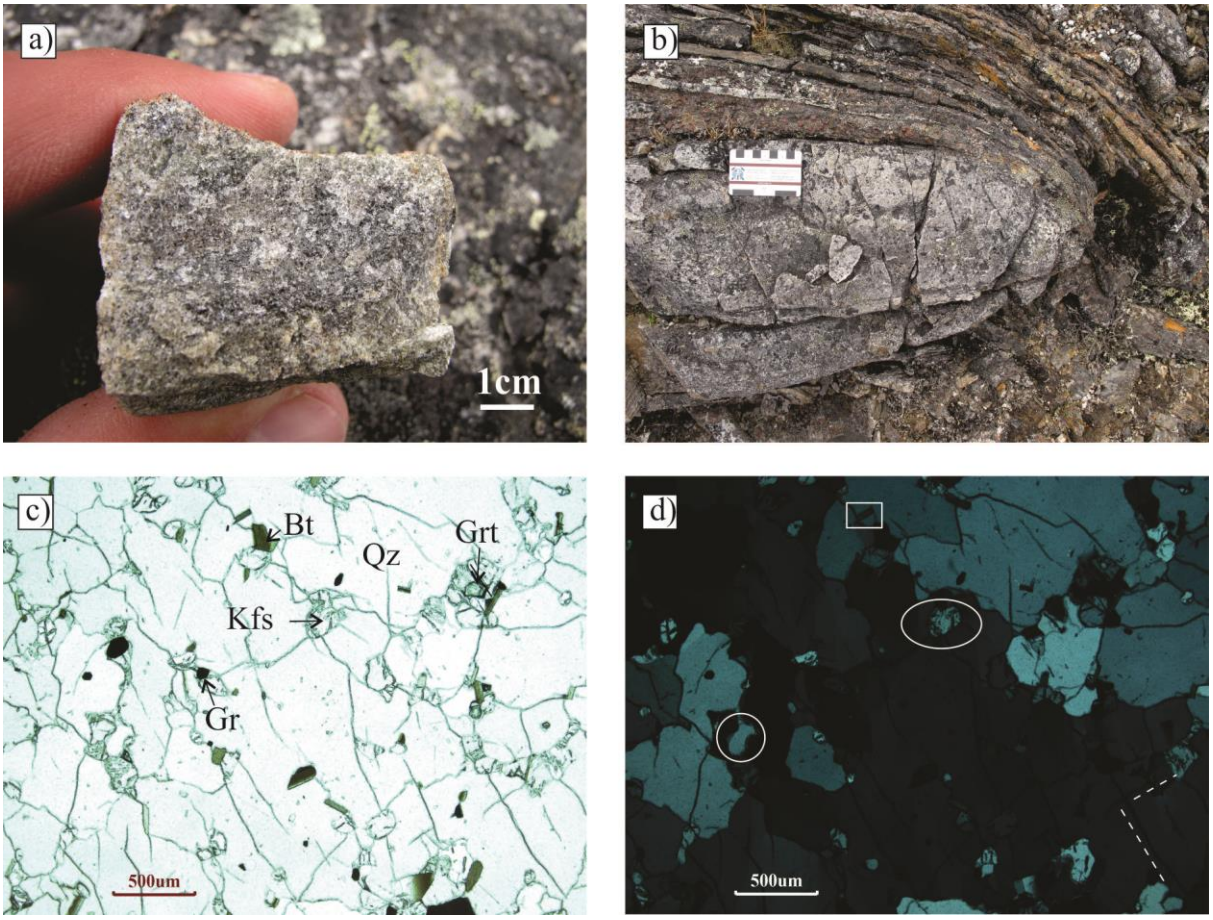

Figure 2.5 – Images of quartzite. a) Fresh surface of fine to medium grained quartzite hand sample. b) Outcrop photograph of boudinaged quartzite c) Plane polarized light thin section image: Bt – biotite, Grt – garnet, Gr – graphite, Kfs – K-feldspar, Qz – quartz. d) Cross-polarized light image of b), note visible undulose extinction in many grains and the ~4mm grain in the centre of the image. White circle surrounds a lobate, interfingering grain suture; white box indicates where quartz is overgrowing biotite; white ellipse indicates where quartz growth is pinned by K-feldspar; dashed lines indicate orientation of dominant deformation lamellae. See Figure 2.10 for outcrop photo location.

2.2.4 Pelite

Pelite is found throughout the supracrustal package and ranges from centimetre-scale layers within the micaceous psammite to discrete intervals up to 2 m thick. The dominant regional (S1) fabric is nearly always observed in pelites and is defined by the preferred orientation and elongation of biotite and sillimanite (Figure 2.6a). Near fold hinges, garnet porphyroblasts greater than 10cm in length are observed (Figure 2.6b). Mineralogically, the

pelite contains biotite – plagioclase – quartz ± garnet ± sillimanite ± K-feldspar (Figure 2.6b, c). Minor phases include apatite, ilmenite and zircon.

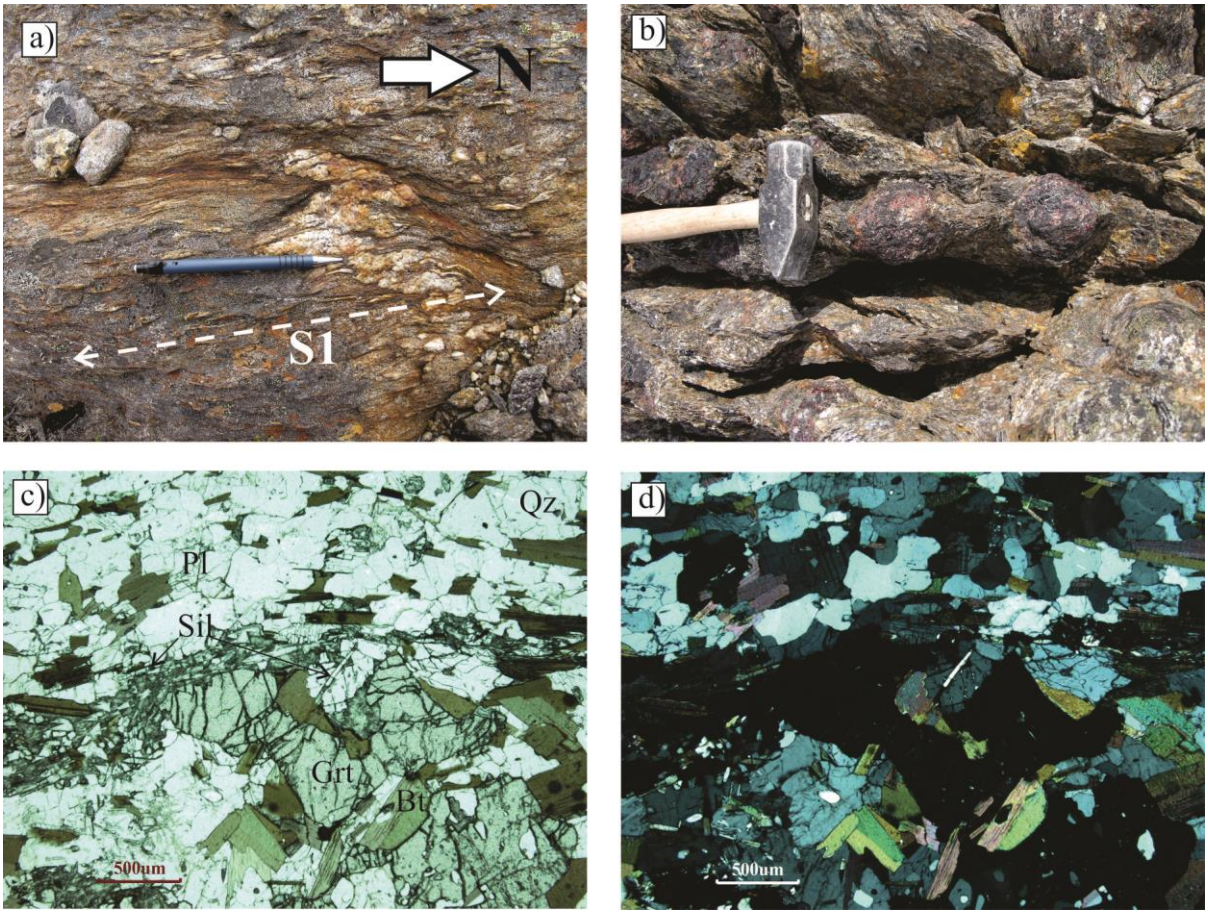

Figure 2.6 – Images of pelite. a) Outcrop photo of pelite displaying S1 fabric. Arrow points north. Pen is 15 cm long. b) Outcrop photograph of pelite with dm-scale garnet porphyroblasts. Hammer head is 12 cm. c) Plane polarized light thin section image: bt – biotite, grt – garnet, plag – plagioclase, qtz – quartz, sil – sillimanite. d) Cross-polarized light image of c). See Figure 2.10 for outcrop photo location.

2.2.5 Mafic and ultramafic rocks

Mafic rocks of the QA range from thin (<2 m), continuous and discontinuous amphibolite layers within the siliciclastic supracrustal rocks to thick (>5 m), discrete, laterally continuous amphibolite units and nearly are found within 500 m of the underlying contact with the tonalite gneiss complex (Figure 2.2). Mafic rocks are commonly emplaced between discrete sedimentary

units which may indicate they were intruded between rheologically contrasting units. Alternatively, interbedding between discrete metasedimentary units may suggest mafic layers represent distinct pulses of volcanism. Primary features which would allow the true nature (intrusive/extrusive) of the mafic rocks to be determined with certainty, such as pillows, vesicles or distinct cross-cutting relationships, have been erased by subsequent deformation and metamorphism. On the west limb of the QA adjacent to the contact with the tonalite gneiss complex, mafic rocks occur as thin, discontinuous, highly deformed layers (Figure 2.7a). Higher in the supracrustal package, on the west limb, there is a thicker (3 – 5 m), discrete mafic layer within the supracrustal rocks. On the east limb of the QA, mafic rocks occur as three thick (3 – 5 m), laterally continuous layers, and as minor, thin (<1 m) discontinuous layers near the contact with the tonalite gneiss complex. Hornblende – plagioclase ± biotite ± garnet is the dominant mineral assemblage in the mafic rocks. Mafic rocks are described in more detail in chapter 3.

Ultramafic rocks occur primarily within a distinct, layered, boudinaged unit traceable along strike (Figure 2.2). Isolated ultramafic pods also occur near the contact with the tonalite gneiss complex; one such pod is thoroughly recrystallized and contains abundant actinolite, talc and clinopyroxene (Figure 2.7b).

Figure 2.7 –a) Mafic sills emplaced between metasedimentary rocks. Hammer handle is 30 cm. b) Ultramafic pod which has been altered to actinolite, clinopyroxene and talc. See Figure 2.10 for outcrop photo locations.

2.2.6 Monzogranite dykes

Dikes and sills, up to 2 m thick, of white-weathering, medium-grained monzogranite are found throughout the supracrustal sequence but occur primarily in contact with mafic rocks. The monzogranite intrusions are predominantly emplaced between mafic rocks and a supracrustal unit. The position of intrusion is likely controlled by the rheological contrast between the mafic and the supracrustal rocks. Monzogranite dykes are observed cross-cutting individual metasedimentary units as well as the mafic rocks (Figure 2.8a and b), but are themselves deformed by and the dominant regional fabric (S1). Monzogranite intrusions make up less than 1% of the total rock volume in the QA, therefore individual intrusions are too small to be shown on the map (Figure 2.2). Minor phases include biotite, garnet and sillimanite (Figures 2.8b and c). The presence of these aluminum-rich minor phases indicates that the monzogranite sills and dykes are peraluminous.

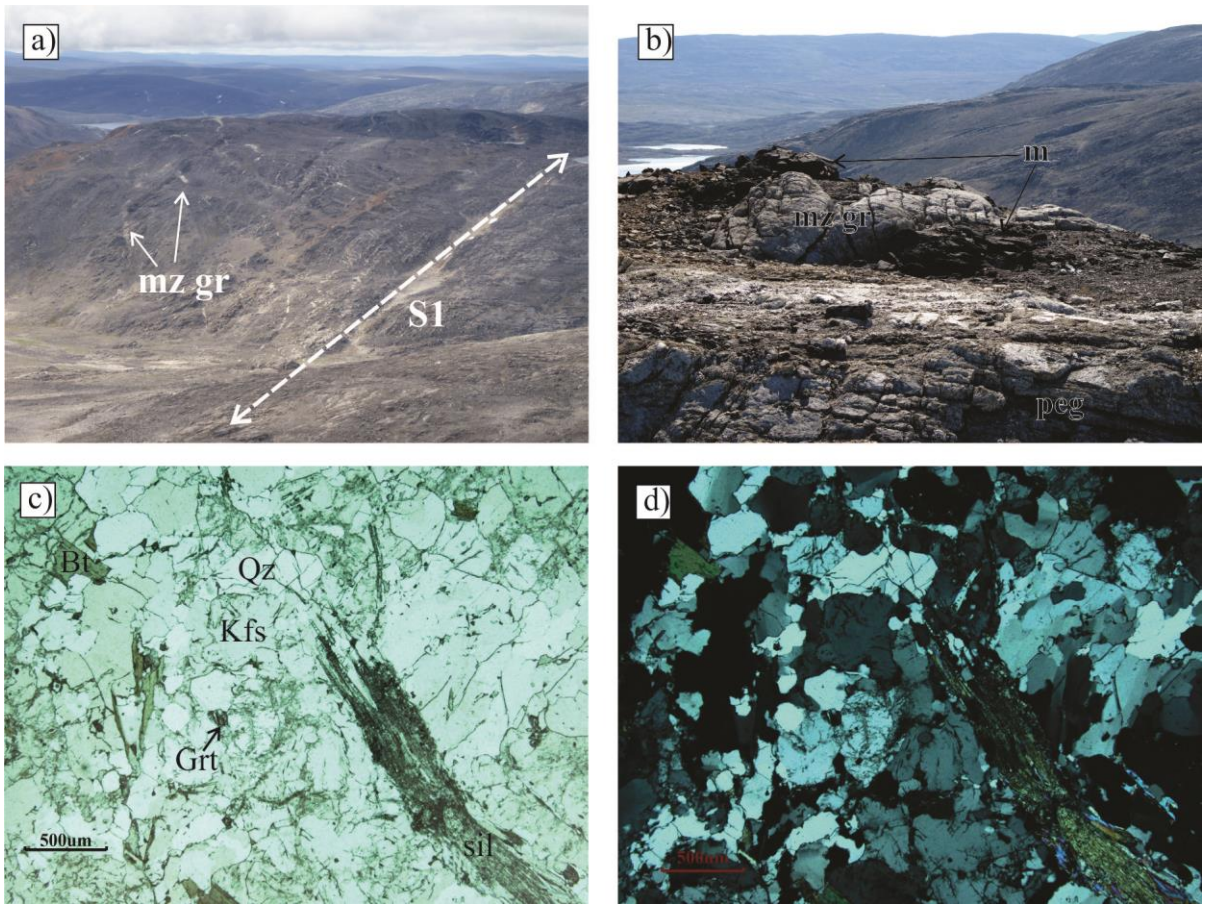

Figure 2.8 – Images monzogranite dykes. a) Air photograph of monzogranite dykes (mz gr) cross-cutting S1. b) Outcrop image of monzogranite dyke (mz gr) cross-cutting a mafic unit (m) with a granitic pegmatite (peg) in the foreground. Monzogranite dyke is approximately 1 m wide. c) Plane polarized light thin section image of monzogranite dyke: Bt – biotite, Grt – garnet, Kfs – K-feldspar, Qz – quartz. d) Cross-polarized light image of b).

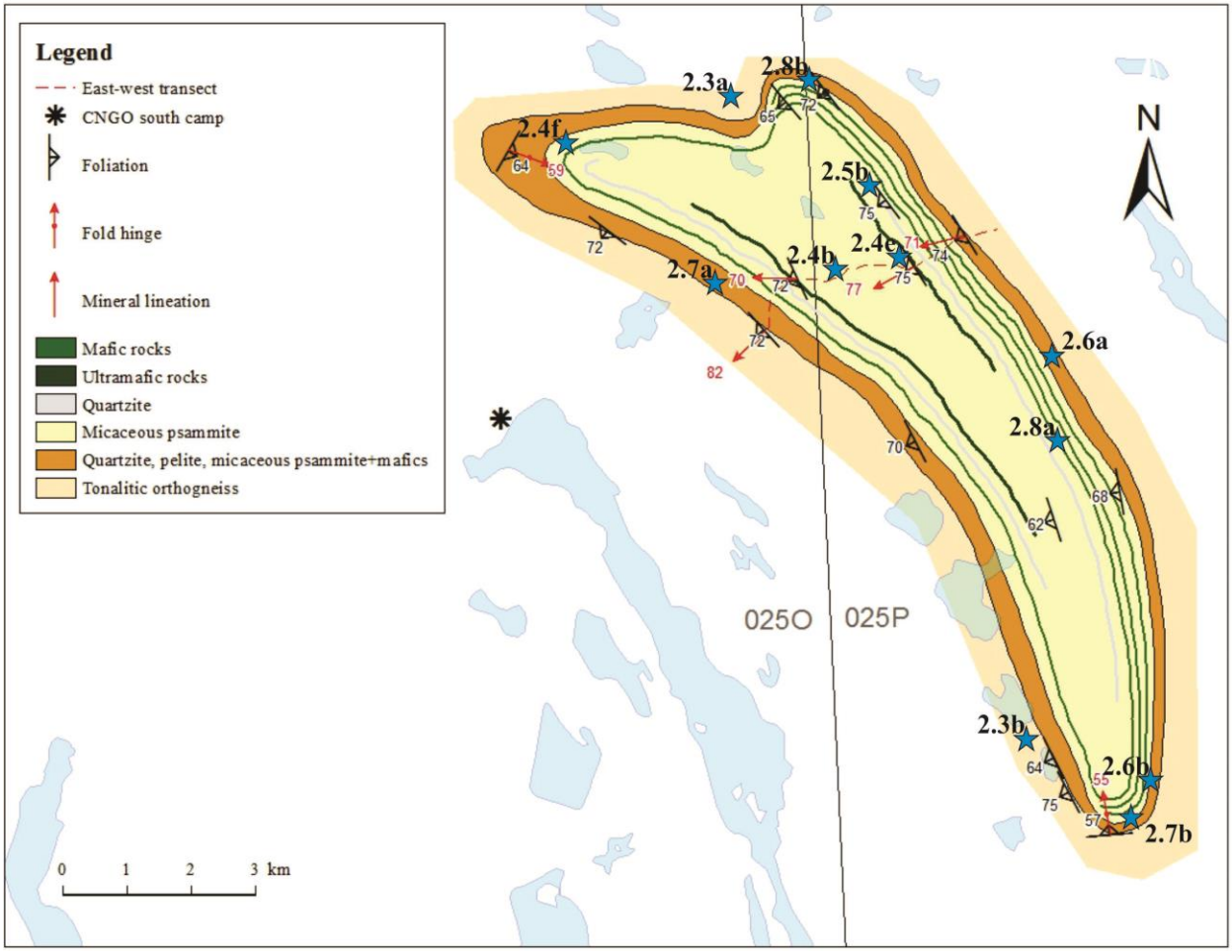

Figure 2.9 – Geology of Qaqqanituaq area. Blue stars show locations of outcrop images from Figures 2.3-2.8.

2.3 Structural observations

The QA is an approximately 50 km^2 northwest-southeast striking, doubly-plunging synformal structural basin (Figure 2.11). There is clear evidence that the area was subjected to at least two distinct deformational events. Nearly all lithological contacts are tectonically transposed into the dominant regional (S1) fabric which resulted from east-west compression during D1. The exception to this is observed in the two fold hinges in the north and the one in the south as well as with some monzogranite dykes which cross-cut the mafic rocks and the interpreted primary bedding in the metasedimentary rocks (S0) at a high angle when they were

originally emplaced and thus were not completely transposed during (D1) deformation. The D1 event also resulted in tight, nearly isoclinal folding (F1) the QA, with all units striking southeast (using right-hand-rule) and steeply dipping (60º-80º) to the west (Figure 2.9 and 2.10). F1 is demonstrated by fold repetition of all major lithological units across the width of the QA (Figure 2.9, 2.10 and 2.11). D2, post-thermal thrusting (Figure 2.12a) – see section 1.3.2 – is not recorded in the QA, but as it is recognized in other parts of the Hall Peninsula, the naming of structural events in the QA takes this event into consideration. The second deformation event recognized in the QA is thus termed D3. D3 is a north-south compression event that resulted in F3 open folding of the QA; this is evident from the reversal in plunge of hinge-parallel lineations from the south to the north (Figure 2.12c), which defines the overall synformal geometry of the basin. D3 also resulted in the development of an S3 crenulation cleavage observed in the parasitic fold limb in the northeast QA (Figure 2.12b).

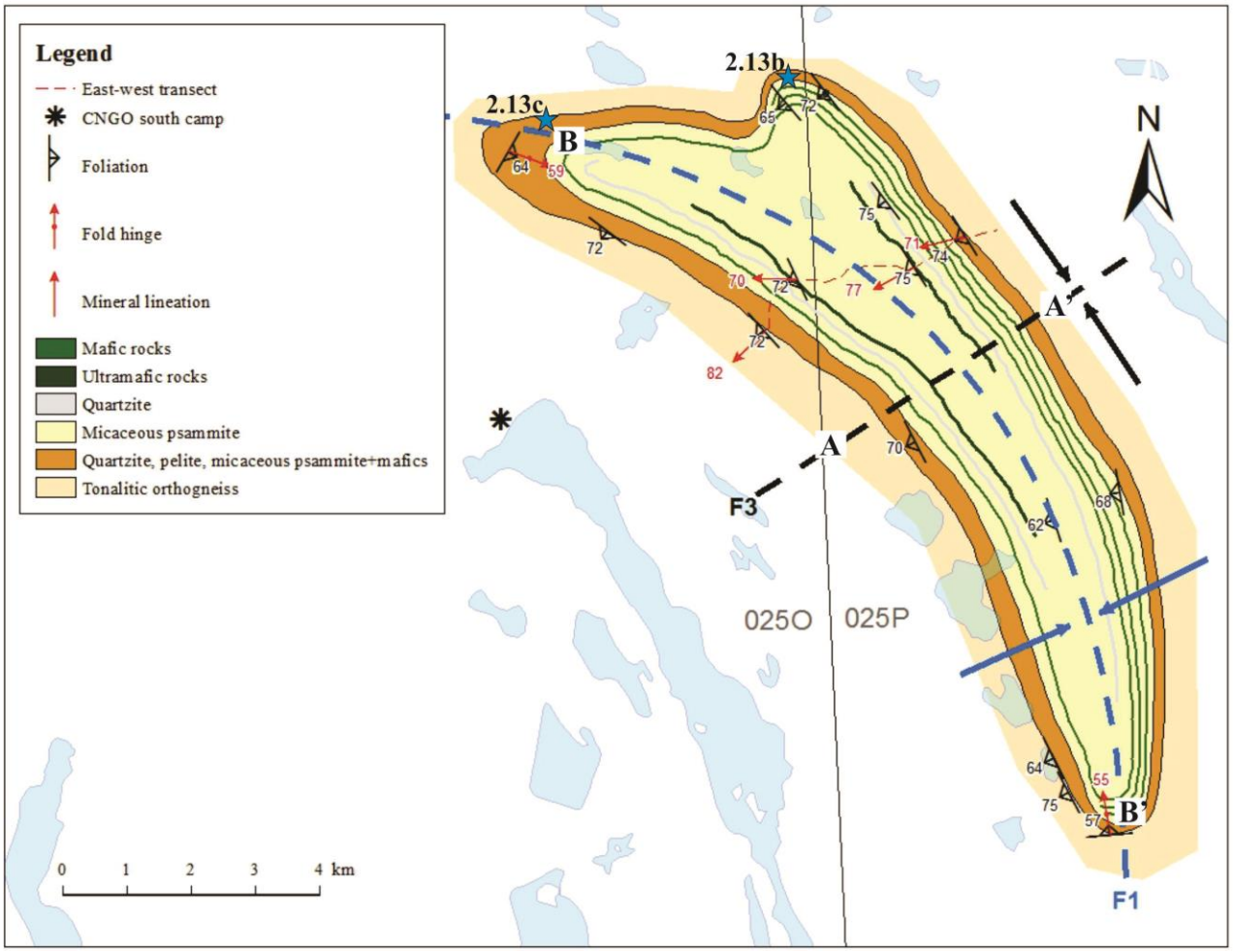

Figure 2.10 – Simplified structural geology of Qaqqanituaq area. Blue dashed line traces F1 fold axis. Black dashed line traces F3 fold axis. Blue stars indicate location of outcrop images (b) and (c) from Figure 2.13.

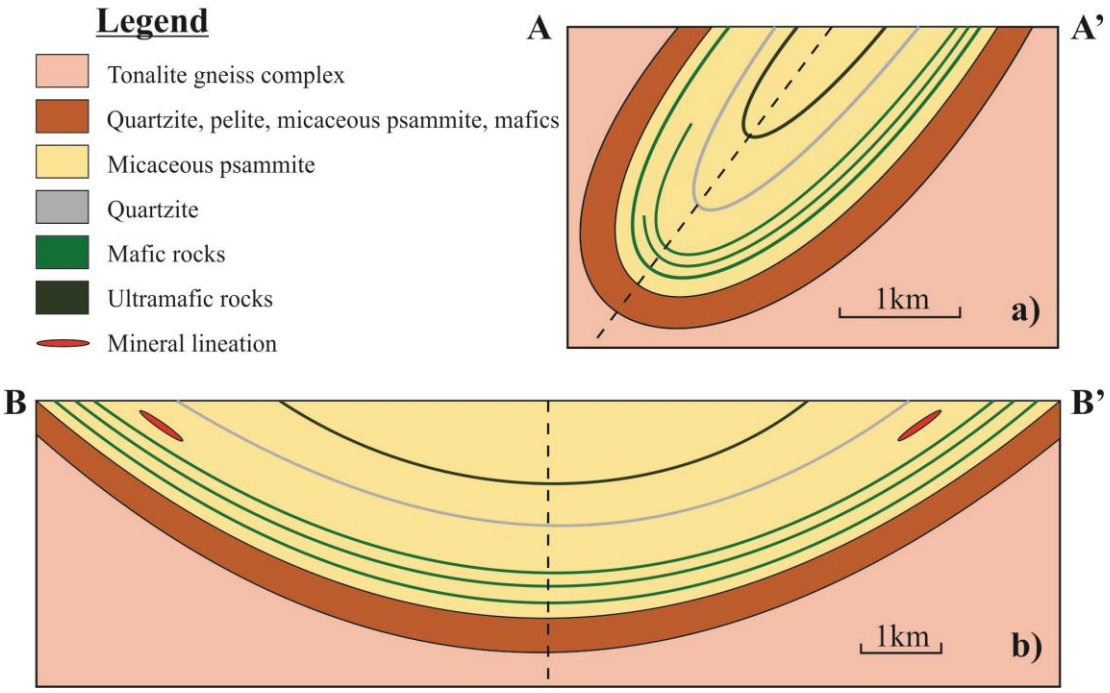

Figure 2.11 – Schematic cross sections of the QA across F1 fold axis (a) and F3 fold axis (b).

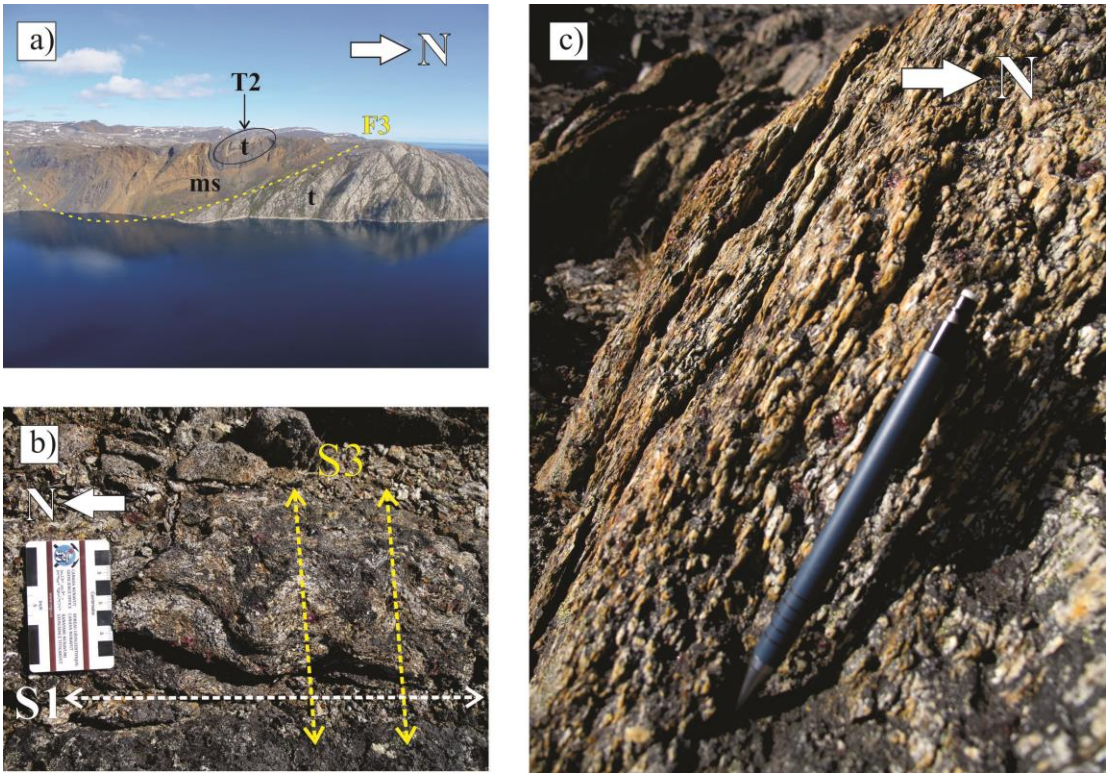

Figure 2.12 – a) Cliff face near Ptarmigan Fiord showing T2 thrust of Archean tonalite orthogneiss (t) onto Paleoproterozoic metasediments (ms) folded by F3 fold. b) S3 crenulation cleavage observed in pelite. c) hinge-parallel faserkeisel lineations observed in micaceous psammite. White north arrows provided for reference. Pen is 15cm long. For outcrop image locations see Figure 2.10b and c and Figure 2.13a.

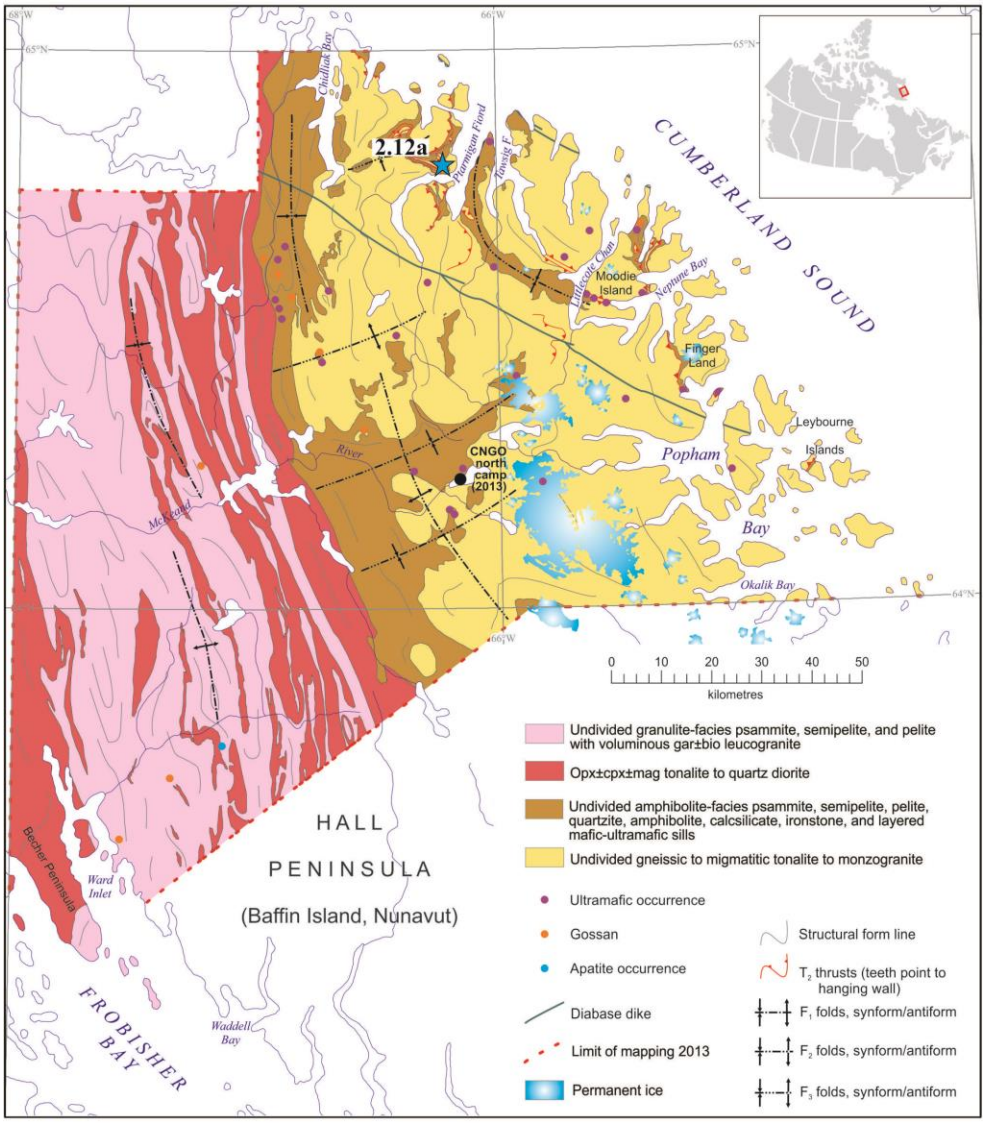

Figure 2.13 – Geology of northern Hall Peninsula Baffin, Island, Nunavut. Blue star indicates location of cliff face image shown in Figure 2.12a.

Along the eastern contact of the QA (Figure 2.14a), there is a transition from the structurally lower tonalite gneiss upward through a 20 m thick zone containing blocks of tonalite gneiss in a pelitic to psammitic matrix (Figure 2.14b and c) into the siliciclastic supracrustal rocks and mafic intrusions/flows. This blocky zone may represent a locally preserved paleoregolith, which would imply that the supracrustal units originally accumulated on top of the underlying tonalite gneiss complex prior to subsequent infolding. Alternatively, the tonalite

blocks may have been tectonically entrained, in which case, the original substrate onto which the metasedimentary rocks of the QA were originally deposited remains unclear.

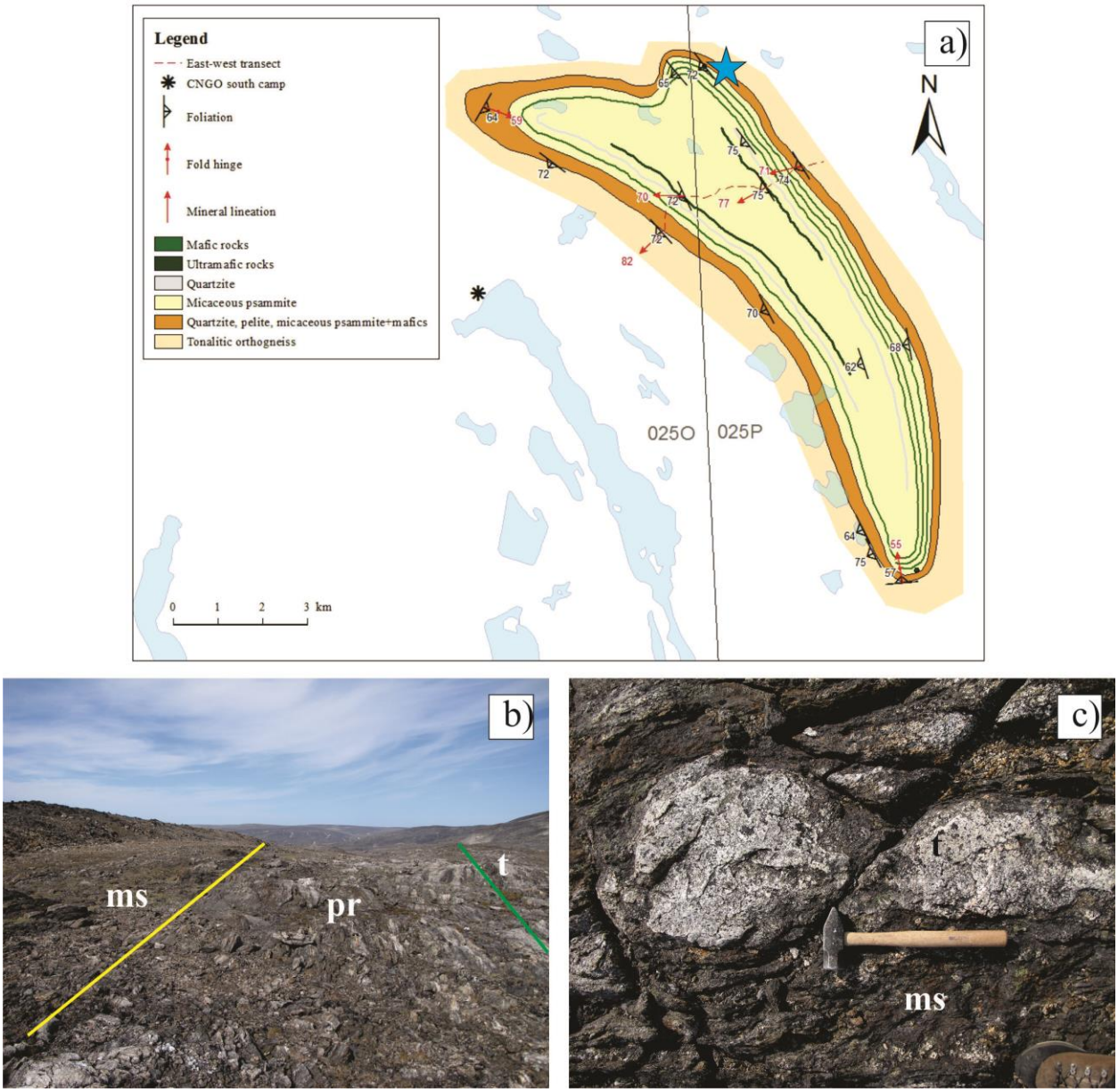

Figure 2.14 – a) Geology of QA, blue star indicates area of potential paleoregolith. b) Outcrop photograph of location in a). Green line denotes approximate contact between tonalite orthogneiss (t) and the potential paleoregolith (pr); yellow line denotes approximate contact between potential paleoregolith (pr) and metasediments and mafic intrusions (ms) of the QA. Note hammer on tonalite block below "pr" label. c) Tonalite block (t) in metasedimentary matrix (ms). Hammer handle is 30cm.

2.4 Metamorphic Observations

2.4.1 Methodology

Garnet – biotite – sillimanite – K-feldspar mineral assemblages indicate that rocks in the QA were subjected to upper-amphibolite-facies metamorphic conditions. In order to confirm this observation, and determine the peak metamorphic conditions recorded by these rocks, a polished thin section of a pelitic sample, K119A with the garnet – biotite – sillimanite – K-feldspar mineral assemblage was cut at the University of Saskatchewan thin section laboratory. Next, transmitted and reflected light petrography was utilized to select grains of garnet, biotite, and plagioclase for analysis based on their proximity, as well as textural equilibrium with one another, and with sillimanite and quartz so that geothermobarometry could be employed. Transmitted light petrography and backscatter electron (BSE) imaging with an accelerating voltage of 15kV and a beam current of 10nA were used to evaluate chemical zonation within individual grains. Wavelength-dispersive electron microprobe analysis was conducted at the University of Saskatchewan department of Geological Sciences on a JEOLJXA-8600 microprobe operating at 15kV with a beam size of 5μm and a current of 50nA, in order to obtain quantitative compositional data of garnet, biotite and plagioclase. Following electron microprobe analysis, the garnet-biotite exchange geothermometer was employed comparing refinements made by Bhattacharya (1992), Hodges and Spear (1982) and Thompson (1976). Next, the GASP geobarometer (Hackler and Wood, 1989; and Ganguly and Saxena, 1984) was employed in order to obtain a pressure estimate of K119A. Finally, winTWQ software (Berman, 2007), which utilizes an internally consistent thermodynamic dataset (Berman et al., 2007) was used to obtain a P-T estimate which could then be compared with the results obtained from the independent implementation of the garnet-biotite exchange geothermometer and the GASP geobarometer.

2.4.2 Results

Table 2.1 gives the results of electron microprobe analysis conducted on sample K119A. Three locations having garnet-biotite-plagioclase-sillimanite mineral assemblages in close proximity and displaying the best evidence of textural equilibrium were analyzed (Figure 2.16). Core and rim spot analyses were taken of garnet, biotite and plagioclase at each location. Chemical zonation in garnet has long been used to study the effects of progressive metamorphism (Spear et al., 1990; Kohn and Spear, 2000). Furthermore, pronounced increased in Mn at the rim of garnet grains is indicative of post-peak-metamorphic diffusional resorption (Kohn and Spear, 2000). No chemical zonation was detected using transmitted light petrography or backscatter electron (BSE) imaging (Figure 2.16). In this study, detailed transects across individual mineral grains were not conducted. However, the core and rim spot analyses which were conducted can be used as a proxy for a more detailed transect. No significant increase or decrease in measured values was observed from core to rim in the grains analyzed. It was thus concluded that the minerals are reflective of a homogenous peak metamorphic assemblage.

Table 2.1 – Mineral compositions from sample K119A used for P-T calculations.

Location	Mineral	SiO_2	TiO_2	Al_2O_3	Cr_2O_3	Fe_2O_3	FeO	MnO	MgO	CaO	Na_2O	K_2O	Total
1, core	gnt	37.66	0.01	21.24	0.00	0.00	35.16	0.91	3.96	1.00	0.00	0.00	99.93
1, core	plag	61.11	0.00	23.50	0.00	0.05	0.00	0.00	0.00	4.86	8.99	0.13	98.64
1, core	bt	35.48	4.03	19.03	0.11	0.00	19.78	0.00	8.49	0.00	0.10	8.99	96.04
1, rim	gnt	37.43	0.00	20.92	0.06	0.00	35.10	0.92	3.89	1.01	0.04	0.00	99.37
1, rim	plag	63.46	0.01	23.29	0.00	0.09	0.00	0.00	0.00	4.47	8.80	0.12	100.27
1, rim	bt	35.08	4.15	18.39	0.03	0.00	20.48	0.02	8.66	0.00	0.10	9.53	96.47
2, core	gnt	37.43	0.00	20.80	0.03	0.00	35.06	0.89	3.85	1.11	0.02	0.00	99.19
2, core	plag	62.10	0.01	23.63	0.00	0.04	0.00	0.00	0.00	5.09	8.59	0.13	99.61
2, core	bt	35.06	3.90	18.57	0.05	0.00	20.25	0.04	8.84	0.00	0.13	9.09	95.94
2, rim	gnt	37.47	0.00	20.95	0.00	0.00	35.68	0.99	3.09	1.07	0.02	0.00	99.25
2, rim	plag	62.32	0.02	23.47	0.00	0.09	0.00	0.00	0.00	4.79	8.78	0.15	99.62
2, rim	bt	35.11	3.86	18.72	0.00	0.00	19.65	0.01	8.85	0.00	0.10	9.28	95.60
3, core	gnt	37.68	0.02	20.84	0.01	0.00	35.65	0.98	3.76	0.99	0.00	0.00	99.94
3, core	plag	60.79	0.02	23.55	0.00	0.01	0.00	0.00	0.00	5.48	8.53	0.24	98.63
3, core	bt	35.34	3.84	18.09	0.07	0.00	20.11	0.02	8.98	0.01	0.12	9.24	95.84
3, rim	gnt	37.51	0.00	21.13	0.04	0.00	34.87	1.03	3.62	0.97	0.02	0.00	99.19
3, rim	plag	60.52	0.02	23.33	0.00	0.12	0.00	0.00	0.00	4.96	8.77	0.18	97.92
3, rim	bt	35.06	3.77	18.41	0.09	0.00	19.28	0.04	8.85	0.03	0.13	9.09	94.77

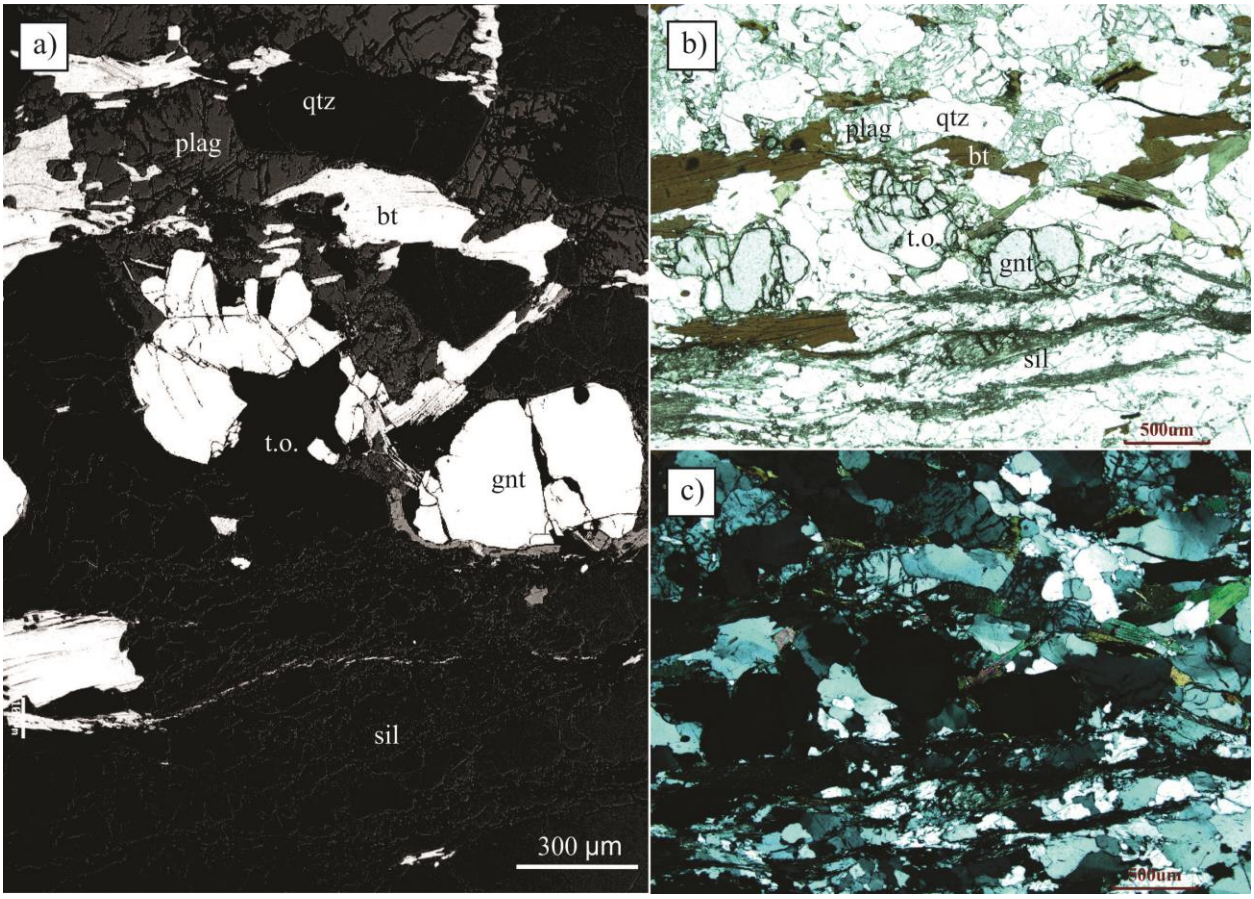

Figure 2.15 – Images of sample K119A location 3 showing garnet – biotite – quartz – plagioclase mineral assemblage in close proximity. No textural evidence such as embayments or chemical zoning to indicate disequilibrium. a) Backscatter electron (BSE) image of sample K119A location 3. b) Plane polarized light image of sample K119A location 3. c) Cross-polarized light image of sample K119A location 3. Bt – biotite; gnt – garnet; Qtz – quartz; plag – plagioclase; sil – sillimanite; t.o. – tear out.

2.4.2 Garnet-biotite exchange geothermometer

The garnet-biotite exchange geothermometer is an experimentally derived quantitative geothermometer based on the reaction:

$$KMg_3AlSi_3O_{10}(F,OH)_2 + Fe_3Al_2Si_3O_{12} = KFe_3AlSi_3O_{10}(F,OH)_2 + Mg_3Al_2Si_3O_{12}$$
(Flouro) Phlogopite + Almandine = Annite + Pyrope

(2.1)

The first experimental calibration of the garnet-biotite exchange geothermometer was conducted by Ferry and Spear (1978) who ran *reversed* experiments where equilibrium values of Fe and Mg in garnet and biotite were measured for given temperatures running the equilibration process with both low and high initial Fe concentrations in biotite to ensure the experiment reflected a true equilibrium value and not simply an interrupted value. Using the measured microprobe data a distribution coefficient (K_D) can be calculated (Equation 2.2):

$$K_D = \left(\frac{X_{Fe}^{Bt}}{X_{Mg}^{Bt}} \times \frac{X_{Mg}^{Grt}}{X_{Fe}^{Grt}}\right) \tag{2.2}$$

and when the natural log of K_D is plotted against the inverse of temperature (in kelvins) the data yields a straight line suggesting that partitioning of Mg and Fe in biotite and garnet behaves as a temperature-dependent ideal solution. The equation for the line using thermodynamic terms for the slope and intercept is given in equation (2.4-3):

$$lnK_D = -\Delta H^o/R \cdot 1/T + \Delta S^o/R \tag{2.3}$$

The values for enthalpy (ΔH) and entropy (ΔS) have been derived from experimental data obtained by many authors including Ferry and Spear (1978), Hodges and Spear (1982) and Thompson (1976) and are assumed to be constant as temperature varies. This assumption is supported when a straight line is achieved by graphing equation 2.3. Equation 2.3 can then be rearranged and solved for temperature using only the measured values from K_D. The formulation of garnet-biotite geothermometer described herein is based on experiments in which garnet is Ca-free. Adding Ca to the system results in a non-ideal pyrope-almandine solution which

requires the implementation of an activity – composition (a-X) model. Many a-X models have been proposed including Bhattacharya (1992), Ganguly and Saxena (1984), Hackler and Wood (1989), Berman (1990) and Holdaway (2000). Similarly, the effects of Ti in the phlogopite-annite system have also been investigated (Henry et al., 2005). The calculated temperatures of K119A based on calibrations made to the garnet-biotite geothermometer by Bhattacharya (1992), Hodges and Spear (1982) and Thompson (1976) are listed in Table 2.2 and shown in Figure 2.16. Calculations were completed using Excel spreadsheets developed by Waters (2004). With the exception of the rim analyses of point 2 there is a strong correlation of peak temperature estimates for each calibration of the garnet-biotite geothermometer. There is a much larger spread in the temperature estimates between calibrations, but all estimates lie between 640±50 ºC and 750±50 ºC.

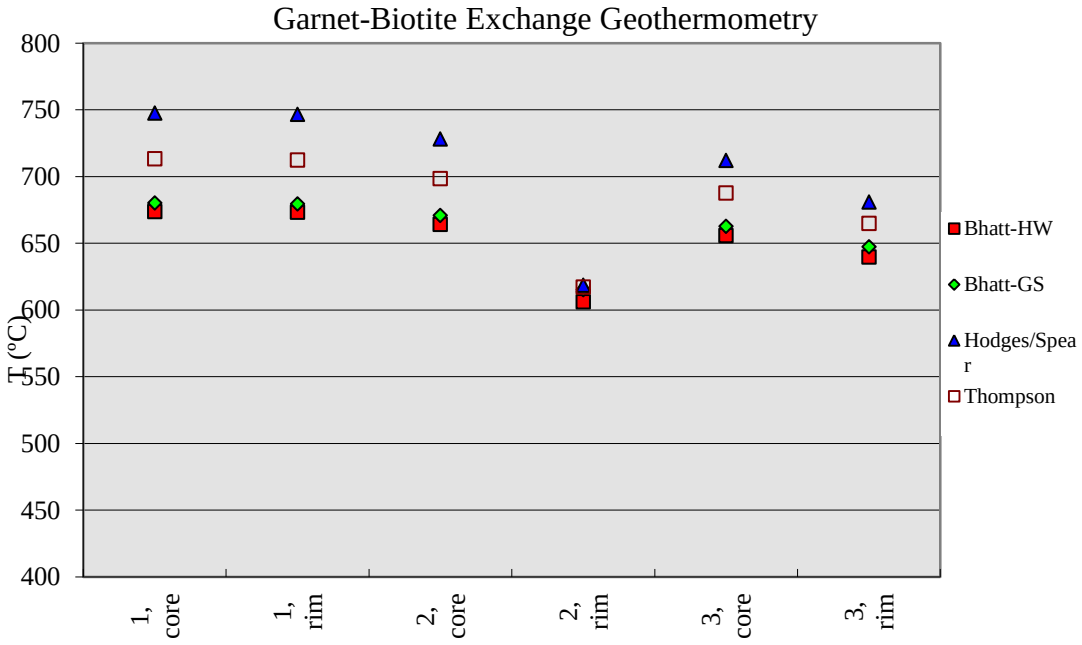

Figure 2.16 – Temperature calculations for K119A based on calibrations made to the garnet-biotite geothermometer by Bhattacharya (1992), Hodges and Spear (1982) and Thompson (1976). Bhatt-HW and Bhatt-GS use mixing parameters for the non-ideal pyrope-almandine solution of Hackler and Wood (1989) and Ganguly and Saxena (1984) respectively.

Table 2.2 – Temperature estimates (ºC) using 4 calibrations: B92 - Bhattacharya (1992); HS82 - Hodges and Spear (1982); and T76 - Thompson (1976). Bhatt-HW and Bhatt-GS utilize mixing parameters for the non-ideal pyrope-almandine solution of Hackler and Wood (1989) and Ganguly and Saxena (1984) respectively

Sample	Ref P(kbar)	B92-HW	B92-GS	HS82	T76
1, core	5	675±40	680±50	750±50	715±50
1, rim	5	675±40	680±50	745±50	710±50
2, core	5	665±40	670±50	730±50	700±50
2, rim	5	605±40	615±50	620±50	620±50
3, core	5	655±40	660±50	710±50	690±50
3, rim	5	640±40	650±50	680±50	665±50

2.4.3 GASP continuous net-transfer geobarometer

The garnet – aluminosilicate – silica –plagioclase (GASP) geobarometer is based on the net-transfer (the production and consumption of phases) reaction:

$$3CaAl_2Si_2O_8 = Ca_3Al_2Si_3O_{12} + 2Al_2SiO_5 + SiO_2$$
$$3\text{Anorthite} = \text{Grossular} + 2\text{Kyanite} + \text{Quartz} \qquad (2.4)$$

This reaction, like many net-transfer reactions, results in a large volume change (ΔV) making the equilibrium constant (K) sensitive to changes in pressure (Equations 2.5 and 2.6).

$$\Delta G = \Delta VP - \Delta ST \qquad (2.5)$$

At equilibrium:

$$\Delta G = \Delta G^o + RTlnK \qquad (2.6)$$

where ΔG^o is the Gibbs free energy for the reaction at a given temperature and pressure.

In order to utilize this pressure sensitive net-transfer reaction, Koziol and Newton (1988) ran *reversed* experiments where sample charges containing given amounts of finely ground $CaAl_2SiO_8$, $Ca_3Al_2Si_3O_{12}$, Al_2SiO_5 and SiO_2 were subjected to measured temperature and pressure conditions. Following each experiment the sample charges were re-analyzed and increases in either $CaAl_2SiO_8$ or $Ca_3Al_2Si_3O_{12}$, Al_2SiO_5 and SiO_2 were noted. In this way they were able to create a best fit line in pressure-temperature space defined as:

$$P(MPa) = 2.28T(^oC) - 109.3 = 2.28T(K) - 731.7 \quad (2.7)$$

Drawbacks of the GASP net-transfer geobarometer include the need for an independent estimation of temperature (Equation 2.7) and the fact that neither anorthite-albite nor grossular-pyrope-almandine solutions are ideal. Table 2.3 lists the calculated values of pressure for sample K119A using Excel spreadsheets developed by Waters (2004) in which the non-ideal mixing parameters of Hackler and Wood (1989) and Ganguly and Saxena (1984) for the grossular-pyrope-almandine solution are utilized.

Table 2.3. Pressure estimates using the *GASP* geobarometer.

Sample	P (kbar) HW	P (kbar) GS
Core, 1	4.6±2.4	4.4±2.6
Rim, 1	4.9±2.5	4.6±2.4
Core, 2	4.7±2.4	4.4±2.6
Rim, 2	3.9±1.1	3.8±1.2
Core, 3	3.9±1.9	3.7±2.4
Rim, 3	4.0±1.8	3.8±2.2

HW and GS utilize mixing parameters for the non-ideal grossular-pyrope-almandine solution of Hackler and Wood (1989) and Ganguly and Saxena (1984) respectively.

2.4.4 winTWQ software

Following electron microprobe analysis, winTWQ (version 2.36) software (Berman, 2007), using the Dec06.dat database (Berman et al., 2007), was utilized to obtain a pressure-temperature estimate for the QA pelites. The program winTWQ uses an internally consistent thermodynamic dataset developed and maintained by Rob Berman at the Geological Survey of Canada. Internally consistent thermodynamic data is measured against all other data in the dataset and adjusted so that it is correlative. This is done because combining end-member thermodynamic data, such as Gibbs Free energy values, from, for example, the Koziol and Newton (1988) GASP geobarometer (Equation 2.4) with the Ferry and Spear (1978) garnet-biotite geothermometer is inherently flawed because: i) the calibrations are different; and ii) different studies using different methods have different amounts of uncertainty. The way in which internally consistent thermodynamic datasets correct for this inherent flaw when simultaneously employing multiple geothermometers and geobarometers, is eloquently laid out by Winter (2010) and summarized here.

Imagine that three different labs independently studied the three Al_2SiO_5 polymorph conversion reactions (And = Ky, Ky = Sil, Sil = And) then extracted the thermodynamic data for the two phases in the reaction they were studying. If they then constructed the equilibrium curves in P-T space, it is highly unlikely that the three curves would intersect at a single invariant point (which they must do), given the errors associated with each experimental method. What internally consistent thermodynamic datasets do is to compare the data derived for all three phases and adjust the values within the experimental limits so that they intersect at a single point. In this way, the data is internally consistent and likely more accurate because it takes into account multiple, experimentally calibrated reactions and not just one.

There are further advantages of winTWQ over "classical" geothermobarometry. For instance, based on the mineral compositions which are input, the program finds other reactions involving the stable mineral assemblage. Also, the geothermometers and geobarometeres employed are commonly based on reactions involving end-member species in a continuous solid solution, for example, anorthite, and grossular garnet in the GASP geobarometer (Equation 2.4). In an ideal situation such as that in equation 2.8, a simple mixing model for an ideal solution (Winter, 2010) can be employed:

$$a_i^A = (X_i^A)^y \tag{2.8}$$

where *a* is the activity, X_i^A is the mole fraction of mixture component *i* in *A* and the exponent y indicates the number of crystallographic sites on which mixing can take place. Real-world mineral compositions nearly always vary from ideal end-member cation concentrations. In these cases activity coefficients (γ_i) are derived which can vary with X (Equation 2.9) effectively making the activity a thermodynamic analog of concentration (Winter, 2010).

$$a_i^A = (\gamma_i X_i^A)^y \tag{2.9}$$

WinTWQ allows the activities/concentrations of each end-member mineral to vary within the uncertainty of each activity model. This defines bands between which the reaction can take place within the activity model's uncertainty. Using all relevant reactions the program then calculates an optimal point in P-T space within correlated uncertainty. Any reaction curves with slopes less than 15 degrees apart and any intersection points outside 1.5 standard deviations are discarded.

Mineral composition data from sample K119A was run in winTWQ software. Three internally consistent reactions, Equations 2.1, 2.4 and 2.10:

$$\underset{\text{Pyrope}}{Mg_3Al_2Si_3O_{12}} + \underset{\text{Grossular}}{2Ca_3Al_2Si_3O_{12}} + \underset{\text{Eastonite}}{3K(Mg_2Al)(Si_2Al_2)O_{10}(OH)_2} + \underset{\text{Quartz}}{6SiO_2}$$

$$= \underset{\text{Anorthite}}{6CaAl_2Si_2O_8} + \underset{\text{Phlogopite}}{3KMg_3(AlSi_3)O_{10}(OH)_2} \qquad (2.10)$$

were identified by the program and applied. Of the six locations analyzed on sample K119A, location 3 (rim) produced the best result. At this location a near perfect 3 point intersection of the 3 reaction curves was obtained (Figure 2.17). Berman (1991) suggested that such a tight intersection of independent reactions indicates that equilibrium has been attained. The peak pressure and temperature conditions reached in the QA are approximately 4.8±2.1 kbars and 645±50°C. Empirical data for P-T intersections is provided in Table 2.4.

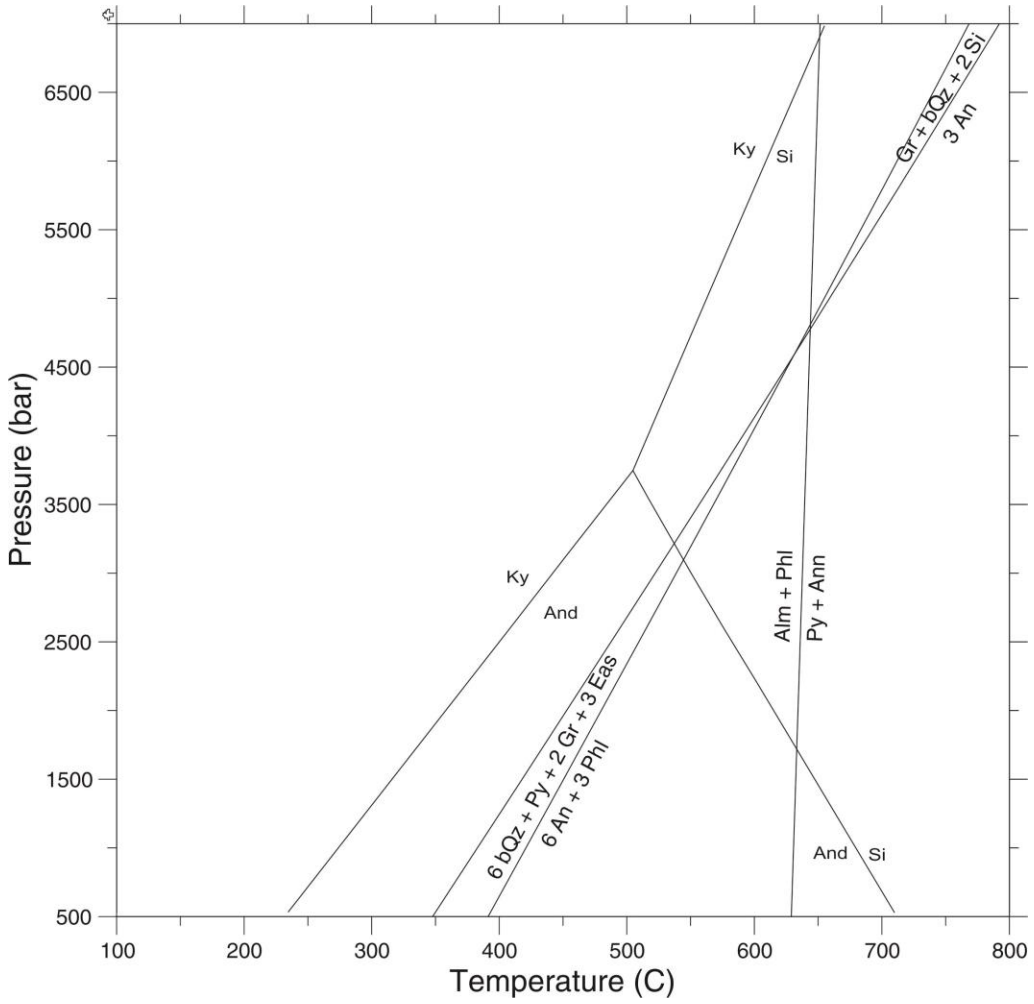

Figure 2.17 – Multi-equilibrium pressure-temperature phase diagram calculated using winTWQ version 2.36 for sample K119A, Rim, 3. An – anorthite; And – andalusite; Ann – annite; Eas – eastonite; Gr – grossular; Ky – kyanite; Phl – phlogopite; Py – pyrope; Qz – quartz.

Table 2.4. Pressure and temperature estimates for sample K119A, Rim, 3 using winTQW version 2.36 software.		
Reaction 1: Gr + Qz + 2Sil = 3An		
Reaction 2: Alm + Phl = Py + Ann		
Reaction 3: 6Qz + Py + 2Gr + 3Eas = 6An + 3Phl		
P-T Intersection	P (bars)	T (°C)
1 and 2	4776.4	643.85
2 and 3	4811.48	643.97

2.5 Age Constraints

2.5.1 Introduction

As a part of the broader HPIGP, the determination of absolute ages of for key rock units was integral to the success of the project. Absolute ages were determined through the use of U-Pb zircon geochronology carried out using the Geological Survey of Canada's Sensitive High Resolution Ion Microprobe (SHRIMP) by Nicole Rayner. Results reported herein are based on interpretations made by Rayner (2014) and on conversations with N. Rayner. As funding was limited, so too was the number of U-Pb age dates that were able to be obtained. As such, all members of the HPIGP gave input to determine the most strategically significant samples for analysis. Two samples from the QA were chosen for geochronology. First, a quartzite (Section 2.2.3), sample K097A (Figure 2.2) was chosen for U-Pb detrital zircon geochronology and second, a cross-cutting monzogranite dyke (Section 2.2.6), sample K079B (Figure 2.2) for U-Pb geochronology to determine its crystallization age. These samples were chosen because the QA is the type locality which serves as an analogue for all metasedimentary-mafic rock packages in the central and eastern regions of the Hall Peninsula and it is therefore crucial that absolute age constraints be obtained.

2.5.2 Sensitive high resolution ion microprobe

The SHRIMP is a double-focusing, large diameter secondary ion mass spectrometer (SIMS). For U-Pb geochronology studies, a primary beam of $(O_2)^{-1}$ ions are accelerated at the sample where it causes secondary ions from the sample to "sputter". The secondary ions are then measured to successively determine the relative isotopic abundance of the various species of U, Th and Pb. The measured, relative isotopic abundances do not correlate to real relative

isotopic abundances since the sputtering yield differs between ionic species. As such, sample-specific calibration factors determined by analyzing reference material and unknowns are applied (Stern, 1997).

The main advantage of SHRIMP U-Pb geochronology over other approaches like isotope dilution chemistry and thermal ionization mass spectrometry (ID-TIMS) is that when using the SHRIMP, much smaller amounts of sample are able to analyzed. For instance, rims and cores on an individual zircon can be analyzed whereas using the ID-TIMS technique the result would likely produce a discordant "blended age", which amalgamates the individual growth episodes. ID-TIMS U-Pb geochronological studies however, produce far more precise ages than SHRIMP analyses.

2.5.3 Quartzite U-Pb detrital zircon geochronology

Sample K097A was analyzed for U-Pb detrital zircon geochronology in order to characterize the metasedimentary rocks of the central and eastern regions of the Hall Peninsula. The detrital zircons recovered from K097A were colourless to medium brown and commonly well rounded presumably due to sedimentary transport (Figure 2.18). There is a significant 2.7 – 2.9 Ga Archean detrital component which corresponds to known ages of the orthogneiss basement in the central and eastern regions of Hall Peninsula (Rayner, 2014). The maximum age of deposition for K097A is 2126±16 (2σ) Ma. This age is defined by the four analyses on grain 42, the youngest detrital zircon (Figure 2.18).

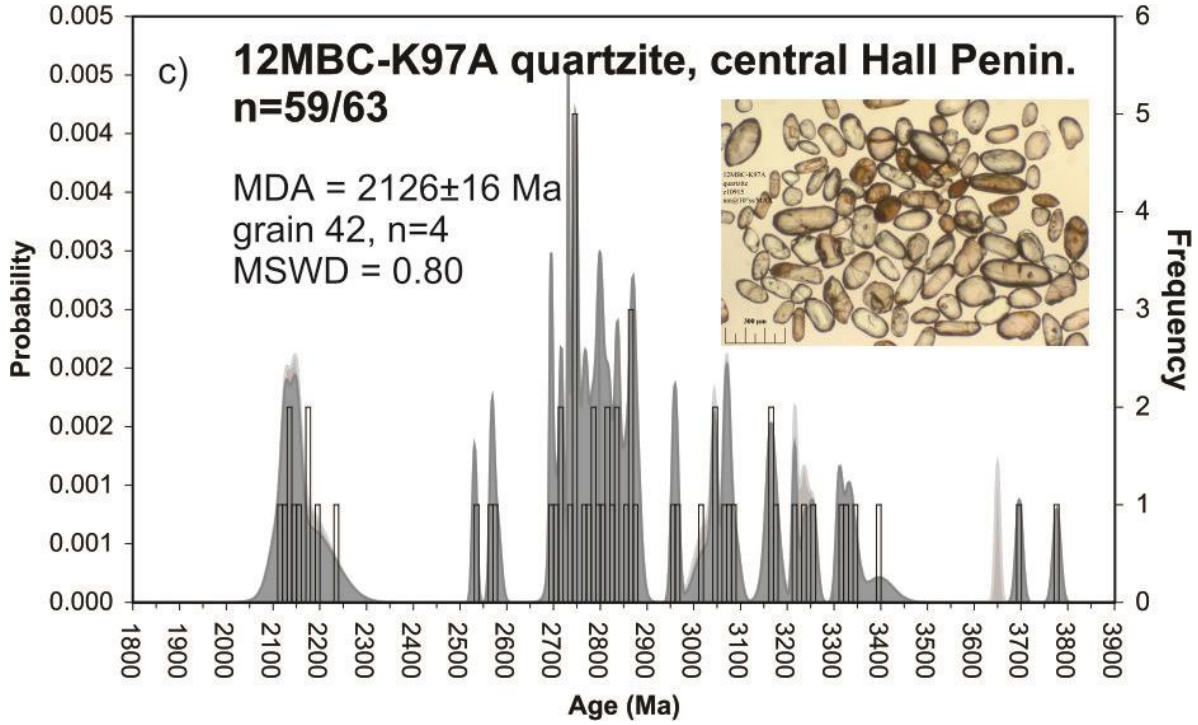

Figure 2.18 – Histogram showing absolute ages of a population of detrital zircons obtained from sample K097A and the frequency and probability that a zircon is a given age. Bars indicate actual measurements corresponding to that age, light grey probability curve represents all data, dark grey probability curve represents concordant data only. MDA – maximum depositional age; n – number of analyses; MSWD – mean square of weighted deviates.

2.5.3 Monzogranite dyke U-Pb geochronology

Sample K079B, a monzogranite dyke which cross-cuts metasedimentary rocks as well as the mafic sills and dykes of the QA, also records the dominant regional (S1) fabric, was analyzed to determine its crystallization age. As reported in Section 2.5.1 above, the metasedimentary rocks of the QA are Paleoproterozoic in age (2126±16 Ma); therefore the monzogranite dykes which cross-cut these metasedimentary rocks must be younger. Zircons recovered from K079B were commonly colourless to medium brown and euhedral to subhedral in shape due to their igneous origin (Figure 2.19). Figure 2.19 shows the concordia diagram for analyses made to K079B. The crystallization age is recorded in high-U zircon and zircon rims with a weighted

mean $^{207}Pb/^{206}Pb$ age of 1873±6 Ma. The linear nature of the discordia curve suggests inheritance from a unimodal source. Also, the analyses that yield older ages are generally found in zircon cores and low-U zircons. These are interpreted as inherited zircon, but multiple analyses in specific cores and grains commonly do not yield reproducible results. This suggests that the linear spread in the older ages is due to recrystallization or Pb-loss during the Paleoproterozoic.

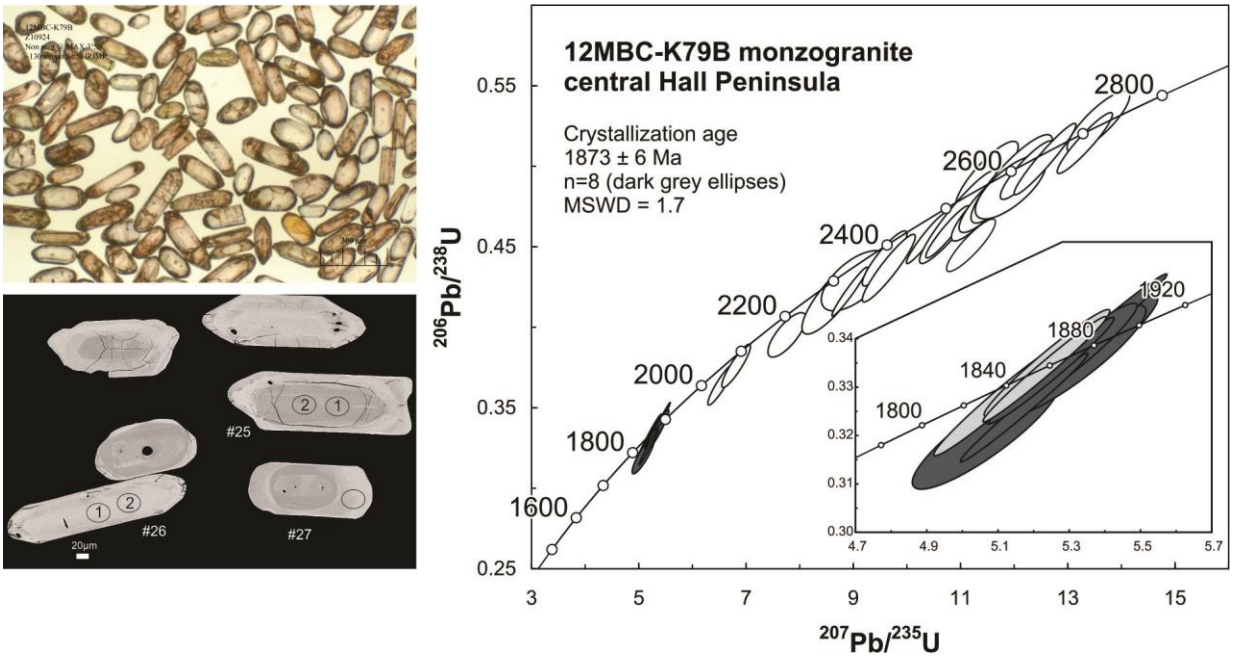

Figure 2.19 – Concordia curve for K079B U-Pb geochronology obtained using SHRIMP. n – number of analyses; MSWD – mean square of weighted deviates.

CHAPTER 3

MAFIC AND ULTRAMAFIC GEOCHEMISTRY

3.1 Introduction

Mafic and ultramafic rocks are most commonly found interbedded with metasedimentary rocks in the east and central regions of the Hall Peninsula. However, there are also mafic and ultramafic enclaves within the Archean-tonalitic-orthogneiss basement in the central and eastern regions and rare mafic and ultramafic units in the western region of the Hall Peninsula. All mafic and ultramafic rocks have undergone multiple phases of deformation and been metamorphosed to at least amphibolite-grade conditions (See Chapters 1 and 2), and thus only locally preserve primary igneous textures (Steenkamp et al., 2014). Because of multiple phases of deformation and metamorphism it is impossible to say for certain whether the mafic rocks are intrusive or extrusive as there are no distinctive defining primary features such as pillows, vesicles or distinct cross-cutting relationships preserved.

Age constraints provided by detrital zircons from quartzite within supracrustal panels in the central and eastern regions, and from cross-cutting monzogranite dykes, as described in the QA described in Chapter 2 and by MacKay et al. (2013a and b) and Rayner (2014), indicate that the mafic map units within supracrustal packages are Paleoproterozoic in age. However, it is not known whether all mafic and ultramafic bodies are the same age, or whether some of the enclaves in the tonalitic gneisses are possibly Archean in age.

Samples were taken from all mafic and ultramafic rock types and were chosen so as to maximize the geographic distribution of the sample data set both in the detailed QA study area and on the Hall Peninsula as a whole (Figure 3.1a and b).

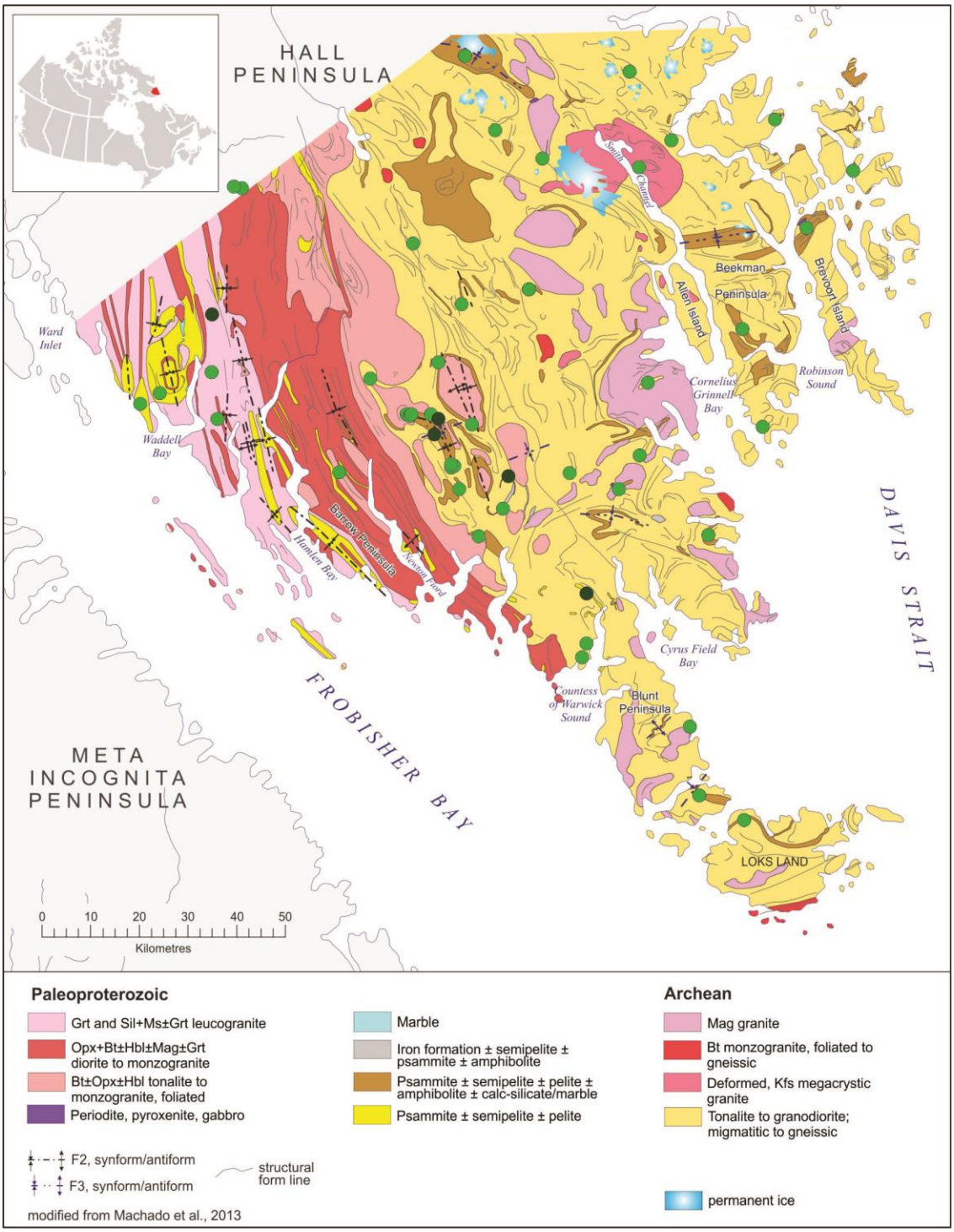

Figure 3.1a – Geology of southern Hall Peninsula from Machado et al (2013). Light green dots indicate the location of 2012 mafic geochemical samples. Dark green dots indicate the location of 2012 ultramafic geochemical samples.

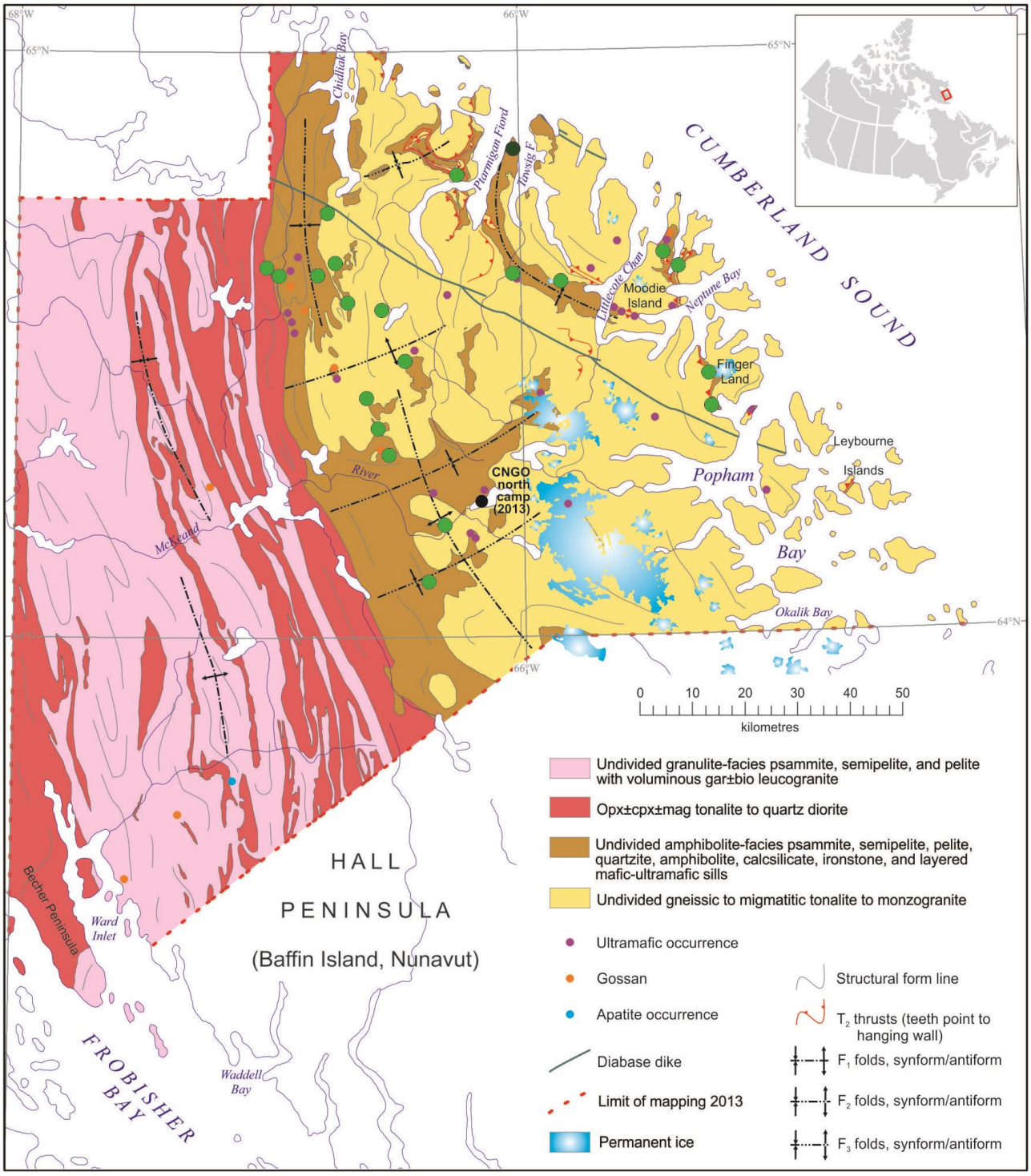

Figure 3.1b – Geology of northern Hall Peninsula from Steenkamp and St-Onge (2014). Light green dots indicate the location of 2013 mafic geochemical samples. Dark green dots indicate the location of 2013 ultramafic geochemical samples.

3.2 Sample Screening, Analytical Procedure and Methodology

Care was taken to collect fresh, large fist-sized, unaltered samples in the field. All weathered edges were removed with a rock saw. Geochemical preparation and analysis was carried out by Activation Laboratories Ltd. (Actlabs) on a total of 91 samples, 67 sampled in 2012 from the southern Hall Peninsula and 24 sampled in 2013 from northern Hall Peninsula. Samples were pulverized using mild steel to reduce contamination, then mixed with a flux of lithium metaborate and lithium tetraborate and fused in an induction furnace. Major oxides were analyzed using simultaneous/sequential Thermo Jarrell-Ash ENVIRO II inductively coupled plasma (ICP). For trace element analysis the solutions prepared for major oxide analysis were spiked with Actlabs internal standard, diluted and run on a Perkin Elmer SCIEX ELAN inductively coupled plasma mass spectrometer (ICP-MS). Sample introduction methodology is proprietary to Activation Laboratories Ltd. Upon completion of geochemical analysis, thirteen samples that had high (>1.5 wt.%) loss on ignition values (LOI) suggesting they had been altered were discarded. Four other samples whose composition was not within the scope of this thesis were discarded from this study, two ultramafic lamprophyres and two which had SiO_2 wt% values >60%. Spatial (latitude and longitude) and contextual (station notes) data was extracted from the CNGO database and appended to the geochemical dataset based on unique sampleIDs. This allowed for the geochemical data to be analyzed and interpreted with spatial relationships and the broader geological context in mind. For tables containing all major and trace element geochemical data see Appendix 2.

3.3 Results

3.3.1 Element Mobility

Samples were tested for evidence of major and trace element mobility that may have occurred during deformation and/or metamorphism. This was done by plotting major and trace element values against Zr, which due to its moderate ionic potential is typically immobile in hydrothermal solutions (Cann, 1970). Major element oxides CaO, Fe_2O_3 and Na_2O show a high degree of scatter when plotted vs. Zr (Figure 3.2a-c) indicating that elements with low ionic potential were most likely mobilized during late thermotectonic events limiting their potential usefulness in geochemical investigations. Conversely, the trace elements Nb, Ce and Ti, with the exception of a few notable outlier analyses, show a much higher degree of correlation (Figure 3.2d-f) allowing for elements with moderate ionic potential (HFSE) to be used in primary geochemical discriminations. The outliers in Figure 3.2d-f may have been mobilized during deformation and/or metamorphism or may indicate that the samples were obtained from rocks that formed during different igneous events resulting from the melting of different parent materials.

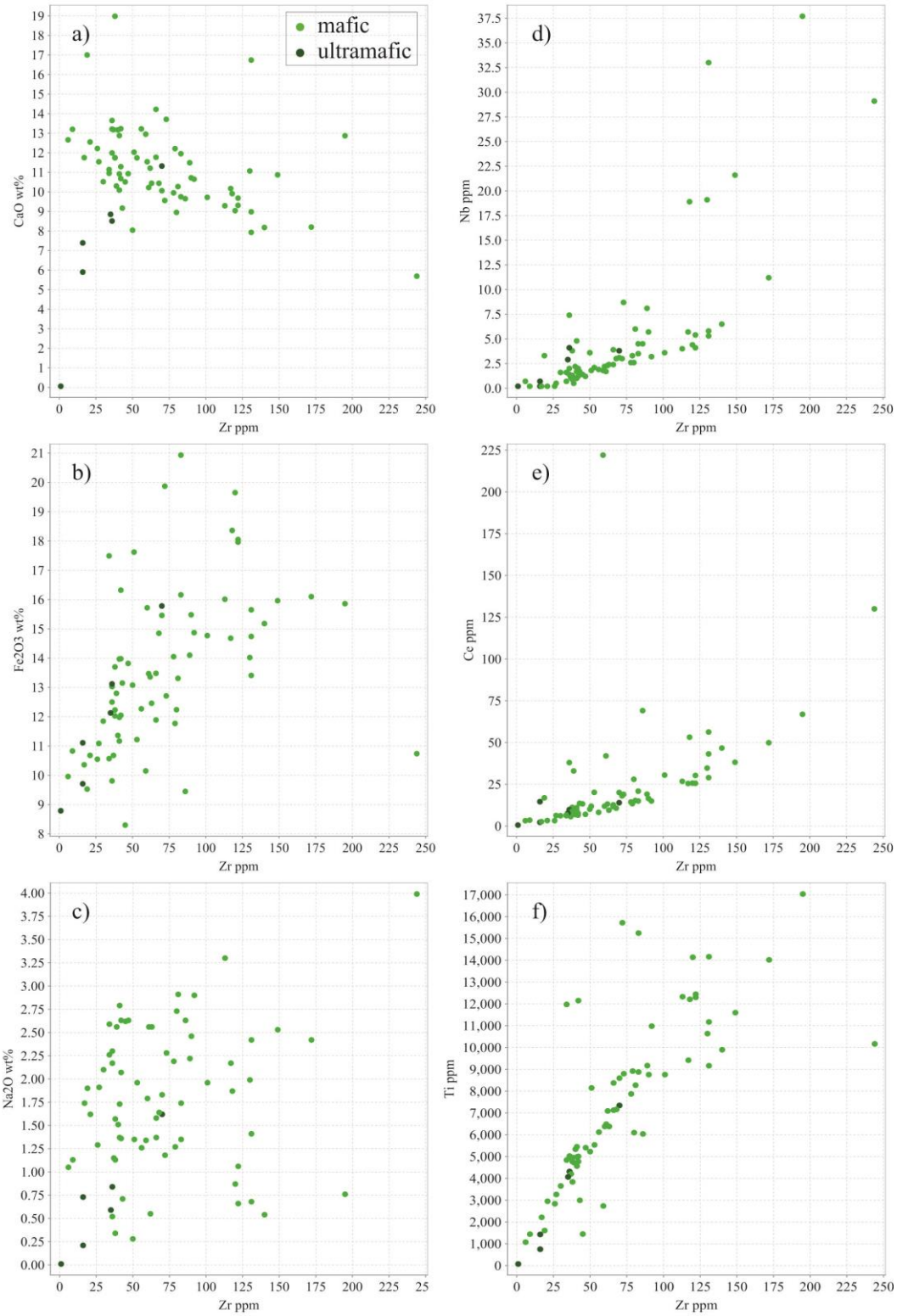

Figure 3.2 – Binary plots of Zr vs a) CaO b) Fe_2O_3 c) Na_2O, d) Nb, e) Ce, f) Ti, used to detect element mobility. Low ionic potential elements a-c show high degree of scatter suggesting mobilization, while moderate ionic potential elements (HFSE) d-f show much stronger correlation suggesting they reflect primary igneous compositions.

3.3.2 Mafic rock classification

The Zr/Ti vs Nb/Y diagram was first proposed by Floyd and Winchester (1978) using immobile trace elements as proxies for silica content (SiO_2) and alkalinity ($Na_2O + K_2O$), the two axes of the IUGS recommended TAS (total alkali-silica) discrimination diagram (Le Maitre et al., 2002). The ratio of Zr/Ti is used as a proxy for silica content, i.e. the degree of fractionation, because fractionation is accompanied by the development of an increasingly negative Ti anomaly relative to N-MORB (Figure 3.3a). The extent of fractionation is indicated by the ratio:

$$M1/Ti \tag{3.1}$$

where M1 is an element that is incompatible throughout fractionation. Zr, (Winchester and Floyd, 1977; Stillman and Williams, 1978; Pearce and Norry, 1979) is the most commonly used element.

The trend from tholeiitic to alkalic is marked by a strong enrichment in Th and Nb relative to N-MORB, and no significant increase of Ti or Y relative to N-MORB (Figure 3.3b). The degree of alkalinity is measured by the ratio:

$$M1/M2 \tag{3.2}$$

where, M1 is a strongly enriched element, and M2 is an element with very weak or no enrichment. Nb/Y (Pearce and Cann, 1973; Floyd and Winchester, 1978) is the least susceptible to alteration and the most commonly used proxy for alkalinity.

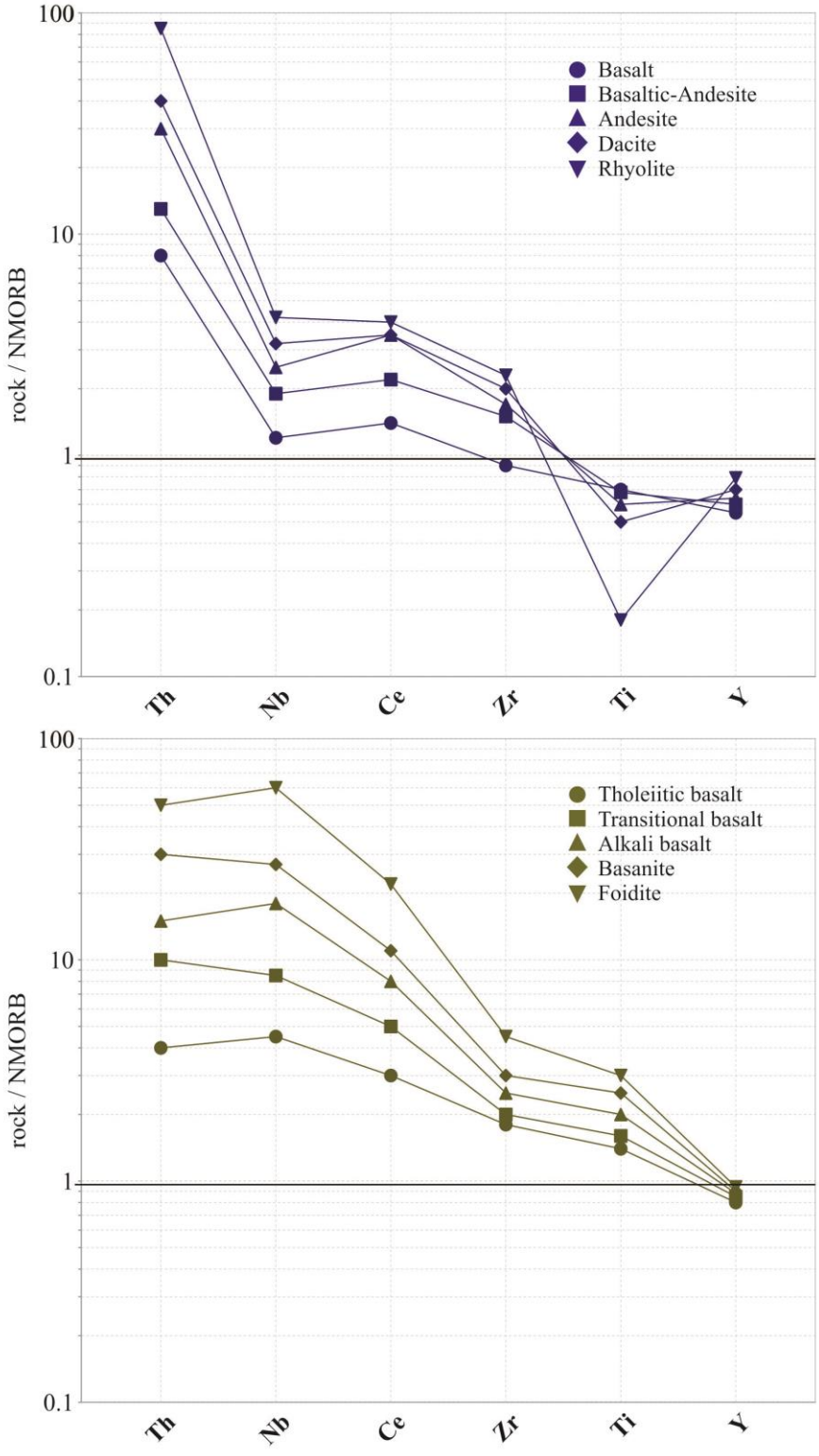

Figure 3.3 – Schematic N-MORB normalized trace element diagrams modified from Pearce (1996) of: a) the volcanic fractionation series, and b) basaltic series of increasing alkalinity.

When plotted on the modified Zr/Ti vs Nb/Y rock classification diagram (Pearce, 1996) which utilizes statistically drawn boundaries, the majority of the mafic samples plot in the sub-alkaline basalt field with four plotting in the alkali basalt field and two plotting in the basaltic andesite field (Figure 3.4a). The majority of sub-alkaline mafic rocks exhibit characteristics typical of tholeiitic or transitional sequences based on the refined sub-alkaline basalt classification scheme of Ross and Bédard (2009) (Figure 3.4b).

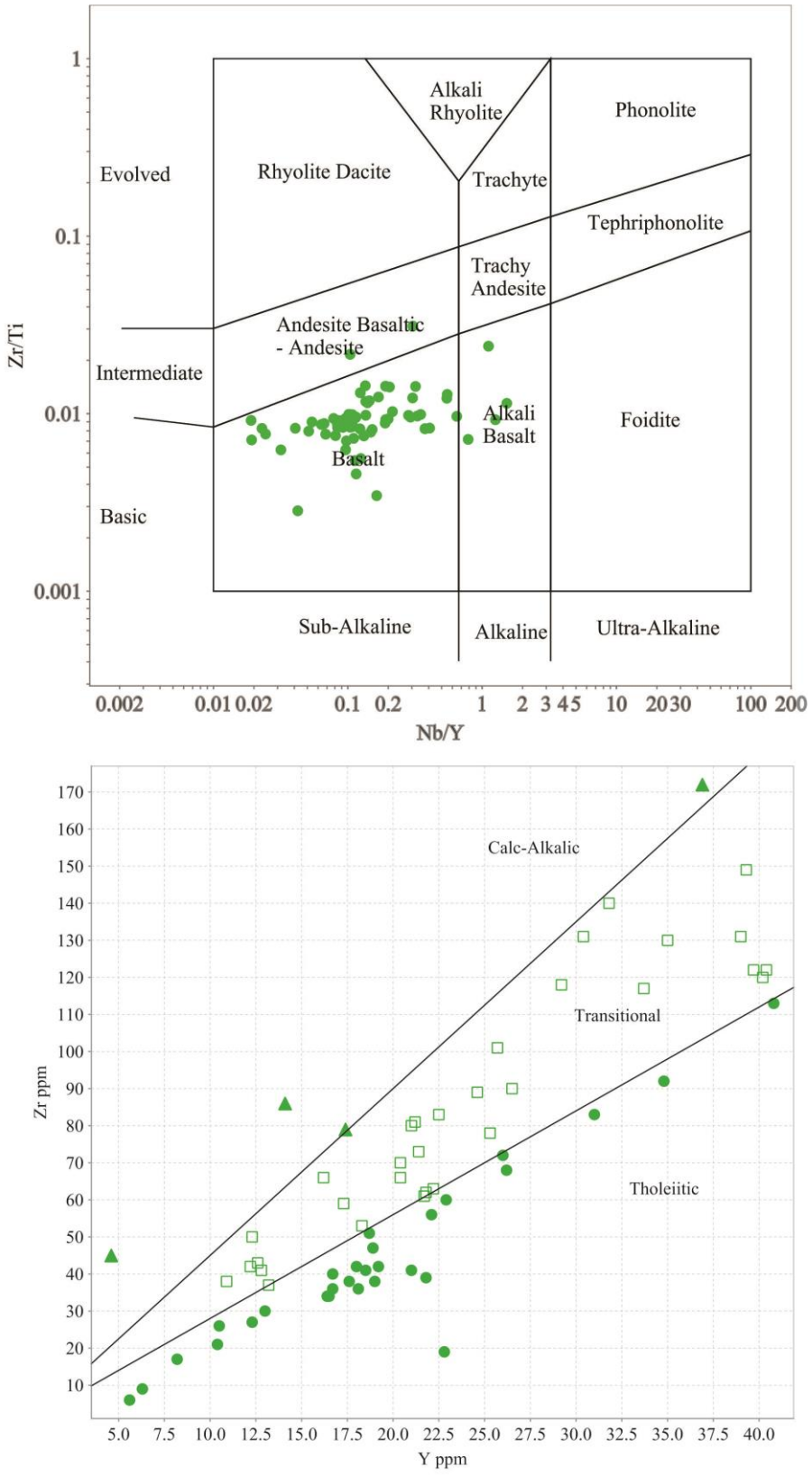

Figure 3.4 – a) Volcanic rock type classification diagram (Zr/Ti vs Nb/Y; Pearce, 1996). b) Sub-alkali basalt classification diagram (Zr vs Y; Ross and Bédard, 2009).

Based on these classification schemes mafic rocks have been subdivided into five broad categories that will form the basis for further examination: alkaline, calc-alkaline, transitional, tholeiitic, and ultramafic. Symbols from Figure 3.4b will be applied in all subsequent diagrams to denote the mafic sub-groups. Ultramafic samples will be denoted with a dark green circle and will be described separately in Section 3.3.5. Table 3.1 provides major and trace element geochemical data for a representative sample from each category. All except sample F140B1 (Figure 3.5) are located in the QA (Figure 3.6) and have been further studied using electron microprobe analysis (Chapter 3.2).

Table 3.1 - Selected representative geochemistry samples					
SampleID	K091B1	F140B1	K093A1	K069A1	K074A1
Unit	alkaline	calc-alkaline	transitional	tholeiitic	ultramafic
Latitude	63.20160002	63.21528166	63.20663502	63.30754668	63.30706168
Longitude	-65.91684146	-65.14472016	-65.92070812	-65.9988414	-65.99365307
(wt%)					
SiO_2	44.73	48.84	48.82	49.9	42.78
Al_2O_3	11.04	16.56	14.22	15.08	11.31
Fe_2O_3(T)	15.86	11.77	14.77	10.57	13.12
MnO	0.228	0.164	0.22	0.165	0.197
MgO	8.68	5.99	5.55	8.33	20.23
CaO	12.87	12.21	9.72	11.14	8.51
Na_2O	0.76	1.27	1.96	2.59	0.84
K_2O	0.39	0.4	0.68	0.2	0.15
TiO_2	2.843	1.488	1.461	0.807	0.719
P_2O_5	0.26	0.09	0.17	0.06	0.08
LOI	0.45	0.76	0.36	0.71	1.42
Total	98.1	99.55	97.93	99.55	99.36
(ppm)					
Sc	35	29	43	44	30
V	451	361	442	300	219
Cr	540	80	40	370	2590
Co	64	44	42	45	95
Ni	160	110	< 20	140	890
Cu	30	140	40	230	50
Zn	120	90	110	70	90
Be	2	< 1	< 1	< 1	< 1
Ga	21	25	20	17	12
Ge	2.9	1.5	1.6	2	1.6
As	< 5	< 5	< 5	< 5	< 5
Rb	1	5	10	3	< 1
Sr	252	225	240	98	34
Y	24.7	17.4	25.7	16.4	10.2
Zr	195	79	101	34	36
Nb	37.7	3.3	3.6	1.6	4.1
Mo	< 2	< 2	< 2	< 2	< 2
Ag	1.3	< 0.5	0.6	< 0.5	< 0.5
In	< 0.1	< 0.1	< 0.1	< 0.1	< 0.1
Sn	2	1	< 1	< 1	< 1
Sb	0.3	0.2	0.3	0.3	0.2
Cs	< 0.1	< 0.1	0.1	< 0.1	< 0.1
Ba	24	67	265	33	10
Hf	4.5	1.9	2.4	0.9	0.9
Ta	2.55	0.23	0.23	0.11	0.31
W	< 0.5	< 0.5	< 0.5	< 0.5	< 0.5
Tl	< 0.05	< 0.05	0.06	< 0.05	< 0.05
Pb	< 5	< 5	< 5	< 5	< 5
Bi	0.1	< 0.1	< 0.1	< 0.1	< 0.1
Th	3.25	0.39	2.12	0.22	0.44
U	0.84	0.16	0.5	0.05	0.1
La	32.8	5.36	14.1	2.86	4.42
Ce	66.9	13.4	30.5	6.24	9.83
Pr	9.07	2.17	4.17	1.05	1.42
Nd	38.3	11.3	18	5.23	6.09
Sm	7.61	3.61	4.09	1.87	1.72
Eu	2.25	1.18	1.26	0.66	0.491
Gd	7.2	3.51	4.16	2.31	1.75
Tb	1	0.59	0.75	0.42	0.32
Dy	5.23	3.33	4.27	2.76	1.86
Ho	0.88	0.62	0.91	0.58	0.38
Er	2.33	1.64	2.67	1.64	1.03
Tm	0.316	0.232	0.4	0.245	0.144
Yb	1.9	1.38	2.55	1.62	0.93
Lu	0.256	0.183	0.39	0.234	0.147

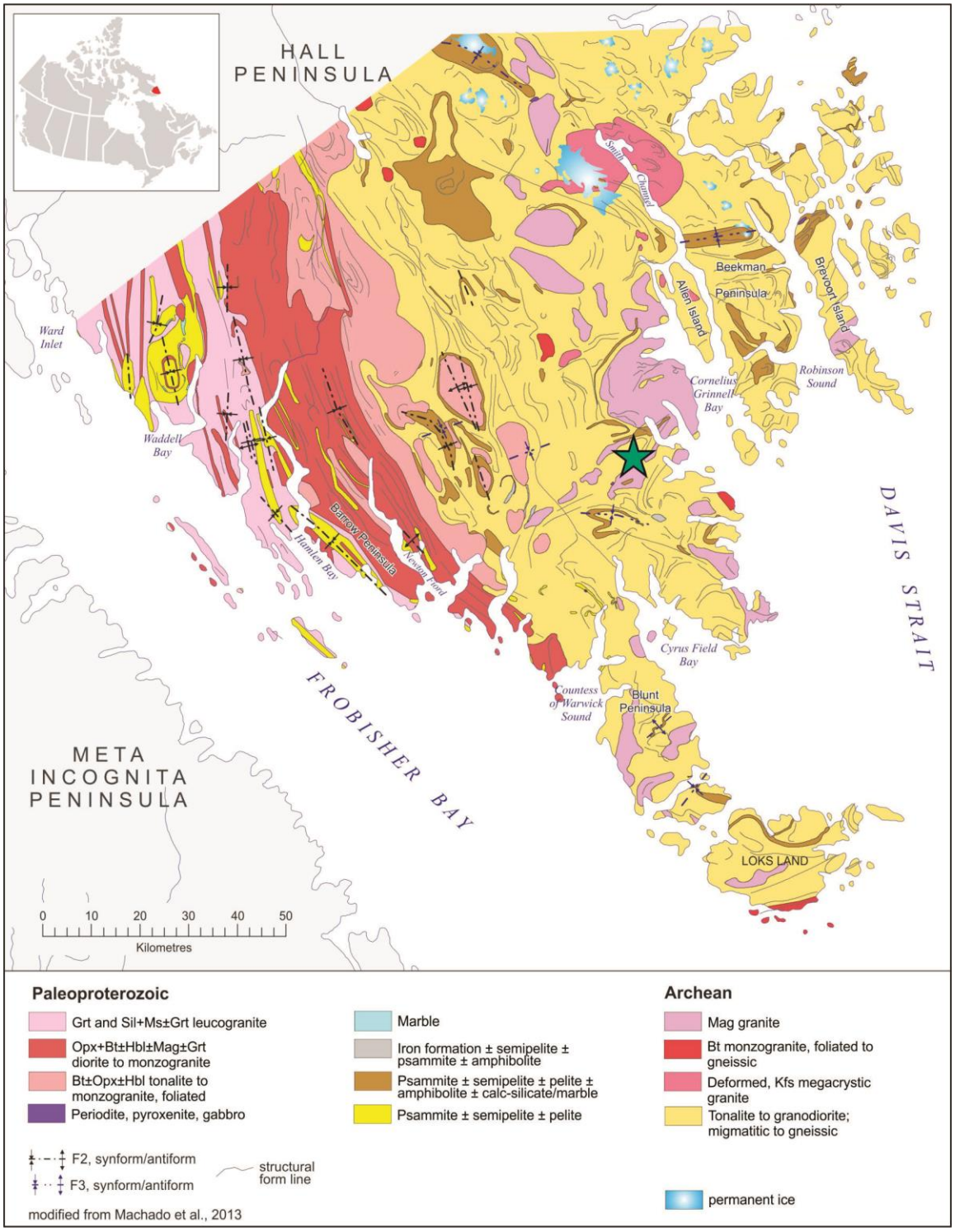

Figure 3.5 – Geology of southern Hall Peninsula from Machado et al. (2013). Green star indicates location of representative sample F140B1 (calc-alkaline).

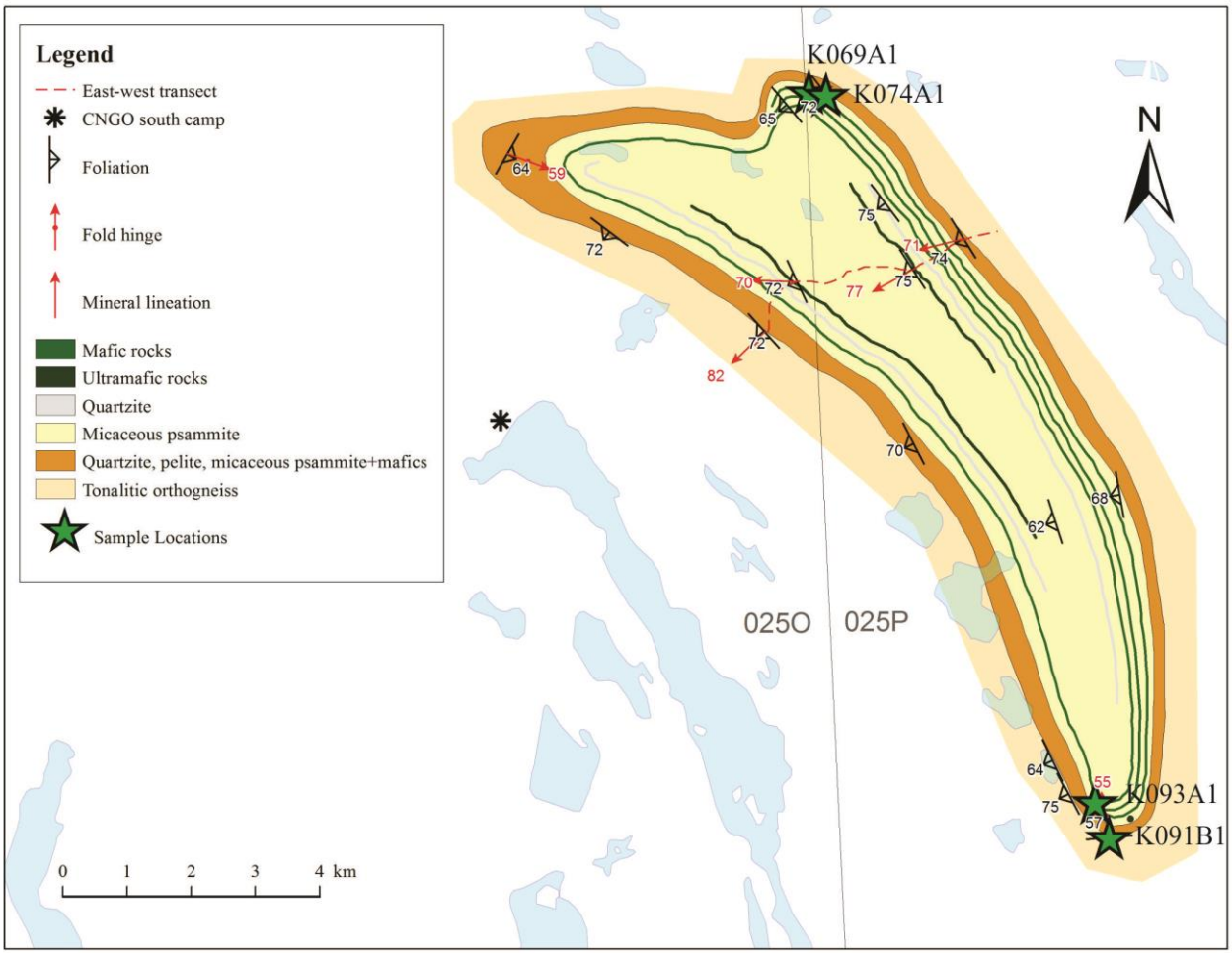

Figure 3.6 – Geology of QA showing location of representative samples K091B1 (alkaline), K093A1 (transitional), K069A1 (tholeiitic), and K074A1 (ultramafic).

3.3.3 Trace Element Profiles

Trace element profiles normalized to NMORB (Sun and McDonough, 1989) are shown in Figure 3.7a-d for all four basaltic sub-groups. With the exception of two alkaline basalt samples, all other samples show a pronounced negative Nb anomaly with respect to Th and Ce typical of volcanic arcs and back arcs. The negative anomaly arises during subduction when Nb is fractionated from Th and Ce during dehydration of subducted crust. Nb is retained in amphibole and other minor minerals such as rutile and titanite while Th and Ce preferentially

enter the fluid phase (Pearce and Peate, 1995). In addition, the alkaline, calc-alkaline and to a lesser extent the transitional samples are enriched in the most incompatible elements relative to NMORB typical of within-plate basalts (Pearce, 1996). The tholeiitic samples are only enriched in the most incompatible elements while the rest of the trace element profile is flat. Ten samples have high $(Ti/Y)_N$ ratios (2.4-5.0) suggesting the involvement of residual garnet during the melting process. Y has a significantly higher bulk distribution coefficient than Ti for melting of garnet lherzolite, and thus is selectively retained within residual garnet, resulting in elevated $(Ti/Y)_N$ in the melt phase (Pearce and Parkinson, 1993). The consistent and subtly different trends seen in the trace element normalized diagrams supports the earlier imposed sub-group classification scheme. Four samples from both the tholeiitic and transitional suites have been excluded from Figure 3.7 for cosmetic purposes. These samples do however, display the diagnostic traits described herein.

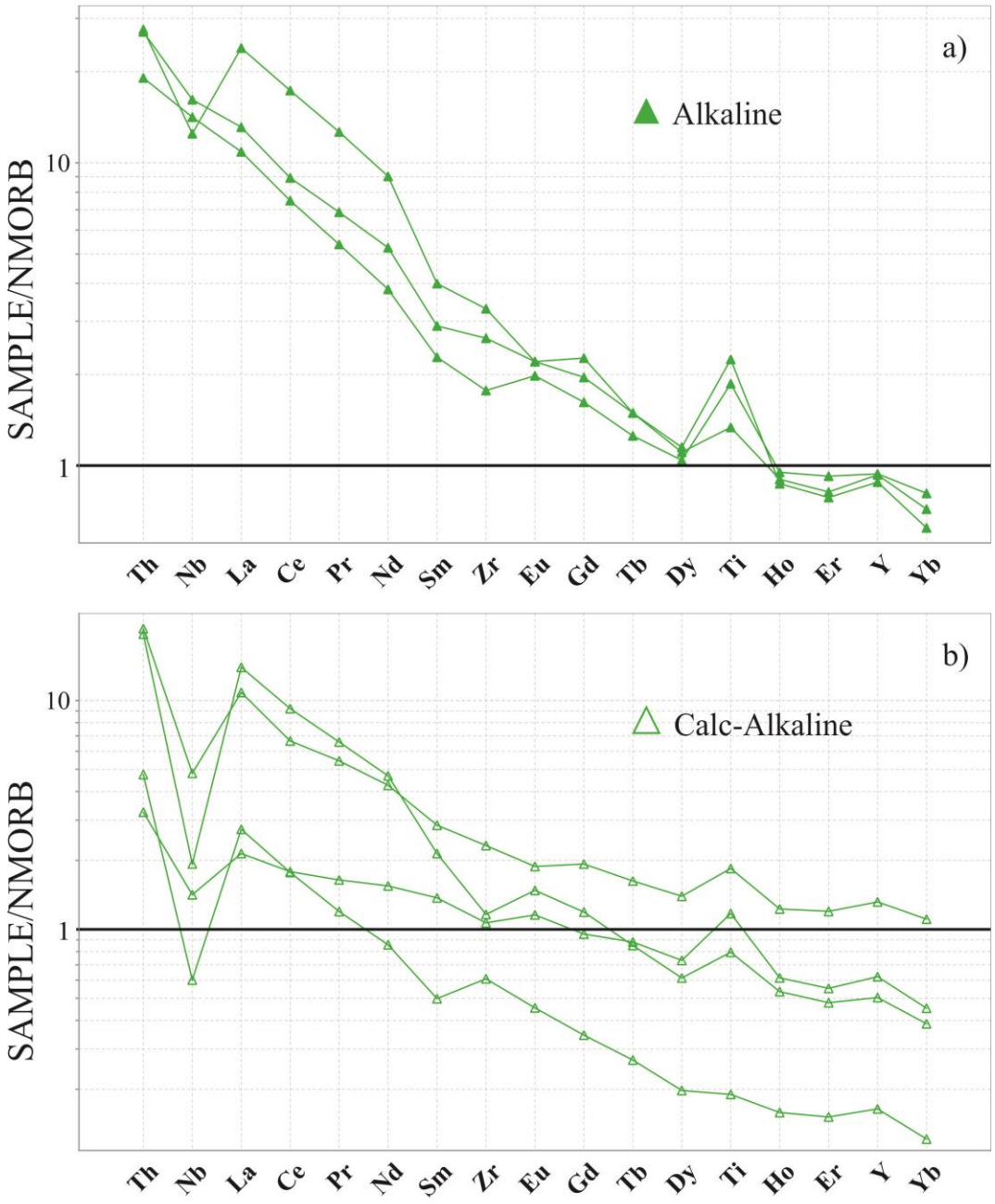

Figure 3.7 – Trace element diagrams normalized to NMORB (Sun and McDonough, 1989) of a) Alkaline basalt composition, b) calc-alkaline basalt composition.

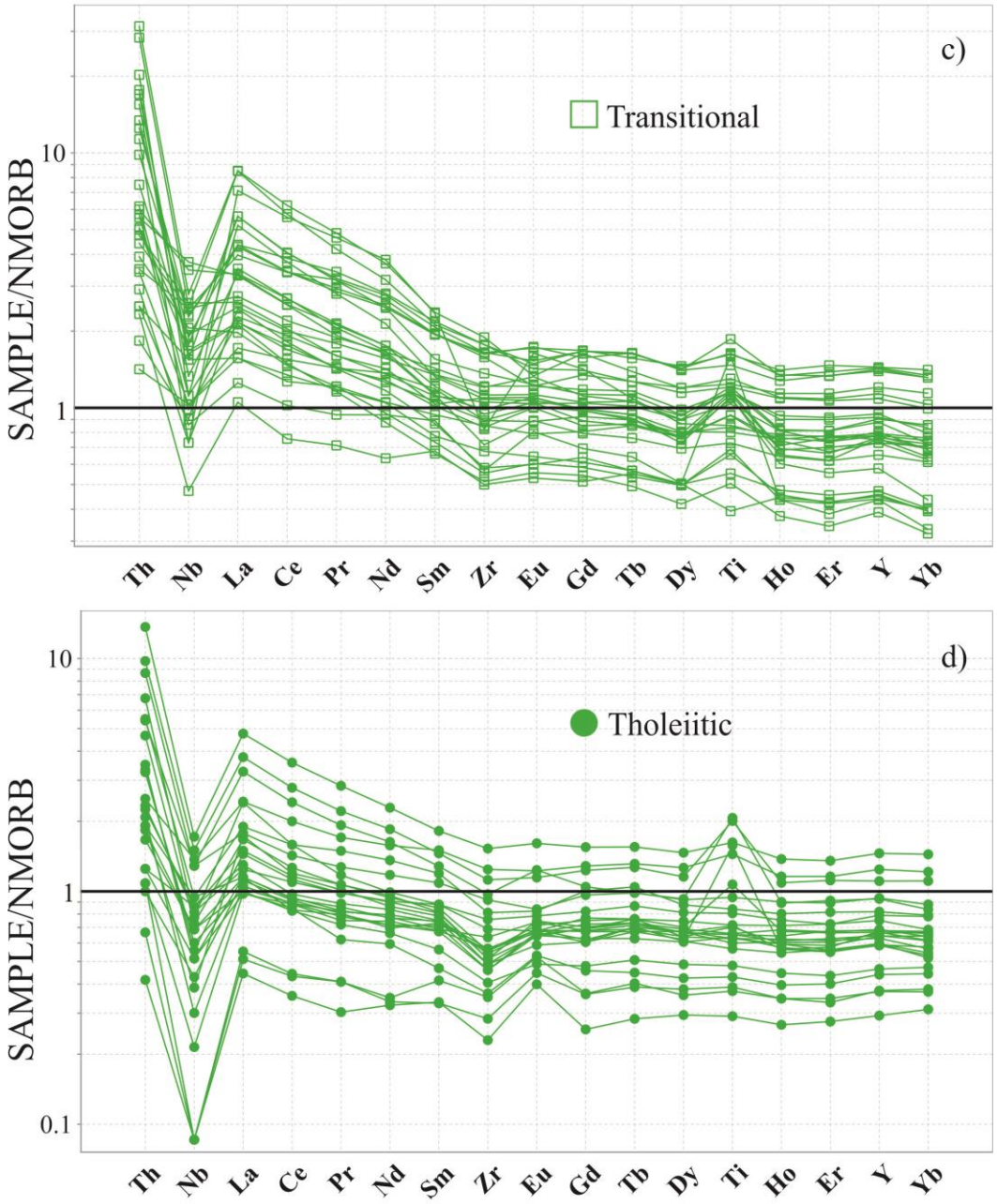

Figure 3.7 continued – Trace element diagrams normalized to NMORB (Sun and McDonough, 1989) of c) transitional basalt composition and d) tholeiitic basalt composition.

3.3.4 Tectonic Discrimination

Tectonic discrimination diagrams are derived from geochemical datasets of rocks whose tectonic setting is known with certainty. Most samples are taken from modern environments,

and as such their accuracy and applicability – especially to rocks older than the Phanerozoic – is contentious (Pearce, 1973, 2008). That being said, tectonic discrimination diagrams can be used to identify chemical variations in similar rock types and form the basis for interpreting processes that give rise to identified differences. Samples plotted on the Th-Zr-Nb tectonic discrimination diagram (Wood, 1980) reveal a large scatter, but plot with some noticeable trends (Figure 3.8). The tholeiitic samples tend to concentrate in volcanic arc and N-MORB like fields (VAB CAB, NMORB, Trans NMORB WPT); all but one of the calc-alkaline samples plot within the volcanic arc – calc alkaline basalt (VAB CAB) field; all but one of the alkaline samples plot within the alkaline – within plate basalt (Alk WPB) field; and the transitional samples show the highest degree of scatter. The Wood (1980) tectonic discrimination diagram utilizes trace elements (Ta, Hf) not employed for mafic rock classification in this thesis, so the consistency of trends within the imposed mafic-rock sub-groups continues to add validity to their selection.

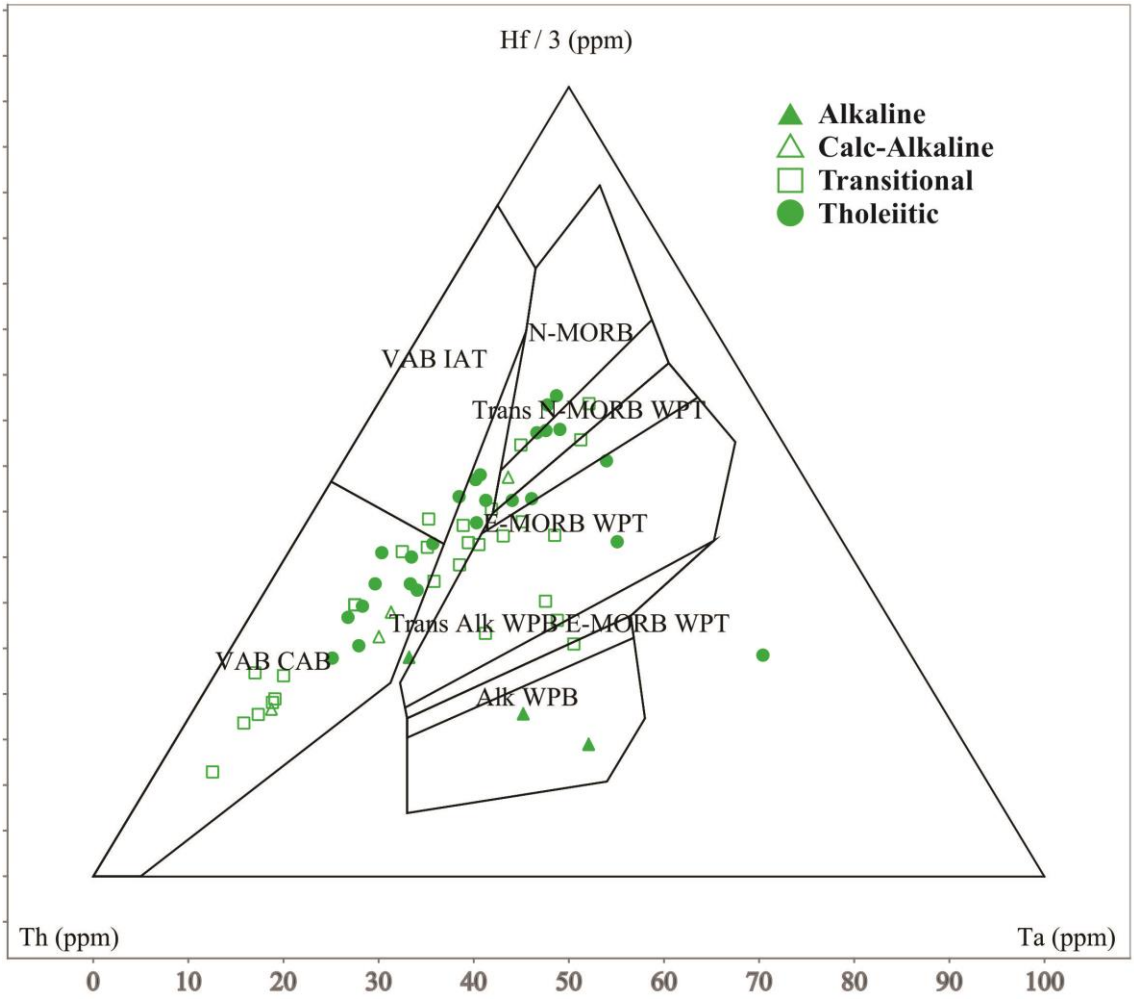

Figure 3.8 – Tectonic discrimination ternary diagram (Wood, 1980). Alk WPB – alkali within plate basalt; E-MORB WPT – enriched mid-ocean ridge basalt within plate transition; N-MORB – normal mid-ocean ridge basalt; Trans N-MORB WPT – transitional normal mid-ocean ridge basalt within plate transition; Trans Alk WPB E-MORB WPT – transitional alkali within plate basalt enriched mid-ocean ridge within plate transition; VAB CAB – volcanic arc basalt calc-alkaline basalt; VAB IAT – volcanic arc basalt island arc transition.

3.3.5 Ultramafic Rocks

Ultramafic rocks on the Hall Peninsula are scarce, occurring as isolated enclaves across the Hall Peninsula (Figures 3.1a and b). Ultramafic rocks were identified in the field based on mineral composition – containing mafic minerals, with less than 10% plagioclase and no visible

quartz. Geochemically, total silica is not less than 45% in all cases (Appendix 2) which is higher than expected, but silica concentration does not likely reflect a primary composition.

Ultramafic rocks have commonly undergone intense hydrothermal alteration. In many cases this hydrothermal alteration has resulted in the formation of talc and serpentine. These altered ultramafic rocks are being evaluated for use by Inuit artisans as a carving stone (Beauregard et al., 2013; Senkow, 2013; and Steenkamp et al., 2014).

Fresh unaltered ultramafic rocks are present, but in very low volume. Enclaves range in size from one meter to hundreds of meters in diameter. Enclaves are present in all regions of Hall Peninsula and were sampled for geochemical analysis (Figures 3.1a and b). Many enclaves comprise of olivine cumulates intercalated with pyroxenite cumulates (Figure 3.9).

Figure 3.9 – Olivine cumulate intercalated with pyroxenite cummulate. Photo taken approximately 1km southeast along strike from sample K074A1 (Figure 3.5) and is interpreted as the extension of the same unit.

The geochemical classification of ultramafic rocks is poorly constrained and poorly understood. Figure 3.10a shows trace element profiles for ultramafic rocks normalized to NMORB (Sun and McDonough, 1989). Like the mafic samples, all ultramafics except sample K127B1 (3 on Figure 3.10a) show a negative Nb anomaly with respect to Th and Ce suggesting a volcanic arc source. All samples (1-5 on Figure 3.10 a), with the exception of B045A1 have flat, slightly depleted profiles. B045A1 (6 on Figure 3.10a) displays a negative slope and strong depletion in to more compatible elements.

Based on the cation-percentage ternary geochemical classification scheme of Jenson (1976) (Figure 3.10b) two samples plot as ultamafic komatiites, three as basaltic komatiites and one plots as a high-Mg tholeiitic basalt. The Jenson (1976) cation percentage ternary plot does not – with the exception of Al_2O_3 – use elements considered to be immobile during secondary alteration processes such as deformation and metamorphism and so must be regarded with skepticism. Ultramafic rock names are therefore better determined based on their mineralogy which is discussed in Section 3.4.6 below.

Plotting of ultramafic geochemical data on discrimination diagrams designed for mafic rocks is sometimes practised because of a lack of any alternative, but will not be undertaken for this thesis. For the complete ultramafic geochemical dataset, see Appendix 2.

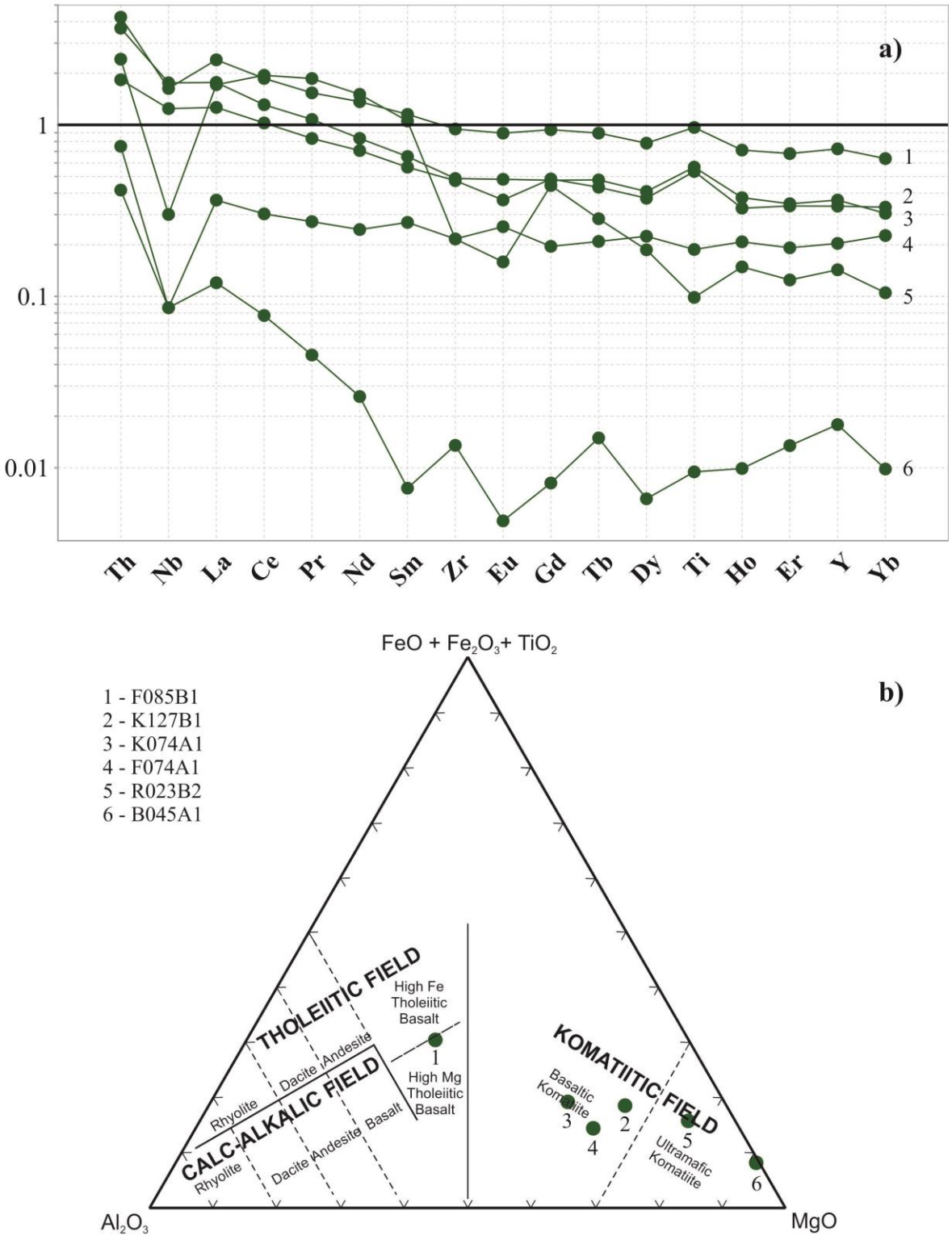

Figure 3.10 – a) Trace element diagram normalized to NMORB (Sun and McDonough, 1989) of ultramafic samples. b) Ternary plot which uses cation % to classify sub-alkalic rocks after Jenson (1976). Corresponding samples in both a) and b) are numbered for comparison.

3.4 Mineral Chemistry and Petrography

3.4.1 Introduction

The four samples from the QA, one tholeiitic (K069A1), one transitional (K093A1), one alkaline (K091B1), and one ultramafic (K074A1), that served as representative geochemical samples (Section 3.3) were also studied both petrographically and using electron microprobe analysis in order to better characterize the rocks in this important area. As indicated in Chapter 2 above, all samples have been subjected to amphibolite-grade conditions or higher and as such, mineral assemblages are metamorphic, not primary. Therefore, normative mineral calculations have been made in cases where mineralogical classifications are employed. The samples were analyzed using wavelength dispersive electron microprobe analysis (EMPA) at the University of Saskatchewan Department of Geological Sciences on a JEOLJXA-8600 microprobe. The analytical procedures are described in detail in Section 2.4.1. Each sample is treated as being representative of the geochemical sub-group for which it is named, however, deviations from the type-sample-mineralogy exist within each sub-group. The results of electron microprobe analysis will be presented first, followed by a detailed description of the petrography and EMPA mineral classification for each mafic and ultramafic sub-group.

3.4.2 Electron microprobe results

The tholeiites, transitional and alkaline mafic rocks are composed primarily of plagioclase and amphibole. A single sample from each sub-group was analyzed using EMPA. The alkaline sample analyzed also contains clinopyroxene. The mineral chemistry for K069A1 (tholeiite), K093A1 (transitional), and K091B1 (alkaline) is displayed in Tables 3.1 to 3.3,

respectively. The ultramafic sample is composed primarily of amphibole, orthopyroxene and olivine. The mineral chemistry for K074A1 is displayed in Table 3.4.

Table 3.2 - Mineral compositons for sample K069A1 tholeiitic basalt

Site	1	2	3	4	1	2	3	4
Mineral	Amp	Amp	Amp	Amp	Pl	Pl	Pl	Pl
SiO_2	46.50	46.75	46.78	47.04	55.75	55.31	55.68	55.02
TiO_2	1.0289	1.2348	0.8589	0.8804	0.0039	0.0000	0.0091	0.0104
Al_2O_3	9.00	8.50	8.04	8.42	27.92	27.48	27.84	27.64
Cr_2O_3	0.0563	0.0465	0.1519	0.1254	-	-	-	-
FeO	13.86	14.03	13.66	13.15	-	-	-	-
Fe_2O_3	-	-	-	-	0.0411	0.0633	0.0145	0.0170
MgO	12.39	13.30	13.67	13.66	0.0134	0.0000	0.0014	0.0000
MnO	0.2372	0.2275	0.2190	0.2267	-	-	-	-
CaO	11.80	11.78	11.88	11.69	10.70	10.50	10.71	10.71
BaO	-	-	-	-	0.0000	0.0000	0.0207	0.0209
Na_2O	1.2618	1.2952	1.1209	1.1997	5.65	5.90	5.71	5.61
K_2O	0.2736	0.2720	0.2405	0.2324	0.0595	0.0363	0.0843	0.0614
Cl	0.0000	0.0074	0.0005	0.0055	-	-	-	-
Total	96.41	97.44	96.62	96.62	100.15	99.30	100.08	99.09
Number of cations on the basis of 23O for Amp and 32O for Pl								
Si	6.908	6.882	6.873	6.944	10.027	10.041	10.027	10.009
Ti	0.1149	0.1367	0.0970	0.0977	0.0005	0.0000	0.0012	0.0014
Al	1.5752	1.4749	1.4222	1.4641	5.9190	5.8790	5.9090	5.9270
Cr	0.0066	0.0054	0.0180	0.0146	-	-	-	-
Fe	1.7215	1.7272	1.7150	1.6230	0.0056	0.0086	0.0020	0.0023
Mg	2.7433	2.9175	3.0590	3.0050	0.0036	0.0000	0.0004	0.0000
Mn	0.0298	0.0284	0.0278	0.0283	-	-	-	-
Ca	1.8785	1.8577	1.9113	1.8494	2.0616	2.0426	2.0668	2.0866
Ba	-	-	-	-	0.0000	0.0000	0.0015	0.0015
Na	0.3634	0.3697	0.3263	0.3434	1.9712	2.0777	1.9953	1.9801
K	0.0518	0.0511	0.0461	0.0438	0.0137	0.0084	0.0194	0.0142
Cl	0.0000	0.0019	0.0001	0.0014	-	-	-	-

Table 3.3 - Mineral compositons for sample K093A1 transitional basalt

Site	1	2	3	4	5	1	2	3	4	5
Mineral	Amp	Amp	Amp	Amp	Amp	Pl	Pl	Pl	Pl	Pl
SiO_2	42.46	43.04	42.12	42.08	42.53	55.26	56.67	55.88	55.86	55.87
TiO_2	1.6726	1.3372	1.5133	1.5294	1.4973	0.0000	0.0102	0.0029	0.0000	0.0100
Al_2O_3	11.65	11.21	11.56	11.57	11.59	27.52	27.03	27.32	26.88	27.65
Cr_2O_3	0.0000	0.0145	0.0048	0.0000	0.0000	-	-	-	-	-
FeO	18.96	18.91	18.94	19.28	19.11	-	-	-	-	-
Fe_2O_3	-	-	-	-	-	0.0614	0.0404	0.0317	0.0334	0.0093
MgO	8.40	8.81	8.77	8.70	8.64	0.00	0.00	0.01	0.00	0.01
MnO	0.2999	0.3391	0.2738	0.3355	0.3174	-	-	-	-	-
CaO	11.21	11.43	11.41	11.34	11.33	10.81	10.57	10.78	10.31	10.80
BaO	-	-	-	-	-	0.0000	0.0048	0.0000	0.0000	0.0124
Na_2O	1.3711	1.2872	1.3939	1.4478	1.4038	5.5600	5.5200	5.5800	5.7800	5.5600
K_2O	0.9334	0.8092	0.8523	0.8864	0.9619	0.1489	0.1766	0.1577	0.1658	0.0147
Cl	0.0101	0.0126	0.0083	0.0190	0.0137	-	-	-	-	-
Total	96.97	97.20	96.85	97.17	97.39	99.36	100.02	99.76	99.03	99.93
Number of cations on the basis of 23O for Amp and 32O for Pl										
Si	6.4840	6.5490	6.4490	6.4350	6.4770	10.0290	10.1890	10.0920	10.1550	10.0650
Ti	0.1921	0.1530	0.1742	0.1759	0.1715	0.0000	0.0014	0.0004	0.0000	0.0014
Al	2.0970	2.0105	2.0858	2.0851	2.0795	5.8870	5.7280	5.8160	5.7580	5.8700
Cr	0.0000	0.0017	0.0006	0.0000	0.0000	-	-	-	-	-
Fe	2.4217	2.4058	2.4253	2.4654	2.4333	0.0084	0.0055	0.0043	0.0046	0.0013
Mg	1.9129	1.9977	2.0022	1.9828	1.9608	0.0012	0.0005	0.0035	0.0005	0.0026
Mn	0.0388	0.0437	0.0355	0.0435	0.0409	-	-	-	-	-
Ca	1.8349	1.8627	1.8712	1.8575	1.8484	2.1029	2.0358	2.0860	2.0086	2.0842
Ba	-	-	-	-	-	0.0000	0.0003	0.0000	0.0000	0.0009
Na	0.4060	0.3797	0.4138	0.4293	0.4144	1.9558	1.9240	1.9535	2.0358	1.9405
K	0.1818	0.1571	0.1665	0.1729	0.1868	0.0345	0.0405	0.0363	0.0385	0.0034
Cl	0.0026	0.0032	0.0022	0.0049	0.0035	-	-	-	-	-

Table 3.4 - Mineral compositons for sample K091B1 Alkali basalt

Site	1	2	3	4	5	1	2	3	4	5	1	2	3	4	5
Mineral	Amp	Amp	Amp	Amp	Amp	Cpx	Cpx	Cpx	Cpx	Cpx	Pl	Pl	Pl	Pl	Pl
SiO_2	47.64	45.13	45.85	44.02	45.5	51.18	51.39	51.77	50.99	51.53	46.59	44.9	46.55	46.17	46.63
TiO_2	0.7982	1.1967	1.0205	1.2024	1.0729	0.1169	0.2375	0.1568	0.1725	0.1185	0.0000	0.0002	0.0135	0.0006	0.0056
Al_2O_3	8.41	9.86	9.51	10.36	9.83	1.2189	1.8087	1.4839	1.6205	1.2853	33.56	34.25	33.71	33.82	33.56
Cr_2O_3	0.0999	0.1117	0.0752	0.1046	0.1753	0.0619	0.0569	0.0248	0.0421	0.0893	-	-	-	-	-
FeO	14.85	15.73	16.47	15.47	15.31	9.33	9.89	9.46	9.39	9.5	-	-	-	-	-
Fe_2O_3	-	-	-	-	-	-	-	-	-	-	0.2005	0.2053	0.1823	0.1425	0.1126
MgO	12.67	11.16	11.26	11.4	11.58	13.01	12.3	12.81	12.55	12.57	0.0058	0.0056	0	0	0.0049
MnO	0.2115	0.2106	0.2912	0.2003	0.2474	0.3325	0.3161	0.3163	0.3303	0.2654	-	-	-	-	-
CaO	12.17	11.81	11.91	11.97	11.89	23.37	23.12	23.1	23.09	23.24	18.5	19.02	18.52	18.69	18.51
BaO	-	-	-	-	-	-	-	-	-	-	0.0000	0.0000	0.0107	0.0029	0.0000
Na_2O	0.8651	1.0773	0.9554	1.0960	1.1360	0.2148	0.2824	0.2314	0.2304	0.2060	1.0864	0.7336	1.0153	0.8989	1.0272
K_2O	0.4110	0.6232	0.5620	0.5715	0.5481	0.0179	0.0000	0.0000	0.0000	0.0027	0.0144	0.0052	0.0194	0.0078	0.0169
Cl	0.0000	0.0094	0.0020	0.0047	0.0028	0.0000	0.0050	0.0104	0.0000	0.0000	-	-	-	-	-
Total	98.13	96.91	97.91	96.4	97.29	98.85	99.41	99.36	98.42	98.81	99.96	99.11	100.01	99.74	99.87
Number of cations on the basis of 23O for Amp, 6O for Cpx, and 32O for Pl															
Si	6.9750	6.7540	6.8040	6.6330	6.7660	1.9498	1.9475	1.9575	1.9491	1.9614	21.78	20.99	21.76	21.58	21.79
Ti	0.0879	0.1347	0.1139	0.1363	0.1200	0.0034	0.0068	0.0045	0.0050	0.0034	0.0000	0.0001	0.0081	0.0004	0.0034
Al	1.4504	1.7399	1.6632	1.8391	1.7235	0.0547	0.0808	0.0661	0.0730	0.0577	17.76	18.12	17.84	17.9	17.76
Cr	0.0116	0.0132	0.0088	0.0125	0.0206	0.0019	0.0017	0.0007	0.0013	0.0027	-	-	-	-	-
Fe	1.8182	1.9687	2.0436	1.9494	1.9038	0.2973	0.3133	0.2991	0.3002	0.3024	0.1402	0.1436	0.1275	0.0996	0.0788
Mg	2.7658	2.4885	2.4911	2.5613	2.5667	0.7385	0.6950	0.7221	0.7153	0.7134	0.0035	0.0034	0.0000	0.0000	0.0030
Mn	0.0262	0.0267	0.0366	0.0256	0.0312	0.0107	0.0101	0.0101	0.0107	0.0086	-	-	-	-	-
Ca	1.9093	1.8933	1.8944	1.9320	1.8946	0.9539	0.9388	0.9359	0.9457	0.9479	13.22	13.59	13.23	13.36	13.23
Ba	-	-	-	-	-	-	-	-	-	-	0.0000	0.0000	0.0095	0.0026	0.0000
Na	0.2456	0.3126	0.2749	0.3202	0.3275	0.0159	0.0208	0.0170	0.0171	0.0152	0.8060	0.5442	0.7532	0.6669	0.7620
K	0.0768	0.1190	0.1064	0.1099	0.1040	0.0009	0.0000	0.0000	0.0000	0.0001	0.0120	0.0043	0.0161	0.0065	0.0140
Cl	0.0000	0.0024	0.0005	0.0012	0.0007	0.0000	0.0003	0.0007	0.0000	0.0000	-	-	-	-	-

Table 3.5 - Mineral compositions for sample K074A1

Site	1	2	3	4	1	2	3	4	1	2	3	4
Mineral	Amp	Amp	Amp	Amp	Ol	Ol	Ol	Ol	Opx	Opx	Opx	Opx
SiO_2	45.38	44.67	47.46	47.29	37.44	36.65	37.46	37.59	53.72	54.05	54.62	54.17
TiO_2	0.5793	0.8495	0.7034	0.6261	0.0000	0.0000	0.0000	0.0000	0.0187	0.0568	0.0109	0.0424
Al_2O_3	11.3600	12.2300	11.6600	11.5600	0.0000	0.0000	0.0022	0.0000	1.5610	2.3197	2.3550	2.0992
Cr_2O_3	0.2303	0.2549	0.2973	0.2575	0.0262	0.0000	0.0015	0.0193	0.0320	0.0288	0.0649	0.0384
FeO	5.96	6.62	6.81	6.78	25.16	23.66	25.08	23.94	15.49	15.47	15.18	15.70
MgO	16.21	16.91	16.97	17.1	36.88	36.79	36.36	36.34	28.30	27.64	26.94	27.63
MnO	0.1000	0.1279	0.1073	0.1280	0.4020	0.3791	0.3967	0.3719	0.3434	0.4167	0.3988	0.4598
NiO	-	-	-	-	0.2701	0.1916	0.2071	0.2483	0.0260	0.0826	0.0376	0.0451
CaO	11.13	11.57	12.02	11.95	0.0000	0.0000	0.0015	0.0037	0.1635	0.2065	0.3089	0.1650
Na_2O	1.2570	1.3687	1.2276	1.2845	0.0000	0.0098	0.0000	0.0594	0.0000	0.0924	0.0000	0.0000
K_2O	0.2391	0.2214	0.2301	0.2452	-	-	-	-	-	-	-	-
Cl	0.0000	0.0118	0.0068	0.0000	-	-	-	-	-	-	-	-
Total	92.45	94.83	97.5	97.23	100.18	97.67	99.51	98.58	99.66	100.37	99.92	100.35
Number of cations on the basis of 23O for Amp and 32O for Pl												
Si	1.7621	1.7045	1.7550	1.7543	-	-	-	-	-	-	-	-
Ti	0.0169	0.0244	0.0196	0.0175	-	-	-	-	-	-	-	-
Al	0.5200	0.5498	0.5084	0.5055	-	-	-	-	-	-	-	-
Cr	0.0071	0.0077	0.0087	0.0076	-	-	-	-	-	-	-	-
Fe	0.1937	0.2111	0.2106	0.2103	-	-	-	-	-	-	-	-
Mg	0.9383	0.9618	0.9355	0.9454	-	-	-	-	-	-	-	-
Mn	0.0033	0.0041	0.0034	0.0040	-	-	-	-	-	-	-	-
Ca	0.4629	0.4731	0.4763	0.4750	-	-	-	-	-	-	-	-
Ba	-	-	-	-	-	-	-	-	-	-	-	-
Na	0.0946	0.1013	0.0880	0.0924	-	-	-	-	-	-	-	-
K	0.0118	0.0108	0.0109	0.0116	-	-	-	-	-	-	-	-
Cl	0.0000	0.0008	0.0004	0.0000	-	-	-	-	-	-	-	-

The mineral chemistry data was used to better characterize the major minerals present in each sample. The anorthite content of plagioclase was calculated for each of the representatve samples. The results are displayed in Figure 3.11.

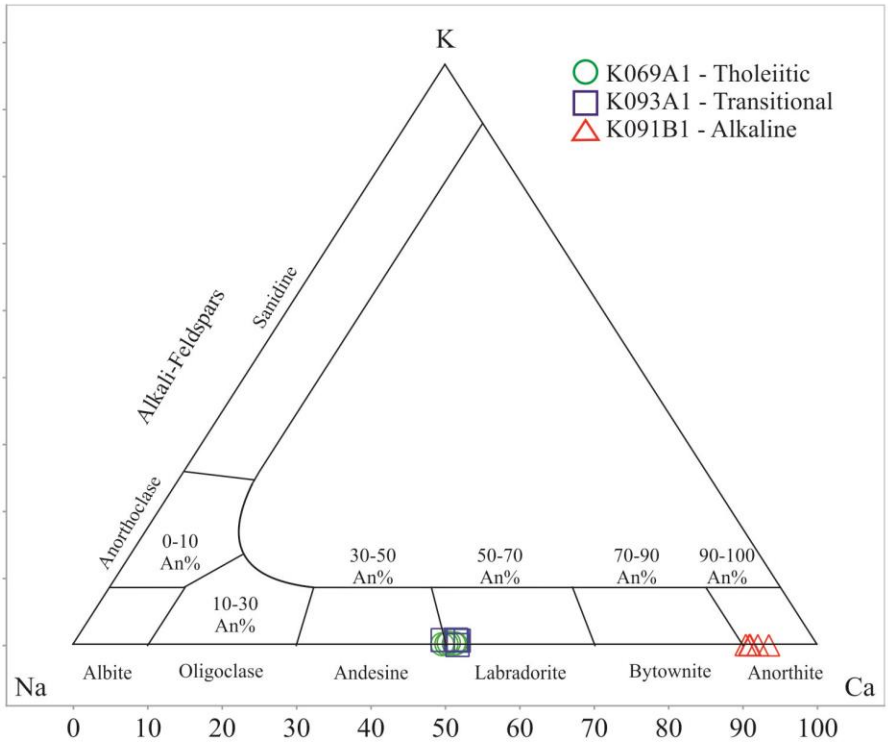

Figure 3.11 – Feldspar Ternary diagram showing the plagioclase composition of samples K069A1 (tholeiitic), K093A1 (transitional) and K091B1 (alkaline). Symbols for the sub-groups have been changed here for the sake of clarity.

Amphibole was classified based on the divisions and criteria proposed by Leake et al. (1997). For all samples, $Ca_B \geq 1.5$; $(Na + K)_A < 0.50$; and $Ca_A < 0.5$, where A are cations occupying the A sites and B are cations occupying the M4 sites based on the general form of the standard amphibole formula:

$$A_{0-1}\, B_2\, C_5^{VI}\, T_8^{IV}\, O_{22}\, (OH, F, Cl)_2 \qquad (3.3)$$

In accordance with the amphibole classifications of Leake et al. (1997) Figure 3.12 was used to classify the amphibole present in the mafic and ultramafic rocks.

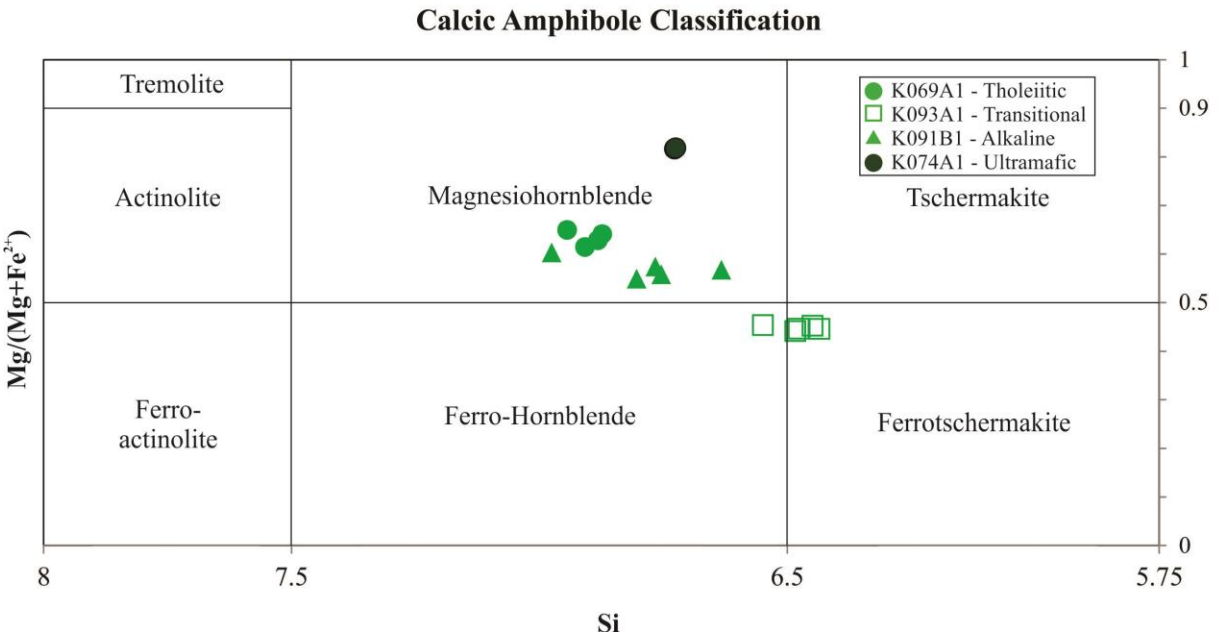

Figure 3.12 – Calcic amphibole classification of samples K069A1 (tholeiitic), K093A1 (transitional), K091A1 (alkaline) and K074A1 (ultramafic) after Leake et al. (1997). Location analyses 1 and 2 from sample K074A1 have been excluded due to low totals, but are consistent with calling them magnesiohornblende.

Clinopyroxene is present in the alkaline mafic rock analyzed whereas orthopyroxene is present in ultramafic rocks. Sample compositions were plotted on the pyroxene ternary diagram (Figure 3.13) using the PX-NOM script developed for Excel spreadsheets (Sturm, 2002) which uses the pyroxene classification criteria of Morimoto et al. (1988).

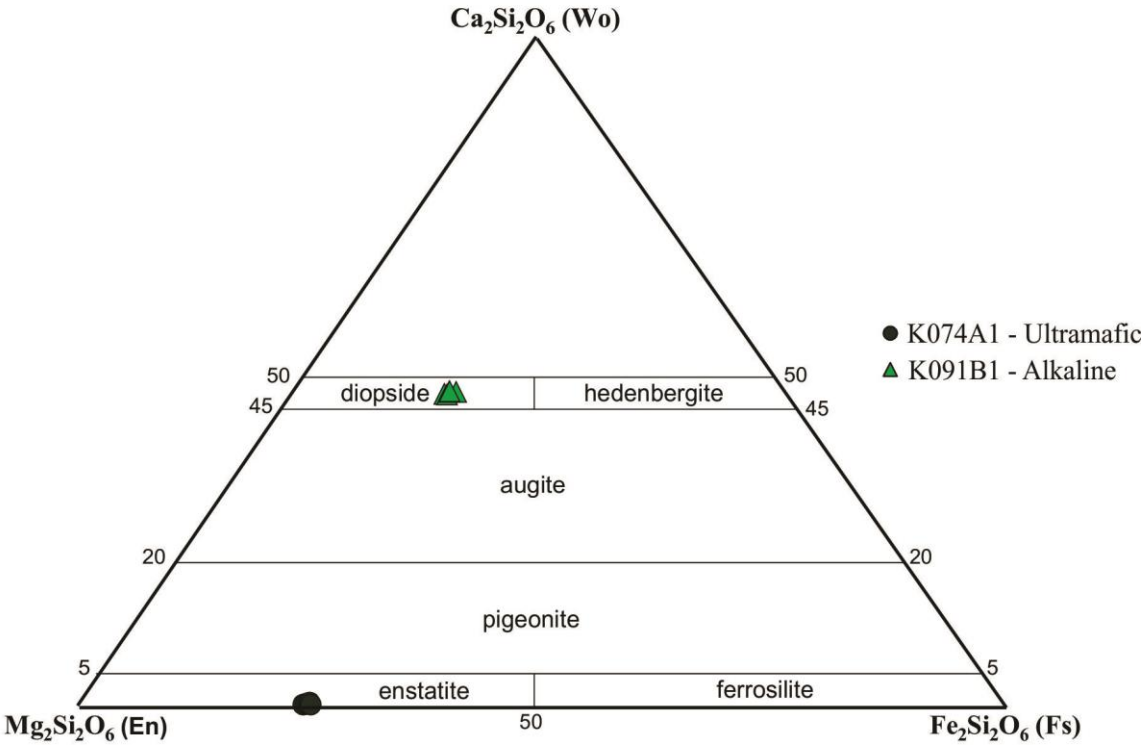

Figure 3.13 – Pyroxene ternary diagram displaying compositions of samples K074A1 (Ultramafic), and K091B1 (Alkaline) constructed using PX-NOM Excel spreadsheets (Sturm, 2002).

3.4.3 Petrography of tholeiites

The tholeiitic mafic rocks are composed dominantly of plagioclase and amphibole with these two minerals comprising approximately 40% and 55% of the rock, respectively (Figure 3.14a and b; and Figure 3.15).

No primary igneous textures are preserved as samples have recrystallized under amphibolite facies metamorphic conditions (Chapter 2.4). A strong S1 foliation defined by aligned amphibole is visible at outcrop scale but is difficult to see in the sample K069A1 thin section (Figure 3.14a and b; and Figure 3.15). The S1 foliation is visible in other tholeiitic thin sections defined by the preferential orientation and elongation of hornblende (Sample B118B1,

Figure 3.14c and d). Relict clinopyroxene, which does not occur in sample K069A1, is also present in sample B118B1 (Figure 3.14c and d).

EMPA studies indicate that the mineral species corresponding to these phases are An_{49-51} plagioclase (andesine/labradorite) (Figure 3.11); amphiboles occuring in tholeiitic mafic rocks are magnesiohornblende (Figure 3.12). Minor phases include apatite, ilmenite (Figure 3.14a and b; and Figure 3.15) and sphalerite.

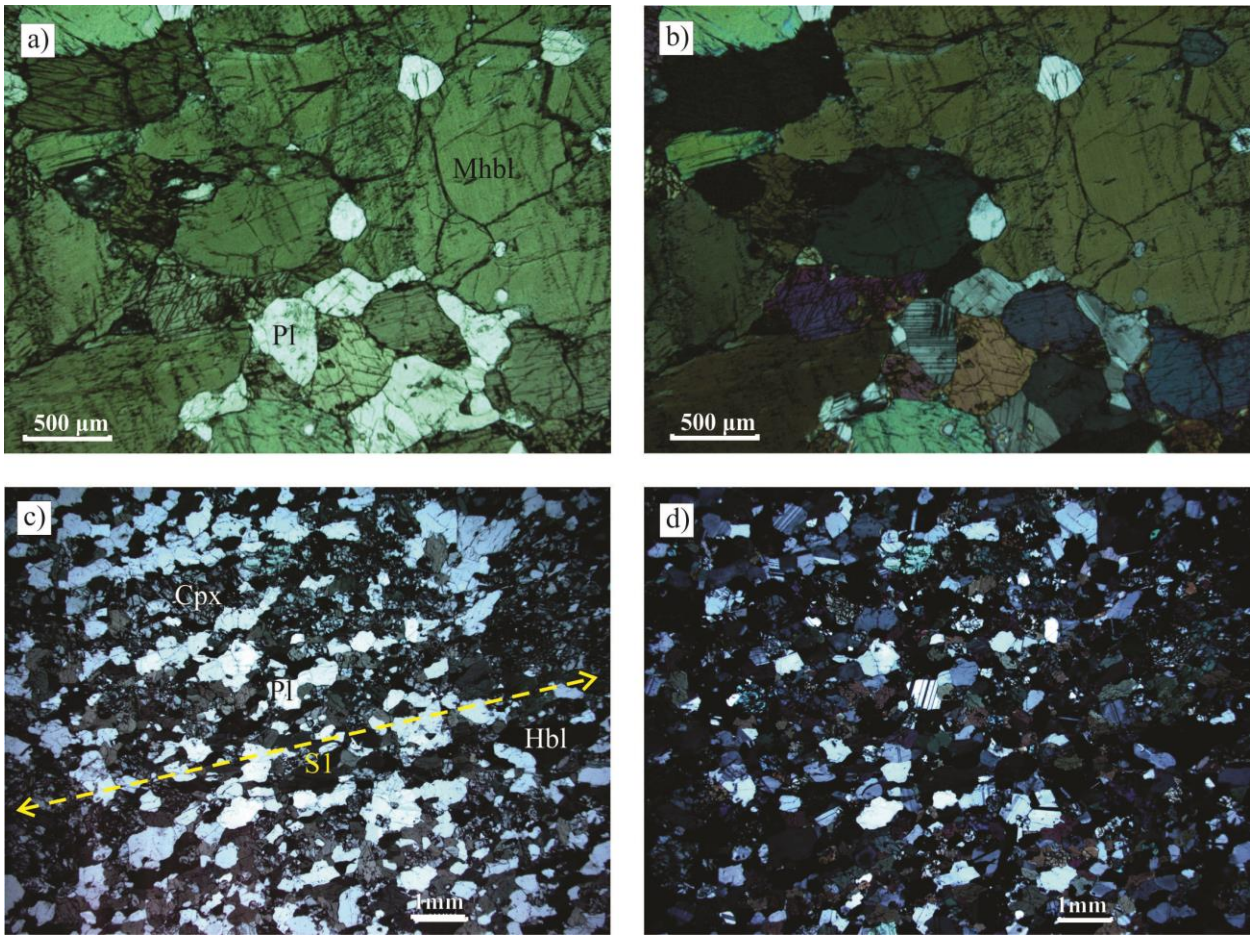

Figure 3.14 –a) Plane polarized light thin section image of K069A1. b) Crossed polarized light thin section image of a). c) Plane polarized light thin section image of tholeiitic sample B118B1 displaying S1 fabric. d) Crossed polarized light image of b). Ap – apatite; Ilm – ilmenite; Mhbl – magnesio-hornblende; Pl – plagioclase; T.O. – tear out.

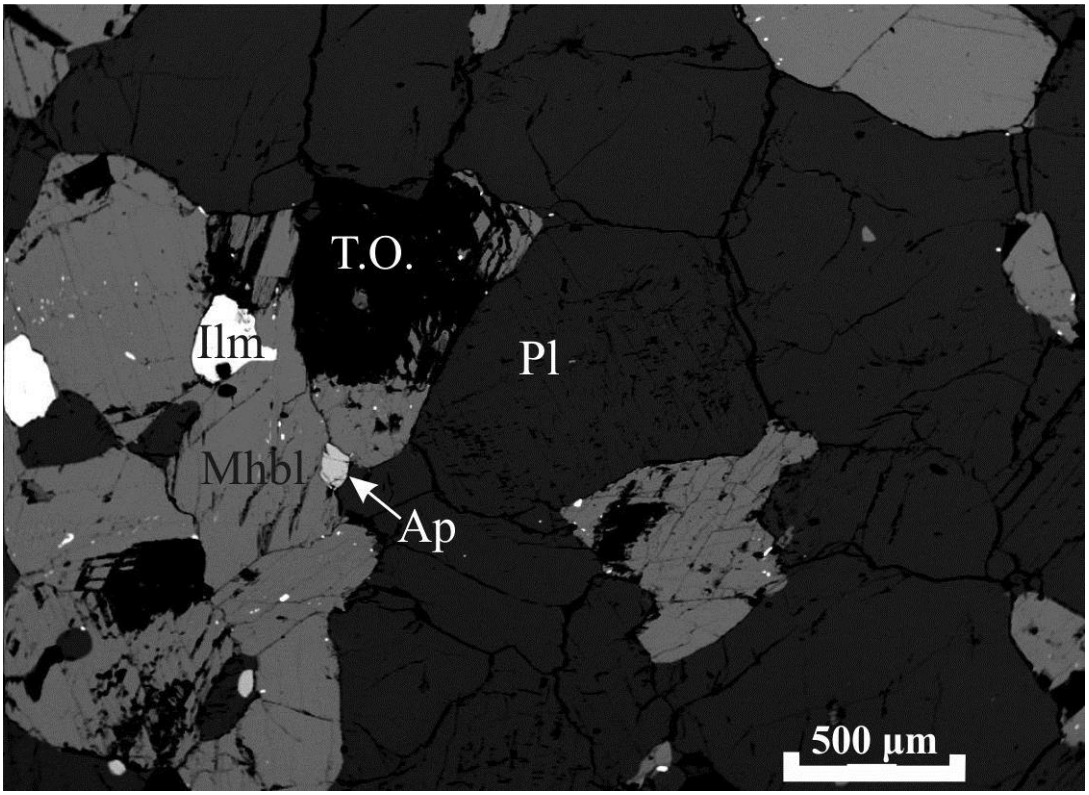

Figure 3.15 – Backscatter electron image of sample K069A1. Ap – apatite; Ilm – ilmenite; Mhbl – magnesio-hornblende; Pl – plagioclase; T.O. – tear out.

3.4.4 Petrography of transitional mafic rocks

Transitional mafic rocks are composed dominantly of plagioclase and amphibole with these two minerals occuring in roughly sub-equal proportions ammounting to approximately 95% of the total rock volume (Figures 3.16a and b; and Figure 3.17).

Minor phases include apatite, ilmenite and quartz (Figure 3.16a and b; and Figure 3.17). Similar to the tholeiitic mafic rocks, no primary igneous textures are preserved and the S1 foliation defined by aligned amphibole visible at outcrop scale is difficult to see in the sample K093A1 thin section (3.16a and b; and Figure 3.17). In other transitional mafic samples relict

clinopyroxene appears and the S1 fabric is more readily observable (Sample B070B1, Figure 3.16c and d).

EMPA analysis indicate a plagioclase composition of An_{49-51} (andesine/labradorite) (Figure 3.11); amphiboles are ferrohornblende and ferrotschermakite (Figure 3.12).

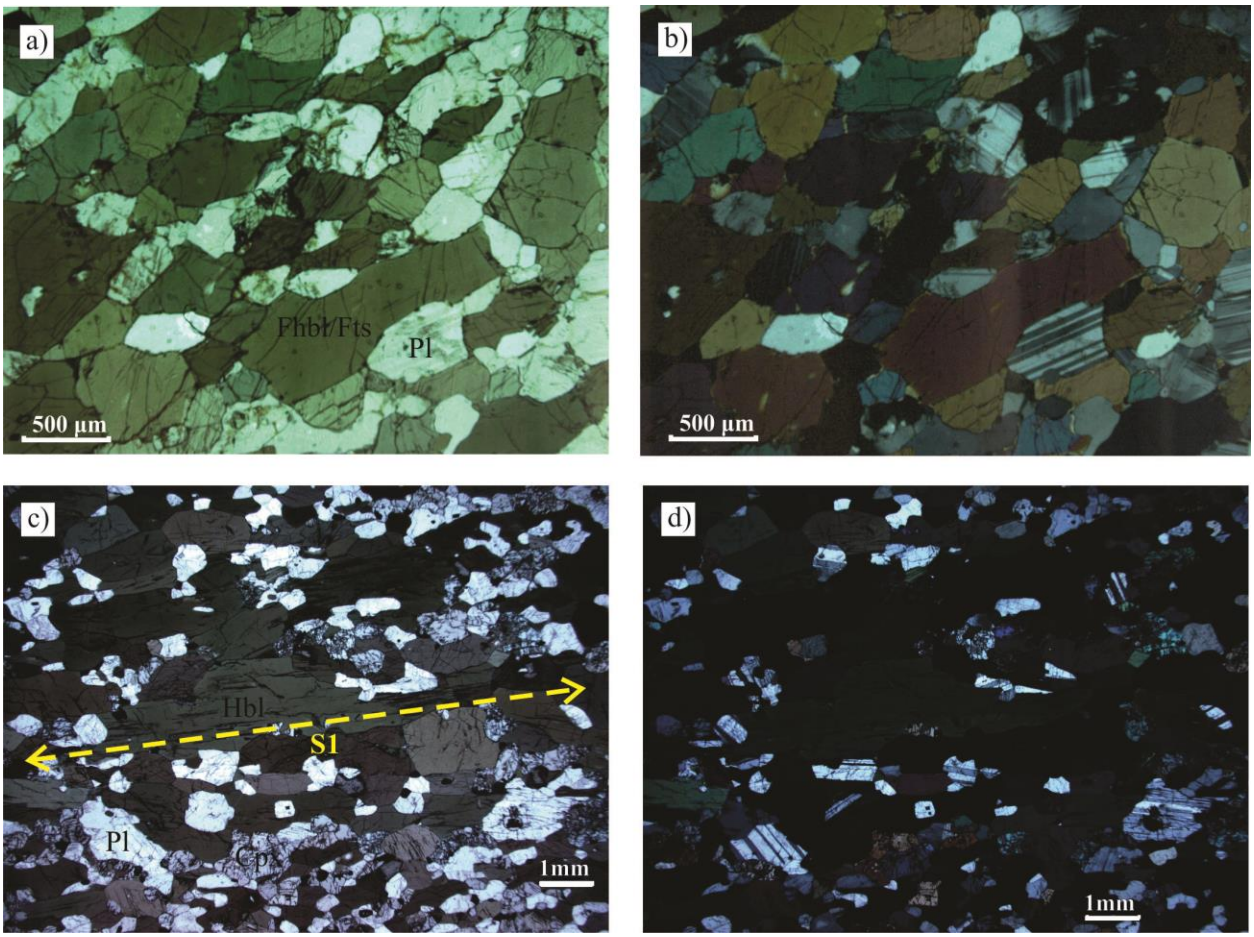

Figure 3.16 –a) Plane-polarized light thin section image of sample K093A1. b) Crossed- polarized light thin section image of a). c) Plane-polarized light thin section image of tholeiitic sample B070B1 displaying S1 fabric. d) Crossed-polarized light image of b) Fhbl/Fts – ferro-hornblende/ferro-tschermakitic hornblende; Ilm – ilmenite; Pl – plagioclase.

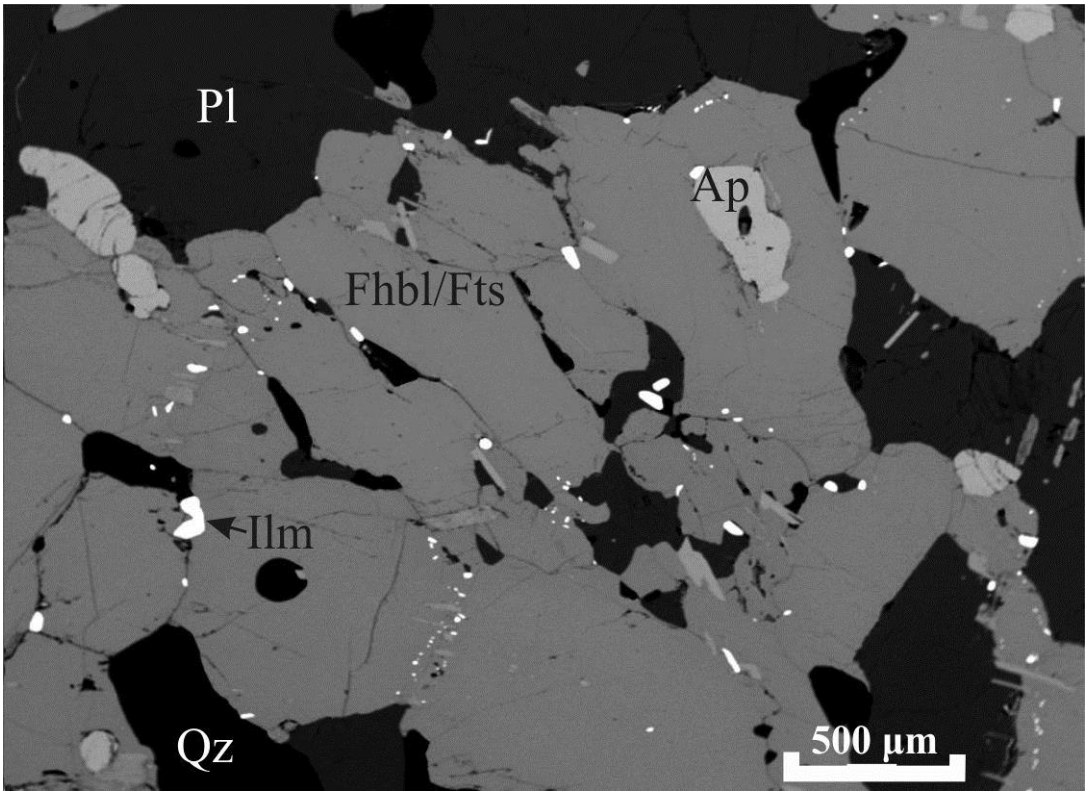

Figure 3.17 – Backscatter electron image of sample K093A1. Ap – apatite; Fhbl/Fts. – ferro-hornblende/ferro-tschermakitic hornblende; Ilm – ilmenite; Pl – plagioclase; Qz – quartz.

3.4.5 Petrography of calc-alkaline mafic rocks

Calc-alkaline mafic rocks are composed primarily of hornblende and plagioclase in sub-equal proportions totalling 95% of the total rock volume (Figure 3.18a and b). Relict clinopyroxene (Figure 3.18a and b) and minor phases apatite and ilmenite comprise the remainder. Electron microprobe analysis was not conducted on any calc-alkaline mafic samples so specific mineral names are not provided.

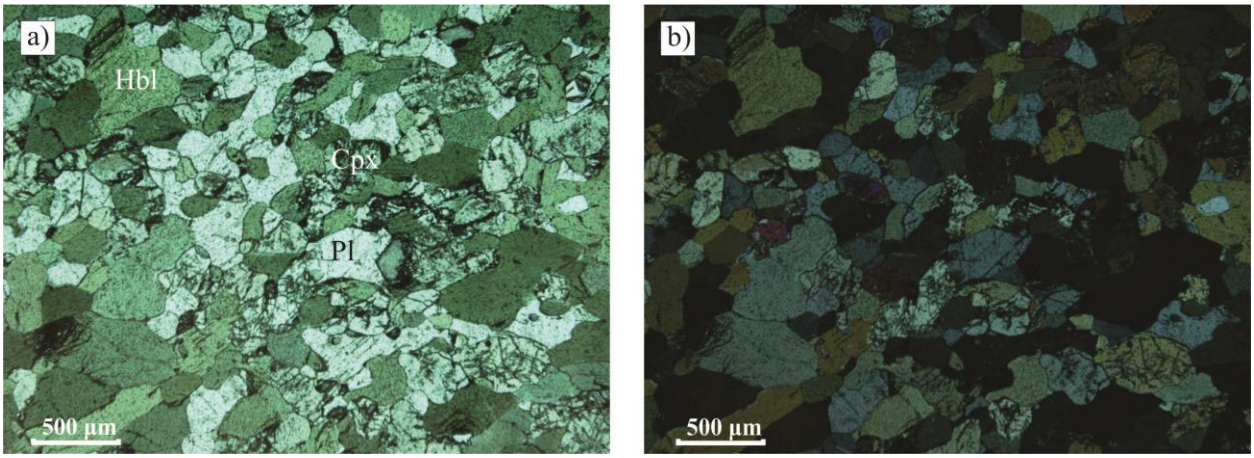

Figure 3.18 –Plane-polarized light thin section image of sample F140B1. b) Crossed-polarized light thin section image of a). Cpx – clinopyroxene; Hbl – Hornblende; Pl – plagioclase.

3.4.6 Petrography of alkaline mafic rocks

Alkaline mafic rocks are composed dominantly of magnesiohornblende (Figure 3.12) and anorthitic plagioclase (An_{90-93}) with these mineral species accounting for approximately 60% and 35% of the rock, respectively (Figure 3.19a-c). Relict igneous diopside (Figures 3.13, and 3.19a and b; and Figure 3.20) is present in sample K091B1. Other minor phases include ilmenite and apatite (Figure 3.20).

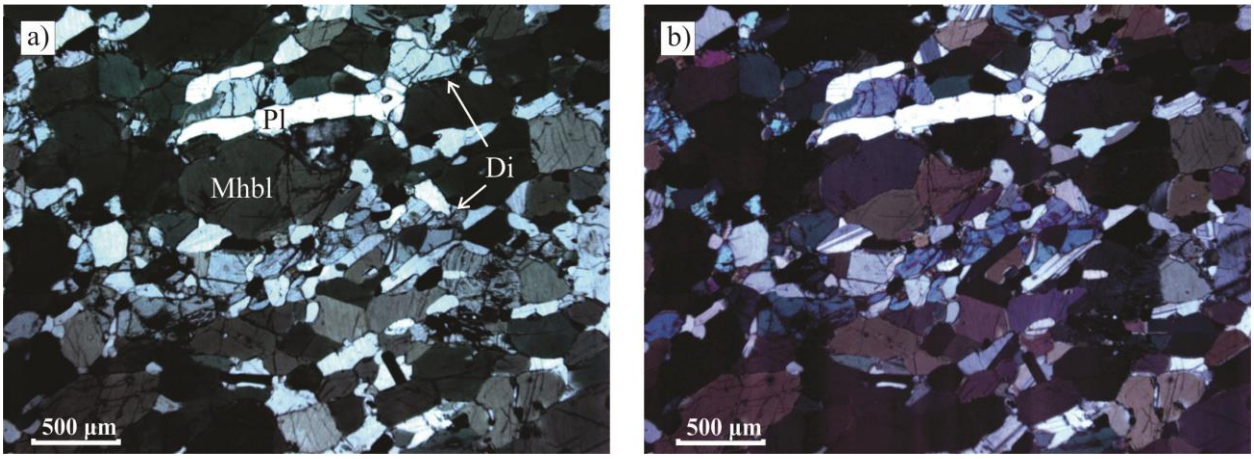

Figure 3.19 –Plane-polarized light thin section image of sample K091B1. b) Crossed-polarized light thin section image of a). Di – diopside; Mhbl – magnesiohornblende; Pl – plagioclase.

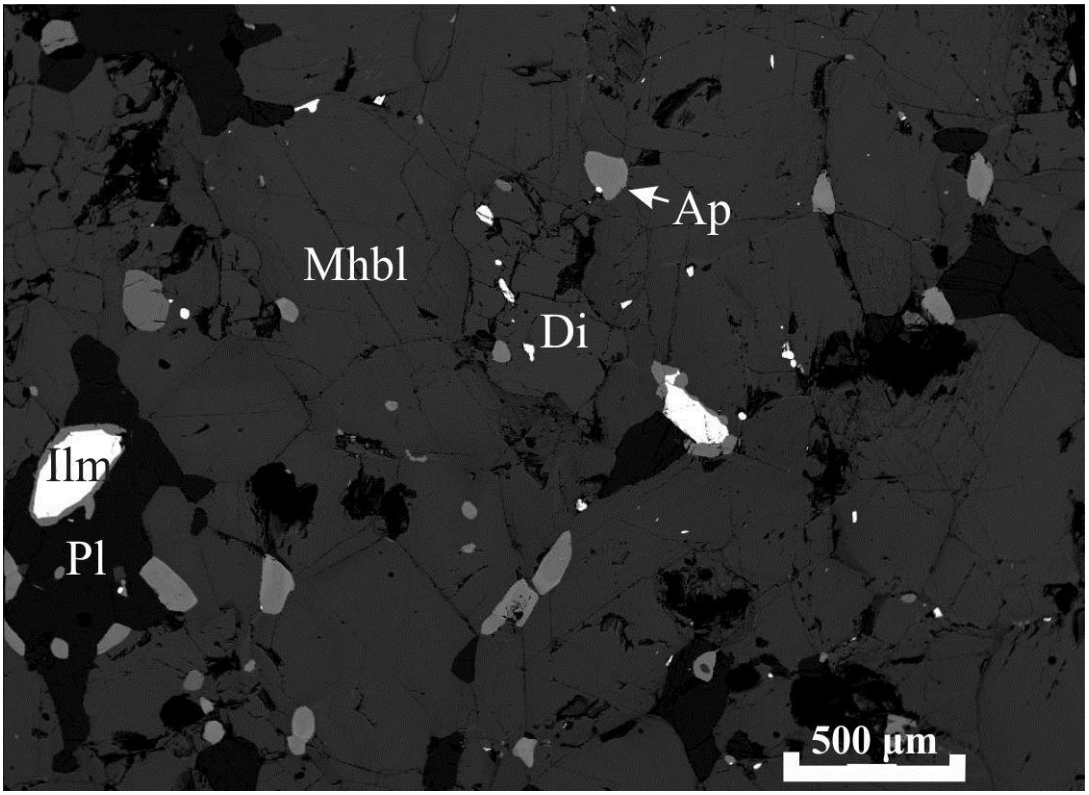

Figure 3.20 –Backscatter electron image of K091B1. Ap – apatite; Di – diopside; Ilm – ilmenite; Mhbl – magnesiohornblende; Pl – plagioclase.

3.4.7 Petrography of ultramafic rocks

The ultramafic rocks are quite variable in their mineralogy. Sample K074A1 comprises 20% olivine (Fo_{71-74}), 40% enstatite (Figure 3.13), 30% magnesiohornblende (Figure 3.12), 8% spinel, with the minor phases ilmenite and apatite making up the remainder (Figure 3.21a and b; and Figure 3.22. Sample K074A1 does not display serpentization of olivines, however sample K127B1, also from the QA, has the same mineralogy and shows minor serpentinization of olivine (Figure 3.21b and c). Some ultramafic rocks contain no olivine and are instead composed of orthopyroxene and clinopyroxene cumulates with interstitial plagioclase (Figure 3.21c and d). However, as indicated in Section 3.4.1 above, these are metamorphic mineral assemblages. Therefore normative mineral abundances have been calculated using Excel

spreadsheets developed by Hollocher (2014) (Table 3.6). Based on normative mineralogy, only one sample (B045A1) meets the <10% plagioclase threshold required for classification as an ultramafic rock under the IUGS classification scheme (Le Maitre et al., 2002). All rock names based on normative mineralogy and following the IUGS classification scheme (Le Maitre et al., 2002) are displayed in Table 3.6.

Table 3.6 - Normative mineralogy of ultramafic rocks

Sample	Qz	Pl	Or	Di	Hyp	Ol	Ilm	Mag	Hem	Ap	Ttn	Total	IUGS Name
B045A1	0.00	0.18	0.08	0.14	13.81	80.06	0.01	0.21	5.49	0.02	0.00	100.00	harzburgite
F085B1	13.54	46.41	0.07	11.55	15.91	0.00	0.42	0.00	9.97	0.02	2.10	99.99	gabbronorite
K074A1	0.00	40.26	1.10	10.49	20.42	18.00	0.29	0.00	8.13	0.18	1.13	100.00	olivine gabbronorite
K127B1	0.00	25.33	0.90	20.18	37.32	7.30	0.26	0.00	7.51	0.12	1.09	100.01	olivine gabbronorite
R023B2	13.04	10.57	0.30	17.34	52.50	0.00	0.17	0.09	5.96	0.05	0.00	100.02	cpx norite
F074A1	0.00	40.00	0.36	6.32	18.83	27.33	0.21	0.00	6.74	0.05	0.16	100.00	olivine gabbronorite

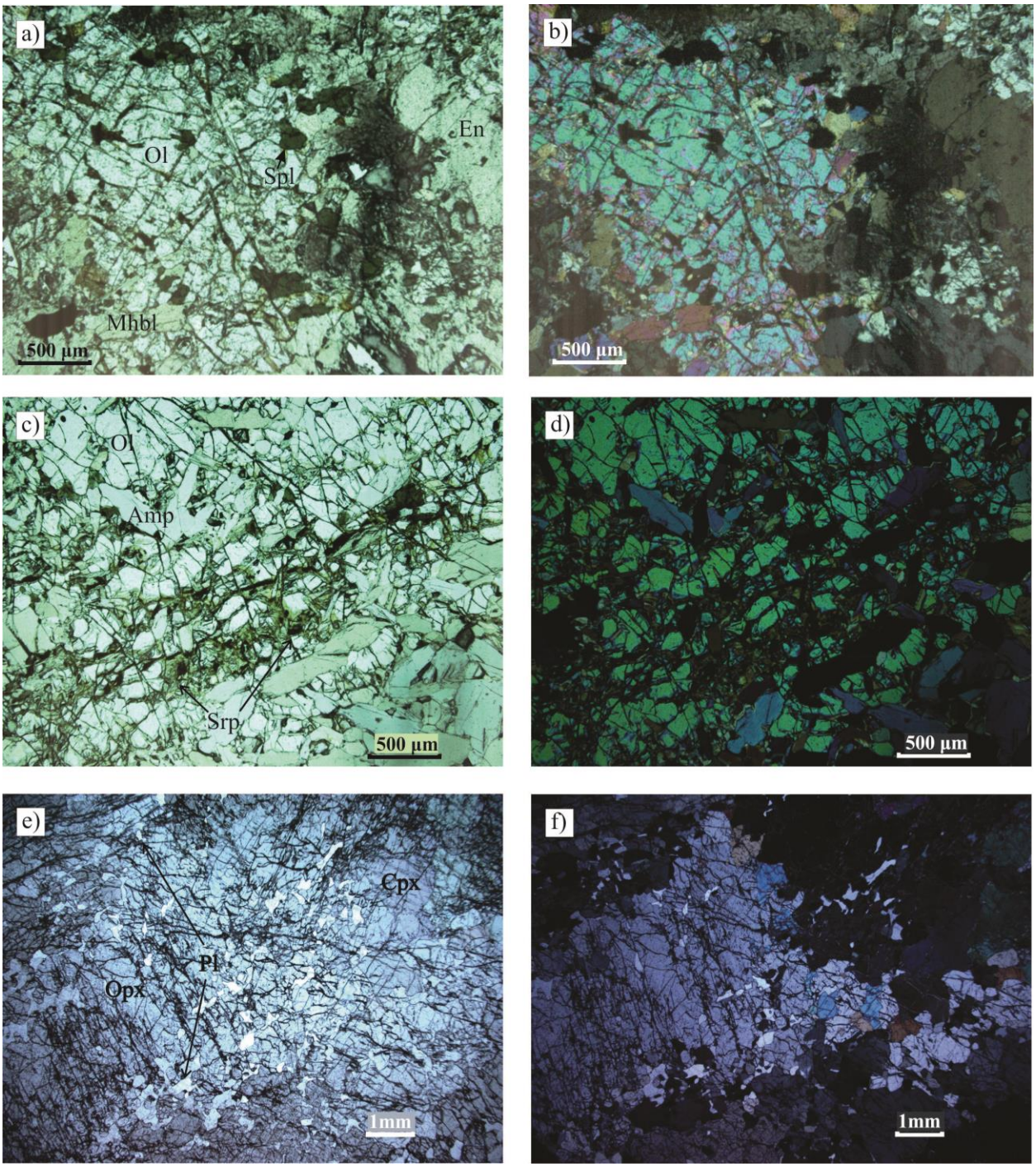

Figure 3.21 –a) Plane-polarized light thin section image of K074A1. b) Crossed-polarized light thin section image of a). c) Plane-polarized light thin section image of K127B1. d) Crossed-polarized light thin section image of c). e) Plane-polarized light thin section image of R023B2. f) Crossed-polarized light thin section image of e) Amp – amphibole; En – enstatite; Ilm – ilmenite; Mhbl – magnesio-hornblende; Ol – olivine; Pl – plagioclase; Spl – spinel; Srp – serpentine.

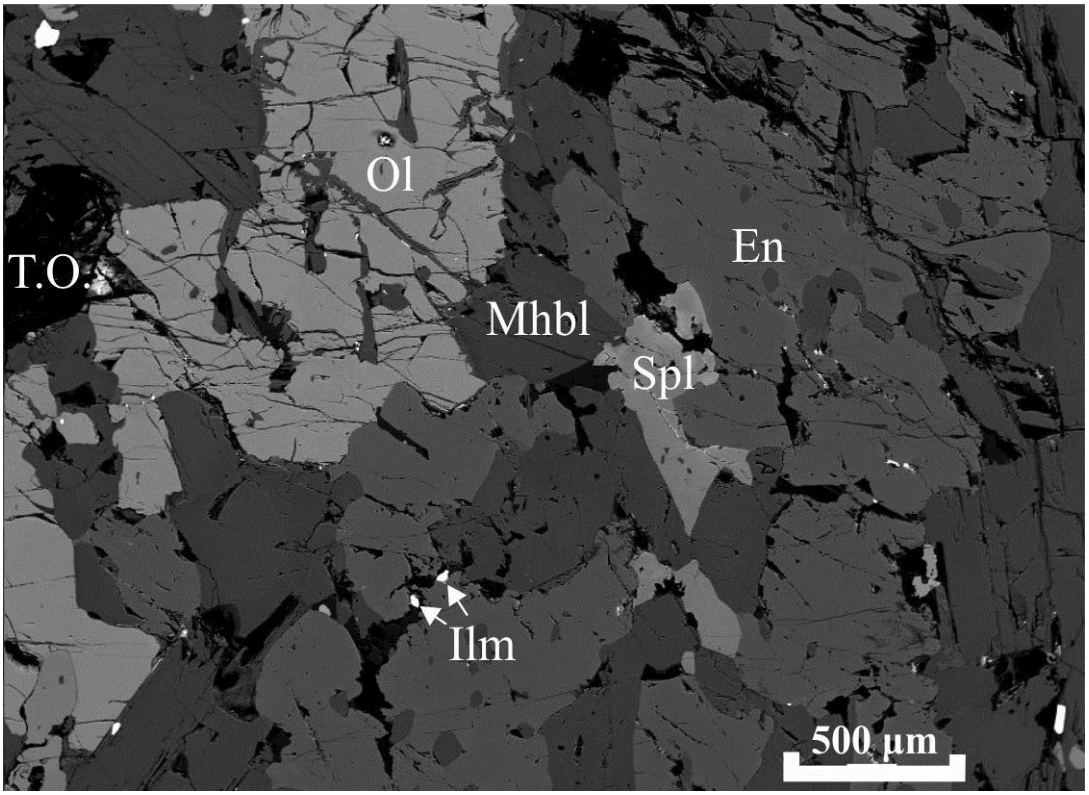

Figure 3.22 – Backscatter electron image of K074A1En – enstatite; Ilm – ilmenite; Mhbl – magnesio-hornblende; Ol – olivine; Spl – spinel; T.O. – tear out.

3.4.8 Summary

The geochemical sub-groups identified at the outset of this chapter are not reflected in the rocks' mineralogy. Relict igneous cpx, while not present in the representative tholeiitic or transitional samples, is found in other samples from these sub-groups. Samples from all four mafic sub-groups have very similar mineralogy, all being composed dominantly of amphibole and plagioclase. Samples from the western region, where granulite-grade metamorphic conditions were reached, contain metamorphic orthopyroxene in place of amphibole, although relict amphibole can be seen in the core of some orthopyroxrene crystals (Figure 3.23a). This is interpreted as metamorphic overgrowth of opx on hornblende. The mafic rocks in the west also tend to contain biotite (Figure 3.23a and b). The mineral chemistry between the mafic sub-

groups is also very similar for the dominant mineral species. The only notable exception being anorthitic plagioclase found in alkaline mafic rocks.

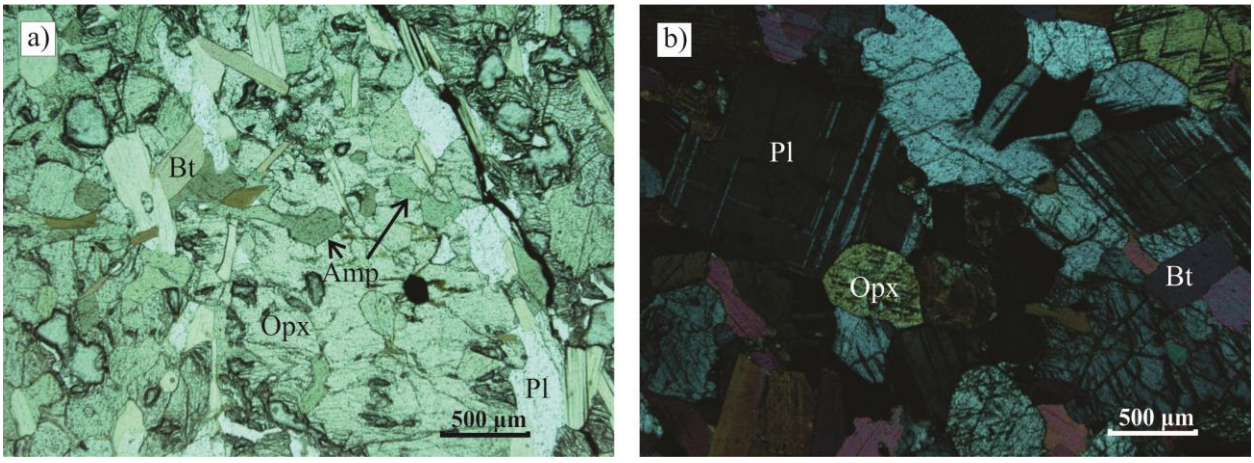

Figure 3.23 – a) Plane-polarized light thin section image of S067B1 showing relict amphibole (Amp) in the core of orthopyroxene (Opx). b) Crossed-polarized light thin section image of S043B1. Bt – biotite; Pl – plagioclase.

Only two types of ultramafic rocks from Hall Peninsula have been included in this study, three olivine-hornblende-pyroxenite cumulates and three websterite cumulates. Since the geochemical classification of ultramafic rocks is so poorly constrained these rock names will be employed for this thesis.

\

CHAPTER 4

DISCUSSION

4.1 Regional Comparisons

4.1.1 Introduction

One of the major goals of the HPIGP is to better understand the tectonostratigraphic evolution of the Hall Peninsula and surrounding area by correlating known regional-scale structures, rock units and cratonic blocks. The position of structures and delineation of cratonic block boundaries in the eastern Canadian Arctic is especially difficult and poorly defined in areas subjected to Trans-Hudson orogenic processes (Figure 1.3). Numerous studies have been conducted to try and elucidate the position of important boundaries between cratonic blocks in the eastern Canadian Arctic, northern Quebec and Labrador, and across Davis Strait into Greenland (e.g., Hoffman, 1989; van Gool et al., 2002; St-Onge et al., 2009; Corrigan, 2012). This section will highlight regions adjacent to the Hall Peninsula (Figure 4.1) which have similar Archean basement ages, comparable supracustal suites and mafic-ultramafic rocks, and previously correlated regions which can be compared with the new data provided in this thesis. The regions which will be presented for comparative analysis are the Cumberland Peninsula, the Ungava Peninsula, south Baffin Island, central Baffin Island, and western Greenland and northern Labrador (Figure 4.1). The available trace element normalized geochemical data of mafic and ultramafic samples from these regions is shown in Figure 4.2.

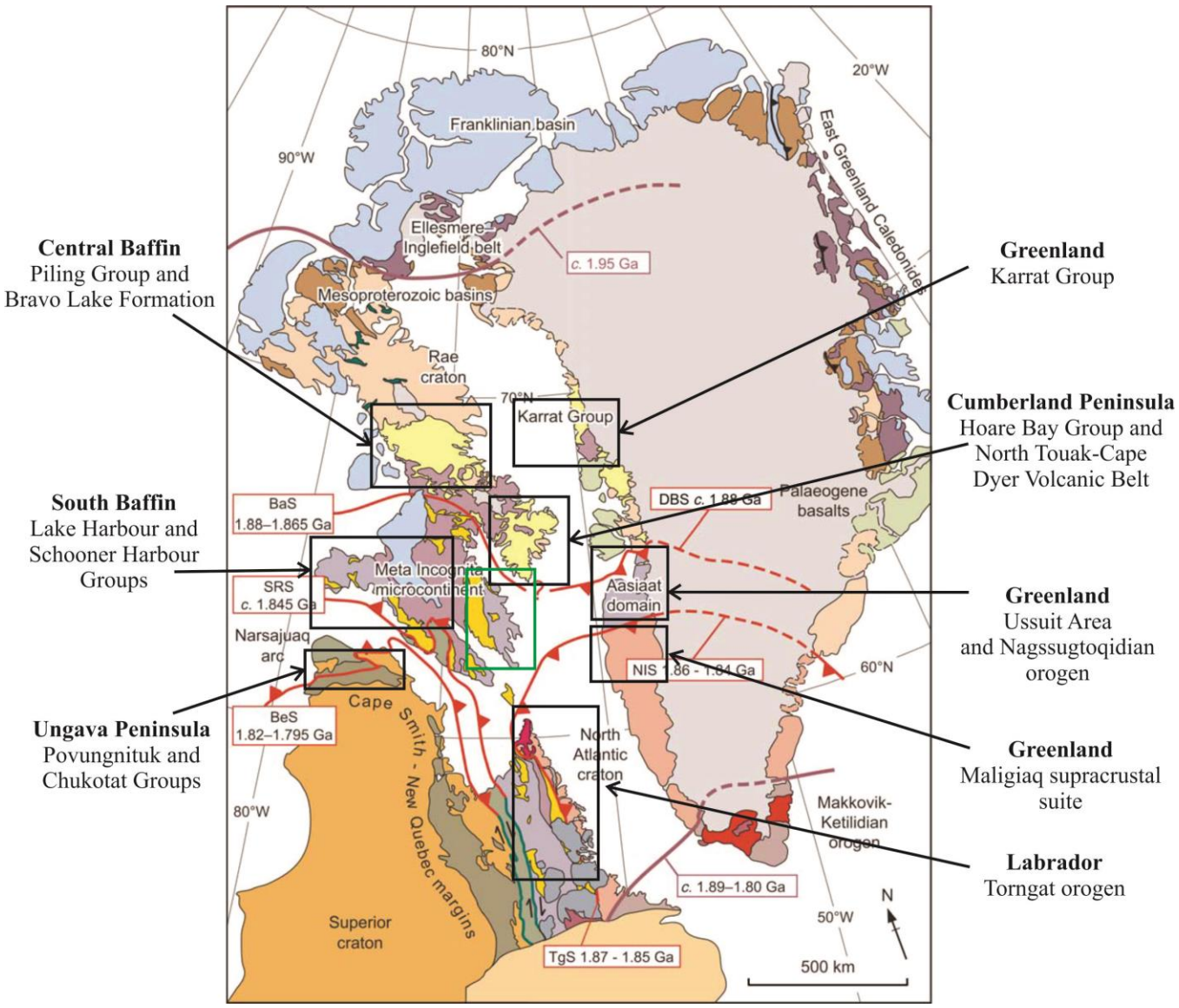

Figure 4.1 – Map showing location of Paleoproterozoic supracrustal rock groups/suites, mafic and ultramafic rock occurrences and previously correlated regions adjacent to the Hall Peninsula (green box). Modified from St-Onge et al. (2009).

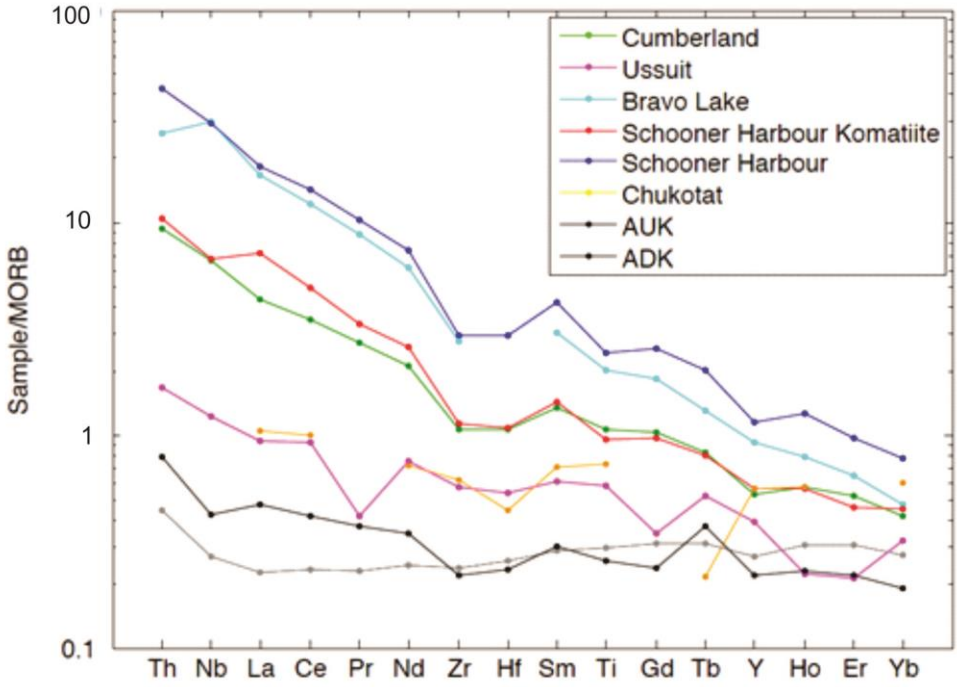

Figure 4.2 – Trace element diagram normalized to NMORB (Sun and McDonough, 1989) for samples from the Cumberland Peninsula (ultramafic, Totnes Road formation) (Keim, 2012), Ussuit area SW Greenland (Ultramafic) (Connelly et al., 2006; and Kalsbeek and Manatschal, 1999), Bravo Lake Formation central Baffin (mafic volcanic) (Johns et al., 2006), Schooner Harbour sequence of south Baffin (mafic and ultramafic) (Sanborn-Barrie et al., 2008), Chukotat group from the Ungava Peninsula (mafic) (St-Onge et al., 1992; and St-Onge et al., 2000), alkali undepleted komatiites (AUK) (Fan and Kerrich, 1997), and alkali depleted komatiites (ADK) (Viljoen et al., 1983). From Keim (2012).

4.1.1 Cumberland Peninsula

Complex plutonic gneisses of ages 2991 ±4 Ma, 2938 ±4, 2782 ±4 Ma, as well as discrete Neoarchean plutons of ages 2772 ±6 Ma, 2759 ±3 Ma and 2700 ±4 Ma (Rayner et al., 2012) form the crystalline structural basement of the Cumberland Peninsula. The Archean gneissic basement is overlain by Paleoproterozoic Hoare Bay Group metasediments and associated mafic and ultramafic volcanic rocks of the North Touak-Cape Dyer volcanic belt (Keim, 2012). Both the Archean, crystalline gneissic basement and Hoare Bay Group supracrustal rocks are cut by a charnockite-granodiorite-diorite suite, informally termed the Qikiqtarjuaq plutonic suite, two examples of which have been dated at 1894 ±5 Ma and 1889 ±3 Ma. Amphibolite metamorphic

conditions persist throughout the majority of the Cumberland peninsula, sometimes reaching granulite grade near intrusions (Hamilton et al., 2012). The dominant regional fabric associated with Paleoproterozoic collision (D2) is broadly east-west striking and north-dipping, and has produced south-vergent D2 structures. D2 occured between 1863±5 Ma and 1859±7 Ma as determined from *in situ* monazite data (Berman et al., 2013).

The Paleoproterozoic metasediments of the Hoare Bay Group that are cut by the ~1890 Ma Qikiqtarjuaq plutonic suite are age-equivalent and compositionally similiar the 1906±9 Ma (Rayner, 2014a and b) metasediments and cross-cutting 1892±7 Ma (Rayner, 2014a and b) orthopyroxene-bearing plutonic suite on Hall Peninsula, suggesting that they may be related.

Detailed mafic and ultramafic geochemical studies from regions adjacent to the Hall Peninsula are scarce. The one exception comes from the Cumberland Peninsula (Figure 4.1). Keim (2012) studied the mafic and ultramafic geochemistry of the North Touak-Cape Dyer volcanic belt during the Cumberland Peninsula Integrated Geoscience Project. From this work, whole-rock major and trace element geochemistry for eighteen mafic samples and twenty-one ultramafic samples from the Cumberland Peninsula were obtained.

The same mafic rock geochemical classification schemes applied herein to samples from the Hall Peninsula have been used to classify the Cumberland Peninsula samples. Based on the classification scheme of Pearce (1996), thirteen of the eighteen are alkaline basalts and five are sub-alkaline basalts (Figure 4.3a). When the sub-alkaline basalts are further refined using the classification scheme of Ross and Bédard, three are transitional and two are tholeiitic (Figure 4.3b).

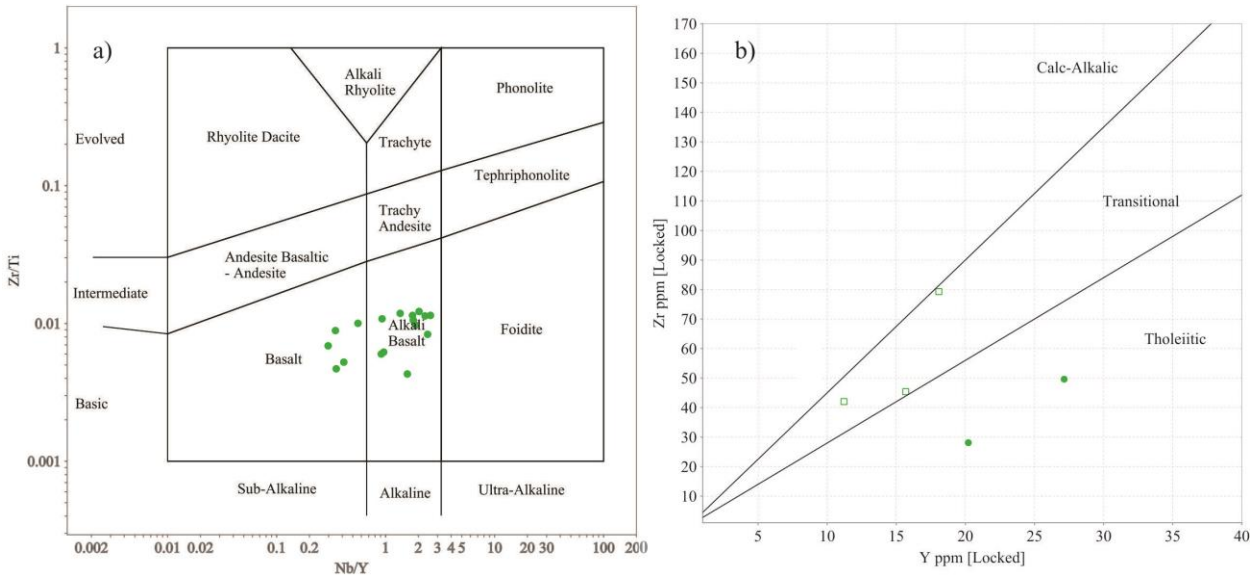

Figure 4.3 – a) Volcanic rock type classification diagram (Zr/Ti vs Nb/Y; Pearce, 1996). b) Sub-alkali basalt classification diagram (Zr vs Y; Ross and Bédard, 2009). Data from Keim, 2012.

Trace element, N-MORB (Sun and McDonough, 1989) normalized diagrams of the Cumberland Peninsula samples display strongly negative slopes typical of within-plate basalts (Pearce, 1996) (Figure 4.4). All alkaline composition samples have high Ti/Y ratios (~2.0) suggesting a garnet lherzolite parent material (Pearce and Parkinson, 1993).

Ultramafic rocks of the Cumberland Peninsula display N-MORB (Sun and McDonough, 1989) normalized trace element profiles similar to those of the Cumberland Peninsula mafic rocks (Figure 4.5a). They show a strong enrichment of the most incompatible elements, a negative slope and a strong positive Ti anomaly. This profile is very different from those of the Hall Peninsula ultramafic rocks which display a negative Nb anomaly with respect to Th and Ce and flat depleted profiles with respect to N-MORB (Sun and McDonough, 1989). Based on the ternary cation-percentage classification scheme of Jenson (1976), the ultramafic rocks of the Cumberland Peninsula plot dominantly as basaltic komatiites (Figure 4.5b).

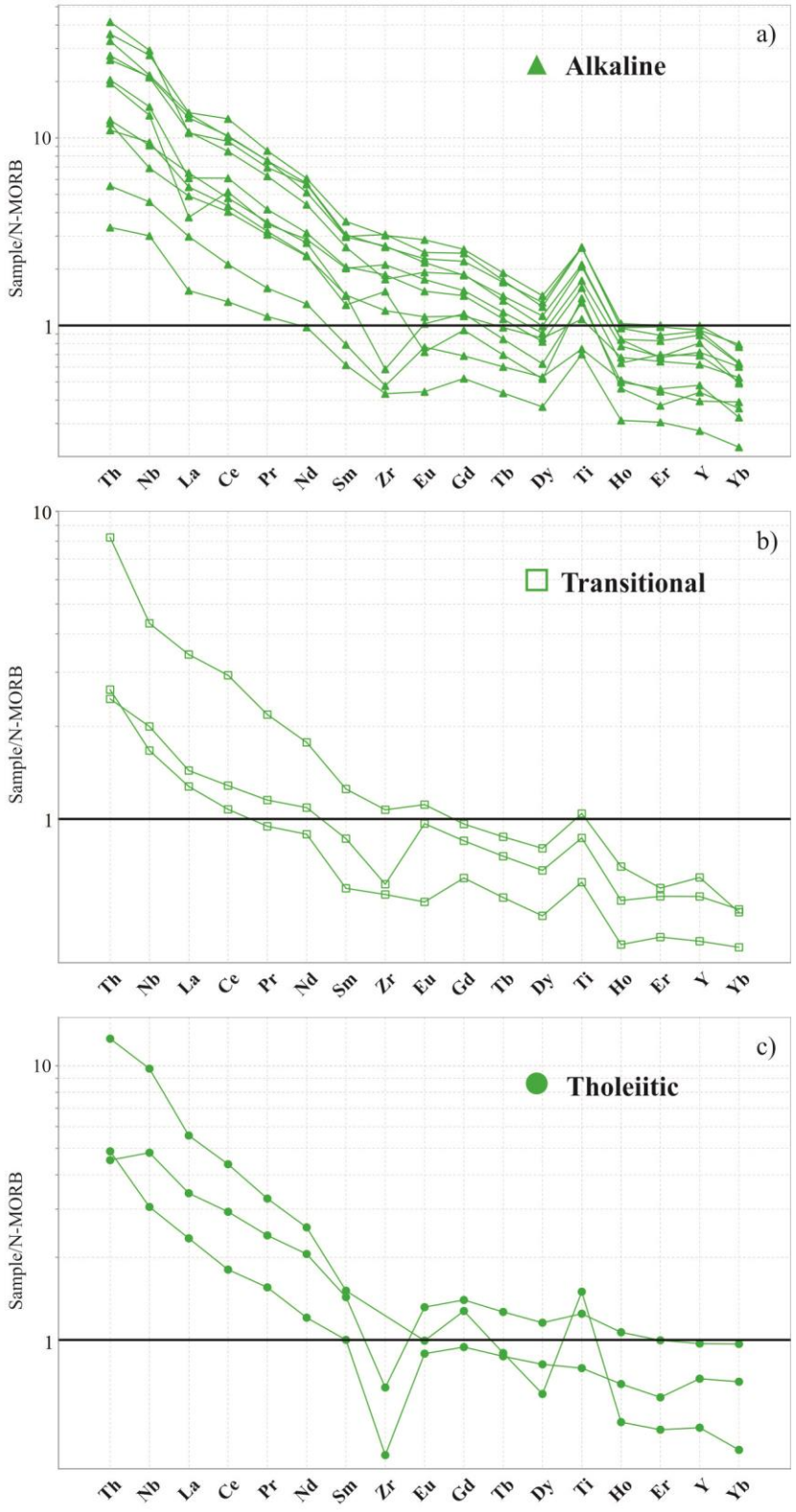

Figure 4.4 – Cumberland Peninsula samples' trace element diagrams normalized to NMORB (Sun and McDonough, 1989) of a) Alkaline basalt composition, b) transitional basalt and d) tholeiitic basalt composition.

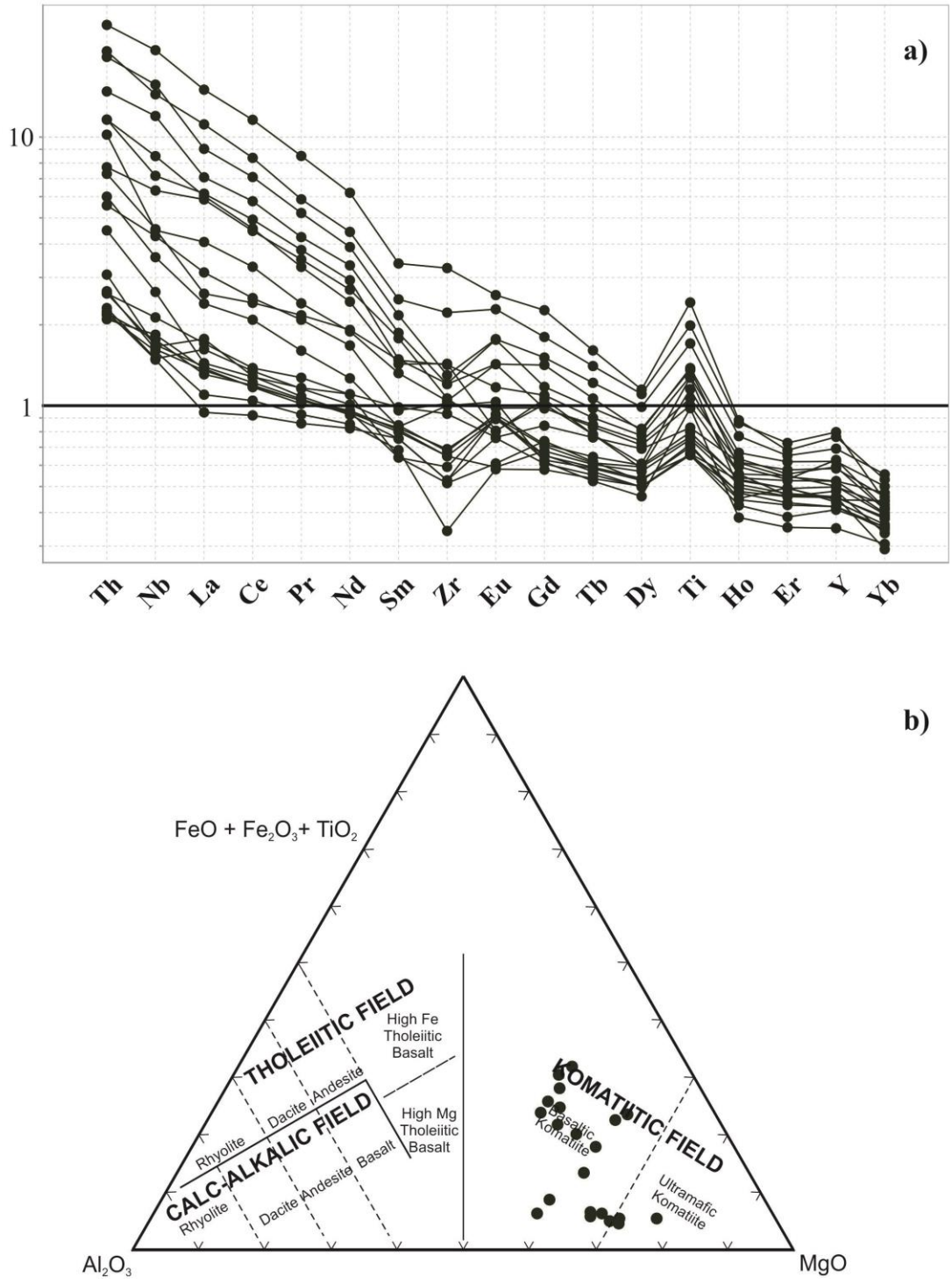

Figure 4.5 – a) Trace element diagram normalized to NMORB (Sun and McDonough, 1989) of Cumberland Peninsula ultramafic samples. b) Ternary plot which uses cation % to classify sub-alkalic rocks after Jenson (1976).

The trace element normalized mafic geochemical signatures of alkaline samples from the Cumberland Peninsula are very similar to alkaline samples from the Hall Peninsula (Figures 4.4 and 3.6, respectively). In contrast, the trace element profiles for tholeiitic and transitional mafic rocks, and ultramafic rocks are very different between the Hall and Cumberland Peninsulas. The Cumberland mafic and ultramafic rocks show a strong enrichment of the most incompatible elements, a negative slope and a strong positive Ti anomaly. Hall Peninsula mafic and ultramafic rocks display a negative Nb anomaly with respect to Th and Ce and flatter profiles, and in the case of ultramafic rocks, a depleted signature with respect to N-MORB (Sun and McDonough, 1989). Enrichment of the most incompatible elements of the Cumberland samples is interpreted by Keim (2012) to be related to subduction modification of the mantle below the Cumberland Peninsula which was then later melted in a mantle plume event. The Cumberland samples do not however, display a negative Nb anomaly with respect to Th and Ce as the Hall Peninsula samples do, which arises when Nb is fractionated during dehydration of subducted crust. The geochemical profile of the Cumberland mafic and ultramafic rocks may instead suggest they were emplaced within a stable – non-rifting, not subduction related – cratonic block. Frey (1982) and Erlank et al. (1982) have used mantle xenoliths to show that metasomatism of sub-continental lithosphere provides at least some of the enrichment observed in within plate basalts. Furthermore, the mantle plumes most commonly associated with within-plate magmatism are themselves enriched relative to NMORB (Pearce, 1996). Whatever the petrogenesis of the Cumberland Peninsula mafic and ultramafic rocks, their profile is very different from those of the Hall Peninsula.

Similar to the Hall Peninsula samples, the mafic and ultramafic volcanic rocks and associated metasediments on Cumberland Peninsula are Paleoproterozoic in age, with a

maximum depositional age for the sediments of ca. 2 Ga (Wodicka, 2011, unpublished data *in* Keim, 2012) providing a broad temporal link with the 1.87 – 2.13 Ga mafic rocks on the Hall Peninsula. However, the divergent geochemical signatures between the Hall and Cumberland Peninsulas suggest melting of different mantle sources, which makes a genetic link between the two unlikely.

4.1.2 Ungava Peninsula and south Baffin

Correlation of crustal terrane boundaries across Hudson Strait from the Ungava Peninsula in northern Quebec to south Baffin Island reveals three distinct structural levels (St-Onge et al., 1999; Thériault et al., 2001; St-Onge et al., 2002). The lowest structural level, the Superior margin (Figure 4.6a and b), identified on the northern part of Ungava peninsula and on Big Island, comprises Superior Provence Archean (3220 +32/-23 Ma – 2740 ±10Ma) tonalitic-dioritic orthogneisses and granitoid plutons (Parish, 1989, St-Onge et al., 1992; Scott and St-Onge, 1995; Wodicka and Scott, 1997). The orthogneiss basement is overlain by two distinct successions of metasedimentary rocks. The first succession has associated LREE-enriched, tholeiitic continental flood basalts of the Povungnituk group and the second sucession has associated tholeiitic basalts of the Chukotat group (Figure 4.1) and gabbro sills (Parrish, 1989; Machado et al., 1993). Both sedimentary packages and associated mafic rocks are interpreted to be the result of multi-stage, Paleoproterozoic rifting of the Superior craton (Parrish, 1989; St-Onge et al., 1992). No Archean basement has been observed on southern Baffin Island (Meta-Incognita). However, variations in εNd (1.85 Ga) values between plutonic rocks identified in structural levels 2 and 3 – Ungava terrane and Meta Incognita terrane, respectively – likely indicate an imprint from an Archean crustal component within each structural level (Thériault et al., 2001). Within structural level 2 there is also a marked difference in εNd values and REE

fractionation across Hudson Strait interpreted to result from northward-dipping subduction below the Narsajuaq arc, resulting in continental-arc magmas intruding a northward-thickening Archean block (Thériault et al., 2001). Further differences in εNd values and REE fractionation in structural level 3, led Thériault et al. (2001) to assert that a second northward-directed subduction zone was present to the north, between the Narsajuaq arc and Meta Incognita microcontinent (Figure 4.6a).

The dominant regional fabric on southern Baffin is east-west striking and north dipping, but changes to NE-SW striking and west dipping eastwards towards the Hall Peninsula. Metamorphic grade increases from amphibolite to granulite facies northwards and up structural section and eastwards towards the Hall Peninsula (St-Onge et al., 2001).

Given the extensive work that has been done on the transition between the Superior craton, Narsajuaq arc and Meta Incognita microcontinent (e.g., Parrish, 1989; St-Onge et al., 1992; Machado et al., 1993; Scott and St-Onge, 1995; Wodicka and Scott, 1997; St-Onge et al., 2001, Thériault et al., 2001) there is no evidence to link Archean gneissic basement, or Paleoproterozoic metasediments or mafic intrusions from the east-central region of Hall Peninsula with the rift-related Paleoproterozoic metasediments and associated flood basalts of the Povungnituk group, or with tholeiitic basalts of the Chukotat group on the Superior craton.

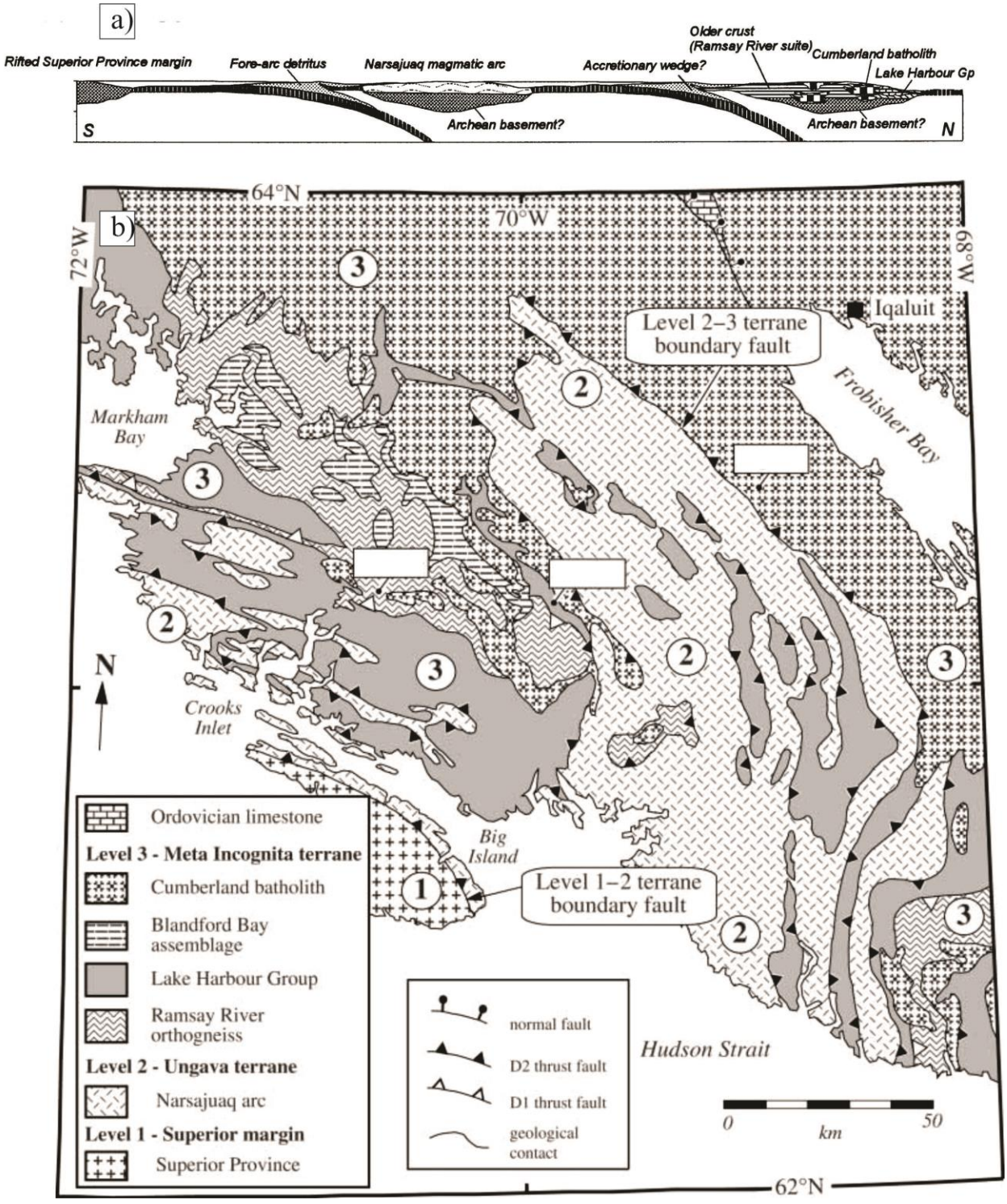

Figure 4.6 – a) Schematic tectonic diagram from Thériault et al. (2001) showing two northward dipping subduction zones beneath the Narsajuaq arc and the Meta Incognita microcontinent. b) Geological map of southern Baffin Island from St-Onge et al. (2002).

Paleoproterozoic cover rocks on south Baffin comprise the north-dipping Lake Harbour Group, interpreted as a clastic – carbonate shelf succession (Scott, 1997; Scott et al., 2002). The Lake Harbour Group metasediments are cut by a large suite of monzogranite plutons (Cumberland Batholith). U-Pb geochronology from detrital zircons and the cross-cutting monzogranite plutons brackets the age of deposition for the Lake Harbour Group to between 1934 ± 2 Ma and 1865 +4/-2 Ma. On the Foxe Peninsula of southwest Baffin Island, stratigraphically above the Lake Harbour Group is the Schooner Harbour sequence, which is a heterogeneous supracrustal sequence interlayered with mafic and ultramafic volcanic rocks (Sanborn-Barrie et al., 2008). Trace element normalized diagrams for Schooner Harbour mafic and ultramafic rocks display a negative slope and strong enrichment of the most incompatible elements (Figure 4.2). This trace element profile mirrors that of the Cumberland Peninsula ultramafic rocks which lead Keim (2012) to suggest there may be a genetic link between the two.

4.1.3 Central Baffin

The southwestern margin of the Rae craton on central Baffin Island is dominated by the Paleoproterozoic Piling Group supracrustal suite. The Piling Group has traditionally been interpreted as a continental margin succession (Morgan et al., 1975, 1967) comprising shallow-water siliciclastic and calc-silicate units, mafic and ultramafic volcanic rocks and deep-water turbidite successions (e.g., Morgan et al., 1976; Tippet, 1984; Jackson, 2000). Recent work by Wodicka et al. (2014) integrating U-Pb geochronology, whole rock geochemistry, Sm-Nd isotopic studies and sequence stratigraphy suggests that the Piling Group depositional basin was formed during Paleoproterozoic (<2160 Ma and >1890 Ma) rifting of the Rae craton, associated at a broad scale with the ca. 2.1 – 2.0 breakup of Kenorland (Williams et al., 1991; Aspler and Chiarenzelli, 1998). In addition to the initiation of sedimentation, rifting also resulted in

theoleiitic to picritic volcanism of lower Bravo Lake formation (Johns et al., 2006) (Figure 4.1) at ca. 1980 Ma (Wodicka et al., 2014). No published mafic geochemical data is available from the lower Bravo Lake formation for comparative analysis. In the upper Bravo Lake formation, alkaline volcanism and sill emplacement, which display trace element geochemical profiles typical of within-plate basalts (Figure 4.2) occured by ca. 1923 Ma (Wodicka et al., 2014). This geochemical profile is nearly identical to the mafic rocks from Cumberland Peninsula and the Schooner Harbour sequence on southwest Baffin Island (Figure 4.2).

4.1.4 Southwest Greenland and northern Labrador

In southwest Greenland, the northern margin of the North Atlantic craton is dominated by 2.87 – 2.81 Ga diorite, granodiorite, tonalite and granite orthogneiss (e.g., Kalsbeek etal. 1984, 1987; Kalsbeek and Nutman, 1996; Connelly and Mengel, 2000, van Gool et al., 2002; St-Onge et al, 2009) which are of similar ages and compositions to the Archean orthogneiss complex of the east-central region of the Hall Peninsula. The Maligiaq supracrustal suite (Figure 4.1) is stratigraphically above the Archean orthogneisses and is characterized by metasedimentary rocks dominated by psammite interpreted as continental margin deposits, and which contain a large proportion of 2.85 Ga detrital zircons, but also a significant ca. 2.1 Ga component (Scott et al., 1998; Marker et al., 1999; Nutman et al., 1999). These detrital zircon ages match closely to those obtained from the QA (Chapter 2.5.1). The Maligiaq supracrustal suite is thought to demarcate the northern limit of the North Atlantic craton in southwest Greenland. However, the North Atlantic craton may extend significantly further north, but its position is obscured by the Assiat domain collisional zone (Figure 4.1). Further south, near Arfersiorfik fjord, 1921 ± 15 to 1885 +6/-3 Ma calc-alkaline mafic rocks of the Arfersiorfik suite intrude metasedimentary and metavolcanic rocks of the Strømfjord supracrustal suite. The Arfersiorfik intrusive suite has

been interpreted as being related to south-directed subduction of oceanic crust beneath the Aasiaat domain prior to the collision of the Rae craton to the north and the North Atlantic craton to the south during the ca. 1.86 – 1.84 Ga Nagssugtoqidian orogeny (Garde et al., 2007; St-Onge et al., 2009).

In northern Labrador the Torngat orogenic belt defines the westernmost known margin of the North Atlantic craton (Figure 4.1). The Torngat orogen is interpreted to have resulted from the collision of the Meta Incognita microcontinent in the west and the North Atlantic craton in the east (Corrigan, 2012). The closure of these two blocks is thought to have resulted from east-directed subduction beneath the North Atlantic craton and concurrent east-directed subduction beneath the 1910 ±2 Ma to 1869 +3/-2 calc-alkaline Burwell arc (Scott and Machado, 1995; Van Kradendonk and Wardle, 1996) located between the two blocks. The collision resulted in east-directed thrusting at the margin of the North Atlantic craton between c. 1870 and 1845 Ma and granulite-facies metamorphism within the core of the orogen (Van Kradendonk, 1996; Scott, 1998; Connelly, 2001). Continued deformation resulted in north – south-trending shearing between 1844 ±4 and 1822 Ma which is most strongly developed in the Tasiuyak gneiss (Bertrand et al, 1993) which has been interpreted to continue northward through the Hall Peninsula (Jackson and Taylor, 1972; Hoffman, 1989; Chapter 1.2).

4.2 Interpretations and Correlations Based on New Findings

4.2.1 Introduction

The QA mapping project is an important study completed with the aim of characterizing the rock units, their structural and metamorphic relationships and age constraints of the metasedimentary-mafic packages of the central and east regions of the Hall Peninsula, Baffin

Island, Nunavut. Within this geological framework, the geochemistry and petrogenesis of the mafic and ultramafic rocks of the Hall Peninsula has been studied to add to a growing body of knowledge in a poorly understood portion of the eastern Canadian Arctic Archipelago. This information can now be compared with data from adjacent regions in the Canadian arctic, northern Quebec, Labrador and Greenland with the aim of making geological correlations of crustal structures, rock units and cratonic blocks.

4.2.2 East-central region Archean basement

Geological relationships studied at the QA show that Archean, crystalline gneissic rocks, dominantly of tonalite composition form its structural base. No tonalitic sample from the QA was dated, but the QA basement is correlated with a 2841 ± 3 Ma (Rayner, 2014) tonalite (sample F105A) dated on Beekman Peninsula (Figure 4.7). The Beekman Peninsula tonalite age agrees with tonalite ages reported by Scott (1999) from Okalik Bay (sample D354A – 2848 ±3 Ma), Breevort Island (sample D352A – 2844 ±6 Ma) and Allen Island (sample D353B – 2835 ±11 Ma) (Figure 4.7). The Archean orthogneiss basement ages most closely resemble the 2.87 – 2.81 Ga diorite, granodiorite, tonalite and granite orthogneiss from the northern margin of the North Atlantic craton in southwest Greenland. These age dates, combined with the correlation of airborne magnetic surveys from the Tasiuyak paragneiss in northern Quebec and Labrador through the Hall Peninsula suggests that the east-central region of the Hall Peninsula is a part of the North Atlantic craton as suggested by Hoffman, 1989, Scott, 1999 etc.

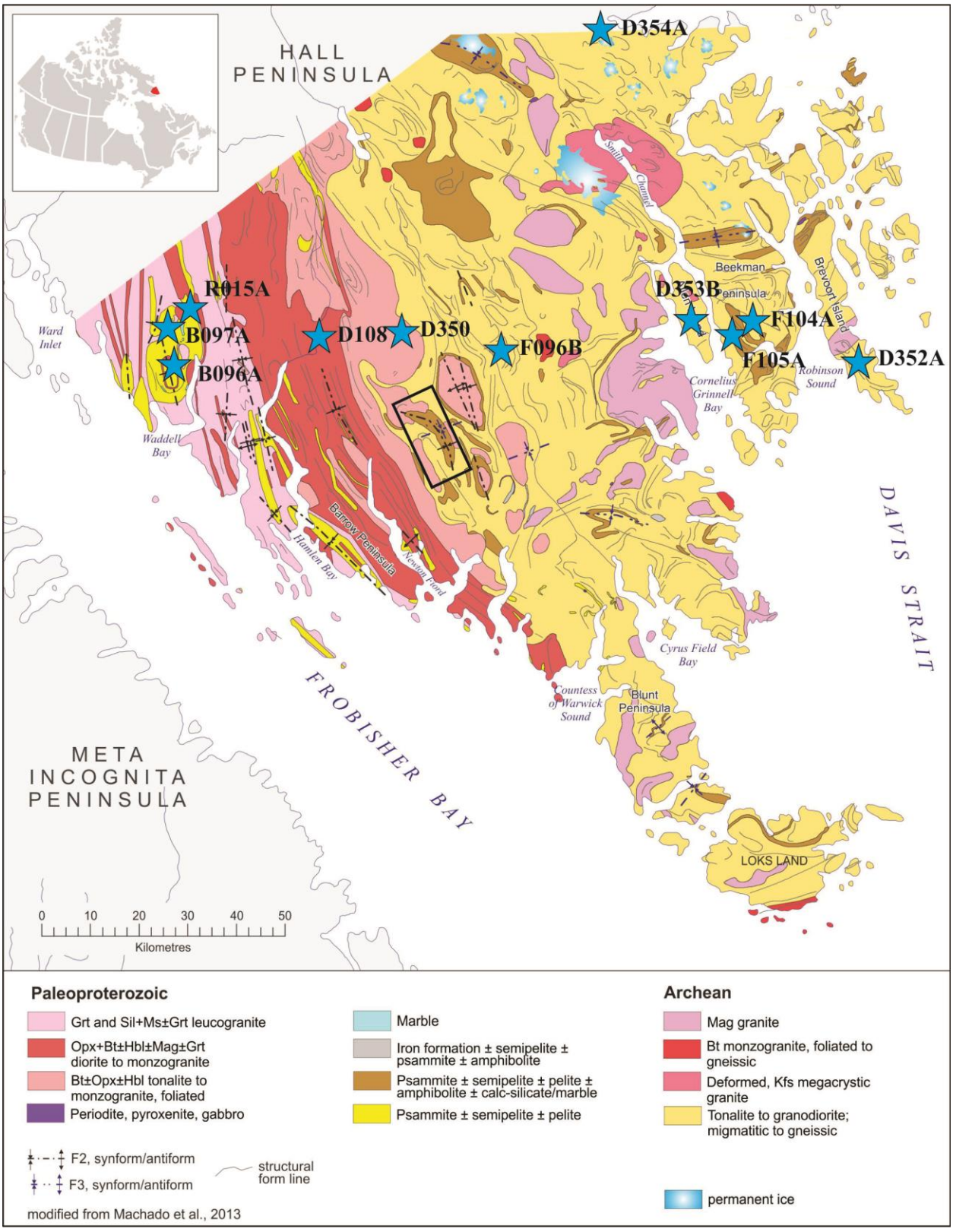

Figure 4.7 – Geology of southern Hall Peninsula, Baffin Island, Nunavut. Blue star indicates location of U-Pb geochronology samples from Rayner, (2014), and Scott (1999). Black box outlines the QA.

4.2.3 East-central region supracrustal rocks

Metasedimentary rocks in the QA comprised dominantly micaceous psammite with lesser quartzite and pelite, which may have been deposited directly onto the underlying tonalite orthogneiss indicated by the potential paleoregolith discussed in Chapter 2.3. The QA supracrustal rocks were folded and tectonically imbricated within the basement during D1 and subsequently refolded during D3.

Pelitic rocks are found most commonly near the contact with the tonalite orthogneiss, near the inferred stratigraphic base of the QA supracrustal rocks. Mafic and ultramafic rocks are found intercalated with metasediments, and particularly near the structural base of the QA. In general, there is a coarsening of detritus stratigraphically upwards in the QA. This trend is consistent with progradational basin fill (Figure 4.9).

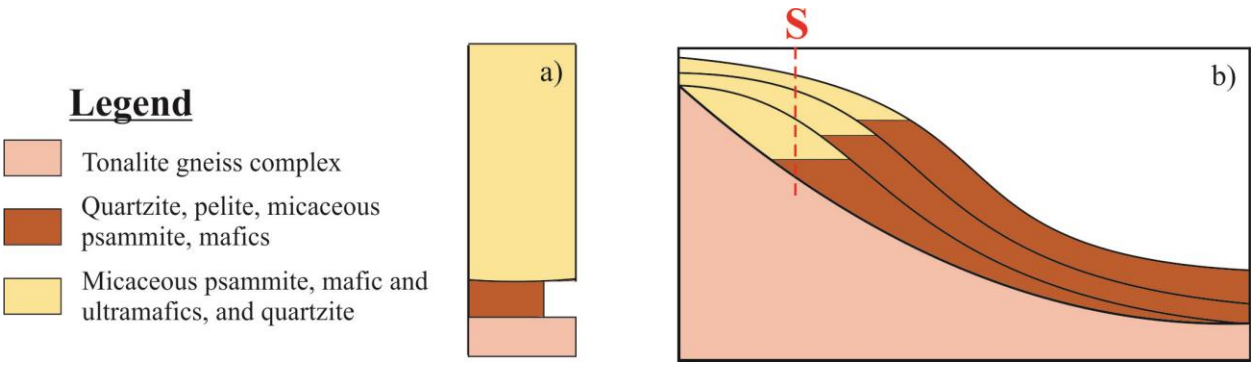

Figure 4.8 – a) Schematic stratigraphic column through the QA along line "S" from (b) illustrating how sediments deposited in deep water appear at the base of the QA when invoking a progradational basin fill model (b).

All sediments in the QA are interpreted as being broadly contemporaneous. U-Pb detrital zircon geochronology performed on quartzite sample K097A from the QA give a maximum deposition age of 2126 ± 16 Ma, with significant detrital input from 2.7-2.9 Ga sources (Rayner,

2014). This U-Pb age detrital zircon profile best correlates with the Maligiaq supracrustal suite on the northern margin of the North Atlantic craton in southwest Greenland which has a maximum depositional age of 2.1 Ga, but significant 2.85 Ga detritus (Scott et al., 1998; Marker et al., 1999; Nutman et al., 1999). The similar U-Pb detrital zircon between the QA and southwest Greenland supports the interpretation that the east-central region of the Hall Peninsula may be a part of the North Atlantic craton. Later 1873 ± 6 Ma (Rayner, 2012) monzogranite dykes cross-cut all metasediments and mafic/ultramafic rocks. These two age dates bracket both sediment accumulation and mafic intrusion/volcanism between 2126 ± 16 Ma and 1873 ± 6 Ma.

Other metasedimentary rocks have been dated from the east-central region of the Hall Peninsula during the HPIGP. A psammite from Beekman Peninsula (sample F104A) which contains detrital input of similar age source rocks to K097A has a maximum depositional age of 1959 ±12 Ma (Rayner, 2014a and b) (Figure 4.7). In addition, a psammite 40km west of Allen Island (sample F096B) yielded only Archean detritus and is interpreted to represent a locally derived basal sedimentary package (Rayner, 2014a and b) (Figure 4.7).

4.2.4 Mafic and ultramafic geochemistry

Mafic and ultramafic rocks interlayered within metasedimentary rocks throughout the central and eastern regions of the Hall Peninsula are analogous to those found in the QA. No primary features are preserved in these rocks so it is impossible to determine for certain whether they are intrusive or extrusive. The consistency of mafic geochemical signatures based on the sub-classifications described herein and the correlations observed in binary trace element Harker diagrams (Figure 3.2) may indicate that, with the possible exception of some notable outliers (Figure 3.2), the mafic rocks across the whole Hall Peninsula are genetically related.

Alternatively, multiple events derived from the same mantle source may have occurred. In either case, this would suggest that mafic enclaves found in the Archean, crystalline, gneissic basement of the east and central regions represent the feeder system for the sills and dykes found in Paleoproterozoic metasediments. Outlier samples (Figure 3.2) may be the result of distinct igneous events which are derived from compositionally distinct mantle sources or may indicate the mobilization of HFSE during deformation and/or metamorphism.

The mafic sub-groupings applied herein are validated by the consistency of trace element normalized geochemical trends observed (Figure 3.6), discernable clustering based on tectonic environment discrimination (Figure 3.7) and plagioclase and amphibole chemistry variations between sub-groups (Figures 3.11 and 3.12). Notably, alkaline mafic rocks contain plagioclase with very high anorthite (An_{90-93}) content (Figure 3.11 and Table 3.3). This likely indicates the pre-metamorphic mafic rock was enriched in calcium. The mafic sub-groups appear to be genetically linked – sampling the same subduction-modified mantle source if not temporally linked; theytherefore likely represent distinct pulses melt, transport and intrusion/extrusion which resulted in the observed geochemical differences. However, no discernable spatial clustering of samples based on any of the sub-classifications described is observed.

Geochemically, all Hall Peninsula alkaline and calc-alkaline mafic samples show characteristics that are intermediate between volcanic-arc-related basalts and within-plate basalts. The much more numerous transitional and tholeiitic samples show characteristics of volcanic-arc-related basalts, within-plate basalts and MORB/depleted MORB. The mixed geochemical character is revealed by negative Nb anomalies typical of volcanic arc basalts; enrichment in the most incompatible elements relative to NMORB and high Ti/Y ratios indicative of within-plate basalts; and a flat NMORB normalized trace element profile for the more compatible elements

associated with spreading centres. The mixed geochemical signature is best explained by subduction-related geochemical modification of the mantle below the Hall Peninsula (Figure 4.10a) which later underwent partial melting, possibly initiated by or within a mantle plume, leading to the emplacement of the mafic magmas during a rifting event (Figure 4.10b).

Sediment deposition and mafic and ultramafic intrusion/extrusion in the east central region of the Hall Peninsula occurred between 2126 ± 16 Ma and 1873 ± 6 Ma (Chapter 2.5.2 and 2.5.3); therefore, subduction-related geochemical enrichment of the mantle below the Hall Peninsula must have occurred earlier in the Paleoproterozoic or in the Archean (Figure 4.11b). Southward-directed subduction beneath the North Atlantic craton occurred prior to the ca. 1.86 – 1.84 Ga Nagssugtoqidian orogeny (Garde et al., 2007; St-Onge et al., 2009) and, eastward-directed subduction beneath the North Atlantic craton prior to the 1.87 – 1.85 Ga Torngat orogeny also occurred (St-Onge et al., 2009) (Figure 4.1; Figure 4.11a and b). Operating on the interpretation that the Hall Peninsula is a part of the North Atlantic craton, temporally, it is possible that either or both of these pre-orogenic subduction systems could be responsible for enrichment of the mantle below the Hall Peninsula prior to mafic intrusion/extrusion. Alternatively, Archean geochemical modification of the mantle below the North Atlantic craton may have occurred. Following geochemical enrichment, incipient rifting of the North Atlantic craton, possibly due to the upwelling of a mantle plume could have produced a basin into which the sediments of the QA (and by extension those from the whole of the east-central Hall Peninsula) as well as those of the Maligiaq supracrustal suite could have been deposited (Figure 4.11b). Further rifting of the North Atlantic craton due to mantle plume upwelling may have melted the subduction-modified mantle resulting in the intrusion/extrusion of the mafic and ultramafic rocks with the mixed geochemical signature observed in the Hall Peninsula.

Mafic and ultramafic geochemical data from regions adjacent to the Hall Peninsula is scarce, and the data that are available (Figure 4.2) do not closely resemble those from the Hall Peninsula. Drawing regional correlations of structural and cratonic architecture would not be validated based solely on similarities in mafic geochemistry. However, it is also true that variation in mafic and ultramafic geochemical profiles between adjacent regions do not negate a spatial or temporal correlation.

4.2.5 Western region supracrustal rocks

In the western region of the Hall Peninsula metasediments have a maximum depositional age of 1906±9 Ma (Sample R015A) (Rayner, 2014a and b) (Figure 4.7). Metasediments from the west region of the Hall Peninsula may be correlated with the Hoare Bay Group from Cumberland Peninsula, however, no detailed detrital zircon geochronology has been published, other than that the Hoare Bay Group metasediments are Paleoproterozoic (<2 Ga) in age (Keim, 2012). Western region metasediments may instead be correlated with the Piling Group from south Baffin Island which has a maximum depositional age of 1934 ± 2 Ma. Alternatively, if the east central region is a part of the North Atlantic craton, then the boundary between the western region and east-central region of Hall Peninsula may represent a shelf edge of the Meta Incognita microcontinent where detritus was being sourced from the west from similar aged rocks to both the Hoare Bay and Piling Groups.

4.2.6 Western region plutonic rocks

Western region metasediments are cut by a plutonic suite of orthopyroxene-bearing monzogranite, granodiorite and diorites. An orthopyroxene-bearing monzogranite (Sample B97A) was dated at 1892±7 Ma (Rayner, 2014a and b), Scott dated a similar rock-type (orthopyroxene tonalite, sample D350) at 1890 +3/-2 Ma (Figure 4.7). This date matches perfectly with the ~1890 Ma Qikiqtarjuaq plutonic suite from Cumberland Peninsula. This plutonic suite had not been recognized prior to the Cumberland Peninsula Integrated Geoscience Project, as it was thought that the plutonic rocks from western Cumberland Peninsula were all part of the ~1860 Ma Cumberland Batholith found in central and southern Baffin Island. This was also the case for the orthopyroxene-bearing plutonic suite in western Hall Peninsula prior to U-Pb geochronology by Scott (1999) and Rayner (2014). Whalen et al., (2010) proposed, based on a 900 km geochemical-isotopic (Nd – O) transect, that the ~1860 Ma Cumberland Batholith resulted from post-collision lithospheric mantle delamination which resulted in upwelling of hot asthenospheric mantle and large volume partial melting of the crust. However, there has been no study of the chemical and isotopic variation between ~1890 Ma Qikiqtarjuaq plutonic suite and the ~1860 Ma Cumberland Batholith. From the Whalen transect (Figure 4.10) it is impossible to know the actual age of all the plutons that were studied. It may be that the older Qikiqtarjuaq plutonic suite is the result of continental arc accretion between the under-riding North Atlantic craton (Hall Peninsula 'Block' – Figure 4.10) with the Meta Incognita microcontinent and Rae craton prior to delamination which produced the Cumberland Batholith (proper) (Figure 4.11c).

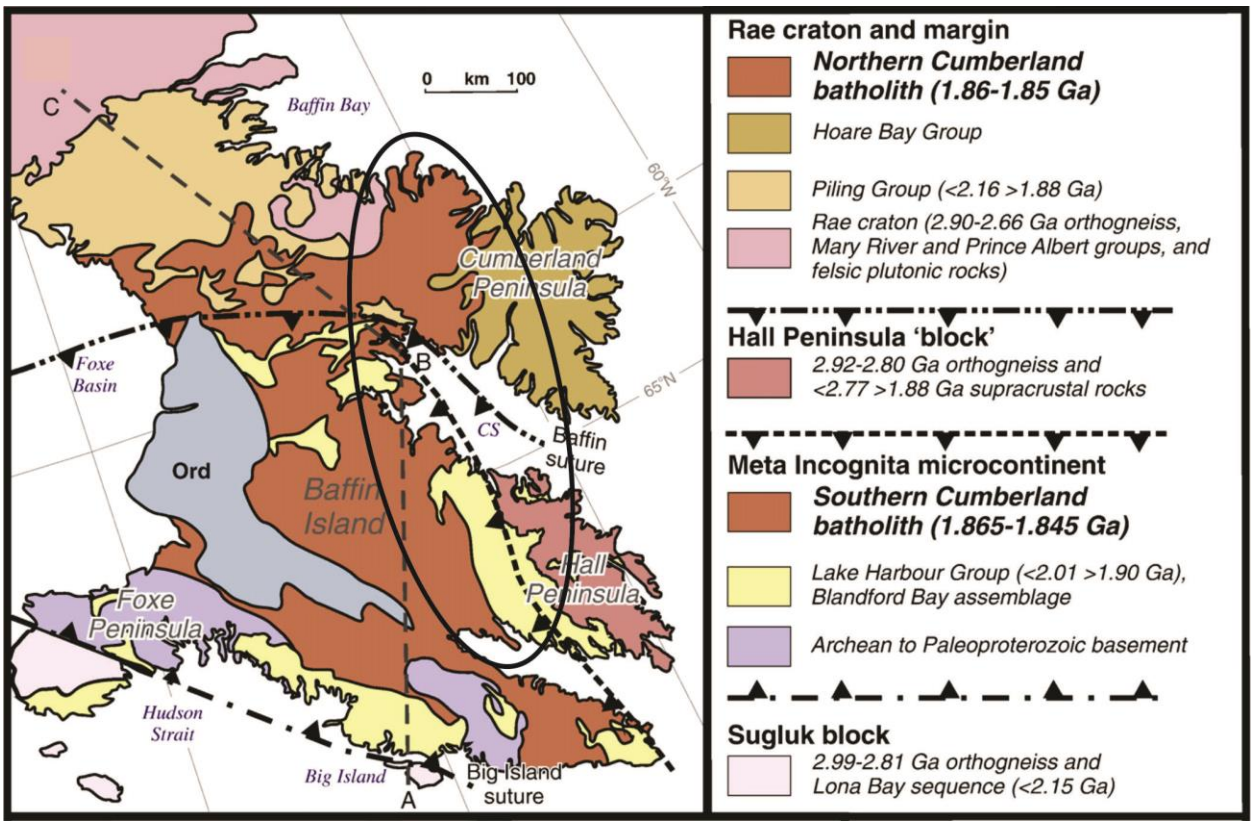

Figure 4.9 – Simplified geology of south and central Baffin Island modified after Whalen et al., 2010. Black ellipse highlights the approximate area in which the ~1890 Ma Qikiqtarjuaq plutonic suite occurs. Grey dashed line (A-B-C) indicates approximate position of Whalen et al. (2010) geochemical and isotopic transect.

Mafic rocks in the western region of Hall Peninsula are scarce. Operating on the interpretation that the western region of the Hall Peninsula is a part of the Meta Incognita microcontinent and the east-central region is a part of the North Atlantic craton (Figure 4.12) it follows that the mafic rocks between regions may not be genetically related. The mafic rocks in the western region may represent a minor phase of the Qikiqtarjuaq plutonic suite. One explanation for the indiscernible geochemical profile between the east-central and western regions is that similar geochemical modification of the mantle below the Meta Incognita microcontinent may have occurred prior to emplacement of the Qikiqtarjuaq plutonic suite.

4.2.7 Deformation and metamorphism

All rocks in the QA have undergone at least two distinct deformational events. The first, an east-west compression (D1), with west over east transport resulted in the dominant regional (S1) fabric as well as tight, nearly isoclinal folding (F1). As regional T2 thrust nappes are not observed in the QA, the next deformation event recorded in the QA resulted from north-south compression producing open F3 folds and an S3 crenulation cleavage. Since the 1873 ± 6 Ma monzogranite dykes are themselves deformed this places a maximum age on D1 deformation.

The deformation events which resulted in the observed fabrics in the QA and the Hall Peninsula as a whole require careful study which is beyond the scope of this thesis. However based on the geometry of the observed fabrics, D1 and D2 may be the result of the collision between the North Atlantic craton and the Meta Incognita microcontinent as both result from east-west compression based on their current orientation (Figure 4.11c). D3 may then be the result of the collision of the southern Superior craton with the upper Churchill plate collage as this event is marked by north-south compression (Figure 4.11d).

Garnet – biotite – sillimanite – K-feldspar mineral assemblages observed in QA pelites indicate that amphibolite facies metamorphic conditions were reached during M1. This preserved mineral assemblage was subsequently folded during D3. Empirical confirmation of the inferred metamorphic conditions based on observed mineral assemblage was made by EMPA using the garnet-biotite exchange geothermometer (Bhattacharya, 1992; Hodges and Spear, 1982; and Thompson, 1976), the GASP geobarometer (Hackler and Wood, 1989; and Ganguly and Saxena, 1984) as well as winTWQ software (Berman, 2007). Results from winTWQ indicate that maximum temperature and pressure conditions recorded in the QA were 645±50°C

and 4.8±2.1 kbars. In the western region of the Hall Peninsula granulite-facies conditions were reached as suggested by orthopyroxene-bearing mineral assemblages and numerous melt pods/sweats interpreted as locally derived anatexis.

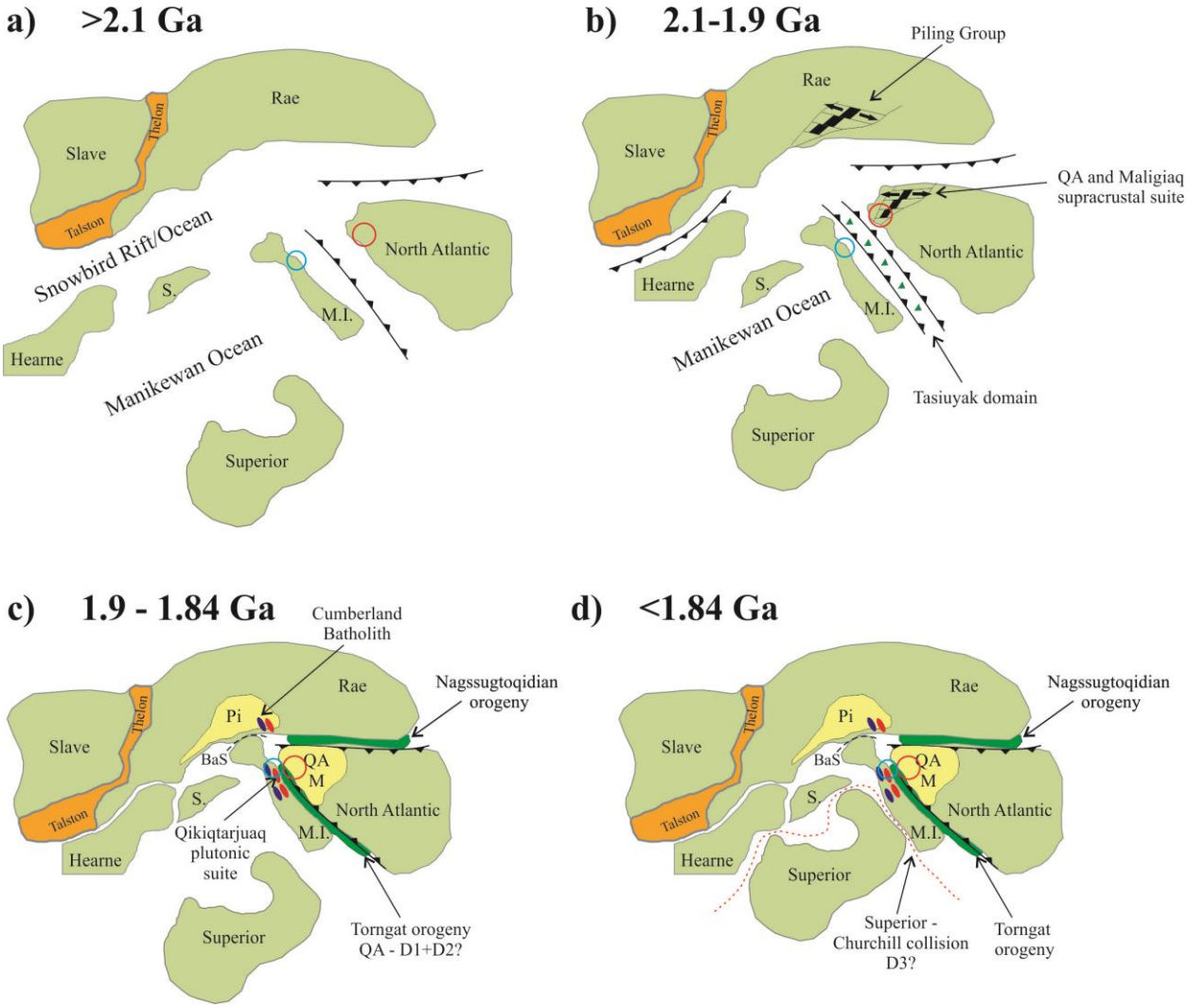

Figure 4.10 – Map view diagram (modified after Corrigan, 2012) showing a) subduction occurring beneath the North Atlantic craton prior to 2.1 Ga enriching the underlying mantle. b) Rifting of the Rae and North Atlantic cratons between 2.1 and 1.9 Ga, possible related to upwelling of a mantle plume, creates basins into which the Piling and, QA and Maligiaq supracrustal + mafic/ultramafic, respectively could be deposited/intruded. c) Terminal collision of the Torngat and Nagssugtoqidian orogenies between 1.9 and 1.84 Ga which creates S1, F1 and T2 on Hall Peninsula and initiates emplacement of the Qikiqtarjuaq plutonic suite at ~1890 Ma. Cumberland batholith emplaced at ~1860 Ma. d) Collision of the under-riding Superior craton and upper Churchill plate-collage which creates S3 and F3 on Hall Peninsula. Blue and red circles indicate approximate positions of western and east-cental Hall Peninsula, respectively. BaS – Baffin suture; M; Maligiaq supracrustal suite; M.I. – Meta Incognita microcontinent; Pi – Piling Group; QA – Qaqqanituaq Area; S – Sugluk craton.

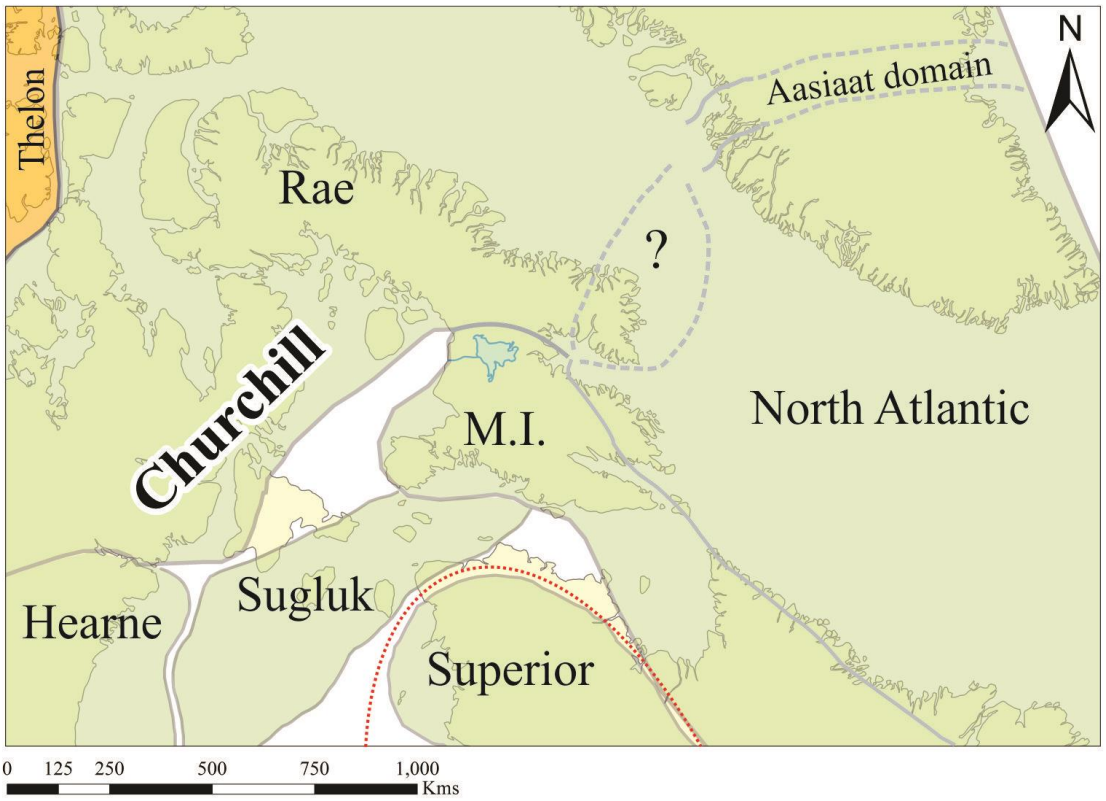

Figure 4.11 – Map showing position of land masses in their current position based on the interpretations shown in Figure 4.11d. Red dotted line indicates boundary between the lower plate, Superior craton and the upper Churchill plate collage. It is not known if the Aasiaat domain in Greenland comprises the North Atlantic craton, the Rae craton, an as yet to be determined new microcontinent or some combination of the three. M.I. – Meta Incognita microcontinent. Modifed after Corrigan, 2012.

CHAPTER 5

CONCLUSIONS

5.1 Introduction

The purpose of this thesis was twofold, with each part necessary for and complimentary to the other. The first part was to study the geology of the Qaqqanituaq area including its metamorphic, deformational and geochronological history. This was accomplished by a detailed transect to identify and sample all major rock units across the QA structural basin and by focused mapping in key areas of the QA, most notably the exposed fold hinges where the most valuable structural information could be observed. Field descriptions of rock units as well as petrographic analysis were used to characterize the QA lithologies. Electron microprobe analysis of QA pelites was conducted at the University of Saskatchewan so that the garnet-biotite geothermometer, GASP geobarometer and winTWQ software could be used to obtain estimates of the maximum pressure and temperature conditions achieved in the QA. U-Pb ages of both detrital zircons from a QA quartzite and a monzogranite dyke which cross-cuts all QA lithologies were obtained by N. Rayner of the Geological Survey of Canada using a sensitive high resolution ion microprobe (SHRIMP).

The second part of this thesis involved the first detailed description of the mafic and ultramafic rocks of the Hall Peninsula. Mafic and ultramafic rocks on the Hall Peninsula most commonly occur intercalated with metasedimentary packages, analogous to the QA, found in the east-central region of the Hall Peninsula. As such, the relationships studied in the QA could be extrapolated to other metasedimentary-mafic-rock-occurrences across the Hall Peninsula. Whole-rock major and trace element geochemistry was obtained for 75 mafic and ultramafic

samples from across the Hall Peninsula using ICP-MS analysis carried out by Activation Laboratories Inc. To better characterize the mafic and ultramafic rocks, they were also studied using petrographic analysis and EMPA. Interpretations were then made about the petrogenesis, and tectonic setting of the mafic and ultramafic rocks.

All of the new data obtained in this thesis project was integrated then compared with existing published data from regions adjacent to the Hall Peninsula. Using all of this information, interpreted correlations have been suggested.

5.2 The Qaqqanituaq Area

The QA is a doubly-plunging, synformal structural basin. Tonalite orthogneiss correlated with a 2841 ± 3 Ma (Rayner, 2014) tonalite dated on Beekman Peninsula forms the structural base of the QA. Structurally above the Archean basement are metasedimentary rocks dominated by micaceous psammite with lesser quartzite and pelite intercalated with mafic and ultramafic rocks all of which are cross cut by later monzogranite dykes. Observation of a potential paleoregolith may indicate that the Archean tonalite gneiss is also the stratigraphic base of the QA and therefore the QA metasedimentary rocks are essentially autochthonous. All QA rocks have underwent at least two distinct deformational events which affect all lithologies. The first, D1 resulted in the dominant regional fabric S1, tight F1 folds, and the observed garnet – biotite – K-feldspar – sillimanite metamorphic mineral assemblage. EMPA analysis and the implementation of winTWQ software indicate that the maximum pressure and temperature conditions achieved in the QA were 4.8±2.1 kbars and 645±50°C. The second deformational event recorded in the QA is D3 which resulted in open F3 folds and an S3 crenulation cleavage.

D2 post-thermal peak thrusting is not evident in the QA, but is observed in other regions of the Hall Peninsula and as such is taken into account when naming structural events.

U-Pb detrital zircon geochronology and U-Pb geochronology of the cross-cutting monzogranite dykes bracket sedimentation and, mafic and ultramafic intrusion/extrusion between 2.13 and 1.87 Ga and place a maximum age on D1 of 1.87 Ga.

5.3 Mafic and Ultramafic Geochemistry and Petrogenesis

The metasedimentary rocks of the east-central region of the Hall Peninsula are intercalated with a series of mafic and ultramafic rocks which may be either successive flows or intrusive sills and dykes. However, no primary igneous textures are preserved which would allow for the intrusive/extrusive nature of these mafic and ultramafic rocks to be known with certainty. Whole-rock major and trace element geochemical analysis of 69 mafic and 6 ultramafic rocks from across the Hall Peninsula was carried out. On the basis of N-MORB (Sun and McDonough, 1989) normalized geochemical profiles and the sub-alkaline mafic rock discrimination diagram of Ross and Bédard (2009), the mafic rocks were classified as being alkaline, calc-alkaline, transitional or tholeiitic. Petrographic variation between these sub-groups was negligible except when comparing samples obtained from the western region of the Hall Peninsula, where granulite-facies metamorphic conditions were reached. Comparisons of mineral chemistry between sub-groups revealed distinct clustering of mineral compositions which gives credence to the imposition of the proposed sub-groups. Geochemical variation between ultramafic samples was broad, therefore ultramafic rocks were classified on the basis of mineralogy as either olivine-hornblende-pyroxenite cumulates or websterite cumulates.

With the exception of the alkaline mafic rocks, all samples show a pronounced negative Nb anomaly with respect to Th and Ce which likely resulted from the melting of a mantle source enriched during subduction beneath the North Atlantic craton prior to the Torngat and/or Nagssugtoqidian orogenies. Enrichment of the most incompatible elements relative to N-MORB and high Ti/Y ratios in calc-alkaline, alkaline and transitional mafic rocks suggest a within-plate origin to these mafic rocks possibly resulting from a mantle plume. Flat, N-MRB depleted profiles observed in tholeiites suggest they may be associated with a spreading centre. The mixed geochemical profile and the tendency for mafic and ultramafic rocks to be intercalated within metasediments may indicate that the QA, and by extension metasedimentary-mafic-rock-occurrences throughout the east-central region of the Hall Peninsula, formed in an extensional environment initiated by the upwelling of a mantle plume below the Hall Peninsula.

5.4 Regional Correlations

Possible correlations of the Hall Peninsula with adjacent regions were explored in Chapter 4. Based on the available data, the western region of Hall Peninsula is interpreted as being a part of the Meta Incognita microcontinent with western metasediments representing a shelf-edge and sourcing similar detritus to that of both the Hoare Bay and Piling Groups. Western plutonic rocks dated at 1892±7 Ma (Rayner, 2014a and b) are correlated with the ~1890 Ma Qikiqtarjuaq plutonic suite from Cumberland Peninsula.

The east-central region is interpreted as being a part of the North Atlantic craton based on a pronounced geophysical anomaly that divides the Hall Peninsula and extends southward through the Tasiuyak paragneiss in northern Quebec and Labrador as well as similar detrital

zircon age populations between the QA quartzite and the Maligiaq supracrustal suite on the northern margin of the North Atlantic craton in southwest Greenland.

REFERENCES

Aspler, L.B., and Chiarenzelli, J.R., 1998, Two Neoarchean supercontinents? Evidence from the Paleoproterozoic: Sedimentary Geology, v. 120, pp. 75-104.

Barker, A.J., 1990, Intoduction to Metamorphic Textures and Microstructures. Blackie, Glasgow, U.K.

Berman, R.G., 1988, Internally-consistent thermodynamic data for minerals in the system Na2O-K2O-CaO-MgO-FeO-Fe2O3-Al2O3-SiO2-TiO2-H2O-CO2: Journal of Petrology, v. 29, pp. 445-522.

Berman, R.G., 1991, Thermobarometry using multi-equilibrium calculations: a new technique, with petrological implications; in, Quantitative methods in petrology: an issue in honor of Hugh J. Greedwood; Eds. Gordon, T M; Martin, R F. Canadian Mineralogist, v. 29, pp. 833-855.

Berman, R.G., 2007, winTWQ (version 2.3): a software package for performing internally-consistent thermobarometric calculations. Geological Survey of Canada, Open File 5462, (ed. 2.32) 2007, 41 pages.

Berman, R.G., Aranovich, L.Y., Rancourt, P. and Mercier, P.H., 2007, Reversed phase equilibrium constraints on the stability of Mg-Fe-Al biotite: American Mineralogist, v. 92, pp. 139-150.

Berman, R.G., Sanborn-Barrie, M., Hamilton, B.M., Rayner, N., and Young, M., 2013, Preliminary in situ SHRIMP geochronological constraints on the tectonometamorphic evolution of Cumberland Peninsula, Baffin Island, Nunavut: Geological Survey of Canada, Current research 2013-7, 19p. doi:10.4095/292215.

Bertrand, J.-M., Roddick, J. C., Van Kranendonk, M. J., and Ermanovics, I., 1993, U–Pb geochronology of deformation and metamorphism across a central transect of the Early Proterozoic Torngat Orogen, North River map area, Labrador: Canadian Journal of Earth Sciences, v. 30, pp. 1470–1489.

Bhattacharya, A., Mohanty, L., Maji, A., Sen, S.K., Raith, M., 1992, Non-ideal mixing in the phlogopite-annite binary: constraints from experimental data on Mg-Fe partitioning and a reformulation of the biotite-garnet geothermometer: Contributions to Mineralogy and Petrology, v. 111, pp. 87-93.

Blackadar, R.G., 1967, Geological reconnaissance, southern Baffin Island, district of Franklin, Geological Survey of Canada, Paper 66-47.

Cann, J.R., 1970, Rb, Sr, Y, Zr and Nb in some ocean floor basaltic rocks: Earth and Planetary Science Letters, v. 10, pp. 7-11.

Clarke, D.B., 1981, The mineralogy of peraluminous granites: a review: Canadian Mineralogist, v. 19. Pp. 3-17.

Connelly, J. N. 2001, Constraining the timing of metamorphism: U–Pb and Sm–Nd ages from a transect across the northern Torngat Orogen, Labrador, Canada. Journal of Geology, v. 109, pp. 57–77.

Connelly, J.N., Thrane, K., Krawiec, A.W., and Garde, A.A, 2006, Linking the Palaeoproterozoic Nagssugtoqidian and Rinkian orogens through the Disko Bugt region of West Greenland: Journal of the Geological Society of London, v. 163, pp. 319-335.

Corrigan, D., Pehrsson, S., Wodicka, N., de Kemp, E. 2009, The Palaeoproterozoic Trans-Hudson Orogen: a prototype of modern accretionary processes; Geological Society of London, Special Publications, v. 327, p. 457-479.

Corrigan, D., 2012, Paleoproterozoic crustal evolution and tectonic processes: Insights from the LITHOPROBE program in the Trans-Hudson orogeny, Canada. Chapter 4 *In* Tectonic Styles in Canada: The LITHOPROBE Perspective. *Edited by* J.A. Percival, F.A. Cook, and R.M. Clowes. Geological Association of Canada, Special Paper 49, pp. 237-284.

Dumont, R., and Dostaker, F., 2010, Geological Survey of Canada, Open File 6413, 1:100 000 first vertical derivative magnetic field map, doi: 10.4095/261656.

Erlank, A,J., Allsopp, H.L., Hawkesworth, C.J., and Menzies, M.A., 1982, Chemical and isotope characterization of upper mantle metasomatism in peridotite nodules from the Bulfontein kimberlite: Terra Cognita, v. 2, pp. 216-263.

Fan, J. & Kerrich, R., 1997, Geochemical characteristics of aluminum depleted and undepleted komatiites and HREE-enriched low-Ti tholeiites, western Abitibi greenstone belt: A heterogeneous mantle plume-convergent margin environment: Geochimica et Cosmochimica Acta, v. 61, pp. 4723-4744.

Faure, G., 1986, Principles of isotope geology, 2nd ed. John Wiley and Sons, Inc.

Ferry, J.M. and Spear, F.S., 1978, Experimental calibration of the partitioning of Fe and Mg between biotite and garnet: Contributions to Mineralogy and Petrology, v. 66, pp. 113-117.

Floyd, P.A., and Winchester, J.A., 1975, Magma type and tectonic discrimination using immobile elements: Earth and Planetary Science Letters, v. 27, pp. 211-218.

Floyd, P.A., and Winchester, J.A., 1978, Identification and discrimination of altered and metamorphosed volcanic rocks using immobile elements: Chemical Geology, v. 21, pp. 291-306.

Frey, F.A., 1982, Rare earth element abundances in upper mantle rocks, *in* Henderson, P., ed., Rare Earth Element Geochemistry: Elsevier, Amsterdam, p. 153-203.

Ganguly, J., and Saxena, S.K., 1984, Mixing properties of aluminosilicate garnets: constraints from natural and experimental data, and application to geothermo-barometry: American Mineralogist, v. 69, pp. 88-97.

Garde, A.A., Hollis, J.A. and Mazur, S., 2007, Paleoproterozoic greenstones and pelitic schists in the northern Nagssugoqidian orogeny, West Greenland: evidence for a second subduction zone?: Geological Association of Canada – Mineralogical Association of Canada (GAC-MAC) Programs with abstracts, v. 32, pp. 30.

Garde, A.A., Whitehouse, M., and Christensen, R., 2012, Mesoarchean epithermal gold mineralization preserved at upper amphibolite-facies grade, Qussuk, southern West Greenland: Economic Geology, v. 107, no. 5, pp. 881-908. Doi: 10.2113/econgeo.107.5.881

Hackler, R.T., and Wood, B.J., 1989, Experimental determination of Fe and Mg exchange between garnet and olivine and estimation of Fe-Mg mixing properties: American Mineralogist, v. 74, pp. 994-999.

Hamilton, B.M., Pattison, D.RM., Sanborn-Barrie, M., and Young, M.D., 2012, Preliminary characterization of metamorphism on Cumberland Peninsula, Baffin Island, Nunavut: Geological Survey of Canada, Current Research 2012-9, 17 p. doi: 10.4095/291530.

Hastie, A.R., Kerr, A.C., Pearce, J.A., Mitchell, S.F., 2007, Classification of altered volcanic arc rocks using immobile trace elements: Development of the Th-Co discrimination diagram: Journal of Petrology, v. 48, pp. 2341-2357.

Henry, D.J., Guidotti, C.V., and Thomson, J.A., 2005, The Ti-saturation for low-to-medium pressure metapelitic biotites: Implications for geothermometry and Ti substitution mechanisms: American Mineralogist, v. 90, pp. 316-328.

Herzberg, C., et al., 2007, Temperatures in ambient mantle and plumes: Constraints from basalts, picrites and komatiites: Geochemistry, Geophysics, Geosystems: an Electronic Journal of the Earth Sciences, v. 8, doi:10.1029/2006GC001390.

Hodges, K.V., and Spear, F.S., 1982, Geothermometry, geobarometry and the Al_2SiO_5 triple point at Mt. Moose; Lauke, New Hampshire: American Mineralogist, v. 67, p. 1118-1134.

Hoffman, P.F., 1989 a, United Plates of America, The Birth of a Craton: Early Proterozoic Assembly and Growth of Laurentia: Annual Review of Earth and Planetary Sciences, v. 16, pp. 543-603.

Hoffman, P.F., 1989 b, Precambrian geology and tectonic history of North America; in The Geology of North America – An Overview, (ed.) A.W. Bally and A.R. Palmer: Geological Society of America, v. A, pp. 447-512.

Hollocher, K., "Calculation of a CIPW Norm from a Bulk Chemical Analysis." 1 Jan. 2014. Web. 28 Dec. 2014.

Holm, P.E., 1982, Non-recognition of continental tholeiites using the Ti – Y – Zr diagram: Contributions to Mineralogy and Petrology, v. 79, pp. 308-310.

Humphris, S.E., and Thompson, G., 1978, Trace element mobility during hydrothermal alteration of oceanic basalts: Geochemica et Cosmochemica Acta, v. 42, pp. 127-136.

Jackson, G.D., 2000, Geology of the Clyde-Cockburn Land map area, north-central Baffi n Island, Nunavut: Geological Survey of Canada Memoir 440, 303 p.

Jackson, G.D., and Taylor, F.C., 1972, Correlation of major Aphebian rock units in the northeastern Canadian Shield: Canadian Journal of Earth Sciences, v. 9, pp. 1650–1669, doi: 10 .1139 /e72 -146 .

Johns, S.M., Helmstaedt, H.H., Kyser, T.K., 2006, Paleoproterozoic submarine intrabasinal rifting, Baffin Island, Nunavut, Canada: volcanic structure and geochemistry of the Bravo Lake Fromation: Canadian Journal of Earth Sciences, v. 43, pp. 593-616.

Kalsbeek, F., and Manatschal, G, 1999, Geochemistry and tectonic significance of peridotitic and metakomatiitic rocks from the Ussuit area, Nagssugtoqidian orogen, West Greenland: Precambrian Research, v. 94, pp. 101-120.

Keim, R.D., 2012, Stratigraphy, petrology and geochemistry of the North Touak-Cape Dyer volcanic belt, and implications for the Paleoproterozoic Hoare Bay group, eastern Baffin Island. Unpub. M.Sc. thesis, University of Saskatchewan. 124pp.

Kohn, M.J., and Spear, F.S., 2000, Retrograde Net Transfer Reaction (ReNTR) Insurance for P-T Estimates: Geology, v. 28, pp.1127-1130.

Koziol, A.M. and Newton, R.C., 1988, Redetermination of the anorthite breakdown reaction and improvement of the plagioclase-garnet-Al2SiO5-quartz barometer: American Mineralgist, v. 73, pp. 216-233.

Le Bas, M.J., Maitre, R.W., Streckeisen, A. and Zanettin, B., 1985, A chemical classification of volcanic rocks based on the total alkali – silica diagram: Journal of Petrology, v. 27, pp. 745-750.

Le Maitre, R.W., Streckeisen, B., Zanettin, B., Le Bas, M.J., Bonin, B., Bateman, P., Bellieni, G., Dudek, A., Efremova, S., Keller, J., Lameyre, J., Sabine, P.A., Schmid, R., Sorensen, H., and Wooley, A.R., 2002, Igneous Rocks: A Classification and Glossary of Terms: Recommendations of the International Union of Geological Sciences Subcommission on the Systematics of Igneous Rocks, 2nd Ed. Cambridge University Press.

Leake, B.E., 1978, Nomenclature of amphiboles: American Mineralogist, v. 63, pp. 1023–1052.

Leake, B.E., et al., 1997, Nomenclature of amphiboles: Report of the Subcommittee on amphiboles of the International Mineralogical Association, Commission on New Minerals and Mineral Names: The Canadian Mineralogist, v. 35, pp. 219-246.

Lichtblau, A. 1997: Baffin Island Project – report of work, International Capris Resources assessment report, Nunavut Geoscience Report 083824.

Machado, G., Biloodeau, C., Takpanie, R., St-Onge, M., Rayner, N., Skipton, d., From, R., MacKay, C.B., Creason, G., and Braden, Z., 2013, Hall Peninsula regional bedrock mapping, Baffin Island Nunavut: summary of fieldwork, *in* Summary of Activities 2012, Canada-Nunavut Geoscience Office. P. 13-22.

Machado, G., Bilodeau, C., St-Onge, M.R., 2013, Geological Survey of Canada, Canadian Geoscience Map 135, doi: 10.4095/292443.

MacKay, C.B., Ansdell, K.M., St-Onge, M.R., Machado, G., Bilodeau, C., 2013, *in* Summary of Activities 2012, Canada-Nunavut Geoscience Office. P. 55-64.

Meschede, M., 1986, A method of discriminating between different types of mid-ocean ridge basalts and continental tholeiites with the Nb – Zr – Y diagram: Chemical Geology, v. 56, pp. 207-218.

Morgan, W.C., Bourne, J., Herd, R.K., Pickett, J.W., and Tippett, C.R., 1975, Geology of the Foxe Fold Belt, Baffin Island, District of Franklin, *in* Report of Activities,Part A: Geological Survey of Canada Paper 75-1A, pp. 343–347.

Morgan, W.C., Okulitch, A.V., and Thompson, P.H., 1976, Stratigraphy, structure and metamorphism of the west half of the Foxe Fold Belt, Baffi n Island, *in* Report of Activities, Part A: Geological Survey of Canada Paper 76-1A, pp. 387–391.

Morimoto, N., Fabries, J., Ferguson, A.K., Ginzburg, I.V., Moss, M., Seifert, F.A., Zussman, J., 1988, Nomenclature of pyroxenes: American Mineralogist, v. 73, pp. 1123-1133.

Niu, Y., et al., 2011, The origin of intra-plate ocean island basalts (OIB): the lid effect and its geodynamic implications: Journal of Petrology, v. 52, pp. 1443-1468.

Parissh, R.R., 1989, U-Pb geochronology of the Cape Smith Belt and Sugluk block: Geoscience Canada, v. 16, pp. 126-130.

Pearce, J.A., 1996, A User's Guide to Basalt Discrimination Diagrams *in* Wyman, D.A., ed., Trace Element Geochemistry of Volcanic Rocks: Applications for Massive Sulphide Exploration: Geological Association of Canada, Short Course Notes, v. 12, p. 79-113.

Pearce, J.A., 2008, Geochemical fingerprinting of oceanic basalts with applications to ophiolite classification and the search for Archean oceanic crust: Lithos, v. 100, pp. 14-48.

Pearce, J.A. and Cann, J.R., 1973, Tectonic setting of basic volcanic rocks determined using trace element analyses: Earth and Planetary Science Letters, v. 19, pp. 290-300.

Pearce, J.A. and Norry, M.J., 1979, Petrogenetic implications of Ti, Zr, Y, and Nb variations in volcanic rocks: Contributions to Mineralogy and Petrology, v. 69, pp. 33-47.

Pearce, J.A. and Parkinson, I.J., 1993, Trace element models for mantle melting: application to volcanic arc petrogenesis. *In*: Prichard, H.M., Alabaster, T., Harris, N.B.W. and Neary, C.R. (eds) Magmatic Processes and Plate Tectonics. Geological Society, London, Special Publications, v. 76, pp. 373-403.

Prestvik, T., 1982, Basic volcanic rocks and tectonic setting. A discussion of the Zr – Ti – Y discrimination diagram and its suitability for classification purposes: Lithos, v. 15, pp. 241-247.

Rayner, N.M, 2014a, New U-Pb geochronological results from Hall Peninsula, Baffin Island, Nunavut; *in* Summary of Activities 2013, Canada-Nunavut Geoscience Office, pp. 39-52.\

Rayner, N.M., 2014b, Data table accompanying "New U-Pb geochronological results from Hall Peninsula, Baffin Island, Nunavut", Canada_nunavut Geoscience Office, Geoscience Data Series GDS2014-001, Microsoft® Excel® file.

Rutherford, E., and Soddy, F., 1903, Radioactive Change: The London, Edinburgh, and Dublin Philosophical Magazine and Journal of Science (6), v. 5, pp. 576-591.

Sanbron-Barrie, M., St-Onge, M.R., Young, M.D., and James, D.T., 2008, Bedrock geology of southwestern Baffin Island, Nunavut: expanding the tectonostratigraphic framework with relevance to mineral resources: Geological Survey of Canada, Current Research 2008-6, 16p.

Sanborn-Barrie, M., and Young, M., 2011, Bulk Compositional Data for Sulfidic and Gossanous Rocks from Cumberland Peninsula, Baffin Isalnd, Nunavut: Geological Survey of Canada Open file 6916.

Scott, D.J., 1996, Geology of the Hall Peninsula east of Iqaluit, southern Baffin Island, Northwest Territories: in Current Research 1996-C; Geological Survey of Canada, pp. 83-91.

Scott, D. J. 1998, U–Pb ages of Archean crust in the southeast arm of the Rae Province, southeastern Ungava Bay, Quebec. In: Radiogenic age and isotopic studies: report 2. Geological Survey of Canada Paper, 1998-F, pp. 41–45.

Scott, D.J., 1999, U-Pb geochronology of the eastern Hall Peninsula, southern Baffin Island, Canada: a northern link between the Archean of West Greenland and the Paleoproterozoic Torngat Orogen of northern Labrador: Precambrian Research, v. 93, pp. 5-26.

Scott, D. J., and Machado, N., 1995, U–Pb geochronology of the northern Torngat Orogen, Labrador, Canada: A record of Paleoproterozoic magmatism and deformation: Precambrian Research, v. 70, pp. 169–190.

Scott, D.J., and St-Onge, M.R., 1995, Constraints on Pb closure temperature in titanite based on rocks from the Ungava orogeny, Canada: implications for U-Pb geochronology and P-T-t path determinations: Geology, v. 23, pp. 1123-1126.

Scott, D.J., St-Onge, M.R., Wodicka, N., and Manmer, S., 1997, Geology of the Markham Bay – Crooks Inlet area, southern Baffin Island, Northwest Territories. *In* Paper 1997-C. Geological Survey of Canada, pp, 157-166.

Shervais, J.W., 1982, Ti – V plots and the petrogenesis of modern and ophiolitic lavas: Earth and Planetary Science Letters, v. 59, pp. 101-118.

Smith, R.E. and Smith, S.E., 1976, Comments on the use of Ti, Zr, Y, Sr, K, P and Nb in classification of basaltic magmas: Earth and Planetary Science Letters, v. 32, pp. 114-120.

Spear, F.S., Kohn, M.J., Florence, F. and Menard, T., 1990, A model for garnet and plagioclase growth in pelitic schists: Implications for thermobarometry and P-T path determinations: Journal of Metamorphic Geology, v. 8, pp. 683-696.

Stern, R.A., 1997, The GSC Sensitive High Resolution Ion Microprobe (SHRIMP): analytical techniques of zircon U-Th-Pb age determinations and performance evaluation: *in* Radiogenic Age and Isotopic Studies: Report 10, Geological Survey of Canada, Current Research 1997-F, pp. 1-31.

Stipp, M.J., Searle, M.P., Waters, D.J. and Horstwood, M.S.A., 2010, The eastern Tonale fault zone: a natural laboratory for crystal plastic deformation of quartz over a temperature range from 250 to 700ºC: Journal of Structural Geology, v. 24, pp. 1861-1884.

Steenkamp, H.M., and St-Onge, M.R., 2014, Overview of the 2013 regional bedrock mapping program on northern Hall Peninsula, Baffin Island, Nunavut: *in* Summary of Activities 2013, Canada-Nunavut Geoscience Office, p. 27-38.

St-Onge, M.R., Lucas, S.B., Parrish, R.R., 1992, Terrane accretion in the internal zone of the Ungava orogeny, northern Quebec. Part 1: tectonostratigraphic assemblages and their tectonic implications: Canadian Journal of Earth Sciences, v. 29, pp. 746-764.

St-Onge, M.R., Scott, D.J., and Wodicka, N., 1999, Geological maps and descriptive notes and legends, parts of Meta Incognita Peninsula, Nunavut: Geological Survey of Canada maps 1979A to 1985A: scale 1:1000 000.

St-Onge, M.R., Scott, D.J., and Lucas, S.B., 2000, Early partitioning of Quebec: Microcontinent formation in the Paleoproterozoic: Geology, v. 28, pp. 323-326.

St-Onge, M.R., Scott, D.J., Wodicka, N., 2001, Terrnane boundaries within Trans-Hudson Orogen (Quebec – Baffin segment), Canada: changing structural and metamorphic character from foreland to hinterland: Precambrian Research, v. 107, pp. 75-91.

St-Onge, M.R., Scott, D.J., Wodicka, N., 2002, Review of crustal architecture and evolution in the Ungava Peninsula – Baffin Island area: connection to the Lithoprobe ECSOOT transect: Canadian Journal of Earth Sciences, v. 39, pp. 589-610.

St-Onge, M.R., Jackson, G.D., and Henderson, I., 2006, GSC Open File 4931, doi: 10.4095/222520.

St-Onge, M.R., Van Gool, J.A.M., Garde, A.A., and Scott, D.J., 2009, Correlation of Archean and Paleoproterozoic units between northeastern Canada and western Greenland: constraining the pre-collisional upper plate accretionary history of the Trans-Hudson orogeny: Geological Society, London, Special Publications, v. 318, pp. 193-235.

Sturm, R., 2002, PX-NOM an interactive spreadsheet program for the computation of pyroxene analyses derived from the electron microprobe: Computers and Geoscience, v. 28, pp. 473-483.

Thériault, R.J., St-Onge, M.R., and Scott, D.J., 200, Nd isotopic and geochemical signature of the Paleoproterozoic Trans-Hudson Orogen, southern Baffin Island, Canada: implications for the evolution of eastern Laurentia: Precambrian Research, v. 108, pp. 113-138.

Thompson, A.B., 1976, Mineral relations in pelitic rocks: II. Calculation of some P – T – X (Fe – Mg) phase relations: The American Journal of Science, v. 276, pp. 425-454.

Tippett, C.R., 1984a, Geology of a transect through the southern margin of the Foxe Fold Belt, central Baffin Island, District of Franklin: Geological Survey ofCanada Open File Report 1110, 77 p.

Van Kradendonk, M. J. 1996, Tectonic evolution of the Paleoproterozoic Torngat Orogen; evidence from P–T–t–d paths in the North River map area, Labrador: Tectonics, v. 15, pp. 843–869.

Van Kradendonk, M. J., and Wardle, R. J., 1996, Burwell domain of the Palaeoproterozoic Torngat orogen, northeastern Canada: Tilted cross-section of a magmatic arc caught between a rock and a hard place. In: Brewer, T. S. (ed.) Precambrian Crustal Evolution in the North Atlantic Region. Geological Society, London, Special Publications, v. 112, pp. 91–115.

van Hunen, J. and Moyen, J.F., 2012, Archean Subduction: Fact or Fiction?: Annual Review of Earth and Planetary Sciences, v. 40, pp. 195-219.

Viljoen, M.J., Viljoen, R.P., Smith, H.S., Erlank, A.J., 1983, Geological, textural and geochemical features of komatiitic flows from the Komati Formation: Geological Society of South Africa, Special Publication, v. 9, pp. 1-20.

Waters, D.J., “Practical Aspects of Mineral Thermobarometry”, http://www.earth.ox.ac.uk, 12 October 2004. web. 5 May 2014.

Whalen, J.B., Wodicka, N., Taylor, B.E., and Jackson, G.D., 2010, Cumberland Batholith, Trans-Hudson Orogen, Canada: Petrogenesis and implications for Paleoproterozoic crustal orogenic processes: Lithos, v. 117, pp. 99-118.

Williams, H., Hoffman, P.F., Lewry, J.F., Monger, J.W.H., and Rivers, T., 1991, Anatomy of North America: Thematic geologic portrayals of the continent: Tectonophysics, v. 187, pp 117-134.

Winchester, J.A. and Floyd, P.A., 1977, Geochemical discrimination of different magma series and their differentiation products using immobile elements: Chemical Geology, v. 20, pp. 325-343.

Winter, J.D., 2010, Principles of Igneous and Metamorphic Petrology, 2nd ed. Pearson Prentice Hall.

Wodicka, N., and Scott, D.J., 1997, A preliminary report on the U-Pb geochronology of the Meta Incognita Peninsula, southern Baffin Island, Northwest Territories: Geological Survey of Canada Paper 1997-C, pp. 167-178.

Wodicka, N., St-Onge, M.R., Corrigan, D., Scott, D.J., and Whalen, J., 2014, Did a proto-ocean basin form aloing the southeastern Rae cratonic margin? Evidence from U-Pb geochronology, geochemistry (Sm-Nd and whole-rockA), and stratigraphy of the Paleoproterozoic Piling Group, northern Canada: Geological Society of America Bulletin, doi: 10.1130/B31028.1

Wood, D.A., Joron, J.L. and Treuil, M., 1979, A re-appraisal of the use of trace elements to classify and discriminate between magma series erupted in different tectonic settings: Earth and Planetary Science Letters, v. 45, pp. 326-336.

APPENDIX A:

COMPLETE PELITE MINERAL CHEMISTRY DATA

This appendix contains complete, mineral chemistry data obtained from electron microprobe analysis for pelitic rocks. Data obtained from pelitic samples K118A1 and K124A1 not included in Chapter 2 due to evidence that mineral assemblages are not in chemical equilibrium are included here.

Plagioclase compositions for sample K118B pelite								
Site	1	2	3	4	5	6	7	8
SiO_2	60.89	61.17	60.52	60.30	60.00	60.30	59.16	60.19
TiO_2	0.0162	0.0246	0.0217	0.0106	0.0220	0.0000	0.0053	0.0372
Al_2O_3	23.61	24.05	23.89	24.89	24.19	24.51	24.06	24.30
Fe_2O_3	0.0497	0.0358	0.0318	0.1385	0.1259	0.1106	0.0280	0.0808
CaO	5.83	5.43	5.61	6.34	6.16	6.12	6.24	6.25
BaO	0.0081	0.0105	0.0093	0.0242	0.0238	0.0156	0.0027	0.0183
Na_2O	8.21	8.34	8.32	7.84	8.56	7.99	8.73	7.95
K_2O	0.0955	0.0811	0.0657	0.0748	0.0511	0.0942	0.1020	0.0898
Total	98.70	99.14	98.47	99.62	99.13	99.15	98.33	98.92
Number of cations on the basis of 32O								
Si	10.956	10.942	10.913	10.766	10.794	10.815	10.750	10.823
Ti	0.0022	0.0033	0.0029	0.0014	0.0030	0.0000	0.0007	0.0050
Al	5.006	5.070	5.077	5.238	5.128	5.181	5.153	5.151
Fe	0.0067	0.0048	0.0043	0.0186	0.0171	0.0149	0.0038	0.0109
Ca	1.1234	1.0401	1.0837	1.2128	1.1878	1.1755	1.2141	1.2034
Ba	0.0006	0.0007	0.0007	0.0017	0.0017	0.0011	0.0002	0.0013
Na	2.8626	2.8942	2.9101	2.7154	2.9843	2.7795	3.0750	2.7726
K	0.0219	0.0185	0.0151	0.0170	0.0117	0.0215	0.0236	0.0206

Plagioclase compositions for sample K118B pelite continued									
Site	9	10	11	12	13	14	15	16	17
SiO_2	59.45	60.58	59.44	59.14	59.82	59.26	60.19	58.97	59.51
TiO_2	0.0080	0.0000	0.0000	0.0232	0.0281	0.0151	0.0000	0.0461	0.0013
Al_2O_3	24.45	24.87	24.20	24.29	24.45	24.42	24.66	24.17	24.32
Fe_2O_3	0.1133	0.0298	0.0786	0.1358	0.2073	0.1365	0.1285	0.0053	0.1378
CaO	6.28	6.34	6.27	6.29	6.36	6.63	6.45	6.49	6.37
BaO	0.0203	0.0009	0.0123	0.0401	0.0293	0.0096	0.0296	0.0000	0.0162
Na_2O	8.10	8.03	8.70	7.91	7.98	7.75	7.93	8.71	7.99
K_2O	0.1099	0.0746	0.0886	0.0891	0.0919	0.1318	0.0559	0.1186	0.0910
Total	98.53	99.93	98.79	97.93	98.97	98.35	99.45	98.51	98.44
Number of cations on the basis of 32O									
Si	10.753	10.783	10.748	10.759	10.769	10.740	10.774	10.708	10.770
Ti	0.0011	0.0000	0.0000	0.0032	0.0038	0.0021	0.0000	0.0063	0.0002
Al	5.212	5.217	5.158	5.208	5.187	5.217	5.203	5.173	5.188
Fe	0.0154	0.0040	0.0107	0.0186	0.0281	0.0186	0.0173	0.0007	0.0188
Ca	1.2166	1.2091	1.2148	1.2262	1.2271	1.2868	1.2379	1.2629	1.2359
Ba	0.0014	0.0001	0.0009	0.0029	0.0021	0.0007	0.0021	0.0000	0.0011
Na	2.8403	2.7714	3.0490	2.7904	2.7843	2.7216	2.7519	3.0680	2.8041
K	0.0253	0.0169	0.0204	0.0207	0.0211	0.0305	0.0128	0.0275	0.0210

Garnet compositions for sample K118B pelite								
Site	1	2	3	4	5	6	7	8
SiO_2	37.21	36.90	37.21	37.67	36.84	36.26	37.27	37.28
TiO_2	0.0124	0.0000	0.0084	0.0000	0.0202	0.0205	0.0034	0.0072
Al_2O_3	21.05	21.19	20.90	21.30	21.09	21.41	21.17	21.24
Cr_2O_3	0.0015	0.0164	0.0216	0.0082	0.0000	0.0314	0.0374	0.0112
FeO	36.89	36.47	37.02	36.86	35.83	36.22	36.28	36.45
MgO	2.4836	2.3693	2.6545	2.5991	2.6371	2.6571	3.0800	2.5955
MnO	2.4624	2.7403	1.9776	2.1227	2.5620	2.7160	2.0895	2.6700
CaO	1.1122	1.0680	1.1690	1.2156	1.3274	1.3260	1.4376	1.3113
Na_2O	0.0543	0.0528	0.0248	0.0039	0.4225	0.0181	0.0208	0.0297
Total	101.27	100.80	100.99	101.78	100.73	100.66	101.38	101.60
Number of cations on the basis of 24O								
Si	5.972	5.940	6.000	6.008	5.940	5.861	5.977	5.956
Ti	0.0015	0.0000	0.0010	0.0000	0.0025	0.0025	0.0004	0.0009
Al	3.982	4.022	3.973	4.003	4.008	4.080	4.001	3.999
Cr	0.0002	0.0021	0.0028	0.0010	0.0000	0.0040	0.0047	0.0014
Fe	4.952	4.910	4.992	4.915	4.832	4.896	4.867	4.870
Mg	0.5891	0.6576	0.4753	0.5045	0.6157	0.6544	0.4995	0.6358
Mn	0.3377	0.3231	0.3625	0.3511	0.3602	0.3638	0.4183	0.3512
Ca	0.1913	0.1842	0.2020	0.2077	0.2293	0.2297	0.2471	0.2244
Na	0.0169	0.0165	0.0078	0.0012	0.1321	0.0057	0.0065	0.0092

Garnet compositions for sample K118B pelite contiuned										
Site	9	10	11	12	13	14	15	16	17	18
SiO_2	37.33	36.91	37.02	37.27	37.19	37.05	37.46	37.02	37.23	36.92
TiO_2	0.0000	0.7563	0.0000	0.0197	0.0075	0.0110	0.0000	0.0000	0.0429	0.0076
Al_2O_3	21.18	20.84	21.17	21.13	21.27	20.90	20.82	21.21	21.25	21.07
Cr_2O_3	0.0172	0.0046	0.0337	0.0277	0.0195	0.0307	0.0007	0.0045	0.0000	0.0000
FeO	36.18	31.98	35.80	36.59	36.34	36.31	36.25	36.39	36.21	36.25
MgO	2.7696	2.0852	2.8462	2.8187	2.4166	2.8550	2.6310	2.8182	3.0500	2.4448
MnO	2.5490	3.8400	2.1509	2.5977	2.7952	2.2279	2.6460	2.5175	2.2233	2.9804
CaO	1.3444	1.0467	1.3247	1.1533	1.3969	1.3940	1.4090	1.3200	1.4061	1.1945
Na_2O	0.0653	0.3124	0.1005	0.0402	0.0335	0.0365	0.0327	0.0205	0.0000	0.0167
Total	101.43	97.79	100.45	101.64	101.47	100.82	101.25	101.30	101.41	100.89
Number of cations on the basis of 24O										
Si	5.972	6.007	5.980	5.960	5.945	5.979	6.003	5.941	5.966	5.938
Ti	0.0000	0.0926	0.0000	0.0024	0.0009	0.0013	0.0000	0.0000	0.0052	0.0009
Al	3.993	3.998	4.031	3.982	4.006	3.974	3.932	4.013	4.013	3.994
Cr	0.0022	0.0006	0.0043	0.0035	0.0025	0.0039	0.0001	0.0006	0.0000	0.0000
Fe	4.840	4.352	4.836	4.893	4.858	4.900	4.859	4.884	4.852	4.875
Mg	0.6078	0.9324	0.5178	0.6192	0.6660	0.5358	0.6320	0.6022	0.5310	0.7144
Mn	0.3753	0.2874	0.3894	0.3818	0.3272	0.3902	0.3571	0.3831	0.4144	0.3330
Ca	0.2304	0.1825	0.2292	0.1976	0.2392	0.2410	0.2419	0.2270	0.2414	0.2058
Na	0.0203	0.0986	0.0315	0.0125	0.0104	0.0114	0.0102	0.0064	0.0000	0.0052

Biotite compositions for sample K118B pelite								
Site	1	2	3	4	5	6	7	8
SiO_2	35.04	34.58	34.96	34.84	34.92	35.14	34.36	34.49
TiO_2	2.7313	2.0188	2.1915	2.4247	2.3786	2.4842	2.4603	2.2152
Al_2O_3	18.73	18.68	19.02	18.92	18.42	18.82	18.27	18.30
Cr_2O_3	0.0268	0.0275	0.0513	0.0441	0.0504	0.0300	0.0000	0.1000
FeO	22.09	22.73	21.64	22.73	22.47	21.88	22.02	22.54
MgO	0.0487	0.0658	0.0382	0.0356	0.0507	0.0514	0.0323	0.0375
MnO	8.13	8.25	8.71	8.17	8.58	8.53	8.51	8.57
CaO	0.0000	0.0212	0.0215	0.0000	0.0000	0.0352	0.0099	0.0000
Na_2O	0.2416	0.1814	0.2349	0.1789	0.1737	0.1902	0.2708	0.1577
K_2O	9.08	8.57	8.79	8.69	8.70	8.82	8.43	8.77
Cl	0.0237	0.0375	0.0727	0.0412	0.0431	0.0244	0.0459	0.0204
Total	96.13	95.17	95.73	96.08	95.80	96.00	94.41	95.20
Number of cations on the basis of 22O								
Si	5.354	5.347	5.346	5.331	5.358	5.360	5.342	5.337
Ti	0.3139	0.2347	0.2520	0.2790	0.2744	0.2850	0.2877	0.2578
Al	3.372	3.404	3.427	3.413	3.331	3.384	3.347	3.337
Cr	0.0032	0.0034	0.0062	0.0053	0.0061	0.0036	0.0000	0.0122
Fe	2.8232	2.9388	2.7670	2.9093	2.8835	2.7908	2.8635	2.9168
Mg	1.8517	1.9021	1.9863	1.8633	1.9624	1.9397	1.9734	1.9755
Mn	0.0063	0.0086	0.0050	0.0046	0.0066	0.0066	0.0043	0.0049
Ca	0.0000	0.0035	0.0035	0.0000	0.0000	0.0057	0.0016	0.0000
Na	0.0716	0.0544	0.0696	0.0531	0.0517	0.0562	0.0816	0.0473
K	1.7689	1.6896	1.7156	1.6955	1.7036	1.7154	1.6713	1.7316
Cl	0.0061	0.0098	0.0188	0.0107	0.0112	0.0063	0.0121	0.0053

Biotite compositions for sample K118B pelite continued										
Site	9	10	11	12	13	14	15	16	17	18
SiO_2	35.09	35.20	34.34	34.81	34.76	34.25	34.19	34.89	34.81	34.87
TiO_2	2.5589	2.6713	2.3178	2.1652	2.4736	2.5612	2.4757	2.5136	2.7540	2.6657
Al_2O_3	18.80	18.48	18.20	18.57	18.38	18.42	18.46	18.49	18.66	18.35
Cr_2O_3	0.1035	0.0648	0.0473	0.0189	0.0339	0.0591	0.0268	0.0482	0.0625	0.0158
FeO	21.54	21.65	22.04	22.21	22.11	22.40	22.29	21.82	21.04	22.01
MgO	0.0528	0.0574	0.0560	0.0435	0.0415	0.0290	0.0803	0.0316	0.0607	0.0369
MnO	8.33	8.97	8.80	8.66	8.33	8.36	8.26	8.67	8.43	8.29
CaO	0.0221	0.0000	0.0034	0.0092	0.0110	0.0000	0.0079	0.0013	0.0152	0.0013
Na_2O	0.1610	0.1783	0.1948	0.1909	0.2036	0.1657	0.1725	0.1946	0.2602	0.1507
K_2O	8.16	8.67	9.11	8.71	8.85	8.68	9.12	9.16	8.15	8.97
Cl	0.0347	0.0278	0.0471	0.0304	0.0309	0.0158	0.0369	0.0349	0.0463	0.0400
Total	94.85	95.98	95.15	95.42	95.22	94.94	95.11	95.85	94.30	95.41
Number of cations on the basis of 22O										
Si	5.389	5.363	5.320	5.356	5.363	5.311	5.305	5.348	5.374	5.369
Ti	0.2955	0.3061	0.2701	0.2505	0.2871	0.2986	0.2889	0.2897	0.3197	0.3086
Al	3.403	3.319	3.324	3.367	3.343	3.365	3.376	3.340	3.395	3.330
Cr	0.0126	0.0078	0.0058	0.0023	0.0041	0.0072	0.0033	0.0058	0.0076	0.0019
Fe	2.7672	2.7579	2.8563	2.8570	2.8535	2.9040	2.8931	2.7966	2.7161	2.8344
Mg	1.9072	2.0375	2.0315	1.9851	1.9164	1.9316	1.9096	1.9804	1.9405	1.9032
Mn	0.0069	0.0074	0.0073	0.0057	0.0054	0.0038	0.0106	0.0041	0.0079	0.0048
Ca	0.0036	0.0000	0.0006	0.0015	0.0018	0.0000	0.0013	0.0002	0.0025	0.0002
Na	0.0479	0.0527	0.0585	0.0569	0.0609	0.0498	0.0519	0.0578	0.0779	0.0450
K	1.5980	1.6857	1.8007	1.7099	1.7418	1.7171	1.8045	1.7907	1.6048	1.7609
Cl	0.0090	0.0072	0.0124	0.0079	0.0081	0.0042	0.0097	0.0091	0.0121	0.0104

Plagioclase compositions for sample K119A pelite						
Site	1, core	1, rim	2, core	2, rim	3, core	3, rim
SiO_2	61.11	63.46	62.1	62.32	60.79	60.52
TiO_2	0.0000	0.0073	0.0087	0.0204	0.0181	0.0225
Al_2O_3	23.50	23.29	23.63	23.47	23.55	23.33
Fe_2O_3	0.0451	0.0941	0.0419	0.0877	0.0100	0.1190
CaO	4.86	4.47	5.09	4.79	5.48	4.96
BaO	0.0002	0.0289	0.0248	0.0000	0.0146	0.0151
Na_2O	8.99	8.80	8.59	8.78	8.53	8.77
K_2O	0.1336	0.1213	0.1309	0.1480	0.2417	0.1789
Total	98.64	100.27	99.61	99.62	98.63	97.92
Number of cations on the basis of 32O						
Si	10.997	11.182	11.046	11.079	10.956	10.979
Ti	0.0000	0.0010	0.0012	0.0027	0.0025	0.0031
Al	4.984	4.836	4.954	4.918	5.002	4.988
Fe	0.0061	0.0125	0.0056	0.0117	0.0014	0.0162
Ca	0.9377	0.8438	0.9698	0.9126	1.0586	0.965
Ba	0.0000	0.0020	0.0017	0.0000	0.0010	0.0011
Na	3.1380	3.0060	2.9617	3.0280	2.9817	3.0850
K	0.0307	0.0273	0.0297	0.0336	0.0556	0.0414

Garnet compositions for sample K119A pelite						
Site	1, core	1, rim	2, core	2, rim	3, core	3, rim
SiO_2	37.66	37.43	37.43	37.47	37.68	37.51
TiO_2	0.0064	0.0000	0.0000	0.0000	0.0190	0.0004
Al_2O_3	21.24	20.92	20.80	20.95	20.84	21.13
Cr_2O_3	0.0000	0.0605	0.0314	0.0000	0.0067	0.0381
FeO	35.16	35.10	35.06	35.68	35.65	34.87
MgO	3.96	3.89	3.85	3.09	3.76	3.62
MnO	0.9109	0.9189	0.8942	0.9854	0.9836	1.0312
CaO	0.9975	1.0126	1.1097	1.0650	0.9852	0.9739
Na_2O	0.0000	0.0373	0.0163	0.0158	0.0026	0.0164
Total	99.93	99.37	99.19	99.25	99.94	99.19
Number of cations on the basis of 24O						
Si	6.024	5.990	6.042	6.059	6.081	6.045
Ti	0.0008	0.0000	0.0000	0.0000	0.0023	0.0000
Al	4.0050	4.0000	3.9570	3.9940	3.9640	4.0140
Cr	0.0000	0.0078	0.0040	0.0000	0.0009	0.0049
Fe	4.703	4.761	4.733	4.825	4.677	4.701
Mg	0.9452	0.9405	0.9253	0.7446	0.9047	0.8694
Mn	0.1234	0.1262	0.1223	0.1350	0.1344	0.1408
Ca	0.1710	0.1760	0.1919	0.1845	0.1703	0.1682
Na	0.0000	0.0117	0.0051	0.0050	0.0008	0.0051

Biotite compositions for sample K119A pelite						
Site	1, core	1, rim	2, core	2, rim	3, core	3, rim
SiO_2	35.48	35.08	35.06	35.11	35.34	35.06
TiO_2	4.03	4.15	3.90	3.86	3.84	3.77
Al_2O_3	19.03	18.39	18.57	18.72	18.09	18.41
Cr_2O_3	0.1126	0.0311	0.0502	0.0000	0.0694	0.0863
FeO	19.78	20.48	20.25	19.65	20.11	19.28
MgO	8.49	8.66	8.84	8.85	8.98	8.85
MnO	0.0000	0.0190	0.0361	0.0125	0.0243	0.0375
CaO	0.0000	0.0000	0.0000	0.0000	0.0127	0.0320
Na_2O	0.0958	0.1006	0.1326	0.0994	0.1154	0.1323
K_2O	8.99	9.53	9.09	9.28	9.24	9.09
Cl	0.0236	0.0157	0.0140	0.0123	0.0210	0.0201
Total	96.04	96.47	95.94	95.60	95.84	94.77
Number of cations on the basis of 22O						
Si	5.353	5.316	5.321	5.336	5.371	5.366
Ti	0.4572	0.4728	0.4456	0.4409	0.4389	0.4337
Al	3.384	3.284	3.323	3.353	3.241	3.321
Cr	0.0134	0.0037	0.0060	0.0000	0.0083	0.0104
Fe	2.4954	2.5957	2.5701	2.4967	2.5553	2.4676
Mg	1.9093	1.9569	2.0000	2.0049	2.0330	2.0182
Mn	0.0000	0.0024	0.0046	0.0016	0.0031	0.0049
Ca	0.0000	0.0000	0.0000	0.0000	0.0021	0.0052
Na	0.0280	0.0295	0.0390	0.0293	0.0340	0.0393
K	1.7295	1.8424	1.7592	1.7998	1.7915	1.7756
Cl	0.0060	0.0040	0.0036	0.0032	0.0054	0.0052

Plagioclase compositions for sample K124A pelite								
Site	1	2	3	4	5	6	7	8
SiO_2	59.30	58.88	59.02	59.92	59.56	59.47	59.87	60.09
TiO_2	0.0323	0.0180	0.0056	0.0000	0.0270	0.0078	0.0045	0.0135
Al_2O_3	24.35	24.31	24.25	24.79	24.57	24.60	24.61	24.05
Fe_2O_3	0.0220	0.0247	0.0033	0.0653	0.0347	0.0333	0.0000	0.0106
CaO	6.23	5.81	6.07	6.03	6.23	6.19	6.00	6.03
BaO	0.0000	0.0000	0.0172	0.0000	0.0006	0.0051	0.0030	0.0000
Na_2O	8.67	8.81	8.69	8.58	8.52	8.58	8.48	7.87
K_2O	0.2054	0.1591	0.1668	0.1213	0.1631	0.1963	0.2415	0.2345
Total	98.81	98.00	98.22	99.51	99.10	99.08	99.21	98.30
Number of cations on the basis of 32O								
Si	10.725	10.727	10.733	10.737	10.727	10.718	10.759	10.865
Ti	0.0044	0.0025	0.0008	0.0000	0.0037	0.0011	0.0006	0.0018
Al	5.190	5.219	5.198	5.234	5.216	5.225	5.213	5.126
Fe	0.0030	0.0034	0.0005	0.0088	0.0047	0.0045	0.0000	0.0014
Ca	1.2069	1.1334	1.1830	1.1572	1.2021	1.1948	1.1546	1.1673
Ba	0.0000	0.0000	0.0012	0.0000	0.0000	0.0004	0.0002	0.0000
Na	3.0410	3.1130	3.0630	2.9822	2.9766	2.9981	2.9563	2.7602
K	0.0474	0.0370	0.0387	0.0277	0.0375	0.0451	0.0554	0.0541

Garnet compositions for sample K124A pelite								
Site	1	2	3	4	5	6	7	8
SiO_2	37.28	37.13	37.20	37.26	37.37	37.21	37.37	37.27
TiO_2	0.0111	0.0020	0.0000	0.0266	0.0496	0.0150	0.0000	0.0150
Al_2O_3	20.98	21.11	21.01	20.93	21.09	20.73	20.58	20.59
Cr_2O_3	0.0188	0.0173	0.0000	0.0000	0.0181	0.0225	0.0083	0.0233
FeO	34.99	35.01	35.25	35.13	33.96	35.78	35.07	35.18
MnO	1.8099	1.7207	1.6908	1.6469	1.5554	1.7948	1.8926	1.8954
MgO	3.29	3.86	3.72	3.64	3.17	3.10	3.56	3.56
CaO	1.1783	1.1681	1.0152	1.1540	1.0471	1.2002	1.1347	1.1010
Na_2O	0.0865	0.0316	0.0009	0.0646	0.0891	0.0498	0.0456	0.0149
Total	99.64	100.05	99.89	99.85	98.36	99.90	99.66	99.66
Number of cations on the basis of 24O								
Si	6.016	5.966	5.989	5.999	6.069	6.013	6.034	6.023
Ti	0.0013	0.0002	0.0000	0.0032	0.0061	0.0018	0.0000	0.0018
Al	3.989	3.997	3.986	3.972	4.037	3.948	3.918	3.921
Cr	0.0024	0.0022	0.0000	0.0000	0.0023	0.0029	0.0011	0.0030
Fe	4.722	4.704	4.746	4.730	4.612	4.836	4.736	4.754
Mg	0.7915	0.9244	0.8923	0.8746	0.7682	0.7469	0.8559	0.8580
Mn	0.2474	0.2342	0.2305	0.2246	0.2140	0.2457	0.2589	0.2594
Ca	0.2037	0.2011	0.1751	0.1991	0.1822	0.2078	0.1963	0.1906
Na	0.0271	0.0099	0.0003	0.0202	0.0280	0.0156	0.0143	0.0047

Biotite compositions for sample K124A pelite								
Site	1	2	3	4	5	6	7	8
SiO_2	35.80	36.45	36.42	36.05	36.03	36.22	36.19	36.00
TiO_2	1.2342	0.6169	0.8785	1.4048	1.0164	1.2744	1.4843	1.1936
Al_2O_3	19.30	20.06	19.93	19.74	19.94	19.89	19.85	20.12
Cr_2O_3	0.0304	0.0000	0.0065	0.0129	0.0630	0.0389	0.0283	0.0427
FeO	18.01	16.68	16.82	17.33	16.46	15.96	16.38	17.20
MnO	0.0443	0.0144	0.0282	0.0044	0.0445	0.0219	0.0000	0.0407
MgO	11.51	12.31	12.53	11.83	12.35	12.55	12.55	11.42
CaO	0.0000	0.0403	0.0000	0.0028	0.0000	0.0491	0.0124	0.0144
Na_2O	0.1265	0.1705	0.0776	0.1030	0.1016	0.1189	0.0907	0.1058
K_2O	9.65	9.26	9.40	9.84	10.07	9.58	9.81	9.52
Cl	0.0205	0.0278	0.0018	0.0025	0.0116	0.0317	0.0007	0.0000
Total	95.72	95.62	96.09	96.33	96.09	95.74	96.39	95.66
Number of cations on the basis of 22O								
Si	5.389	5.429	5.405	5.372	5.369	5.387	5.362	5.385
Ti	0.1397	0.0691	0.0980	0.1574	0.1139	0.1426	0.1654	0.1343
Al	3.425	3.521	3.486	3.467	3.502	3.486	3.466	3.548
Cr	0.0036	0.0000	0.0008	0.0015	0.0074	0.0046	0.0033	0.0051
Fe	2.2676	2.0773	2.0871	2.1593	2.0513	1.9856	2.0290	2.1524
Mg	2.5819	2.7322	2.7728	2.6280	2.7429	2.7823	2.7708	2.5471
Mn	0.0057	0.0018	0.0035	0.0006	0.0056	0.0028	0.0000	0.0052
Ca	0.0000	0.0064	0.0000	0.0005	0.0000	0.0078	0.0020	0.0023
Na	0.0369	0.0492	0.0223	0.0298	0.0293	0.0343	0.0260	0.0307
K	1.8523	1.7588	1.7790	1.8704	1.9130	1.8186	1.8540	1.8169
Cl	0.0052	0.0070	0.0005	0.0006	0.0029	0.0080	0.0002	0.0000

APPENDIX B:

MAFIC AND ULTRAMAFIC GEOCHEMISTRY

This appendix contains complete, whole rock, major and trace element geochemical data from mafic and ultramafic samples collected during the HPIGP. Samples were analyzed using ICP-MS by Activation Laboratories Ltd. (Actlabs) ("4lithores" package code). Detection limits for major oxides and trace elements are shown below. Actlabs utilizes internal standards in order to ensure quality control. In addition a blind, duplicate of sample 13SUB-K035B1 was submitted during analysis of the 2013 samples. The results of the blind are also listed below.

Geochemical data tables are divided based on the imposed sub-groups (unit) – alkaline, calc-alkaline, transitional, tholeiitic, and ultramafic – described in this thesis and ordered alphabetically within each sub-group based on their unique SampleIDs. SampleIDs with the prefix "12MBC" were collected during the 2012 field season (southern Hall Peninsula), while those with the prefix "13SUB" were collected during the 2013 field season (northern Hall Peninsula). Samples rejected from this thesis reasons outlined in Chapter 3.2 are labeled "R" in the unit row followed by their reason for rejection (LOI – high loss on ignition values; and rock type – rock type not applicable to this thesis).

Analyte Symbol	Detection Limit	13SUB-K035B1	Blind Duplicate
(wt%)			
SiO_2	0.01	48.37	47.8
Al_2O_3	0.01	14.19	13.97
Fe_2O_3(T)	0.01	14.87	15.3
MnO	0.001	0.184	0.179
MgO	0.01	6.72	6.68
CaO	0.01	10.65	10.81
Na_2O	0.01	2.9	2.83
K_2O	0.01	0.65	0.66
TiO_2	0.001	1.832	1.805
P_2O_5	0.01	0.16	0.16
LOI		0.23	0.17
Total	0.01	100.8	100.4
(ppm)			
Sc	1	42	42
Be	1	< 1	< 1
V	5	392	392
Cr	20	120	120
Co	1	42	42
Ni	20	80	70
Cu	10	40	40
Zn	30	140	110
Ga	1	21	21
Ge	0.5	2.5	2.1
As	5	16	< 5
Rb	1	4	4
Sr	2	58	54
Y	0.5	34.8	35.9
Zr	1	92	92
Nb	0.2	3.2	3.5
Mo	2	< 2	< 2
Ag	0.5	< 0.5	< 0.5
In	0.1	< 0.1	< 0.1
Sn	1	< 1	< 1
Sb	0.2	< 0.2	< 0.2
Cs	0.1	0.2	< 0.1
Ba	3	48	43
La	0.05	6.07	6.22
Ce	0.05	15	15.7
Pr	0.01	2.25	2.41
Nd	0.05	11.5	11.5
Sm	0.01	3.95	3.92
Eu	0.005	1.25	1.38
Gd	0.01	4.73	5.17
Tb	0.01	0.88	0.91
Dy	0.01	5.75	5.8
Ho	0.01	1.17	1.23
Er	0.01	3.44	3.56
Tm	0.005	0.55	0.546
Yb	0.01	3.7	3.57
Lu	0.002	0.527	0.548
Hf	0.1	2.1	2.4
Ta	0.01	0.24	0.28
W	0.5	3.1	< 0.5
Tl	0.05	< 0.05	< 0.05
Pb	5	< 5	< 5
Bi	0.1	< 0.1	< 0.1
Th	0.05	0.3	0.3
U	0.01	0.09	0.07

SampleID	12MBC-K091B1	12MBC-K101C1	12MBC-S043B1	13SUB-K041B1
Region	Central	Eastern	Western	Central
Occurrence	Metaseds	Basement	Western	Metaseds
Unit	alkaline	alkaline	alkaline	alkaline
Latitude	63.201600	63.802995	63.376420	64.575972
Longitude	-65.916841	-64.997340	-66.876921	-66.714636
(wt%)				
SiO_2	44.73	52.35	47.24	42.59
Al_2O_3	11.04	16.67	12.94	15.72
Fe_2O_3(T)	15.86	10.74	9.81	13.41
MnO	0.228	0.152	0.157	0.194
MgO	8.68	3.56	12.38	5.16
CaO	12.87	5.69	13.21	16.74
Na_2O	0.76	3.99	0.52	1.41
K_2O	0.39	2.66	2.07	0.98
TiO_2	2.843	1.696	0.838	2.363
P_2O_5	0.26	0.42	0.43	0.36
LOI	0.45	0.58	0.21	1.71
Total	98.1	98.52	99.81	100.6
(ppm)				
Sc	35	11	44	33
V	451	128	272	307
Cr	540	< 20	1000	100
Co	64	31	55	61
Ni	160	< 20	210	60
Cu	30	30	20	10
Zn	120	140	70	220
Be	2	3	1	2
Ga	21	24	14	19
Ge	2.9	1.6	2.1	2.5
As	< 5	< 5	< 5	< 5
Rb	1	117	173	12
Sr	252	606	323	419
Y	24.7	26.1	9.4	26.3
Zr	195	244	36	131
Nb	37.7	29.1	7.4	33
Mo	< 2	< 2	< 2	< 2
Ag	1.3	1.7	< 0.5	< 0.5
In	< 0.1	< 0.1	< 0.1	< 0.1
Sn	2	2	< 1	1
Sb	0.3	0.4	0.3	< 0.2
Cs	< 0.1	1.8	3.1	0.3
Ba	24	630	579	446
Hf	4.5	5.2	0.9	2.9
Ta	2.55	1.21	0.43	2.53
W	< 0.5	< 0.5	< 0.5	< 0.5
Tl	< 0.05	0.55	0.23	< 0.05
Pb	< 5	8	< 5	< 5
Bi	0.1	< 0.1	0.1	< 0.1
Th	3.25	3.31	0.2	2.29
U	0.84	0.85	0.16	1.18
La	32.8	59.9	16.6	27.2
Ce	66.9	130	38	56.3
Pr	9.07	16.7	5.31	7.1
Nd	38.3	65.9	22.8	27.9
Sm	7.61	10.5	3.9	6
Eu	2.25	2.25	0.866	2.02
Gd	7.2	8.34	2.61	5.96
Tb	1	1	0.31	0.84
Dy	5.23	5.04	1.69	4.74
Ho	0.88	0.91	0.33	0.96
Er	2.33	2.43	0.93	2.74
Tm	0.316	0.361	0.142	0.4
Yb	1.9	2.19	0.9	2.47
Lu	0.256	0.291	0.124	0.354

SampleID	12MBC-B110A1	12MBC-B126B1	12MBC-F140B1	12MBC-T026A1
Region	Eastern	Central	Central	Central
Occurrence	Basement	Basement	Basement	Unknown
Unit	calc-alkaline	calc-alkaline	calc-alkaline	calc-alkaline
Latitude	63.741458	63.198267	63.215282	63.164850
Longitude	-65.104922	-65.436760	-65.144720	-65.254202
(wt%)				
SiO_2	51.25	50.18	48.84	50.5
Al_2O_3	12.76	12.39	16.56	15.75
Fe_2O_3(T)	8.3	16.1	11.77	9.45
MnO	0.135	0.214	0.164	0.129
MgO	10.28	5.14	5.99	7.92
CaO	10.51	8.2	12.21	9.65
Na_2O	2.62	2.42	1.27	2.63
K_2O	0.67	1.23	0.4	0.83
TiO_2	0.241	2.339	1.488	1.007
P_2O_5	0.05	0.32	0.09	0.21
LOI	1.21	0.91	0.76	0.99
Total	98.02	99.44	99.55	99.06
(ppm)				
Sc	26	39	29	22
V	107	367	361	124
Cr	440	110	80	180
Co	49	47	44	42
Ni	270	60	110	210
Cu	60	50	140	30
Zn	90	120	90	80
Be	< 1	1	< 1	< 1
Ga	16	22	25	19
Ge	1.5	1.8	1.5	1.6
As	< 5	< 5	< 5	< 5
Rb	9	16	5	18
Sr	226	189	225	964
Y	4.6	36.9	17.4	14.1
Zr	45	172	79	86
Nb	1.4	11.2	3.3	4.5
Mo	< 2	< 2	< 2	< 2
Ag	< 0.5	1.1	< 0.5	0.6
In	< 0.1	< 0.1	< 0.1	< 0.1
Sn	1	1	1	< 1
Sb	< 0.2	< 0.2	0.2	0.4
Cs	< 0.1	< 0.1	< 0.1	0.6
Ba	46	421	67	851
Hf	1.1	4.1	1.9	2.1
Ta	0.16	0.67	0.23	0.27
W	< 0.5	< 0.5	< 0.5	< 0.5
Tl	0.07	0.08	< 0.05	0.14
Pb	< 5	6	< 5	9
Bi	0.5	< 0.1	< 0.1	< 0.1
Th	0.57	2.47	0.39	2.34
U	0.11	0.57	0.16	0.39
La	6.84	27.1	5.36	34.9
Ce	13.3	49.9	13.4	69.1
Pr	1.58	7.19	2.17	8.69
Nd	6.25	31.1	11.3	34.2
Sm	1.31	7.5	3.61	5.64
Eu	0.463	1.92	1.18	1.51
Gd	1.27	7.1	3.51	4.38
Tb	0.18	1.09	0.59	0.57
Dy	0.9	6.35	3.33	2.79
Ho	0.16	1.24	0.62	0.54
Er	0.45	3.56	1.64	1.42
Tm	0.063	0.539	0.232	0.194
Yb	0.37	3.38	1.38	1.18
Lu	0.06	0.491	0.183	0.174

SampleID	12MBC-B033C1	12MBC-B070B1	12MBC-B137B1	12MBC-C042A1	12MBC-F046A1	12MBC-F085A1
Region	Central	Central	Central	Central	Western	Central
Occurrence	Metaseds	Metaseds	Metaseds	Unknown	Western	Basement
Unit	transitional	transitional	transitional	transitional	transitional	transitional
Latitude	63.504945	62.972243	63.084028	63.630140	63.348715	63.169032
Longitude	-65.858868	-65.379858	-65.839273	-66.078995	-67.111011	-65.656962
(wt%)						
SiO_2	48.4	44.66	49.14	46.2	48.74	44.64
Al_2O_3	13.2	13.43	15.65	14.3	6.83	16.52
Fe_2O_3(T)	14.02	16.32	11.22	15.96	12.03	13.47
MnO	0.217	0.186	0.168	0.228	0.182	0.222
MgO	5.37	7.54	7.58	5.78	11.03	7.14
CaO	11.07	13.23	11.74	10.87	18.98	10.22
Na_2O	1.99	1.36	1.96	2.53	0.34	2.56
K_2O	0.56	0.5	0.33	0.46	0.11	1.75
TiO_2	1.775	2.027	0.923	1.935	0.64	1.082
P_2O_5	0.18	0.05	0.09	0.17	0.06	0.27
LOI	1.21	0.26	0.52	0.65	-0.1	0.91
Total	97.99	99.57	99.33	99.08	98.84	98.79
(ppm)						
Sc	46	40	48	50	22	35
V	395	857	304	455	171	287
Cr	140	30	150	110	1800	70
Co	51	58	42	56	95	43
Ni	80	220	50	60	1510	30
Cu	40	460	50	60	70	50
Zn	130	110	70	130	130	120
Be	1	1	< 1	1	2	< 1
Ga	22	25	18	24	14	19
Ge	2	2	1.6	1.9	3.6	1.4
As	< 5	< 5	< 5	< 5	1650	< 5
Rb	7	5	1	4	1	39
Sr	205	178	248	229	139	435
Y	35	12.2	18.3	39.3	10.9	21.7
Zr	130	42	53	149	38	61
Nb	19.1	2	2.1	21.6	3.8	1.7
Mo	< 2	< 2	< 2	< 2	< 2	< 2
Ag	1.1	< 0.5	< 0.5	1	< 0.5	< 0.5
In	< 0.1	< 0.1	< 0.1	< 0.1	0.1	< 0.1
Sn	1	1	< 1	2	5	< 1
Sb	0.4	< 0.2	< 0.2	0.4	28.8	0.3
Cs	0.6	< 0.1	< 0.1	0.2	< 0.1	0.4
Ba	239	51	122	117	31	231
Hf	3.1	1.2	1.3	3.5	1	1.5
Ta	1.22	0.16	0.14	1.37	0.15	0.08
W	< 0.5	< 0.5	< 0.5	< 0.5	4.8	< 0.5
Tl	0.08	< 0.05	< 0.05	< 0.05	< 0.05	0.24
Pb	< 5	< 5	< 5	6	< 5	< 5
Bi	< 0.1	0.2	< 0.1	0.2	70.8	0.3
Th	1.73	0.3	0.22	1.04	2.04	1.36
U	0.73	0.36	0.08	0.5	0.71	0.33
La	16.4	3.13	8.79	17.7	5.31	17.8
Ce	34.7	7.67	20.2	38.2	11.2	42
Pr	4.73	1.24	2.72	5.44	1.53	6.14
Nd	20.8	6.85	12.2	24.3	6.4	27.8
Sm	5.28	2.34	2.96	6.16	1.74	6.16
Eu	1.49	0.823	0.909	1.7	0.568	1.67
Gd	5.68	2.55	2.92	6.68	2	5.23
Tb	1	0.43	0.51	1.1	0.33	0.73
Dy	5.78	2.3	3.15	6.52	1.91	3.94
Ho	1.2	0.44	0.65	1.37	0.38	0.77
Er	3.35	1.14	1.84	4.1	1.02	2.19
Tm	0.507	0.168	0.285	0.627	0.156	0.336
Yb	3.25	1.02	1.87	3.91	0.98	2.1
Lu	0.5	0.128	0.27	0.567	0.135	0.296

SampleID	12MBC-F093A1	12MBC-F103A1	12MBC-F122C1	12MBC-K002B1	12MBC-K004A1	12MBC-K071A1
Region	Central	Eastern	Central	Central	Central	Central
Occurrence	Basement	Metaseds	Metaseds	Metaseds	Metaseds	Metaseds
Unit	transitional	transitional	transitional	transitional	transitional	transitional
Latitude	63.178303	63.437662	63.959228	63.292595	63.308388	63.307633
Longitude	-65.892256	-64.704342	-65.807571	-66.052581	-66.001491	-65.995323
(wt%)						
SiO_2	47.35	49.11	51.66	50.04	45.54	46.64
Al_2O_3	16.45	12.77	11.2	14.68	14.43	12.97
Fe_2O_3(T)	12.46	17.96	18.05	15.18	15.48	18.36
MnO	0.194	0.257	0.262	0.208	0.223	0.257
MgO	7.41	5.15	5.84	5.56	6.98	5.74
CaO	10.44	9.31	9.68	8.18	10.72	9.91
Na_2O	2.56	1.06	0.66	0.54	2.46	1.87
K_2O	1.14	0.57	0.47	0.96	0.27	0.62
TiO_2	1.064	2.052	2.076	1.651	1.461	2.037
P_2O_5	0.1	0.27	0.25	0.22	0.11	0.25
LOI	1.06	0.08	0.08	0.57	0.37	0.16
Total	100.2	98.6	100.2	97.81	98.04	98.8
(ppm)						
Sc	35	48	53	45	44	51
V	271	466	488	416	409	394
Cr	260	50	90	80	170	150
Co	48	46	48	46	62	55
Ni	150	20	< 20	< 20	120	50
Cu	40	40	20	50	70	10
Zn	90	160	150	160	120	190
Be	< 1	1	3	2	< 1	2
Ga	19	22	20	24	22	24
Ge	1.4	2.3	3.2	2.9	2.2	2.3
As	< 5	< 5	< 5	< 5	< 5	< 5
Rb	42	11	3	45	5	3
Sr	169	255	271	388	147	229
Y	22.2	40.4	39.7	31.8	26.5	29.2
Zr	63	122	122	140	90	118
Nb	2.4	4.1	5.4	6.5	5.7	18.9
Mo	< 2	< 2	< 2	< 2	< 2	< 2
Ag	< 0.5	0.9	0.7	0.8	0.5	0.7
In	< 0.1	< 0.1	< 0.1	< 0.1	< 0.1	< 0.1
Sn	< 1	1	1	2	< 1	1
Sb	0.3	0.3	0.3	0.2	0.3	0.3
Cs	0.4	1.5	< 0.1	1.1	< 0.1	< 0.1
Ba	76	186	47	151	30	281
Hf	1.5	2.9	2.8	3.2	2.2	2.8
Ta	0.25	0.27	0.28	0.37	0.37	1.28
W	< 0.5	< 0.5	< 0.5	< 0.5	< 0.5	< 0.5
Tl	0.18	0.08	< 0.05	0.2	< 0.05	< 0.05
Pb	< 5	5	< 5	5	< 5	< 5
Bi	0.5	0.3	0.4	0.1	< 0.1	< 0.1
Th	0.41	0.9	1.5	3.77	0.53	1.27
U	0.26	0.23	0.33	0.86	0.13	0.24
La	3.92	14.1	10.7	21.3	6.85	24.9
Ce	9.52	30.3	25.6	46.7	16.5	53.2
Pr	1.6	4.25	3.78	6.4	2.49	7.11
Nd	7.69	20.2	18.1	26.9	12.1	30.2
Sm	2.47	5.45	5.09	6.23	3.76	6.42
Eu	0.806	1.75	1.56	1.36	1.24	1.77
Gd	2.97	6.18	6.13	6.01	4.34	6.29
Tb	0.57	1.05	1.09	0.93	0.78	0.96
Dy	3.64	6.63	6.5	5.44	4.48	5.33
Ho	0.79	1.42	1.36	1.11	0.94	1.05
Er	2.29	4.36	3.96	3.22	2.72	2.98
Tm	0.359	0.669	0.627	0.498	0.396	0.45
Yb	2.32	4.3	4.01	3.15	2.42	2.97
Lu	0.34	0.637	0.58	0.457	0.319	0.417

SampleID	12MBC-K074B1	12MBC-K076A2	12MBC-K076A3	12MBC-K088A1	12MBC-K089A1	12MBC-K092A1
Region	Central	Central	Central	Central	Central	Central
Occurrence	Metaseds	Metaseds	Metaseds	Metaseds	Metaseds	Metaseds
Unit	transitional	transitional	transitional	transitional	transitional	transitional
Latitude	63.307062	63.306257	63.306257	63.300852	63.298912	63.203228
Longitude	-65.993653	-65.995756	-65.995756	-66.093340	-66.088445	-65.916108
(wt%)						
SiO_2	44.46	50.31	47.42	49.16	50.57	43.57
Al_2O_3	14.83	14.15	12.87	11.78	15.67	15.13
Fe_2O_3(T)	11.17	15.65	19.65	10.68	12.24	16.16
MnO	0.191	0.198	0.257	0.175	0.193	0.233
MgO	12.01	4.86	4.87	11.53	6.1	7.76
CaO	12.88	7.93	9.04	13.18	8.95	11.95
Na_2O	1.73	2.42	0.87	1.15	2.73	1.74
K_2O	0.21	0.73	0.55	0.33	1.22	0.31
TiO_2	0.831	1.864	2.359	0.701	1.017	1.481
P_2O_5	0.08	0.21	0.22	0.05	0.14	0.11
LOI	1.12	0.3	-0.14	1.19	1.05	0.33
Total	99.52	98.63	97.97	99.91	99.88	98.77
(ppm)						
Sc	43	45	47	49	42	41
V	263	429	644	268	313	399
Cr	1170	70	< 20	580	70	130
Co	61	38	52	54	41	60
Ni	420	40	30	270	30	90
Cu	10	60	30	70	< 10	120
Zn	80	140	180	60	80	120
Be	< 1	2	2	< 1	1	< 1
Ga	18	24	24	14	19	21
Ge	1.1	2	2	1.6	2.1	1.5
As	< 5	< 5	< 5	< 5	< 5	< 5
Rb	2	41	5	9	42	3
Sr	190	119	102	115	286	170
Y	12.8	39	40.2	13.2	21	22.5
Zr	41	131	120	37	80	83
Nb	4.8	5.3	4.4	1.1	2.6	4.5
Mo	< 2	< 2	< 2	< 2	< 2	< 2
Ag	< 0.5	0.8	0.7	< 0.5	< 0.5	0.5
In	< 0.1	< 0.1	< 0.1	< 0.1	< 0.1	< 0.1
Sn	< 1	2	3	< 1	< 1	< 1
Sb	0.2	0.4	0.3	< 0.2	0.2	0.3
Cs	< 0.1	1.5	< 0.1	0.3	0.5	0.3
Ba	70	251	95	46	363	55
Hf	1	3.1	3	0.9	1.9	2
Ta	0.28	0.3	0.3	0.13	0.2	0.31
W	< 0.5	< 0.5	0.5	< 0.5	< 0.5	< 0.5
Tl	< 0.05	0.17	< 0.05	< 0.05	0.17	< 0.05
Pb	< 5	< 5	< 5	< 5	< 5	< 5
Bi	< 0.1	< 0.1	0.3	0.1	< 0.1	0.1
Th	0.47	1.18	1.61	0.28	2.43	0.61
U	0.11	0.43	0.57	0.07	0.55	0.14
La	4.93	10.9	10.9	2.63	13	6.21
Ce	11	29	25.7	5.67	28	15
Pr	1.6	4.51	3.89	0.94	3.7	2.36
Nd	6.95	20.5	18.4	4.63	15.6	11.4
Sm	1.93	5.74	5.14	1.78	3.48	3.54
Eu	0.617	1.52	1.77	0.541	1.09	1.15
Gd	2.15	6.14	5.78	1.89	3.65	3.87
Tb	0.36	1.1	1.1	0.37	0.63	0.71
Dy	2.26	6.39	6.43	2.28	3.67	4.1
Ho	0.46	1.29	1.35	0.48	0.76	0.82
Er	1.26	3.98	4.11	1.35	2.31	2.2
Tm	0.191	0.618	0.631	0.202	0.344	0.333
Yb	1.2	4.01	4.09	1.23	2.11	2.09
Lu	0.149	0.597	0.617	0.183	0.327	0.292

SampleID	12MBC-K093A1	12MBC-K095B1	12MBC-M023B1	12MBC-M034A1	12MBC-M047A1	12MBC-M057C1
Region	Central	Central	Central	Central	Central	Central
Occurrence	Metaseds	Metaseds	Basement	Unknown	Unknown	Metaseds
Unit	transitional	transitional	transitional	transitional	transitional	transitional
Latitude	63.206635	63.207903	63.822292	63.401852	63.766068	62.592577
Longitude	-65.920708	-65.928878	-65.705501	-65.986538	-65.875286	-64.933944
(wt%)						
SiO_2	48.82	49.12	53.3	50.55	48.72	50.03
Al_2O_3	14.22	14.61	14.16	13.81	13.93	14.44
Fe_2O_3(T)	14.77	11.89	14.74	14.68	15.46	13.48
MnO	0.22	0.176	0.216	0.202	0.2	0.206
MgO	5.55	7.45	5.28	6.37	5.64	7.21
CaO	9.72	14.22	8.98	10.17	10.06	11.77
Na_2O	1.96	1.37	0.68	2.17	1.83	1.58
K_2O	0.68	0.21	0.83	0.43	0.66	0.44
TiO_2	1.461	1.397	1.529	1.571	1.434	1.189
P_2O_5	0.17	0.09	0.22	0.16	0.12	0.08
LOI	0.36	0.42	0.36	0.16	0.44	0.36
Total	97.93	100.9	100.3	100.3	98.5	100.8
(ppm)						
Sc	43	41	43	46	44	40
V	442	382	400	378	687	346
Cr	40	90	100	170	40	200
Co	42	44	44	50	45	53
Ni	< 20	130	30	90	< 20	140
Cu	40	290	60	150	40	110
Zn	110	160	140	140	100	90
Be	< 1	< 1	1	1	< 1	< 1
Ga	20	22	22	20	20	20
Ge	1.6	1.8	2.6	2.3	2	2.1
As	< 5	< 5	< 5	< 5	< 5	< 5
Rb	10	2	24	23	12	5
Sr	240	206	348	45	227	158
Y	25.7	16.2	30.4	33.7	20.4	20.4
Zr	101	66	131	117	70	66
Nb	3.6	2.4	5.8	5.7	3.1	3.9
Mo	< 2	< 2	< 2	< 2	< 2	< 2
Ag	0.6	< 0.5	1	0.9	< 0.5	0.5
In	< 0.1	< 0.1	< 0.1	< 0.1	< 0.1	< 0.1
Sn	< 1	< 1	2	1	< 1	< 1
Sb	0.3	< 0.2	0.4	0.3	0.4	0.3
Cs	0.1	< 0.1	1.2	0.2	0.2	< 0.1
Ba	265	31	237	203	237	58
Hf	2.4	1.7	3.2	3.3	1.8	1.7
Ta	0.23	0.21	0.38	0.47	0.21	0.27
W	< 0.5	< 0.5	< 0.5	< 0.5	< 0.5	< 0.5
Tl	0.06	< 0.05	0.11	0.12	0.07	< 0.05
Pb	< 5	< 5	< 5	< 5	< 5	< 5
Bi	< 0.1	< 0.1	0.3	< 0.1	< 0.1	< 0.1
Th	2.12	0.17	3.4	0.42	1.86	0.6
U	0.5	0.07	0.83	0.21	0.37	0.16
La	14.1	4.29	21.2	9.93	8.4	5.42
Ce	30.5	11.6	43.2	25.5	20.1	12.7
Pr	4.17	1.89	5.54	4.19	2.83	1.92
Nd	18	10	23.2	19.4	12.8	9.2
Sm	4.09	3.12	5.58	5.11	3.19	2.79
Eu	1.26	1.03	1.45	1.24	1.07	0.901
Gd	4.16	3.58	5.17	4.95	3.27	3.4
Tb	0.75	0.61	0.85	0.85	0.57	0.6
Dy	4.27	3.31	5.21	5.46	3.47	3.5
Ho	0.91	0.61	1.1	1.15	0.69	0.75
Er	2.67	1.65	3.17	3.38	2.08	2
Tm	0.4	0.233	0.478	0.536	0.326	0.297
Yb	2.55	1.33	3.03	3.48	2.15	1.91
Lu	0.39	0.175	0.437	0.51	0.315	0.285

SampleID	12MBC-S065A1	12MBC-S067B1	12MBC-S172B1	13SUB-F044B1	13SUB-S064B1	13SUB-S072A1
Region	Western	Western	Eastern	Central	Central	Western
Occurrence	Western	Western	Metaseds	Metaseds	Basement	Western
Unit	transitional	transitional	transitional	transitional	transitional	transitional
Latitude	63.795872	63.793525	63.742660	64.406665	64.311695	64.569028
Longitude	-66.956184	-66.933831	-64.218461	-66.407588	-66.483934	-66.908042
(wt%)						
SiO_2	44.61	49.78	46.8	52.42	51.11	47.19
Al_2O_3	9.56	6.29	11.14	14.05	14.17	15.04
Fe_2O_3(T)	13.08	13.15	10.15	13.36	14.05	12.71
MnO	0.188	0.222	0.178	0.207	0.222	0.207
MgO	22.17	17.13	12.36	6.99	6.31	6.29
CaO	8.04	9.17	12.95	11.21	9.95	13.71
Na_2O	0.28	0.71	1.34	0.55	2.19	2.28
K_2O	0.07	1.11	1.6	0.29	0.6	0.34
TiO_2	0.872	0.499	0.456	1.183	1.313	1.468
P_2O_5	0.07	0.07	0.46	0.08	0.1	0.12
LOI	0.39	-0.02	1.15	0.57	0.53	1.36
Total	99.33	98.12	98.59	100.9	100.6	100.7
(ppm)						
Sc	31	20	32	49	47	43
V	246	122	207	341	338	325
Cr	2210	1140	930	150	140	230
Co	91	82	55	47	46	50
Ni	1120	1020	350	50	40	100
Cu	130	70	< 10	50	100	130
Zn	80	130	110	120	110	110
Be	< 1	< 1	< 1	1	< 1	< 1
Ga	13	10	14	17	18	18
Ge	2.2	2	2	2.1	2.4	2.2
As	28	< 5	< 5	< 5	< 5	< 5
Rb	< 1	74	167	2	14	3
Sr	155	12	312	109	139	293
Y	12.3	12.6	17.3	21.8	25.3	21.4
Zr	50	43	59	62	78	73
Nb	3.6	1.7	1.8	2.3	2.6	8.7
Mo	< 2	< 2	< 2	< 2	< 2	< 2
Ag	< 0.5	< 0.5	< 0.5	< 0.5	< 0.5	< 0.5
In	< 0.1	< 0.1	< 0.1	< 0.1	< 0.1	< 0.1
Sn	< 1	< 1	< 1	< 1	< 1	< 1
Sb	0.4	0.3	0.4	< 0.2	< 0.2	< 0.2
Cs	< 0.1	2.5	56.5	0.1	0.4	< 0.1
Ba	8	99	271	16	100	172
Hf	1.3	1.2	1.4	1.7	2.1	1.7
Ta	0.27	0.15	0.25	0.26	0.24	0.69
W	< 0.5	0.9	< 0.5	< 0.5	< 0.5	< 0.5
Tl	< 0.05	0.42	0.83	< 0.05	< 0.05	< 0.05
Pb	< 5	< 5	< 5	< 5	< 5	< 5
Bi	< 0.1	0.2	2.1	< 0.1	0.2	< 0.1
Th	0.3	0.35	12.2	0.69	0.74	0.67
U	0.08	0.13	2.28	0.22	0.25	0.19
La	3.92	6.12	108	5.4	5.69	8.25
Ce	10.1	13.6	222	13.2	14.4	19
Pr	1.56	1.88	29.3	1.89	2.12	2.54
Nd	7.64	8.53	119	9.39	9.91	11.9
Sm	2.04	2.28	17.1	2.67	2.92	2.95
Eu	0.657	0.611	2.97	1.02	1.06	1.12
Gd	2.25	2.35	9.95	3.13	3.84	3.59
Tb	0.38	0.38	0.83	0.58	0.68	0.6
Dy	2.26	2.29	3.58	3.48	4.09	3.6
Ho	0.44	0.45	0.59	0.72	0.82	0.7
Er	1.25	1.27	1.62	2.26	2.42	1.97
Tm	0.187	0.19	0.219	0.35	0.379	0.324
Yb	1.22	1.2	1.28	2.27	2.61	2.2
Lu	0.177	0.172	0.186	0.381	0.39	0.319

SampleID	13SUB-S075D1	13SUB-S112B1
Region	Eastern	Central
Occurrence	Metaseds	Unknown
Unit	transitional	transitional
Latitude	64.782625	64.669620
Longitude	-66.210639	-66.784711
(wt%)		
SiO_2	49.03	49.43
Al_2O_3	14.31	14.14
Fe_2O_3(T)	14.1	13.31
MnO	0.214	0.202
MgO	6.37	6.78
CaO	11.49	10.27
Na_2O	2.22	2.91
K_2O	0.28	0.84
TiO_2	1.53	1.38
P_2O_5	0.14	0.11
LOI	0.3	0.82
Total	99.99	100.2
(ppm)		
Sc	39	39
V	376	342
Cr	100	200
Co	48	46
Ni	70	110
Cu	200	< 10
Zn	120	100
Be	< 1	< 1
Ga	19	18
Ge	2.3	2.3
As	< 5	< 5
Rb	3	4
Sr	197	235
Y	24.6	21.2
Zr	89	81
Nb	8.1	6
Mo	< 2	< 2
Ag	< 0.5	< 0.5
In	< 0.1	< 0.1
Sn	< 1	< 1
Sb	< 0.2	< 0.2
Cs	< 0.1	< 0.1
Ba	72	92
Hf	2	1.7
Ta	0.67	0.49
W	< 0.5	< 0.5
Tl	< 0.05	< 0.05
Pb	< 5	< 5
Bi	< 0.1	< 0.1
Th	0.72	0.57
U	0.2	0.17
La	8.35	6.49
Ce	19.1	15.3
Pr	2.79	2.11
Nd	12.8	10.4
Sm	3.55	2.72
Eu	1.35	1.12
Gd	4.1	3.63
Tb	0.71	0.63
Dy	4.23	3.43
Ho	0.83	0.66
Er	2.41	1.85
Tm	0.356	0.297
Yb	2.21	1.96
Lu	0.346	0.294

SampleID	12MBC-B118B1	12MBC-C038B1	12MBC-F013A1	12MBC-F034B1	12MBC-F093B1	12MBC-K004A2
Region	Central	Central	Western	Eastern	Central	Central
Occurrence	Basement	Metaseds	Basement	Metaseds	Basement	Metaseds
Unit	tholeiitic	tholeiitic	tholeiitic	tholeiitic	tholeiitic	tholeiitic
Latitude	63.777628	63.529027	63.200152	63.401995	63.178303	63.308388
Longitude	-65.496642	-65.546688	-66.371111	-64.538422	-65.892256	-66.001491
(wt%)						
SiO_2	47.49	48	47.46	45.77	44.4	49.91
Al_2O_3	13.6	14.4	15.22	12.14	15.06	7.88
Fe_2O_3(T)	12.5	13.03	11.85	19.87	15.72	13.97
MnO	0.297	0.193	0.181	0.228	0.199	0.243
MgO	6.66	7.9	10.07	5.48	7.23	13.37
CaO	13.65	11.99	10.52	9.56	11.54	10.92
Na_2O	2.3	2.17	2.1	1.18	1.79	1.37
K_2O	0.67	0.3	0.35	0.63	0.77	0.14
TiO_2	0.719	0.827	0.609	2.623	1.064	0.909
P_2O_5	0.06	0.06	0.03	0.13	0.05	0.08
LOI	0.66	0.38	0.29	0.18	1.37	0.9
Total	98.6	99.24	98.68	97.8	99.19	99.69
(ppm)						
Sc	41	43	37	52	48	68
V	259	280	216	853	349	372
Cr	250	240	320	90	190	1120
Co	53	54	59	60	53	60
Ni	160	170	360	70	120	190
Cu	60	70	20	30	30	10
Zn	100	90	80	150	110	90
Be	< 1	< 1	< 1	< 1	< 1	< 1
Ga	16	16	15	22	20	13
Ge	1.8	1.7	1.8	2.3	1.4	2.6
As	< 5	< 5	< 5	< 5	< 5	< 5
Rb	6	1	4	9	11	3
Sr	107	154	76	136	91	38
Y	16.7	18.1	13	26	22.9	21
Zr	36	36	30	72	60	41
Nb	1.4	2	1.6	3	2.2	1.7
Mo	< 2	< 2	< 2	2	< 2	< 2
Ag	< 0.5	< 0.5	< 0.5	< 0.5	< 0.5	< 0.5
In	< 0.1	< 0.1	< 0.1	< 0.1	< 0.1	< 0.1
Sn	< 1	< 1	< 1	< 1	< 1	< 1
Sb	0.2	< 0.2	0.2	0.2	0.3	0.4
Cs	< 0.1	< 0.1	< 0.1	0.3	0.2	< 0.1
Ba	71	25	32	128	102	27
Hf	0.9	1	0.9	1.8	1.5	1.2
Ta	0.12	0.11	0.09	0.19	0.22	0.12
W	< 0.5	< 0.5	1.8	< 0.5	< 0.5	< 0.5
Tl	< 0.05	< 0.05	< 0.05	0.1	0.06	< 0.05
Pb	< 5	< 5	< 5	7	< 5	< 5
Bi	< 0.1	< 0.1	0.1	0.3	< 0.1	< 0.1
Th	0.39	0.15	0.2	1.04	0.66	0.56
U	0.2	0.04	0.04	0.29	0.18	0.11
La	2.56	3.74	2.5	8.17	4.74	4.18
Ce	6.68	8.73	6.19	18.1	11.9	9.48
Pr	1.08	1.34	0.95	2.54	1.97	1.41
Nd	5.79	6.29	4.83	11.9	9.93	6.86
Sm	1.94	2.06	1.48	3.37	3.14	2.23
Eu	0.6	0.665	0.497	1.26	0.84	0.729
Gd	2.23	2.54	1.76	3.85	3.7	2.76
Tb	0.47	0.49	0.34	0.66	0.7	0.51
Dy	2.78	3.03	2.21	4.22	3.98	3.39
Ho	0.55	0.62	0.45	0.9	0.81	0.72
Er	1.67	1.86	1.29	2.71	2.42	2.15
Tm	0.254	0.288	0.206	0.4	0.376	0.331
Yb	1.66	1.87	1.44	2.55	2.41	2.09
Lu	0.255	0.269	0.21	0.388	0.336	0.31

SampleID	12MBC-K069A1	12MBC-K076A1	12MBC-K079A1	12MBC-K079A2	12MBC-K114D1	12MBC-M015B1
Region	Central	Central	Central	Central	Central	Central
Occurrence	Metaseds	Metaseds	Metaseds	Metaseds	Metaseds	Basement
Unit	tholeiitic	tholeiitic	tholeiitic	tholeiitic	tholeiitic	tholeiitic
Latitude	63.307547	63.306257	63.305905	63.305905	63.068107	63.112597
Longitude	-65.998841	-65.995756	-66.006033	-66.006033	-64.887145	-65.763260
(wt%)						
SiO_2	49.9	45.34	46.28	46.64	50.13	48.14
Al_2O_3	15.08	11.71	11.63	9.64	13	14.34
Fe_2O_3(T)	10.57	17.62	12.23	13.7	14.85	13.98
MnO	0.165	0.268	0.23	0.243	0.203	0.211
MgO	8.33	9.61	12.51	12.74	6.76	8.3
CaO	11.14	12.03	11.75	11.74	10.44	11.29
Na_2O	2.59	1.35	1.57	1.13	1.64	2.07
K_2O	0.2	0.47	0.2	0.19	0.37	0.3
TiO_2	0.807	1.359	0.795	0.827	1.195	0.835
P_2O_5	0.06	0.06	0.05	0.02	0.1	0.06
LOI	0.71	0.41	1.31	1.16	0.21	0.72
Total	99.55	100.2	98.57	98.04	98.9	100.3
(ppm)						
Sc	44	57	65	62	49	48
V	300	500	349	372	352	299
Cr	370	220	1030	1080	160	310
Co	45	67	51	58	50	54
Ni	140	180	160	180	50	140
Cu	230	< 10	10	< 10	30	30
Zn	70	160	80	90	90	100
Be	< 1	< 1	< 1	< 1	< 1	< 1
Ga	17	18	15	19	20	18
Ge	2	1.7	1.6	1.9	2.7	2.3
As	< 5	< 5	< 5	< 5	< 5	< 5
Rb	3	8	3	5	10	5
Sr	98	34	77	53	78	96
Y	16.4	18.7	17.6	19	26.2	19.2
Zr	34	51	38	38	68	42
Nb	1.6	1.8	0.9	1.3	3	2
Mo	< 2	2	< 2	< 2	< 2	< 2
Ag	< 0.5	< 0.5	< 0.5	< 0.5	< 0.5	< 0.5
In	< 0.1	< 0.1	< 0.1	< 0.1	< 0.1	< 0.1
Sn	< 1	< 1	< 1	< 1	< 1	< 1
Sb	0.3	0.3	0.3	< 0.2	0.4	0.4
Cs	< 0.1	< 0.1	0.1	0.1	< 0.1	0.1
Ba	33	66	51	91	60	34
Hf	0.9	1.1	1	1	1.9	1.2
Ta	0.11	0.15	0.1	0.08	0.22	0.17
W	< 0.5	< 0.5	< 0.5	< 0.5	< 0.5	< 0.5
Tl	< 0.05	< 0.05	< 0.05	< 0.05	0.07	< 0.05
Pb	< 5	< 5	< 5	< 5	< 5	< 5
Bi	< 0.1	< 0.1	< 0.1	< 0.1	< 0.1	< 0.1
Th	0.22	0.81	0.23	0.4	0.65	0.27
U	0.05	0.18	0.06	0.1	0.18	0.07
La	2.86	6.02	4.32	3.62	4.45	3.25
Ce	6.24	11.9	8.97	8.44	10.7	7.3
Pr	1.05	1.55	1.41	1.3	1.68	1.17
Nd	5.23	7.24	7	6.57	8.59	6.1
Sm	1.87	2.31	2.14	2.12	2.86	1.97
Eu	0.66	0.688	0.656	0.761	0.855	0.677
Gd	2.31	2.83	2.55	2.59	3.55	2.66
Tb	0.42	0.51	0.51	0.49	0.66	0.49
Dy	2.76	3.19	2.9	3.02	4.19	3.13
Ho	0.58	0.68	0.63	0.65	0.91	0.69
Er	1.64	1.97	1.83	2.01	2.65	1.99
Tm	0.245	0.293	0.265	0.32	0.412	0.312
Yb	1.62	1.88	1.73	2.05	2.68	1.95
Lu	0.234	0.279	0.266	0.296	0.388	0.286

SampleID	12MBC-S090C1	12MBC-Y014A1	12MBC-Y048A4	13SUB-B050D1	13SUB-F039A1	13SUB-F045A1
Region	Central	Central	Central	Eastern	Central	Central
Occurrence	Metaseds	Metaseds	Unknown	Metaseds	Unknown	Basement
Unit	tholeiitic	tholeiitic	tholeiitic	tholeiitic	tholeiitic	tholeiitic
Latitude	63.279432	63.289263	63.325998	64.600303	64.331430	64.407180
Longitude	-65.828543	-66.062936	-65.315947	-65.826891	-66.512146	-66.409298
(wt%)						
SiO_2	47.9	51.61	45.08	49.05	48.82	49.58
Al_2O_3	12.4	8.18	12.35	14.6	15.64	15.68
Fe_2O_3(T)	11.36	9.53	20.93	16.01	12.05	12.27
MnO	0.195	0.282	0.242	0.221	0.202	0.205
MgO	9.84	10.13	5.3	4	8.66	6.52
CaO	13.17	17	9.75	9.29	10.68	13.22
Na_2O	1.51	1.9	1.35	3.3	2.63	1.26
K_2O	0.35	0.34	0.54	0.53	0.28	0.28
TiO_2	0.89	0.268	2.544	2.057	0.796	1.021
P_2O_5	0.05	0.08	0.14	0.25	0.05	0.08
LOI	0.78	0.57	0.02	1.11	0.64	0.56
Total	98.45	99.87	98.24	100.4	100.4	100.7
(ppm)						
Sc	53	40	50	40	42	41
V	327	167	1054	438	261	295
Cr	510	2910	30	50	350	320
Co	51	81	64	37	47	50
Ni	210	770	80	40	170	180
Cu	170	10	90	50	40	80
Zn	70	90	150	150	110	110
Be	< 1	1	< 1	1	< 1	< 1
Ga	16	14	24	22	16	18
Ge	2.1	3	2	2.1	1.9	2.2
As	< 5	< 5	< 5	< 5	< 5	< 5
Rb	7	2	9	12	7	11
Sr	97	64	111	188	120	122
Y	16.7	22.8	31	40.8	18	22.1
Zr	40	19	83	113	42	56
Nb	2.2	3.3	3.5	4	1.2	1.9
Mo	< 2	< 2	< 2	< 2	< 2	< 2
Ag	< 0.5	< 0.5	0.6	< 0.5	< 0.5	< 0.5
In	< 0.1	< 0.1	< 0.1	< 0.1	< 0.1	< 0.1
Sn	< 1	< 1	< 1	1	< 1	< 1
Sb	0.3	0.3	0.4	0.2	< 0.2	< 0.2
Cs	0.1	< 0.1	0.2	0.8	0.2	0.9
Ba	78	25	195	175	93	41
Hf	1.1	0.6	2.2	2.5	1.1	1.5
Ta	0.17	0.15	0.24	0.38	0.12	0.4
W	< 0.5	< 0.5	< 0.5	< 0.5	< 0.5	< 0.5
Tl	< 0.05	< 0.05	0.06	0.18	0.1	< 0.05
Pb	< 5	< 5	< 5	8	< 5	< 5
Bi	< 0.1	< 0.1	< 0.1	< 0.1	0.3	< 0.1
Th	0.23	0.72	1.17	1.64	0.42	0.28
U	0.06	0.35	0.28	0.37	0.06	0.1
La	2.88	8.53	9.43	11.9	2.44	3.11
Ce	6.96	16.9	20.9	26.8	6.6	8.22
Pr	1.13	2.49	2.92	3.75	0.99	1.3
Nd	5.61	9.6	13.5	16.7	5.43	6.62
Sm	1.96	2.11	3.83	4.78	1.78	2.31
Eu	0.687	0.323	1.17	1.64	0.697	0.8
Gd	2.5	2.44	4.53	5.7	2.47	3.02
Tb	0.46	0.48	0.85	1.04	0.45	0.58
Dy	2.91	3.32	5.26	6.67	3.06	3.69
Ho	0.6	0.71	1.1	1.39	0.6	0.76
Er	1.66	2.1	3.31	4.02	1.74	2.15
Tm	0.251	0.357	0.53	0.653	0.293	0.344
Yb	1.58	2.41	3.38	4.4	1.96	2.38
Lu	0.229	0.365	0.487	0.666	0.307	0.392

SampleID	13SUB-F111B1	13SUB-F127B1	13SUB-F138A1	13SUB-F139B1	13SUB-H082C1	13SUB-H094B1
Region	Central	Eastern	Central	Central	Eastern	Eastern
Occurrence	Metaseds	Metaseds	Unknown	Metaseds	Metaseds	Metaseds
Unit	tholeiitic	tholeiitic	tholeiitic	tholeiitic	tholeiitic	tholeiitic
Latitude	64.377808	64.648782	64.239922	64.180433	64.670630	64.378415
Longitude	-66.567849	-65.340248	-66.285929	-66.351383	-65.407956	-65.220920
(wt%)						
SiO_2	50.72	47.11	47.85	49.31	47.32	48.36
Al_2O_3	9.29	12.98	16.41	15.48	17.19	15.88
Fe_2O_3(T)	9.96	17.49	11.09	11.98	12.8	10.36
MnO	0.223	0.23	0.184	0.149	0.101	0.177
MgO	14.57	6.7	10.11	8.46	8.84	10.51
CaO	12.66	10.95	11.54	10.09	10.3	11.75
Na_2O	1.05	2.26	1.91	2.79	2.56	1.74
K_2O	0.53	0.6	0.3	0.34	0.2	0.27
TiO_2	0.179	1.998	0.544	0.761	0.788	0.369
P_2O_5	0.04	0.05	0.05	0.06	0.12	0.03
LOI	1.49	0.12	0.88	0.61	0.64	1.18
Total	100.7	100.5	100.9	100	100.9	100.6
(ppm)						
Sc	47	72	34	42	44	35
V	195	1088	195	262	220	164
Cr	830	40	410	340	220	520
Co	61	58	50	50	43	52
Ni	310	< 20	260	190	120	270
Cu	< 10	110	20	10	< 10	40
Zn	120	140	110	110	70	110
Be	< 1	< 1	< 1	1	< 1	< 1
Ga	14	19	14	16	18	13
Ge	3.7	2.9	2.4	2.5	2.5	2.3
As	< 5	< 5	< 5	< 5	< 5	< 5
Rb	5	4	22	10	1	7
Sr	42	121	116	186	208	114
Y	5.6	16.5	12.3	18.5	21.8	8.2
Zr	6	34	27	41	39	17
Nb	0.7	0.7	0.5	1	0.5	< 0.2
Mo	5	< 2	< 2	< 2	< 2	< 2
Ag	< 0.5	< 0.5	< 0.5	< 0.5	< 0.5	< 0.5
In	< 0.1	< 0.1	< 0.1	< 0.1	< 0.1	< 0.1
Sn	1	< 1	< 1	< 1	1	< 1
Sb	< 0.2	< 0.2	< 0.2	< 0.2	< 0.2	< 0.2
Cs	< 0.1	0.1	0.6	1.3	< 0.1	0.8
Ba	52	15	106	73	21	38
Hf	0.2	0.9	0.7	0.9	1.1	0.4
Ta	0.18	0.12	0.47	0.11	0.1	0.07
W	< 0.5	1.8	< 0.5	< 0.5	< 0.5	< 0.5
Tl	< 0.05	< 0.05	0.06	< 0.05	< 0.05	< 0.05
Pb	< 5	< 5	< 5	< 5	< 5	< 5
Bi	< 0.1	0.5	< 0.1	0.9	< 0.1	< 0.1
Th	0.08	0.25	0.13	0.12	1.53	< 0.05
U	0.16	0.08	0.04	0.03	0.16	0.03
La	2.04	2.64	2.46	2.78	15.9	1.11
Ce	3.24	6.66	6.34	6.87	33	2.67
Pr	0.52	1.03	0.82	1.06	4.8	0.4
Nd	1.84	5.23	4.34	5.08	20.3	2.37
Sm	0.67	1.77	1.23	1.92	3.88	0.88
Eu	0.43	0.68	0.541	0.698	1.2	0.407
Gd	0.7	2.23	1.68	2.28	3.52	0.94
Tb	0.14	0.45	0.3	0.47	0.56	0.19
Dy	0.85	2.83	1.93	3.04	3.27	1.34
Ho	0.19	0.57	0.4	0.61	0.67	0.27
Er	0.55	1.63	1.19	1.8	2.06	0.82
Tm	0.094	0.267	0.199	0.306	0.329	0.14
Yb	0.64	1.76	1.35	2.04	2.17	0.95
Lu	0.085	0.263	0.203	0.314	0.34	0.147

SampleID	13SUB-K035B1	13SUB-K047A1	13SUB-S153A1	13SUB-S154A1	13SUB-S164C1	13SUB-S165C1
Region	Central	Central	Central	Central	Eastern	Eastern
Occurrence	Metaseds	Basement	Basement	Basement	Metaseds	Metaseds
Unit	tholeiitic	tholeiitic	tholeiitic	tholeiitic	tholeiitic	tholeiitic
Latitude	64.563295	64.502697	64.519473	64.519645	64.445927	64.443793
Longitude	-66.772458	-66.428534	-66.616971	-66.622516	-65.229305	-65.230375
(wt%)						
SiO_2	48.37	48.47	47.8	48.46	49.91	46.71
Al_2O_3	14.19	14.76	13.97	10.68	16.04	16.73
Fe_2O_3(T)	14.87	13.82	15.3	10.83	10.68	10.55
MnO	0.184	0.204	0.179	0.181	0.176	0.171
MgO	6.72	7.68	6.68	14.1	8.3	11.34
CaO	10.65	10.93	10.81	13.2	12.55	12.22
Na_2O	2.9	2.63	2.83	1.13	1.62	1.29
K_2O	0.65	0.65	0.66	0.47	0.23	0.15
TiO_2	1.832	0.902	1.805	0.24	0.492	0.473
P_2O_5	0.16	0.07	0.16	< 0.01	0.03	0.03
LOI	0.23	0.65	0.17	1.41	0.65	0.9
Total	100.8	100.8	100.4	100.7	100.7	100.6
(ppm)						
Sc	42	41	42	45	45	28
V	392	289	392	180	224	174
Cr	120	220	120	700	360	420
Co	42	53	42	67	43	56
Ni	80	160	70	310	110	390
Cu	40	80	40	< 10	30	50
Zn	140	120	110	100	90	80
Be	< 1	< 1	< 1	< 1	< 1	< 1
Ga	21	16	21	10	15	14
Ge	2.5	2.3	2.1	2.6	2.5	2.1
As	16	< 5	< 5	< 5	< 5	< 5
Rb	4	6	4	3	4	2
Sr	58	110	54	57	107	98
Y	34.8	18.9	35.9	6.3	10.4	10.5
Zr	92	47	92	9	21	26
Nb	3.2	1.2	3.5	< 0.2	< 0.2	< 0.2
Mo	< 2	< 2	< 2	< 2	< 2	< 2
Ag	< 0.5	< 0.5	< 0.5	< 0.5	< 0.5	< 0.5
In	< 0.1	< 0.1	< 0.1	< 0.1	< 0.1	< 0.1
Sn	< 1	< 1	< 1	< 1	< 1	< 1
Sb	< 0.2	< 0.2	< 0.2	< 0.2	< 0.2	< 0.2
Cs	0.2	< 0.1	< 0.1	0.2	0.5	0.3
Ba	48	40	43	38	24	28
Hf	2.1	1.2	2.4	0.3	0.5	0.7
Ta	0.24	0.12	0.28	3.61	0.05	0.07
W	3.1	< 0.5	< 0.5	< 0.5	< 0.5	< 0.5
Tl	< 0.05	< 0.05	< 0.05	< 0.05	< 0.05	< 0.05
Pb	< 5	< 5	< 5	< 5	< 5	< 5
Bi	< 0.1	< 0.1	< 0.1	< 0.1	0.2	< 0.1
Th	0.3	0.15	0.3	0.07	0.13	0.08
U	0.09	0.05	0.07	0.08	0.04	0.01
La	6.07	2.87	6.22	2.42	1.38	1.28
Ce	15	7.04	15.7	3.55	3.32	3.24
Pr	2.25	1.09	2.41	0.5	0.54	0.54
Nd	11.5	5.66	11.5	2.24	2.45	2.55
Sm	3.95	1.81	3.92	0.65	0.87	1.09
Eu	1.25	0.753	1.38	0.284	0.455	0.533
Gd	4.73	2.49	5.17	0.97	1.33	1.34
Tb	0.88	0.48	0.91	0.17	0.26	0.27
Dy	5.75	3.04	5.8	1	1.73	1.63
Ho	1.17	0.57	1.23	0.2	0.35	0.35
Er	3.44	1.71	3.56	0.61	1.03	0.99
Tm	0.55	0.287	0.546	0.103	0.169	0.166
Yb	3.7	2.01	3.57	0.7	1.13	1.16
Lu	0.527	0.311	0.548	0.104	0.167	0.182

SampleID	12MBC-B045A1	12MBC-F085B1	12MBC-K074A1	12MBC-K127B1	12MBC-R023B2	13SUB-F074A1
Region	Central	Central	Central	Central	Western	Eastern
Occurrence	Basement	Basement	Metaseds	Metaseds	Western	Unknown
Unit	ultramafic	ultramafic	ultramafic	ultramafic	ultramafic	ultramafic
Latitude	62.968958	63.169032	63.307062	63.282140	63.496643	64.847482
Longitude	-65.377000	-65.656962	-65.993653	-65.969268	-66.885806	-66.010345
(wt%)						
SiO_2	40.83	43.68	42.78	47.48	55.57	43.32
Al_2O_3	0.46	14.15	11.31	7.05	2.99	11.55
Fe_2O_3(T)	8.79	15.78	13.12	12.13	9.71	11.11
MnO	0.114	0.284	0.197	0.179	0.162	0.153
MgO	49.25	8.27	20.23	22.65	23.99	24.62
CaO	0.06	11.32	8.51	8.85	5.9	7.39
Na_2O	0.01	1.62	0.84	0.59	0.21	0.73
K_2O	< 0.01	1.06	0.15	0.12	0.04	0.05
TiO_2	0.012	1.225	0.719	0.678	0.125	0.238
P_2O_5	< 0.01	0.03	0.08	0.05	0.02	0.02
LOI	0.82	0.77	1.42	0.72	0.01	1.44
Total	100.3	98.19	99.36	100.5	98.73	100.6
(ppm)						
Sc	5	39	30	24	7	13
V	32	341	219	193	47	81
Cr	2080	160	2590	1820	1990	580
Co	119	59	95	81	70	93
Ni	2550	150	890	1110	1320	1110
Cu	< 10	< 10	50	< 10	< 10	20
Zn	40	120	90	70	290	70
Be	< 1	< 1	< 1	< 1	2	< 1
Ga	< 1	21	12	10	13	8
Ge	0.9	2.2	1.6	2.6	3.3	1.4
As	< 5	12	< 5	455	< 5	< 5
Rb	< 1	31	< 1	< 1	3	1
Sr	< 2	116	34	46	25	45
Y	< 0.5	20.3	10.2	9.4	4	5.7
Zr	1	70	36	35	16	16
Nb	0.2	3.8	4.1	2.9	0.7	< 0.2
Mo	2	< 2	< 2	< 2	< 2	< 2
Ag	< 0.5	< 0.5	< 0.5	< 0.5	< 0.5	< 0.5
In	< 0.1	< 0.1	< 0.1	< 0.1	< 0.1	< 0.1
Sn	< 1	3	< 1	< 1	< 1	< 1
Sb	0.3	0.9	0.2	1.3	0.3	< 0.2
Cs	< 0.1	0.7	< 0.1	< 0.1	0.1	< 0.1
Ba	< 3	224	10	5	7	12
Hf	< 0.1	1.8	0.9	1	0.6	0.5
Ta	0.07	0.34	0.31	0.24	0.09	0.1
W	< 0.5	< 0.5	< 0.5	< 0.5	< 0.5	< 0.5
Tl	< 0.05	0.13	< 0.05	< 0.05	< 0.05	< 0.05
Pb	< 5	< 5	< 5	< 5	< 5	< 5
Bi	< 0.1	1.5	< 0.1	0.4	< 0.1	< 0.1
Th	< 0.05	0.51	0.44	0.22	0.29	0.09
U	0.02	0.41	0.1	0.06	0.14	0.02
La	0.3	5.99	4.42	3.16	4.29	0.91
Ce	0.58	14	9.83	7.7	14.6	2.27
Pr	0.06	2.03	1.42	1.1	2.46	0.36
Nd	0.19	9.97	6.09	5.17	11	1.79
Sm	0.02	3.03	1.72	1.49	2.77	0.71
Eu	< 0.005	0.913	0.491	0.372	0.162	0.26
Gd	0.03	3.45	1.75	1.78	1.63	0.72
Tb	< 0.01	0.6	0.32	0.29	0.19	0.14
Dy	0.03	3.56	1.86	1.7	0.85	1.02
Ho	< 0.01	0.72	0.38	0.33	0.15	0.21
Er	0.04	2.02	1.03	1	0.37	0.57
Tm	0.006	0.303	0.144	0.162	0.05	0.103
Yb	0.03	1.94	0.93	1.01	0.32	0.69
Lu	0.004	0.285	0.147	0.132	0.046	0.098

SampleID	12MBC-B115A1	13SUB-Y048B1	12MBC-B077A1	12MBC-B080A1	12MBC-B071A1	12MBC-B008B1
Region	Eastern	Eastern	Eastern	Eastern	Eastern	Central
Occurrence	Basement	Metaseds	Basement	Metaseds	Basement	Basement
Unit	R - LOI	R - LOI	R - LOI	R - LOI	R - rock type	R - LOI
Latitude	63.921893	64.609827	63.637283	63.837442	63.266328	63.374857
Longitude	-65.110130	-66.011893	-64.435905	-64.512070	-64.622259	-66.231301
(wt%)						
SiO_2	41.53	46.32	42.97	41.38	57.29	48.37
Al_2O_3	3.6	0.39	4.9	2.82	16.53	8.16
Fe_2O_3(T)	9.87	9.69	9.35	8.62	7.21	13.34
MnO	0.137	0.127	0.128	0.167	0.103	0.278
MgO	35.4	38.21	32.37	41.52	3.61	14.02
CaO	3.26	0.22	4.46	1.48	6.49	10.78
Na_2O	0.2	0.02	0.08	0.05	4.14	1.05
K_2O	0.02	< 0.01	0.06	< 0.01	1.32	1.42
TiO_2	0.191	0.023	0.207	0.137	0.614	0.689
P_2O_5	0.02	< 0.01	0.01	< 0.01	0.18	0.08
LOI	5.45	5.63	4.76	3.62	0.59	1.8
Total	99.68	100.6	99.29	99.81	98.09	99.98
(ppm)						
Sc	16	4	17	11	32	42
V	99	14	98	44	123	217
Cr	2200	1670	2120	1530	60	480
Co	107	110	99	120	22	74
Ni	2170	2330	1810	2690	30	350
Cu	20	30	20	< 10	30	10
Zn	70	150	70	90	110	200
Be	< 1	< 1	< 1	< 1	1	1
Ga	5	< 1	6	3	25	16
Ge	1.1	1.7	1.3	1.4	1.5	2.1
As	< 5	5	< 5	< 5	< 5	< 5
Rb	< 1	< 1	< 1	< 1	41	60
Sr	12	< 2	51	8	423	64
Y	4.6	0.6	5.2	1.2	42.9	15.6
Zr	10	3	11	5	222	42
Nb	< 0.2	< 0.2	< 0.2	< 0.2	4.4	3.3
Mo	< 2	< 2	< 2	< 2	< 2	3
Ag	< 0.5	< 0.5	< 0.5	< 0.5	1.7	< 0.5
In	< 0.1	< 0.1	< 0.1	< 0.1	< 0.1	< 0.1
Sn	< 1	< 1	< 1	< 1	1	3
Sb	0.6	< 0.2	< 0.2	< 0.2	0.2	0.2
Cs	< 0.1	< 0.1	0.1	< 0.1	2.3	2.8
Ba	< 3	< 3	8	< 3	380	186
Hf	0.3	< 0.1	0.3	< 0.1	4.7	1.3
Ta	0.18	< 0.01	0.05	0.04	0.22	0.16
W	< 0.5	< 0.5	< 0.5	< 0.5	< 0.5	0.7
Tl	< 0.05	< 0.05	< 0.05	< 0.05	0.19	0.38
Pb	< 5	< 5	< 5	< 5	6	< 5
Bi	0.2	0.4	0.3	0.1	< 0.1	0.4
Th	0.08	0.09	0.08	0.05	1.51	0.62
U	0.03	0.05	0.03	0.04	0.3	0.27
La	0.61	0.24	0.93	0.38	33.1	9.92
Ce	1.68	0.52	2.17	0.85	76.8	28.9
Pr	0.25	0.06	0.35	0.11	12.7	4.57
Nd	1.54	0.19	1.65	0.56	61.4	20.2
Sm	0.51	0.09	0.5	0.09	13.9	4.9
Eu	0.157	0.017	0.161	0.035	2.03	1.08
Gd	0.62	0.08	0.69	0.2	11.5	4.37
Tb	0.12	0.01	0.14	0.03	1.7	0.6
Dy	0.8	0.09	0.82	0.2	8.86	3.01
Ho	0.17	0.02	0.19	0.04	1.67	0.56
Er	0.47	0.07	0.58	0.15	4.16	1.44
Tm	0.078	0.01	0.092	0.024	0.547	0.211
Yb	0.51	0.07	0.55	0.15	2.91	1.32
Lu	0.07	0.01	0.089	0.029	0.353	0.192

SampleID	12MBC-B151C1	12MBC-B153B1	12MBC-K012A1	12MBC-F155B1	12MBC-F156B1	12MBC-K099A1
Region	Central	Central	Central	Central	Central	Central
Occurrence	Metaseds	Basement	Basement	Basement	Basement	Metaseds
Unit	R - LOI	R - LOI	R - LOI	R - rock type	R - rock type	R - LOI
Latitude	62.537660	62.723018	63.350448	62.876467	62.861295	63.204097
Longitude	-64.794962	-64.942790	-65.099897	-65.336888	-65.360825	-65.909833
(wt%)						
SiO_2	51.69	42.57	51.45	46.05	45.92	57.39
Al_2O_3	15.04	8.3	14.97	8.95	10.05	0.69
Fe_2O_3(T)	10.3	8.62	9.81	8.78	7.96	5.39
MnO	0.128	0.105	0.137	0.102	0.101	0.109
MgO	6.66	9.02	8.03	9.88	10.36	29.85
CaO	8.87	8.22	9.38	6.66	7.99	1.68
Na_2O	2.67	0.89	2.93	1.23	1.6	0.05
K_2O	0.61	6.72	1.46	8.67	7.09	< 0.01
TiO_2	1.03	2.919	0.988	3.618	2.421	0.012
P_2O_5	0.18	1.11	0.23	1.63	0.74	0.05
LOI	2.62	9.71	1.55	2.28	3.06	2.59
Total	99.8	98.18	100.9	97.86	97.29	97.83
(ppm)						
Sc	27	14	23	16	20	4
V	228	130	148	118	126	19
Cr	100	280	150	520	430	1310
Co	44	36	42	41	41	76
Ni	130	230	130	370	150	1660
Cu	100	30	50	40	20	< 10
Zn	70	70	90	130	80	40
Be	< 1	3	1	4	3	< 1
Ga	19	18	18	21	19	3
Ge	1.4	1.2	1.3	1.1	1.3	4.2
As	< 5	< 5	< 5	< 5	< 5	< 5
Rb	5	112	47	200	200	< 1
Sr	297	1413	676	2397	1185	9
Y	16.9	17.8	14.3	19.9	14.7	1.6
Zr	100	448	135	508	250	< 1
Nb	3.5	81.6	4.7	96.8	44.9	0.4
Mo	4	3	< 2	7	< 2	< 2
Ag	0.7	2.8	0.9	3.2	1.4	< 0.5
In	< 0.1	< 0.1	< 0.1	< 0.1	< 0.1	< 0.1
Sn	< 1	2	< 1	3	< 1	< 1
Sb	0.2	0.3	0.2	0.2	0.3	0.3
Cs	0.4	0.6	0.7	1.4	1.4	< 0.1
Ba	93	2235	1061	6341	3780	< 3
Hf	2.3	9.1	2.9	10.7	5.4	< 0.1
Ta	0.27	4.4	0.25	5.48	2.5	0.06
W	2.4	1.6	< 0.5	2.9	< 0.5	< 0.5
Tl	< 0.05	0.12	0.23	0.33	0.31	< 0.05
Pb	< 5	< 5	9	13	9	10
Bi	0.3	< 0.1	< 0.1	< 0.1	< 0.1	< 0.1
Th	1.84	5.91	1.58	9.26	6.31	0.08
U	0.64	1.06	0.32	1.7	0.93	0.3
La	15	99.1	31.5	156	79.3	0.74
Ce	31.3	185	63.3	281	140	1.92
Pr	4.12	22.8	8.22	33	16.3	0.31
Nd	16.8	86.7	32.6	121	62	1.24
Sm	3.46	12.7	5.93	16.7	9.06	0.34
Eu	0.875	3.12	1.6	4.13	2.3	0.095
Gd	3.45	8.95	4.81	11.7	6.82	0.37
Tb	0.53	0.93	0.59	1.15	0.69	0.06
Dy	3.06	3.98	2.76	4.67	2.92	0.29
Ho	0.68	0.64	0.53	0.73	0.51	0.05
Er	1.79	1.59	1.33	1.75	1.29	0.15
Tm	0.283	0.206	0.178	0.212	0.157	0.022
Yb	1.71	1.08	1.13	1.1	0.86	0.13
Lu	0.261	0.123	0.166	0.145	0.119	0.018

SampleID	12MBC-S083B1	12MBC-R023B1	13SUB-S070A1	12MBC-F039C1
Region	Western	Western	Western	Western
Occurrence	Western	Ultramafic	Western	Western
Unit	R - LOI	R - LOI	R - LOI	R - rock type
Latitude	63.301552	63.496643	64.562588	63.334622
Longitude	-66.849299	-66.885806	-66.913476	-67.201831
(wt%)				
SiO_2	44.56	45.04	44.16	72.78
Al_2O_3	7.03	8.15	13.15	10.13
Fe_2O_3(T)	12.58	11.31	10.35	3.22
MnO	0.176	0.183	0.156	0.117
MgO	21.62	20.8	20.01	1.55
CaO	7.77	9.04	9.17	7.6
Na_2O	0.46	0.68	0.78	0.27
K_2O	0.13	0.26	0.09	0.03
TiO_2	1.059	0.685	0.176	0.279
P_2O_5	0.05	0.07	< 0.01	0.04
LOI	2.24	1.65	2.83	2.16
Total	97.69	97.89	100.9	98.18
(ppm)				
Sc	24	25	22	6
V	210	197	93	56
Cr	1600	1770	900	40
Co	82	82	77	6
Ni	910	1020	790	< 20
Cu	< 10	80	90	10
Zn	70	100	80	50
Be	2	< 1	< 1	2
Ga	11	12	9	13
Ge	3.2	1.7	1.7	1.5
As	8	< 5	< 5	< 5
Rb	2	5	1	< 1
Sr	181	145	55	163
Y	11.7	10.4	4.1	9.5
Zr	49	43	9	25
Nb	4.6	3.8	< 0.2	2.7
Mo	< 2	< 2	< 2	< 2
Ag	< 0.5	< 0.5	< 0.5	< 0.5
In	< 0.1	< 0.1	< 0.1	< 0.1
Sn	2	< 1	< 1	< 1
Sb	0.3	0.4	< 0.2	< 0.2
Cs	< 0.1	0.3	< 0.1	< 0.1
Ba	< 3	16	12	26
Hf	1.4	1.1	0.2	0.6
Ta	0.36	0.24	0.08	0.5
W	< 0.5	< 0.5	< 0.5	1.2
Tl	< 0.05	< 0.05	< 0.05	< 0.05
Pb	< 5	< 5	< 5	< 5
Bi	0.2	0.1	< 0.1	< 0.1
Th	< 0.05	0.33	< 0.05	2.36
U	0.01	0.17	< 0.01	0.77
La	4.25	3.57	0.66	10.4
Ce	12.1	8.65	1.42	20.6
Pr	1.9	1.34	0.19	2.51
Nd	9.24	5.95	1.14	9.33
Sm	2.47	1.67	0.34	1.85
Eu	0.791	0.383	0.195	0.407
Gd	2.32	1.78	0.44	1.72
Tb	0.39	0.31	0.09	0.23
Dy	2.27	1.85	0.63	1.3
Ho	0.42	0.37	0.13	0.28
Er	1.11	1.04	0.37	0.83
Tm	0.17	0.159	0.075	0.123
Yb	1.11	1.03	0.53	0.75
Lu	0.157	0.149	0.074	0.122